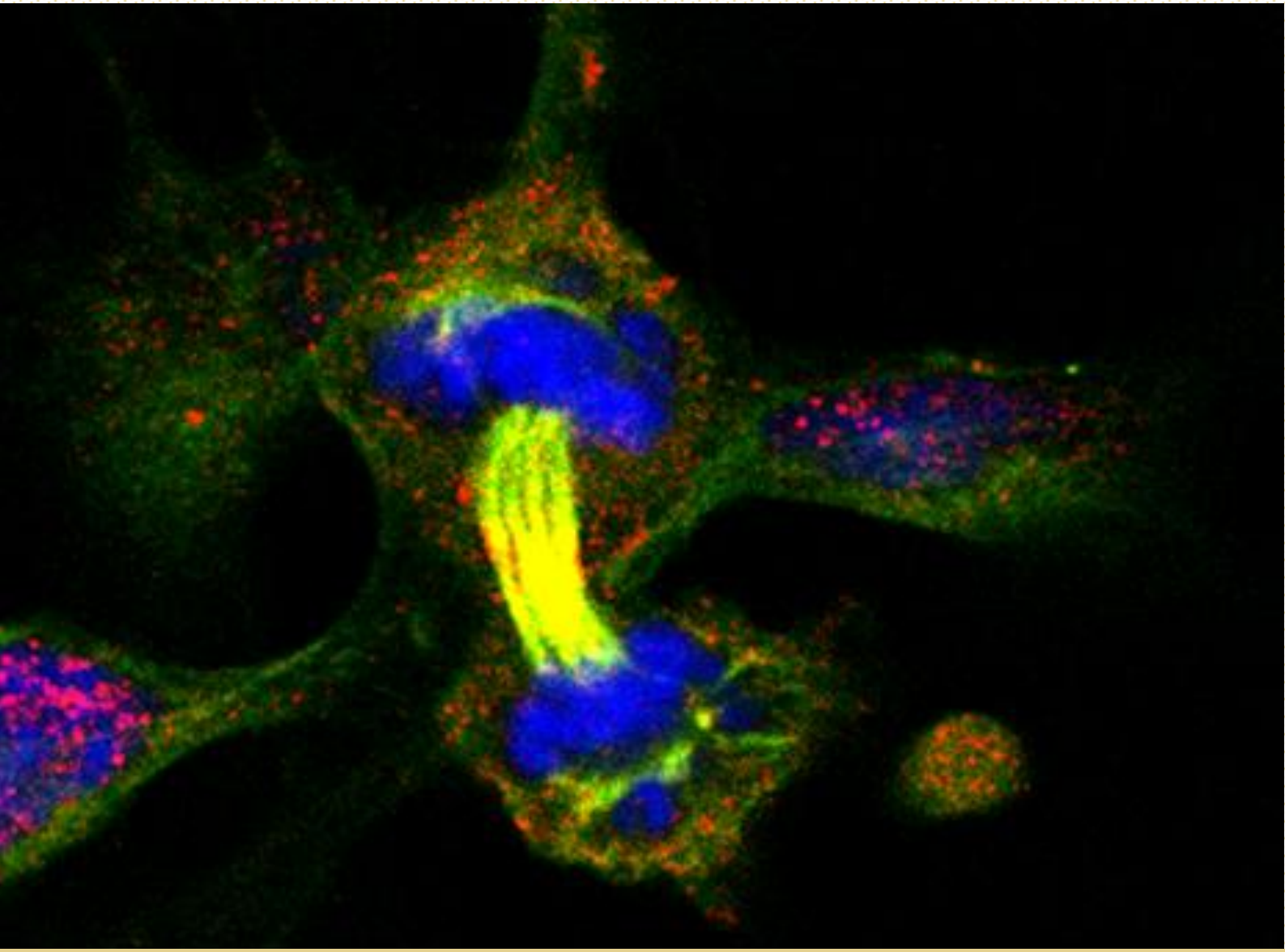

Carla Maria Nunes Lopes

Characterization of human stem cells and therapeutic strategies involving IGF-1 and shRNA in Huntington's disease

Tese de Doutoramento em Biologia Experimental e Biomedicina, Ramo de Neurociências e Doença, orientada por Doutora Ana Cristina Rego e
apresentada ao Instituto de Investigação Interdisciplinar da Universidade de Coimbra (IIIUC)

2015

· U C ·

UNIVERSIDADE DE COIMBRA

Characterization of human stem cells and therapeutic strategies involving IGF-1 and shRNA in Huntington's disease

Dissertação apresentada ao Instituto de Investigação Interdisciplinar da Universidade de Coimbra para cumprimento dos requisitos necessários à obtenção do Grau de Doutor em Biologia Experimental e Biomedicina na especialidade de Neurociências e Doença

Orientada por:

Professora Doutora Ana Cristina Carvalho Rego – Faculdade de Medicina da Universidade de Coimbra e Centro de Neurociências e Biologia Celular, Universidade de Coimbra, Coimbra, Portugal

Co-orientada por:

Professor Doutor Luis Pereira de Almeida –Faculdade de Farmácia e Centro de Neurociências e Biologia Celular, Universidade de Coimbra, Coimbra, Portugal

The research described in the present thesis was performed at the Center for Neurosciences and Cell Biology, University of Coimbra, Coimbra, Portugal.

Carla Lopes received a PhD fellowship from Fundação para a Ciência e Tecnologia (FCT), Portugal (fellowship: SFRH / BD / 51192 / 2010, financed by national founds of MEC CRM:0044390). The research work was funded by European community fund FEDER through "Programa Operacional Temático Factores de Competitividade – COMPETE" and "Fundação para a Ciência e a Tecnologia" (FCT), Portugal.

ACKNOWLEDGEMENTS

Table of Contents

Summary

Huntington's disease (HD) is an autosomal dominant disease caused by an expansion of CAG repeats in the gene encoding for huntingtin (HTT) and characterized by motor, cognitive and psychiatric symptoms. Despite HD monogenic etiology, its pathogenesis is incredibly complex and several mechanisms of neuronal dysfunction have been proposed. Given the diversity of mutant HTT interactions and the fact that there is still no cure or neuroprotective treatment for HD, in this study we aimed to clarify the early pathological mechanisms involving deficits in energy metabolism linked to mitochondrial dysfunction, altered cell cycle and modified signaling pathways, as well as evaluate the influence of treatment approaches targeting distinct cellular mechanisms *in vitro* and *in vivo*.

In the first part of this work we investigated the pathological mechanisms that have been proposed for neurodegeneration, including mitochondrial dysfunction and oxidative stress in HD patient-specific induced pluripotent stem cells (HD-iPSC) and derived HD-NSC *versus* cells expressing normal HTT. We showed that HD-iPSCs possessed hyperpolarized mitochondria and reduced mitochondrial Ca^{2+} storage capacity. HD-iPSCs mitochondria exhibited round shape morphology, but no differences in fission/fusion proteins were found. HD-iPSCs also consumed less O_2, exhibited decreased complex I+III activities and had lower ATP/ADP ratio, which was in accordance with the observation that HD cells relied more on glycolysis. Moreover, HD-iPSCs showed increased phosphorylation of pyruvate dehydrogenase (PDH) subunit E1α at Ser 232, 293 and 300, reflecting its inactivation. Concordantly, increased levels of pyruvate dehydrogenase kinase, isozyme 1 (PDK1) were found. In addition, increased levels of mitochondrial superoxide anion and hydrogen peroxide were observed in HD-iPSCs. These results were consistent with increased acetylation and decreased activity of superoxide dismutase 2 (SOD2) in HD cells. Our study suggests that human HD-iPSC can help to reveal the role of mitochondrial and metabolic dysfunction in early stages of HD.

In the second part of the work we analysed the role of HTT in the control of mitosis, namely whether it has an important impact on asymmetric division and cell fate. Using human embryonic stem cells (hESC) characterized as adult-onset mutant gene carriers, we qualified the role of human HTT in mitotic spindle orientation in human neural stem cells (derived from the hESC) and the effect of the adult-onset HD mutation. RNAi-

mediated silencing of HTT in neural stem cells derived from wild type hESC disrupted spindle orientation and mislocalized dynein, the $P150^{Glued}$ subunit of dynactin and the large nuclear mitotic apparatus NUMA protein. We further addressed the effect of an adult-onset HD mutation on spindle orientation in neural cells derived from HD-specific hESC. After identifying single-nucleotide polymorphism (SNP) we combined SNP-targeting allele-specific silencing and gain of function approaches, showing that expression of human HTT with 46 glutamines was sufficient to induce a dominant negative effect on spindle orientation and alteration of the localization of dynein, $P150^{Glued}$ and NUMA in neural stem cells. These findings revealed that neural derivatives of disease-specific human pluripotent stem cells constitute a relevant biological resource for exploring the impacts of adult onset HTT mutations on neural progenitors division with potential application in HD drug discovery targeting HTT-dynein- $P150^{Glued}$ complex functions.

Following the previous data from *in vitro* studies showing that Akt has a beneficial role on HD phenotype, in the third part of the work, we detailed the changes in an animal model of the disease and treatment response to IGF-1. Thus, we analysed brain metabolic dysfunction and altered Akt signaling and the protective role of insulin-like growth factor-1 (IGF-1)/Akt pathway in HD. We investigated motor phenotype, peripheral and central metabolic profile, and striatal and cortical signaling pathways in HD transgenic YAC128 mice subjected to intranasal administration of recombinant human IGF-1 (rhIGF-1), in order to promote IGF-1 delivery to the brain. IGF-1 supplementation enhanced IGF-1 cortical levels and improved motor activity and both peripheral and central metabolic abnormalities in YAC128 mice. Moreover, decreased Akt activation in HD mice brain was ameliorated following IGF-1 administration. Upregulation of Akt following rhIGF-1 treatment occurred concomitantly with increased phosphorylation of mutant HTT at Ser421. These data suggested that intranasal administration of rhIGF-1 ameliorates HD-associated glucose metabolic brain abnormalities and mice phenotype.

The present work enlightens the mechanisms underlying mitochondrial dysfunction and metabolic impairment as well as the role of HTT in cell cycle and cell fate occurring in early stages of HD. Moreover, we exploit therapeutic approaches targeting different molecular pathways, which were efficient *per se* in delaying disease phenotype, namely the selective inhibition of mutant HTT translation using shRNA in HD-patient's derived neural stem cells and the activation of brain intracellular signaling pathways induced by

IGF-1 in an animal model of HD. These studies provide new insights into HD pathogenesis which, hopefully, may result in improved therapeutic approaches for the disease.

Keywords: ESCs, iPS cells, cell proliferation, cell differentiation, Huntingtonʻs disease, huntingtin

Resumo

A doença de Huntington (DH) é uma doença genética, autossomica dominante, causada por uma expansão de CAGs no gene que codifica a proteína huntingtina e caracterizada por distúrbios motores e psíquicos, e declínio cognitivo. Apesar da etiologia monogénica, a patogenia é extremamente complexa e vários mecanismos de disfunção neuronal têm sido propostos. Tendo em conta a complexidade das interações moleculares e celulares da HTT mutada e o facto de não existirem tratamentos eficazes para a DH, este trabalho teve como principal objetivo esclarecer os mecanismos patológicos envolvidos no défice metabólico associado à disfunção mitocondrial e ao ciclo celular, bem como a alteração das vias de sinalização nas fases iniciais da DH, e aplicar diferentes abordagens terapêuticas *in vitro e in vivo*.

Na primeira parte deste trabalho investigámos os mecanismos fisiopatológicos associados à DH, incluindo a disfunção mitocondrial e o stresse oxidativo. A mitocondria tem sido sugerida como um factor patológico adicional em DH. Utilizando células pluripotentes induzidas provenientes de doentes de Huntington (HD-iPSC) mostrámos que as mitocôndrias se apresentavam hiperpolarizadas com menor capacidade de armazenamento de Ca^{2+}. As HD-iPSCs registaram um menor consumo de oxigénio, diminuição na atividade dos complexos I+III e do rácio ATP/ADP, recorrendo menos à fosforilação oxidativa para produção de ATP. As mitocôndrias das HD-iPSCs apresentaram morfologia alterada, contudo não encontrámos diferenças nos níveis das proteínas de fissão ou fusão Mais ainda, as HD-iPSCs mostraram um aumento da fosforilação da subunidade E1α nas Ser232, 293 e 300 da piruvato desidrogenase (PDH), refletindo a sua inactivação. Concomitantemente, verificou-se um aumento dos níveis da piruvato desidrogenase cinase, isoenzima 1 (PDK1). Além disso, níveis mitocondriais aumentados do ião superóxido e de peróxido de hidrogénio foram observados em HD-iPSCs. Estes resultados foram consistentes com o aumento da acetilação e diminuição da atividade da enzima superóxido dismutase 2 (SOD2) em HD-iPSCs. Este estudo sugere que a disfunção mitocondrial é um evento precoce na etiopatogenia da DH.

Na segunda parte do trabalho analisámos o papel fundamental da HTT no controlo da mitose, nomeadamente na divisão assimétrica e na definição da linhagem celular. Recorrendo a células estaminais embrionárias humanas (hESC) portadoras do gene mutante caracterizámos o papel de HTT humana na orientação do fuso mitótico em

células neurais humanas e o efeito da mutação da forma adulta da DH. O silenciamento mediado por shRNA dos alelos da huntingtina em células estaminais neurais derivadas de células estaminais embrionárias humanas *wild type* alterou a orientação do fuso mitótico e deslocalizou a dineína, a subunidade $p150^{glued}$ da dinactina e a proteína NUMA. Após identificação de um polimorfismo de nucleotídeo único (SNP) no gene HTT, avaliámos o silenciamento de um alelo específico e estratégias de ganho de função, mostrando que uma expansão de 46 glutaminas na proteína humana HTT é suficiente para induzir um efeito negativo dominante na orientação do fuso e alteração da localização de dineína, $p150^{glued}$ e NUMA em células estaminais neurais. Estes resultados revelaram que células estaminais neurais derivadas de células pluripotentes humanas constituem um recurso biológico relevante para explorar os impactos da forma adulta da mutação de HTT na mitose de progenitores neurais com potencial aplicação na descoberta de medicamentos visando as funções complexas da tríade HTT - dineina-$p150^{glued}$.

Estudos prévios *in vitro* mostraram que a cinase Akt desempenha um papel neuroprotector e passível de reverter o fenótipo da doença. Assim, na terceira parte do trabalho detalhámos a disfunção metabólica cerebral e as alterações nas vias de sinalização da Akt num modelo animal da DH (YAC128) e a resposta ao tratamento com fator de crescimento insulínico de tipo 1 (IGF-1). Especificamente investigámos as alterações motoras, o perfil metabólico central e periférico e as vias de sinalização corticais e estriatais no murganho YAC128 submetido à administração intranasal de IGF-1 recombinante humano (rhIGF-1), de modo a ceder IGF-1 ao cerebro. Mostrámos que a administração de rhIGF-1 aumenta os níveis corticais de IGF-1 e melhora a função motora e as alterações metabólicas periféricas e centrais no modelo YAC128. Consequentemente, a diminuição da ativação de Akt observada nos tecidos cerebrais de murganhos de DH foi revertida após administração de IGF-1. O aumento de expressão de Akt após o tratamento com rhIGF-1 ocorreu concomitantemente com o aumento da fosforilação de huntingtina mutante. Estes dados sugerem que a administração intranasal de rhIGF-1 melhora a alterações metabólicas cerebrais de DH e o fenótipo de murganhos YAC128.

Os resultados obtidos neste trabalho permitem esclarecer os mecanismos subjacentes à disfunção mitocondrial e à deficiência metabólica bem como as alterações no ciclo celular encontrados nos estadios iniciais da DH. Mostra-se ainda que abordagens terapêuticas em alvos moleculares distintos podem ser eficazes em retardar o fenótipo

da doença, nomeadamente a inibição da tradução seletiva da HTT mutante usando shRNA em células provenientes de doentes de Huntington e o efeito protetor do IGF-1 num modelo animal da doença. Estes estudos fornecem novos dados sobre as fases iniciais da patogenia da DH, podendo ajudar a encontrar abordagens terapêuticas mais eficazes para esta doença neurodegenerativa e debilitante.

Palavras –chave: Células estaminais embrionárias, Células estaminais pluripotentes induzidas, proliferação, diferenciação, Doença de Huntington, huntingtina

CHAPTER I - GENERAL INTRODUCTION

1.1.Huntington's disease

1.1.1. Historical background

A first attempts to describe Huntington's disease (HD) as a "chronic hereditary disease" was made in the middle 19th century but the most accurate description was done by George Huntington in 1872. He published his report in The Medical and Surgical Reporter (juulMargolis *et al.* 2003) about a hereditary form of chorea, describing "three marked peculiarities of this disease:

1. Its hereditary nature.

2. A tendency to insanity and suicide.

3. Its manifesting itself as a grave disease only in adult life"

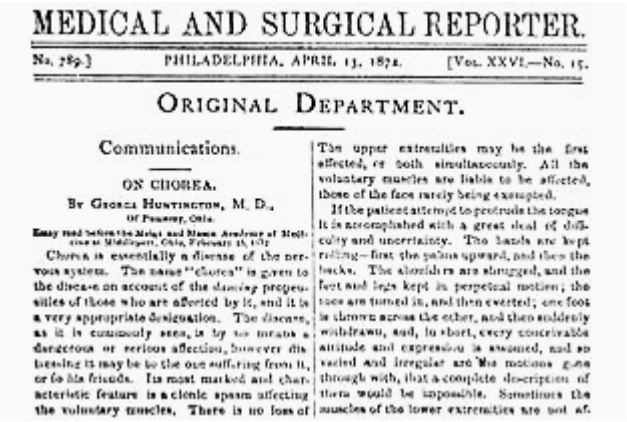

MEDICAL AND SURGICAL REPORTER.

No. 789.] PHILADELPHIA, APRIL 13, 1872. [Vol. XXVI.—No. 15.

ORIGINAL DEPARTMENT.

Communications.

ON CHOREA.

By George Huntington, M. D.,
Of Pomeroy, Ohio.

Essay read before the Medical and Surgical Academy at Middleport, Ohio, February 18, 1872

Chorea is essentially a disease of the nervous system. The name "chorea" is given to the disease on account of the dancing propensities of those who are affected by it, and it is a very appropriate designation. The disease, as it is commonly seen, is by no means a dangerous or serious affection, however distressing it may be to the one suffering from it, or to his friends. Its most marked and characteristic feature is a clonic spasm affecting the voluntary muscles. There is no loss of

The upper extremities may be the first affected, or both simultaneously. All the voluntary muscles are liable to be affected, those of the face rarely being exempted.

If the patient attempt to protrude the tongue it is accomplished with a great deal of difficulty and uncertainty. The hands are kept rolling—first the palms upward, and then the backs. The shoulders are shrugged, and the feet and legs kept in perpetual motion; the toes are turned in, and then everted; one foot is thrown across the other, and then suddenly withdrawn, and, in short, every conceivable attitude and expression is assumed, and so excited and irregular are the motions gone through with, that a complete description of them would be impossible. Sometimes the muscles of the lower extremities are not af-

Figure 1.1. Original paper "On Chorea" published by George Huntington at *The Medical and Surgical Reporter* in April 1872

Despite Mendel's Laws describing the principle of hereditary transmission were still recent and weakly disseminated, Huntington was able to note the autosomal dominant inheritance:

> *"The hereditary chorea, as I shall call it, is confined to certain and fortunately a few families, and has been transmitted to them, an heirloom from generations away back in the dim past……. When either or both the parents have shown manifestations of the disease, and more especially when these manifestations have been of a serious nature, one or more of the*

offspring almost invariably suffer from the disease, if they live to adult age. But if by any chance these children go through life without it, the thread is broken and the grandchildren and great-grandchildren of the original shakers may rest assured that they are free from the disease."

HD usually has a midlife onset, but juvenile (onset < 20 years) and older onset (> 70 years) are also present (Nance *et al.* 2001) progressing inexorably to death 15-20 years after the onset (for review, Rego *et al.* 2005). Only about 5-7% of patients exhibit symptoms before 21 years-old, in what was defined as the juvenile form of HD (Nance et al. 2001).

In early stages of the disease mild symptoms such as subtle psychiatric or motor changes often are neglected by the patient. HD progression involves movement disorder in early stages (also named chorea) evolving to more disabling progressive bradykinesia, incoordination, and rigidity, but also involves emotional and cognitive disturbances, leading to dementia as described in the following section.

1.1.2. Epidemiology

HD is one of the most important genetic disorders of adulthood and is found worldwide but with asymmetric distribution. Europe has the largest number of prevalence studies and, as it can be seen in Figure 1.2., a uniform prevalence of HD. The high prevalence is related with specific HTT haplotypes, namely the haplogroup A where both HD chromosomes and intermediate alleles for HD were almost exclusively found on (Warby *et al.* 2011). Indeed, a prevalence of 4-7 per 100,000 people is found over a large part of the continent. Finland reveals an atypical low prevalence, of about 0.5 per 100,000 individuals, which can be related to genetically distinct features from other populations, probably diverged from the common origin before such mutations occurred (Harper 1992). A previous study in South Wales found a prevalence of 8.85 HD cases per 100,000 people (Quarrell *et al.* 1988). A recent study in the UK reveal that the prevalence of diagnosed adult HD was 12.3 per 100 000 people and that the prevalence raised in the last decade probably due to patient longevity (Evans *et al.* 2013). Morrison, 2010 estimated that the current UK prevalence should be 14 to 16/100,000 or higher and that the prevalence in Caucasian populations is highly underestimates (Morrison 2010, Morrison 2012)

HD was originally described in North America, in families of British descent, as confirmed by the elevated rate of occurrence in descendants of Western European. In 2000, there were 30,000 cases of HD in United States, indicating a prevalence of about 10 cases per 100,000 people. The prevalence of HD in African Americans generates some controversy. Some studies described a much lower rate (Wright *et al.* 1981), but this number was refuted by the Maryland study, which found a prevalence of 5.15 per 100,000 people, based on a population of 4,217,000, a similar number to the population of Western-European origin. In most of these affected families, the HD allele did not have a European origin (Folstein *et al.* 1987).

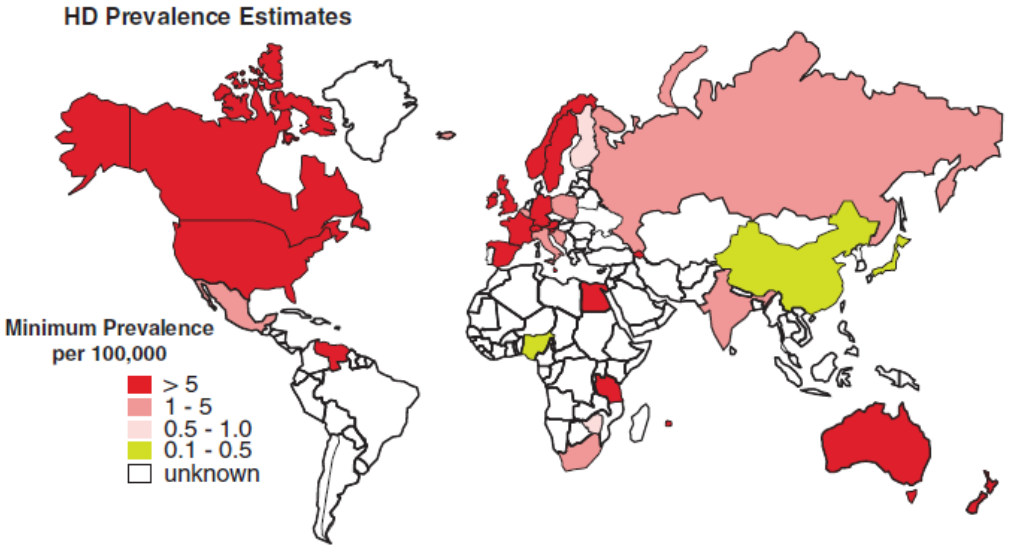

Figure 1.2. Worldwide estimates of the prevalence of HD. Adapted from Warby et al., 2011

In Portugal, the prevalence of HD is estimated to range from 2-5 per 100,000 people, overlapping the European values (Costa *et al.* 2003).

The disorder is rare in Orientals and Africans, suggesting that HD gene is rare (Harper 1992). Japan has a very low rate, of about 0.5 per 100,000 people (Walker 2007). In contrast, there are some regions where the prevalence is unusually high. Some studies were able to track the ancestor by genealogical analysis, mainly due to historical migration and geographic isolation of these areas. Tasmania has a prevalence of 17,4/100,000 people and the region of Lake Maracaibo, Venezuela, has more than 100 living HD patients, all descended from a single ancestor (Conneally 1984, Harper 1992). Importantly, HD affects equally males and females. The total heterozygote frequency in South Wales has been estimated at 20.2 per 100,000 people (Conneally 1984).

1.1.3. Genetics

An expansion of cytosine-adenine-guanine (CAG) repeats was first described in the androgen gene, and since then a class of nine genetically distinct, gain-of-function disorders were described, constituting the polyglutamine-expansion diseases. These include HD, dentatorubralpallidoluysian atrophy, spinal bulbar muscular atrophy (SBMA) or Kennedy‘s disease and spinocerebellar ataxias 1, 2, 3, 6, 7 and 17 (Bates 2005).

The gene affected in HD encodes the protein huntingtin (HTT) and the mutation results in a stretch of glutamine residues located at the N-terminal of mutant HTT (mHTT) (1993). This is believed to confer a deleterious gain-of-function to the mutant protein. The HD gene was mapped in 1983 with the eight polymorphic marker test (G8), which mapped the gene to chromosome 4 (4p) (Gusella *et al.* 1983). However, the HD gene was cloned only in 1993, which allowed the identification of a coding region occurring at the short arm of chromosome 4 (4p16.3), corresponding to an unstable DNA segment containing an expansion of a polymorphic trinucleotide repeat, near the 5‘ end in the exon 1 of the “Interesting Transcript 15” (IT15) gene, that spans over 200 kb and is composed of 67 exons (Group 1993).

Normal alleles are defined as alleles with < 26 CAG repeats; these are non-pathologic and segregated as a stable polymorphic repeat in > 99% of meiosis. In normal individuals, the most frequent allele length contains 17 and 19 CAG repeats (Kremer *et al.* 1994).

Mutable normal alleles are defined as alleles with 27-35 CAG repeats. This repeat range is often referred to as the meiotic instability range or as "intermediate alleles". No case has been associated unequivocally with an HD phenotype (Rubinsztein *et al.* 1996) (Brinkman *et al.* 1997), but they can be meiotically unstable in sperm, and predispose to CAGs expansion from one generation to the next, particularly when the disease is transmitted by males (Myers *et al.* 1993, Rubinsztein et al. 1996). This susceptibility was only described during transmission through the male germline and is associated with advanced paternal age (Goldberg *et al.* 1993).

HD alleles with reduced penetrance are defined as having 36-39 CAG repeats; these are meiotically unstable and associated with HD phenotype in both clinically and neuropathologically documented cases (Nance (Nance et al. 2001) et al., 2001). Few asymptomatic individuals over 75 years, with this allele size, have been documented (Rubinsztein et al. 1996).

Alleles with > 40 CAG repeats are defined as alleles with full penetrance. While there are several reports of elderly clinically asymptomatic HD gene carriers with 40 and 41 CAG repeats, no individuals with >41 CAG repeat length remained asymptomatic after middle life and the probability of an earlier onset is inversely related to number of CAG repeats (Brinkman et al. 1997). The presence of ≥ 60 CAGs is associated with juvenile onset that represents approximately 5-7% of all cases (Nance et al. 2001). A few cases of juvenile-onset disease with more than 200 CAG repeats have been documented (Nance *et al.* 1999, Seneca *et al.* 2004).

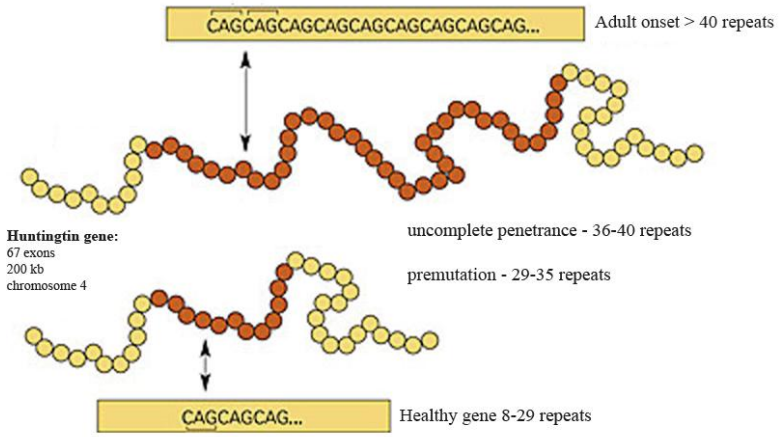

Figure 1.3. Representation of the HD gene and the impact of polyglutamine repeat size on HD onset

As an autosomic dominant disorder, the HD offspring have 50% chance of inheriting the disease in a Mendelian mode.

The number of polyglutamines is inversely correlated with age of onset (Duyao *et al.* 1993, Norremolle *et al.* 1993), but this only accounts for about 40% of the variation, with the remaining due to genetic polymorphisms adjacent to CAG repeat (for review, Rego et al. 2005, Norremolle *et al.* 2009) and environment (Wexler *et al.* 2004). However, some studies did not find a relationship between the number of CAG repeats and the rate of clinical decline (Kieburtz *et al.* 1994), which suggested that CAG repeat length may have a small effect on the rate of progression that may be clinically important over time (Rosenblatt *et al.* 2006).

A large population sample was analyzed in Portugal, showing that CAG ranged between 9 and 40 repeats, with the 17 CAG allele occurring most frequently (37.9%). Intermediate alleles with 27–35 CAGs represented 3.0% and two expanded alleles (0.11%) were found,

one of reduced penetrance (36 CAGs) and other with fully penetrant repeat (40 CAGs) (Costa et al. 2003).

The number of CAG repeats is only highly predictive of the age of onset if CAG≥ 40. The genes encoding for NR2A/B receptor subunits of the *N*-methyl-D-aspartate (NMDAR) receptor may be responsible for the variance on the age of onset in individuals with CAG repeat lengths between 30-40 (ClinicalTrials.gov 2009). In a cohort of HD patients with a CAG repeat length between 41 and 45, 30.8% of the variance in age of onset could be attributed to CAG repeat number, while variations in the NR2A (*N*-methyl-D-aspartate receptor receptor subunit) and NR2B genes accounted for 4.5% and 12.3% of the variance, respectively (ClinicalTrials.gov 2009).

1.1.4. Neuropathology

Basal ganglia are a group of nuclei located subcortically that are involved in motor and cognitive processes. Cerebral cortex and substantia nigra pars compacta (SNpc) send glutamatergic and dopaminergic inputs, respectively, to caudate and putamen, and frontal cortex receives transiently excitatory input from the thalamus (Purves et al. 2004). Connections between basal ganglia output nuclei (GPi/SNr) (globus pallidus interna/ substancia nigra pars reticulata) and striatum are organized in two pathways: direct and indirect.

The direct pathway is a monosynaptic transiently inhibitory projection between medium spiny neurons (MSN) of caudate and putamen to the tonically active inhibitory neurons in GPi/SNr, which in turn provides inhibitory innervation to thalamocortical projections (ventral anterior and ventral lateral thalamic nuclei - VA/VL complex).

The indirect pathway is a polysynaptic connection that involves intercalated neurons in globus pallidus externa (GPe) and STN (subthalamic nucleus) and increases the level of tonic inhibition. Ninety-five per cent of all neurons in striatum are GABAergic and contain mainly the inhibitory neurotransmitter γ-aminobutyric acid (GABA) and enkephalin, dynorphin or substance P (SP) as co-transmitter. When the indirect pathway is activated by excitatory signals from the cortex, MSN discharge and inhibit tonically active GABAergic neurons of GPe. Enkephanin is a reliable marker of indirect pathway while substance P is of the direct pathway (Vonsattel et al. 2011). These neurons project to STN, which in turn sends excitatory inputs to GPi and SNpr that oppose the disinhibitory action

of the direct pathway. Thus, indirect pathway modulates the direct pathway. Most MSNs express D1 (subtype 1 dopamine receptor) and D2 (subtype 2 dopamine receptor) receptors, the majority of D1-expressing neurons being part of direct pathway and containing substance P, whereas D2- bearing neurons are part of indirect pathway, projecting to GPe and contain enkephalin (Purves *et al.* 2004).

SNr also projects its axons to deep layers of superior colliculus, an area of the upper motor neurons that command the saccades (rapid orienting movements of the eyes). Immediately before saccade onset, discharge rate of reticulata neurons is greatly reduced through the input from tonic GABAergic MSNs of caudate, which have been activated by signals from cortex. As a consequence upper motor neurons of superior colliculus are activated, allowing them to generate bursts of action potentials that command the saccade (Purves *et al.* 2004).

In patients with HD, MSN that project to the external segment of GP degenerate, especially those synthesizing enkephalin and GABA. In absence of their normal inhibitory input from spiny neurons, GPe cells become abnormally active; in turn, this activity reduces the excitatory output of STN to GPi, leading to the reduction of the inhibitory outflow of the basal ganglia (Figure 1.4.), (Purves *et al.* 2004).

Without the restricting influence of basal ganglia, upper motor neurons can be activated by inappropriate signals, resulting in choreatic movements and slowing of saccadic movements (Purves *et al.* 2004).

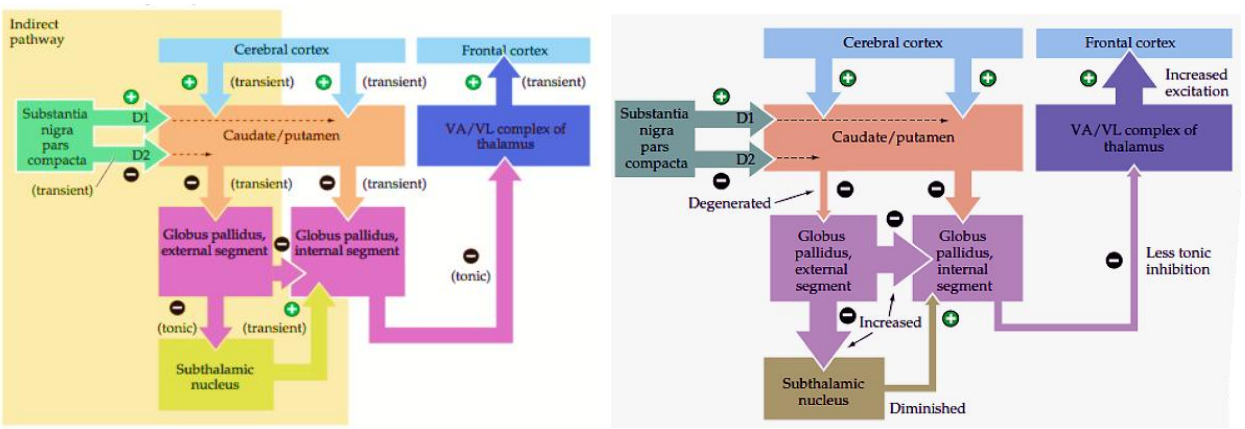

Figure 1.4. - Direct and indirect pathways through basal ganglia in normal and HD.

The balance of inhibitory signals in direct and indirect pathways is altered, leading to a decrease ability of basal ganglia to control the thalamic output to cortex. Projection from caudate and putamen to GPe is decrease (thinner arrow). This effect increases the tonic inhibition from GP to STN (larger arrow), making the excitatory STN less effective in opposing the action of direct pathway (thinner arrow). Thus, thalamic excitation of cortex is increased (larger arrow), leading to greater and often inappropriate motor activity. VA -ventral anterior thalamic nuclei; VL-ventral lateral thalamic nuclei (Purves *et al.* 2004).

As mentioned before, basal ganglia are also involved in other non-motor functions with significant clinical implications. Degeneration of specific subdivisions of prefrontal and limbic loop appears to be related with deterioration of cognitive and emotional function typical in HD (Purves *et al.* 2004). The prefrontal loop regulates the initiation and termination of cognitive processes (e.g. planning, working memory and attention) and the limbic loop regulates emotional behavior and motivation (Purves *et al.* 2004).

Degeneration can be found at different degrees in MSNs. In early and middle stage HD, enkephalinergic striato-GPe projection and SP-containing projection to SNr (indirect pathway) are more severely affected than SP -containing projections to the GPi and SN (direct pathway), resulting in an imbalance between the direct and indirect pathways (Reiner *et al.* 2013). A possible explanation is that SP-containing striato-SNr neurons and enkephalin-containing striato-GPe neurons are lost at a greater rate than either SP-containing striato-SNc or SP-containing striato-GPi neurons. In end-stage HD, all classes of striatal projection neurons are affected (including striate-GPi) which may explain the bradykinesia and rigidity (Reiner *et al.* 1988, Deng *et al.* 2004). In HD, glutamic acid decarboxylase (GAD), the enzyme that is involved in GABA synthesis, is significantly decreased in GPe but not in GPi in early stages, whilst in grade 4 patients the GAD fiber depletion from both structures was much larger. (Deng et al. 2004).

Striatal projecting neurons and parvalbuminergic striatal interneurons degenerate during HD (Vonsattel *et al.* 1998, Reiner et al. 2013) whereas cholinergic striatal interneurons and striatal interneurons containing somatostatin, neuropeptide Y and/or NADPH diaphorase (or nitric oxide synthase) and medium-sized calretinergic striatal interneurons survive in the pathology (Ferrante *et al.* 1985, Ferrante *et al.* 1987, Ferrante *et al.* 1987, Fusco *et al.* 1999, Cicchetti *et al.* 2000) The base for this vulnerability is uncertain but multiple factors seem to contribute for this selective vulnerability including: differential expression of HTT, changes in innervations, the extent of input from cortical or any other huntingtin-rich glutamatergic neurons implicating a prominent excitatory input, a high enrichment in Ca^{2+}-permeable AMPA receptors and the BDNF dependence (Fusco et al. 1999, Reiner et al. 2013). Reactive astrocytosis (gliosis) is also a common find together with neuronal loss (Verkhratsky *et al.* 2013). A 0-4 rating scale (the `Vonsattel scale') of gross and microscopic neurodegeneration, based primarily on changes in caudate and putamen (e.g. Figure 1.5.), has been used to semi-quantitatively describe the severity of HD. Grade 0 appears indistinguishable from normal brains after gross examination. However, 30–40% neuronal loss can be detected in the head of caudate nucleus upon histological examination. Grade 1 shows atrophy in the tail and in some cases the body of caudate nucleus. Neuronal loss and astrogliosis are evident in the head (50% loss), tail and, to a lesser extent, in the body of caudate nucleus. Grade 2 is associated with gross striatal atrophy that is more pronounced than that detected in grade 1 brain. Grade 3 displays severe gross striatal atrophy. Grade 4 includes HD cases with severe atrophy of striatum and up to 95% neuronal loss (Vonsattel *et al.* 1985, Gil *et al.* 2008).

More severe neurodegeneration in caudate and putamen were associated with longer expanded repeat nucleotide, which is associated with a faster deterioration and greater pathological severity and normal CAG repeat sizes can also influence the disease phenotype (Furtado *et al.* 1996, Aziz *et al.* 2009). However, the degree of tissue atrophy may not be solely determined. In advanced cases, total brain weight is reduced by 25-30% (Margolis et al. 2003).

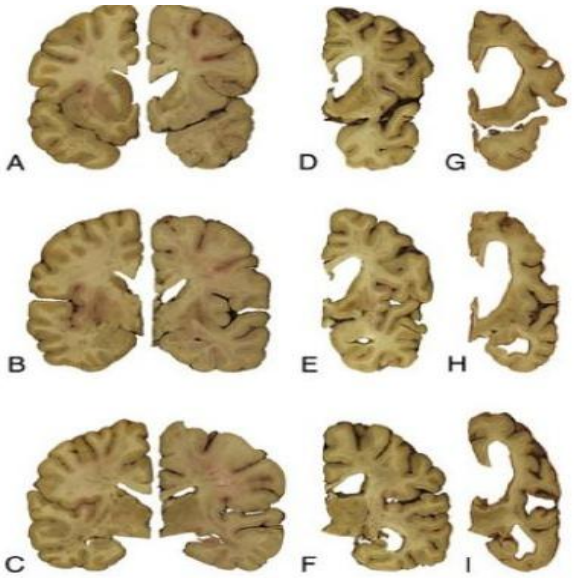

Figure 1.5. Macroscopic image from a normal control (left) and of Huntington's brain (right).
(A,D,G) coronal sections passing through the nucleus accumbes; (B,E,H) through the caudal edge of the anterior commissure; (C,F,I) through the lateral geniculate body. (A, B, C left) 43-years-old man control; (A, B, C right) 24- years-old man with CAG 70/20 (grade 3/4) and onset at 13-years; (D, E, F) 53- years-old man with CAG 46/17 (grade 3/4) and onset at 36-years; (G, H, I) 56- years-old man with CAG 49/22 (grade 4/4) and symptomatic for over 40-years; Photo from (Vonsattel *et al.* 2011).

Hypothalamus is a region of the brain involved in regulation of metabolism and sleep, and includes the pituitary gland that regulates hormonal levels in the body. A substantial trophy and cell death has been described in hypothalamus from HD patients (Kremer *et al.* 1990). Cells more severely affected are located in the lateral tuberal nucleus (nucleus tuberalis lateralis, NTL) of hypothalamus. In NTL of HD patients, about 90% neuronal loss was found and the remaining neurons showed features of degeneration (Kremer et al. 1990, Kremer *et al.* 1991). There was also astrocytosis and reduction of 40% in the number of oligodendrocytes (Kremer et al. 1990).This NTL vulnerability appears to be related to the high density of NMDA receptors in this nucleus (Kremer *et al.* 1993, Timmers *et al.* 1996). There is also a significant loss of orexin-containing neurons in hypothalamus most probably responsible for the sleep disregulation and metabolic changes (Petersen *et al.* 2005, Gabery *et al.* 2010).

1.1.5. Symptoms

HD symptoms typically manifest in midlife, between 35-50 years old and become fatal 15-20 years after the onset and juvenile or late-onset forms have shorter disease (Foroud *et al.* 1999) (Figure 1.6.).

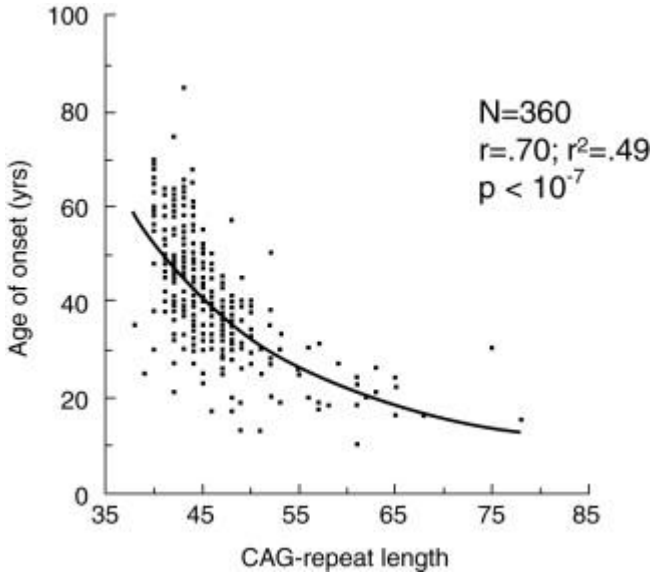

Figure 1.6. Correlation between trinucleotide repeat length and age of onset of symptoms. Adapted from (Andrew *et al.* 1993).

Psychiatric and behavioral problems have shown to be evident at least 15 years before motor hallmarks of the disease and are major constituents of the clinical spectrum of HD (Paulsen *et al.* 2001, Paulsen *et al.* 2006, Paulsen *et al.* 2008). The disease it‘s classically associated with progressive emotional, cognitive, and motor disturbances. In the prodromal phase (presymptomatic) relatively subtle symptoms (*e.g.* changes in personality, cognition, and motor control) may precede the disease onset by several years. Irritability or disinhibition, difficulty in developing multitasking, forgetfulness and anxiety are common, depression, impulsiveness, apathy and also motor changes including minor difficulties in coordination, balance, and slight adventitious movements of the trunk, limbs, and finger can be present (Foroud et al. 1999, Epping *et al.* 2011). Oculomotor abnormalities are primordial features and often the earliest motor sign; delayed initiation and slowing of saccadic movements, and inability to suppress glances at novel stimuli and an occasional nystagmus (Patel *et al.* 2012, Rupp *et al.* 2012).

The most frequently used criteria for diagnosis of clinical HD is ‘Motor 4’- a rating within the Unified Huntington Disease Rating Scale ’99 (1996), made when there are signals of clear motor abnormalities. HD is a multi-system disease with a continuum of both

involuntary and voluntary movement manifestations. Involuntary movements were first described by George Huntington as *Chorea*, derived from the Greek word *χορεία* (a kind of dance). Choreoathetotic movements are clonic spasm affecting voluntary muscles, with a random pattern. The severity varies from restlessness with mild, intermittent exaggeration of gesture and expression, through fidgety movements of hands and unstable dance-like gait, to a continuous flow of disabling and violent movements (Wild *et al.* 2007). Motor symptoms commonly begin by slight twitchings in the muscles of the face, which gradually increase in violence and variety, which may interfere with vocalization, chewing and swallowing. Dysarthria and dysphagia are common in these patients (for review, Walker 2007).

Voluntary movements are also disturbed, leading to bradykinesia and rigidity with slow initiation and poor execution of coordinated movements, especially in later stages of the disease (Purdon *et al.* 1994). In children with the juvenile form, a dominant picture of bradykinesia, rigidity, dystonia, ataxia and epileptic seizures occurs (Seneca et al. 2004, Ruocco *et al.* 2006). Another finding in HD that contributes to patients overactivity is motor impersistence — the inability to maintain a voluntary muscle contraction at a constant level. Incapacity to apply steady pressure during handshake is characteristic of HD and is called milkmaid's grip. Motor impersistence is a good marker of disease severity, since it is independent of chorea and linearly progressive. Fine motor skills, such as finger-tapping rhythm and rate, are useful for establishing an early diagnosis of HD (Walker 2007). Although chorea is the cardinal feature of HD, a significant percentage of patients do not refer it as the first symptom; rather, the patients refer other prominent symptoms, like cognitive or emotional changes (Foroud et al. 1999).

Several studies showed a high frequency of psychiatric disturbances in HD. Depressive symptoms could be a direct result of brain degeneration or a psychological reaction to the disease. Affective component is a major concern given the high risk of suicide, estimated to be 5-10 times more frequent than in general population (Fiedorowicz *et al.* 2011).

As disease progresses, memory deficits tend to appear. Reported impairments range from short-term memory deficits to long-term memory difficulties, including deficits in procedural and working memory. Cognitive problems tend to get worse over time and, in late-stage HD, leads to dementia (Montoya *et al.* 2006).

Sleep disturbances are also common clinical problems in HD and include increased sleep onset latency, reduced sleep efficiency, disruption of sleep, more time spent awake and less slow wave sleep. These abnormalities appear to be related with duration and severity

of the disease, and degree of atrophy of the caudate nucleus. Patients also show an increased density of sleep spindles (Hansotia *et al.* 1985, Wiegand *et al.* 1991, Cuturic *et al.* 2009). Recently, it was shown that HD patients have a disrupted circadian rhythm (Morton *et al.* 2005) probably due to melatonin deficiency (Alders *et al.* 2009). Interestingly, the most frequent primary cause of death in HD is pneumonia and cardiovascular disease (Sorensen *et al.* 1992).

1.1.6. Central and peripheral metabolic changes in HD

The selective permeability of blood brain barrier makes the glucose as the mandatory fuel for cerebral energy metabolism. In particular conditions, such as starvation or extreme physical activity, the brain also consumes monocarboxylic acids, including lactate and ketone bodies, acetoacetate and β-hydroxybutyrate (Mergenthaler et al. 2013). Glucose-6-phosphate does not only generate ATP but it's also used for pentose phosphate pathway (PPP) that generates NADPH to manage oxidative stress and to synthesize nucleic acid precursors. In glycolysis, glucose is degraded to pyruvate and then to lactate (Figure 1.7.). This process is not very energy-efficient, resulting only in the production of 2 mol of ATP/mol of glucose and in regeneration of reducing equivalents (the oxidized form of nicotinamide-adenine dinucleotide, NAD+). The use of lactate as a supplemental fuel varies with its availability and physiological state of the subject. The astrocyte–neuron lactate shuttle hypothesis supports the proposition that lactate (even from the bloodstream) is taken up and used by neurons under normal physiological conditions (Boumezbeur *et al.* 2010). Alternatively, pyruvate enters the tricarboxylic acid cycle (or Krebs cycle) and produce ATP of glucose via mitochondrial oxidative phosphorylation (Mergenthaler et al. 2013).

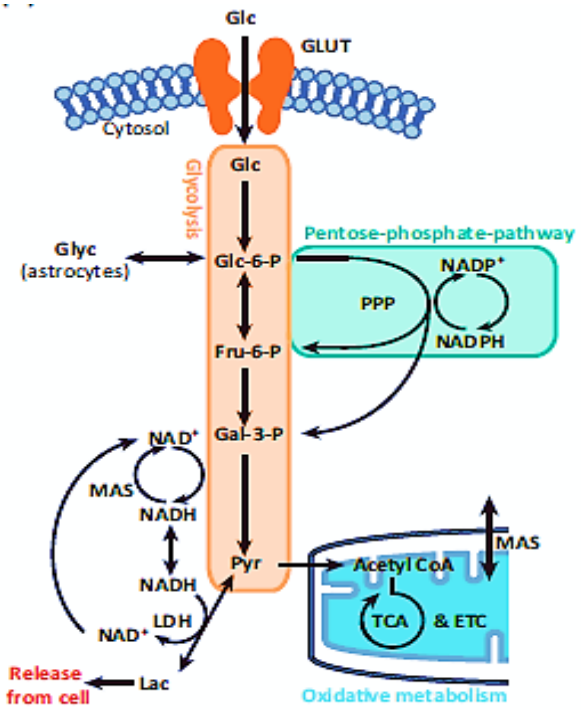

Figure 1.7. - Major pathways of glucose metabolism. Adapted from (Mergenthaler *et al.* 2013)

Bioenergetics defects are emerging as important pathophysiological mechanisms in neurodegenerative disorders. In a recent study, glucose metabolism was found to be significantly decreased in striatum and temporal and frontal cortical lobes, in both preclinical and affected HD patients, with marked striatal hypometabolism seen in later stages of disease reflecting neuronal atrophy (Ma *et al.* 2007). Thalamic hypermetabolism and cortical hypometabolism and hypoperfusion have also been detected in early stage of symptomatic HD patients with Positrons Emission Tomography or Single Photon Emission Computed Tomography (Ma et al. 2007). Also prodromal patients present unique pattern of brain metabolism and dopamine D2 receptor binding that appear to precede significant volumetric changes striatal which may be useful for following progression during different phases of the disease (Feigin *et al.* 2007).

As it was described previously mHTT and its fragments can interfere with energy production, through interaction with a variety of key proteins involved in energy metabolism. HTT interacts with an important enzyme involved in glycolysis GAPDH (glyceraldehyde-3-phosphate dehydrogenase) (Burke *et al.* 1996, Ratovitski *et al.* 2012) and when mutated partially inhibits its activity in a disease progression dependent manner causing a significant decrease in ATP production culminating in cell death but also oxidized GAPDH facilitates nuclear translocation of mHTT by translocating to the nucleus together with Siah (ubiquitin-E3-ligase) (Bae *et al.* 2006, Wu *et al.* 2007, Zala *et al.* 2013). The major cause for energetic deficit involves mitochondrial abnormalities triggered by mHTT which impairs oxidative phosphorylation, the final step in ATP production pathway. Defects in HD respiratory chain seems to be a secondary event involving specific mHTT-mitochondria interactions leading to increased production of reactive oxygen species therefore having a major role in both necrotic and apoptotic mechanisms of cell death. A dramatically decrease of the activity of complex II/III and mildly complex IV in the caudate or putamen, with normal levels in the frontal cortex or cerebellum was observed in postmortem studies of symptomatic patients or models of HD (Gu *et al.* 1996, Maksimovic *et al.* 2001, Benchoua *et al.* 2006, Browne 2008). Nevertheless the preferential decrease of respiratory chain enzymes, in particular complex II (SDH/II - succinate dehydrogenase) and to a lesser extend cytochrome c oxido-reductase (IV) seems to involve oxidative stress to which iron-sulfur cluster–containing proteins are more susceptive (for review, Mochel *et al.* 2011).

It has been widely described that HD patients have increased lactate levels in the basal ganglia and elevated lactate to pyruvate ratio in the CSF as well as reduced ATP synthesis

(Jenkins *et al.* 1993, Koroshetz *et al.* 1997). This findings suggests that damage to mitochondria and impaired energy metabolism occurs in the disease, leading to conversion of pyruvate in lactate to generate ATP (Koroshetz et al. 1997, Martin *et al.* 2007). Although glucose is the primary energy source for neurons and astrocytes, the first can utilize glial-produced lactate as an additional energy substrate under abnormal conditions (Pellerin *et al.* 1994). Increased lactate reflects metabolic and energy impairment, resulting in tissue acidosis which in turn induce glial and neuronal cell swelling (Koroshetz et al. 1997). It has been described that pyruvate concentrations are significantly lower in HD patients group, which may also increase the L/P ratio (Koroshetz et al. 1997).

In HD patients and in several transgenic mouse models, weight lost and muscle wasting is a hallmark of the disease, accompanying its evolution (Djousse *et al.* 2002, Gaba *et al.* 2005, Aziz *et al.* 2008, van der Burg *et al.* 2008). The considerable weight loss, particularly on its final stages, seems directly associated with the number of CAG repeats (Aziz et al. 2008). Patients with higher body mass index were linked with slower progression of HD (Myers *et al.* 1991). HD patients are either underweight (Djousse et al. 2002) or tend to lose weight during the course of their illness, eventually becoming cachectic in end-stage, despite adequate caloric intake (Aziz et al. 2008). Underlying mechanisms of weight loss remain to be clarified but some studies tried to elucidate this matter. Aziz and colleagues found an increased basal resting energy expenditure in early stage HD patients which was primarily due to an increased fat oxidation rate (Aziz *et al.* 2010). One study reported that total energy expenditure was 11% higher in HD patients (Gaba et al. 2005). The majority of presymptomatic HD patients present an altered metabolic profile which may therefore represent an early step in HD pathogenesis and general metabolic derangement (Gaba et al. 2005). Moreover, some studies referred increased motor activity to be involved in weight loss (Pratley *et al.* 2000), whilst others referred a hypermetabolic state, leading to a negative energy balance (Aziz et al. 2008, Goodman *et al.* 2008).

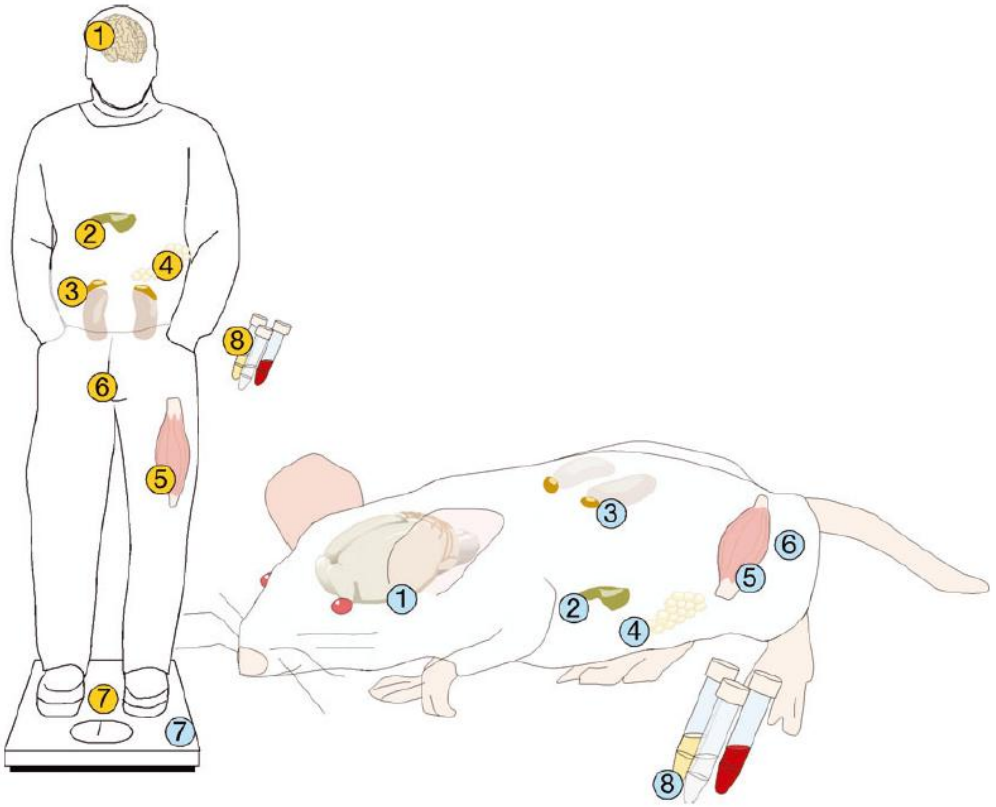

Figure 1.8.- Hypothalamic and endocrine changes found in patients and in mouse models with HD. 1- atrophy, alterations in neuropeptide levels, and neuropathology in the hypothalamus of patients; 2 - Increased prevalence of diabetes; 3- increased levels of cortisol; 4- Reduced levels of leptin in HD patients and and adipocyte dysfunction occurs in R6/2 mice; 5- Alterations in gene expression and muscle pathology; 6-testis atrophy in HD mice and levels of testosterone are reduced; 7- Weight loss; 8- Neuroendocrine factors can be meaured in CSF, serum and/or urine such as ghrelin; leptin, orexin, testosterone, cortisol and insulin. Adapted from (Petersen *et al.* 2006).

Others proclaim that weight loss may be due to hypothalamic dysfunction (Petersen et al. 2006, Gabery et al. 2010). Hypothalamus establishes the connection between peripheral endocrine system activity and central nervous system activity, as this organ facilitates hunger, thirst, reproductive function, and circadian rhythms. Loss of orexin-positive neurons in the lateral hypothalamic area, important for regulation of sleep and wakefulness and feeding behavior, was observed in R6/2 mice (Petersen et al. 2005). N171–82Q HD mice also present significant transcriptomic alterations in the hypothalamus (Martin *et al.* 2012). Alterations in the hypothalamic–pituitary–adrenal axis of HD patients and mice

models point to increase evidences of important pathology of the hypothalamus and the endocrine system in HD (figure 1.8.)

1.1.6.1.Diabetes mellitus in HD

When glucose metabolism is impaired and glucose uptake by cells is reduced, blood glucose levels rise. If this occur chronically a metabolic disease, Diabetes Mellitus, can arise (WHO, 2006). The most common Diabetes mellitus (DM) forms are type I and type II. Type I diabetes is characterized by loss of insulin-producing β-cells in pancreatic islets of Langerhans leading to insulin deficiency. In type II diabetes insulin resistance is the main characteristic and, initially, there is no reduction in insulin secretion, but a deficient response to insulin (James *et al.* 1994).

Neurodegenerative disorders are known to be associated with increased risk for DM. In HD the reports so far in human and mice have been controversy on the prevalence of DM. The leading causes for DM in several mouse models of HD are well known, nonetheless the mechanism for DM in HD patients not yet been elucidated. The first paper describing a higher prevalence of diabetes in HD was (Podolsky *et al.* 1977) in which 50% of the patients studied had impaired carbohydrate metabolism, probably due to decreased insulin secretion. In 1985, Ferrer studied 620 probands with HD and found that 65 of them (10.5%) had diabetes, suggesting that HD patients had 7 times more probability of have diabetes. A more recent study, focused on changes in insulin sensitivity and insulin resistance, major determinants of glucose homeostasis, in a group of consecutive normoglycemic patients with HD, showed impairment in insulin secretion capacity, accompanied by simultaneous decrease in insulin sensitivity and an increase in the insulin resistance (Lalic *et al.* 2008). Post mortem studies in 9 HD patients and controls revealed that islet cell area was unchanged in HD and mRNA insulin quantification by in situ hybridization were similar to levels in control individuals. Also, no cytoplasmic or nuclear inclusions in islet cells were found contrary to R6/2 mice models described previously (Bacos *et al.* 2008). Pancreatic β-cells inclusions are the most probable explanation for pancreatic dysfunction and subsequent DM 2 (Andreassen *et al.* 2002). The development of those inclusions may require a longer CAG repeat, not seen in late onset HD patients, and the slow disease progression may also spare the cells. Aziz *et colleagues* assessed lipid and glucose metabolism during both basal and insulin stimulated conditions in early

stage, medication free HD patients (44,4 CAGs) in comparison with matched controls and found no evidence for insulin resistance but verified an inverse association between mutant CAG repeat size and insulin sensitivity (Aziz et al. 2010). They suggest that peripheral polyQ length interference with insulin signalling therefore become clinically relevant in higher CAG carriers (Aziz et al. 2010).

However, an increase risk among early and middle-stage HD patients was not found in another study perhaps because the patients studied had different anthropometric features (Boesgaard *et al.* 2009). Moreover, multiple HD mice models display metabolic dysregulation, developing glucose intolerance and glycosuria- R6/2 (Bjorkqvist *et al.* 2005); R6/1 transgenic mouse (Josefsen *et al.* 2008) and HD-N171-82Q mice (Schilling *et al.* 1999). Recently, Hunt *et al.* (2005) found that from 9 weeks of age R6/2 glycosuria and glucose intolerance were detectable. It worsens with age, affecting more than 70 % R6/2 mice at 14 weeks and its severity was associated with progressive formation of ubiquitinated inclusions in pancreatic β-cells. Pancreatic aggregates were identified at the same time as neuronal, around 3 weeks age, and its accumulation was associated with selective disruption in expression of transcription factors essential for glucose-responsive insulin gene expression leading to impairment of insulin release rather than insulin resistance (Hunt *et al.* 2005). Bjőrkqvist *et al.* (2005) identified two separate pathological processes that may be responsible for diabetes in R6/2 mice: impaired β-cell replication (resulting in deficient β-cell mass (~35%) most likely due to impaired regeneration of islet cells) and a reduction of insulin-containing secretory granules (abrogating stimulated hormone secretion). R6/1 mice, carrier of a shorter CAG repeat, although not diabetic, shows impaired glucose tolerance (Josefsen et al. 2008).

1.2.Normal function of huntingtin

1.2.1. Development

HTT is a protein with approximately 350 kDa, composed of more than 3100 aminoacids (aa). It is primarily a cytosolic protein, ubiquitously expressed in mammalian tissues, including brain (Trottier *et al.* 1995). Highest levels were found in the brain, particularly in cortical layers II and V and in the Cerebellar Purkinje cells (Trottier et al. 1995). Cellular functions of HTT remains unclear, however it has been associated with the nucleus, endoplasmic reticulum, Golgi complex, synaptic vesicles and mitochondria (Li *et al.* 2004). Some studies suggested that it has an important role during embryogenesis, being essential for gastrulation. Knockout of the gene in mouse during embryonic stage was lethal approximately at day 7.5, whilst the conditional knockout in mouse forebrain at postnatal or later embryonic stages causes a progressive neurodegenerative phenotype, suggesting a constitutive role important for neuron survival (for review, Bhide *et al.* 1996). HTT was also detected through human brain from 19th to 21st week of fetal gestation, suggesting that it may play an important constitutive role in neurons during brain development. This also suggests that the development controls heterogeneity in neuronal expression of HTT and that intraneuronal distribution of the protein may be directly correlated with neuronal maturation (for review, Bhide et al. 1996). Transiently knockdown of endogenous HTT by morpholino oligonucleotides in zebrafish revealed that it may be essential to development and it may be involved in normal blood function and iron utilization (Lumsden *et al.* 2007). Furthermore, HTT appears to be important during adult life. In this regard, deletion of HTT gene in Drosophila showed that it may have an essential role in long-term mobility and survival of adult animals, accelerating the neurodegenerative phenotype (Zhang *et al.* 2009). Additionally, the conditional deletion of HTT in forebrain and testis of adult mice led to degeneration of these tissues (Li et al. 2004).

1.2.2. Structure

The human HTT protein has a polyglutamine stretch at the N-terminus, adjacent to a proline-rich region which is an important mediator of protein-protein interactions (Figure 1.9). This region is followed by four clusters of HEAT repeats (Huntingtin, elongation factor 3 (EF3)) known for been a protein-protein interaction site (Warby et al. 2008). In the N-terminal domain relies a retention signal responsible for cytoplasmic targeting and at C-terminal a nuclear export signal was identified being both subject to posttranslational modifications (PTM) and thus the protein localization (Rockabrand *et al.* 2007).

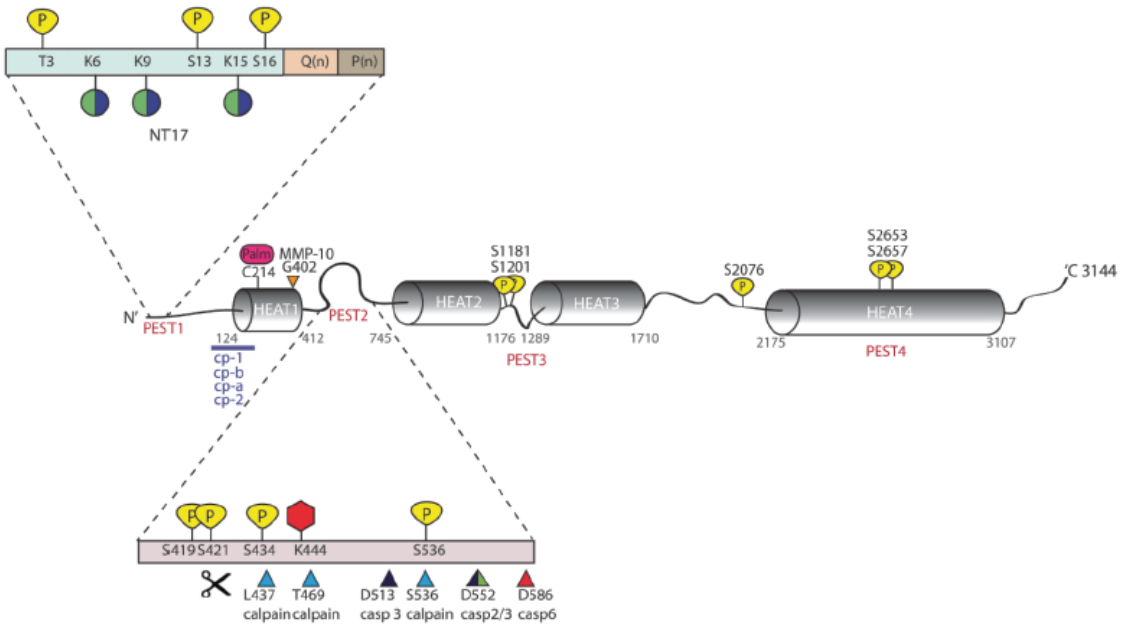

Figure 1.9. – Huntingtin and its post translacional modifications. Predicted HEAT repeats and PEST domains. Phosphorylation sites (yellow) occur at *threonine* (T) or *serine* (S) residues. *Lysines* (K) (green and purple) are modified by the addition of ubiquitin or sumo-1 and *lysine* (K) 444 by acetylation (red) and *cysteine* (C) 214 by palmitoylation (pink). HTT can be cleaved by several proteases: calpain (blue triangle) caspase −2 (green triangle), −3 (black triangle) and −6 (red triangle) and *matrix metalloprotease-10* (ΔΨM-10) site at 404 (orange triangle). Additional proteolytic cleavage sites lie at the N-terminus of HTT and cleavage between amino acid 104-114, 205-214, 81-129 and at R167 generate cp-A, cp-B , cp-1 and cp-2 fragments. Adapted from (Ehrnhoefer *et al.* 2011).

1.2.3. Interactors

HTT interacts with a wide range of cellular proteins through multiple interaction domains. Structural analysis of HTT identified up to 36 HEAT (huntingtin, elongation factor 3, the A subunit of protein phosphatase 2A and TOR1) repeats, with approximately 40-amino acid long, composed of two hydrophobic antiparallel helices that acts as a scaffold protein.

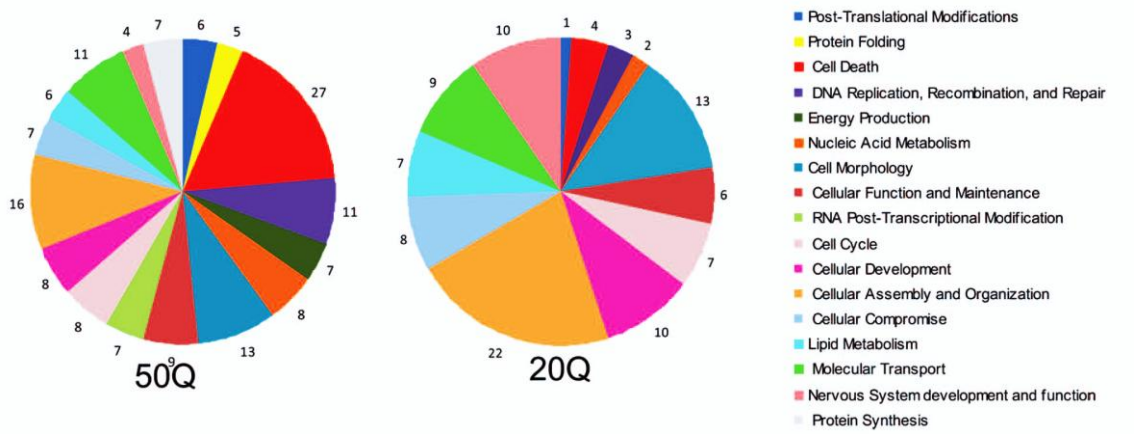

Figure 1.10.- Quantitative analysis of normal and expanded HTT interactome. The graph shows the functional preferential interactors for HTT-20Q and HTT-50Q. Adapted from (Ratovitski et al. 2012)

1.2.4. Functions

Proposed cellular functions of HTT include endocytosis, modulation of synapse structure and synaptic transmission; transcriptional regulation (especially of brain-derived neurotrophic factor (BDNF), essential for survival of striatal neurons in HD; axonal transport of BDNF and vesicles, and anti-apoptotic activity (Ho *et al.* 2001, Leavitt *et al.* 2001, Leavitt *et al.* 2006, Caviston *et al.* 2009).

HD pathogenesis has been suggested to be also related with a loss of function in wild-type HTT. This may be due to a 50% decrease in the expression of HTT and to its cleavage and sequestration into aggregates, thus impairing its neuroprotective function and culminating in neuronal dysfunction and death (Ho et al. 2001). The polyglutamine repeat (polyQ) expansion promotes association with several proteins, leading to their intracellular accumulation into 5-7 μm aggregates

1.2.5.Mitosis

1.2.5.1.Cell cycle

Self-renewal and differentiation of cells is profoundly associated with cell-cycle progression. The main goal of cell cycle is to replicate and transmit genetic material to daughter cells. During S phase and M phase chromosome replication and chromosome transmission occurs, correspondingly, whereas G1 and G2 represent gap phases. In G1 and G2 cells increase in size and represent checkpoints where control mechanisms ensure that all the machinery is properly working for DNA synthesis and to enter M phase and divide. The hESCs maintains the four cell cycle canonical stages, G1, S, G2, and M, with a specific cell-cycle profile characterized, though. The fast proliferation rate is due to a very short overall cell cycle (15-16 h) and a lack of a functional restriction or check point at the G1/S transition (Becker *et al.* 2006, Wang *et al.* 2009). hESCs are characterized by a shortened G1 phase (~ 2.5 h) and accelerated organization of subnuclear domains that mediate the assembly of regulatory machinery for histone-regulated gene expression (Becker et al. 2006). A recent study demonstrated that the duration of G1 in iPSCs is also considerably shorter, compared to somatic cells, only 2.5-3 h, but has a similar duration of S (~8 h), G2 (~4 h), and M phases (~ 1 h) (Ghule *et al.* 2011). Cell cycle progression is controlled by cyclin-dependent kinases (CDKs) that are activated by cyclin binding and inhibited by CDK inhibitors. CDKs regulate check-points and coordinate cell cycle transitions. The G1 →S phase transition is regulated by the activities of cyclin D1/CDK4, cyclin E/CDK2 and cyclin A/CDK2 complexes, whereas G2→M transition is mainly regulated by cyclin B/CDK1. CDK2 had the highest expression in the S phase, cyclin A and c-Myc in S and G2 phase, cyclin B1 in the G2 phase, cyclin E in the G1 and S phase, whilst Cdc25A in the G1 phase of the cell cycle of hESCs (Neganova *et al.* 2008). When hESC are cultured in suspension cyclin E expression is upregulated in Embryoid Bodies and CDK2 was considerably downregulated by day 10 of EB development. Some transcriptional factors could also regulate the cell cycle such as NANOG and Oct4 (Neganova et al. 2008, Zhang et al. 2009). NANOG helps to maintain pluripotency and proliferation by enhancing transition from the G1→S phase in hESCs through the direct binding of the C terminal domain of NANOG to the regulatory regions of Cdk6 and Cdc25A. Another common feature of hESCs and iPSCs is the high expression levels of telomerase activity (Thomson *et al.* 1998). iPSCs also showed reduced levels of histone methylation at telomeres, compared to somatic cells, which facilitates the exchange of

DNA between telomeres showing a bias towards modulation of the pathways involved in senescence (Davy *et al.* 2009).

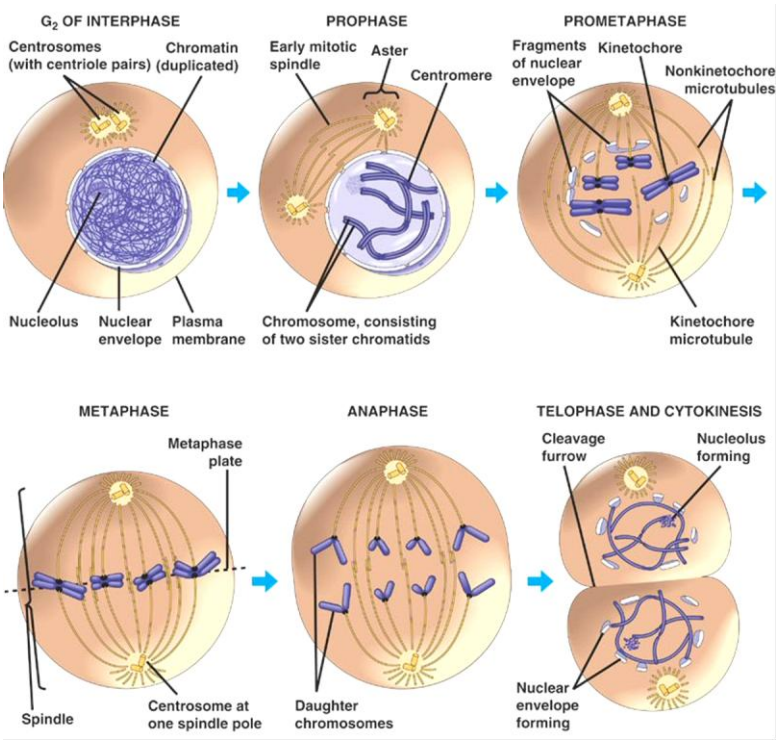

Figure 1.11.- **Mitosis and cytokinesis.** Prophase- chromosomes recruit condensin and begin to undergo a condensation process. Prometaphase- fragmentation of the nuclear envelope for spindle assembly. Metaphase – chromosomes assume their most compacted state. Anaphase - separation of sister chromatids. Telophase and cytokinesis - Mitosis ends and the nuclear membrane then reorganizations and the chromosomes begin to decondense into their interphase conformations. Telophase is followed by cytokinesis where the division of the cytoplasm into two daughter cells happens. Adapted from (http://ehumanbiofield.wikispaces.com).

1.2.5.2.The mitotic spindle

Cell division is a serial of events aiming to transmit genetic content to daughter cells. During mitosis the duplicated chromosomes are divided equally through morphological changes occurring in five stages: prophase, prometaphase, metaphase, anaphase and telophase (Figure 1.11). In prophase chromosomes condense, the spindle starts to assemble and centrosomes move to opposite poles. At the end, nuclear envelope breaks down and prometaphase begins. Instantly, proteins attach to the centromeres creating the

kinetochores and chromosomes attach to the mitotic spindle through sister kinetochores beginning to move. During metaphase spindle fibres align the chromosomes along the middle of the cell nucleus known as metaphase plate allowing for a symmetric split.

At anaphase sister chromatids separate and move towards the opposite sides. This is achieved by the shortening of kinetochore microtubules. Motion results from a combination of kinetochore movement involving grow and shrink of microtubules along the spindle and through the physical interaction of polar microtubules. During telophase chromatids arrive at opposite poles and a new nuclear envelop reassembles around them. The spindle fibers disperse and cytokinesis begins. A cleavage furrow, contractile ring of actin and myosin, forms at the equatorial cortex separating the two daughter cells.

During metaphase a complex macromolecular structure designated the mitotic spindle, where the principal components are centrosomes and microtubules, is formed. Spindle poles consist of polarized array of microtubules, the minus end embedded at the spindle and the plus end pointing the cell cortex. This microtubules antiparallel array comprise kinetochore microtubules that attach to chromosomes, interpolar microtubules and astral microtubules connecting spindle to cell cortex. The spindle alignment is tuned by microtubules dynamical growth and shrinking through the addition and removal of tubulin dimers, referred as 'dynamic instability'. The position and orientation is coordinated by pulling forces acting on astral microtubules, driven by dynein-mediated pulling forces generated at the cell cortex (Kotak *et al.* 2012, Laan *et al.* 2012). The spindle assembly and positioning is dependent on a protein complex comprising cytoplasmic dynein, dynactin, the nuclear mitotic apparatus (NUMA) protein, and the G protein regulator leucine-glycine-asparagine repeat (LGN) protein. During cell division, LGN is recruited to the cell cortex by glycosyl phosphatidylinositol-linked (Gαi/Gαo), which binds LGN carboxy-terminal GoLoco motifs (Zheng *et al.* 2010), which in turn recruits NUMA forming a conserved tripartite complex, NuMA/LGN/Gαi (Zhu *et al.* 2011). NUMA most probably recruits the dynein–dynactin complex to the cortex and this complex exerts pulling forces on astral microtubules that contact this cortical region (Peyre et al. 2011, Collins et al. 2012, Kotak et al. 2012, Laan et al. 2012, Elias et al. 2014). As referred, both dynein, a motor proteins involved in spindle orientation, and microtubule depolymerization are responsible for generate the pulling forces for poleward motion of chromosomes. *In vitro* evidences also showed that dynein can induce a catastrophe simply by holding the microtubule with its growing end against the barrier (Laan et al. 2012). The minus end–directed motor dynein often accumulates at the plus ends of microtubules, and

dynactin (dynein activator) has been shown to modulate this localization (for review, Kardon *et al.* 2009). The mitotic spindle undergoes gentle rocking movements during metaphase allowing proper localization but never diverge far from the apical/basal polarity axis (for review, Siller *et al.* 2009). Another partner required for appropriate spindle orientation is HTT (Godin *et al.* 2010, Elias et al. 2014, Molina-Calavita *et al.* 2014). Has been widely described the interaction of HTT with proteins involved in vesicle trafficking and intracellular transport (Caviston *et al.* 2007, Caviston et al. 2009). Moreover, HTT-associated protein 1 (HAP1) is a huntingtin binding partner that interacts with $p150^{Glued}$ subunit of dynactin (Engelender *et al.* 1997, Li *et al.* 1998). Furthermore was reported that huntingtin binds directly to dynein to enhance dynein-mediated vesicle motility along microtubules (Gauthier *et al.* 2004, Caviston et al. 2007, Zala *et al.* 2008). Elias et al (2014) proposed that HTT is a key regulator of kinesin 1-dependent trafficking of dynein, dynactin, NUMA, and LGN along astral microtubules to the cell cortex and in the cortex dynein/dynactin/NUMA/LGN complex are responsible for generating pulling forces on astral microtubules for mitotic spindle positioning (Figure 1.12) (Elias et al. 2014).

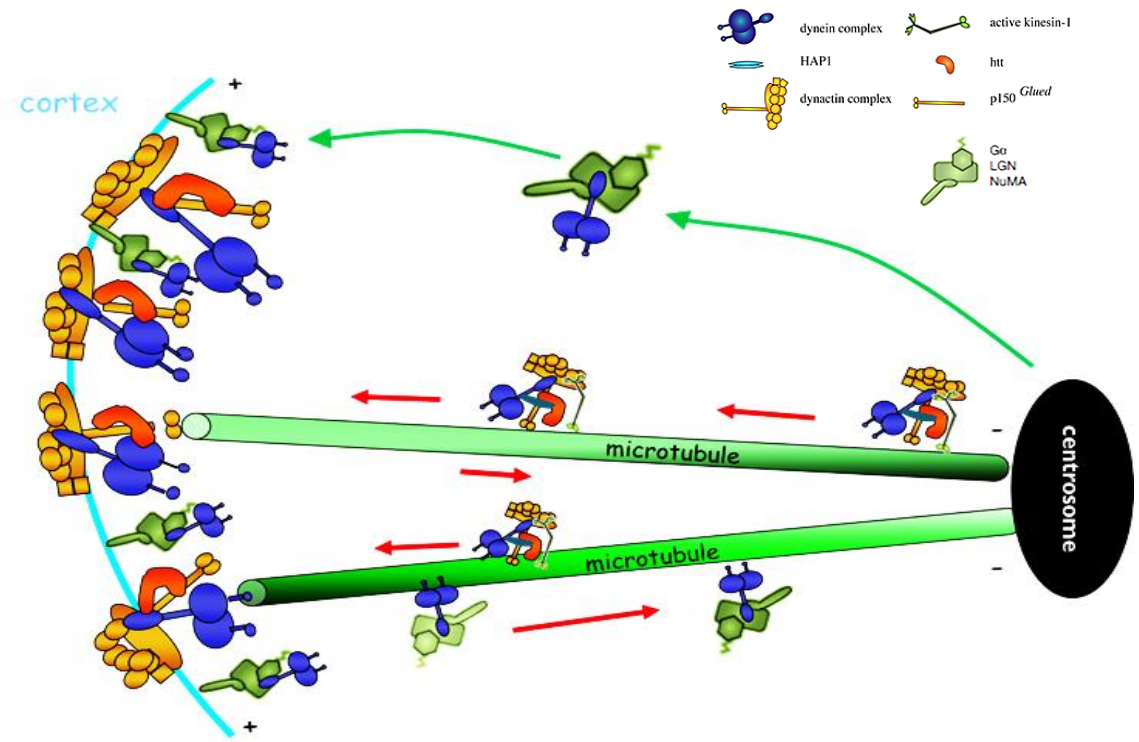

Figure 1.12. - Proteins involved in spindle assembly. HAP1- huntingtin associated-protein 1, HTT- huntingtin, LGN - Leu-Gly-Asn repeat-enriched protein, NuMa – nuclear mitotic apparatus

1.2.5.3.In development and cell fate specification

Spindle orientation seems to be a decisive factor for regulating cell fate particularly in the cortex and retina. In many tissues when progenitors divide symmetrically two identical cell fates are generated (neuroepithelial progenitor/ neuroepithelial progenitor or neuron/neuron, depending neurogenesis timeline occurrence) and if apical/basal spindle orientation predominate two different cell types are formed (Figure 1.13.). Initial studies on ferret neocortex indicated that the apical-basal division were asymmetric and neurogenic, whereas planar divisions were symmetric and proliferative (Chenn et al. 1995). Latter was observed that most neural progenitors divide with a near planar orientation even at stages where asymmetric divisions predominate and slight shifts in spindle orientation may regulate symmetric versus asymmetric division. The cleavage plans can bisect or bypass the apical domain determining the location of cell constituents responsible for cell fate (Kosodo *et al.* 2004, Noctor *et al.* 2008). This concept was reinforced by observation of asymmetric inheritance of regulatory proteins leading to differential gene regulation in daughter. Numb, a cell fate-determinant, display an asymmetrical and apical membrane pattern on dividing ventricular neural progenitors (Noctor et al. 2008, Couturier *et al.* 2012). Asymmetric cell divisions was proposed to comprise 3 steps: (1) a cell polarity axis is specified; (2) cell polarization is translated into the asymmetric localization of cell fate determinants; and (3) the mitotic spindle aligns with the cell polarity axis, leading to the segregation of fate determinants in only one daughter cell (Morin *et al.* 2011). Moreover, HTT was also found to be required in murine neuronal progenitors for appropriate spindle orientation and for cell fate determination (Godin et al. 2010). A recent study associated mHTT expression and increased asymmetric division and depletion of progenitors pool. Additionally the ventricular zone of mutant protein carriers embryos was considerable smaller as the thickness of layer VI was reduced (Molina-Calavita et al. 2014). In the same line, magnetic resonance imaging brain scan of prodromal Huntington's disease patients revealed smaller intracranial adult brain volume suggesting that mHTT can cause abnormal development, which may contribute to the pathogenesis of Huntington's disease (Nopoulos et al. 2011).

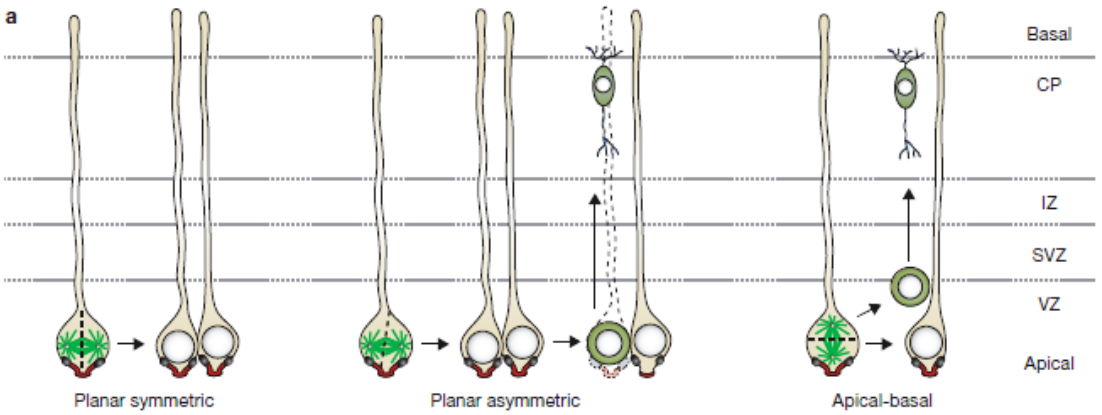

Figure 1.13 - Spindle orientation and positioning in the mammalian neuroepithelium. The mammalian cortex is a pseudostratified epithelium with morphologically distinct layers, including cortical plate (CP), intermediate zone (IZ), subventricular zone (SVZ) and ventricular zone (VZ). Neural epithelial cells or radial glia progenitors in the VZ (tan cells) can undergo planar and molecularly symmetric divisions (left); planar but molecularly asymmetric divisions (centre) or apical/basal molecularly asymmetric divisions (right). Molecularly, asymmetric divisions, generate a basal progenitor/neuron (green) and a neuroepithelial progenitor (tan). Adapted from (Siller et al. 2009)

1.3.Huntingtin and HD

1.3.1. Loss of wild-type huntingtin

Although HTT protein is crucial for embryonic development its constitutive role during lifespan is still controversial. Rigamonti et al (2000) proved that wild-type huntingtin acts by protecting CNS cells from a variety of apoptotic stimuli, including serum withdrawal, death receptors, and pro-apoptotic Bcl-2 homologs through the action of caspase-9. The full-length protein also modulates the toxicity of the poly-Q expansion and cells expressing full-length mutant protein are susceptible to fewer death stimuli than cells expressing truncated mutant huntingtin (Rigamonti et al. 2000). Another study, using a YAC transgenic mouse model, showed that wild type HTT can protect against the gain of function caused by the expanded polyglutamine tract in mutant huntingtin (Leavitt et al. 2001). Wild type HTT seems to protect by reducing the cleavage of mutant full length HTT, as opposed to attenuating the apoptosis caused by the toxic fragment. In YAC transgenic mice was seen that the proapoptotic effect of mutant htt can be completely inhibited by increased levels of murine wild-type HTT (Leavitt et al. 2001).

Wild type HTT was also found to reduce the cellular toxicity of mutant HTT exon 1 fragments in both neuronal and non-neuronal cell lines (Ho et al. 2001). Strehlow et al (2006) found that cells lacking HTT exhibit a significant reduction in transcripts encoding proteins destined for the extracellular space, many of which are components of the extracellular matrix or involved in cellular adhesion, receptor binding and hormone activity (Strehlow et al. 2007). Moreover, in Hdh null cells lysosomal activity and apoptosis are increased suggestive of elevated cellular stress (Strehlow et al. 2007). In a full-length knock-in mouse model of HD cortical HTT was required for the correct establishment of cortical and striatal excitatory circuits, and this function of HTT is lost when the mutant HTT is present (McKinstry et al. 2014). An accumulative number of studies implicate HTT in early neural developmental processes. In ESC, loss of HTT, disrupted the specification for multiple stages of neural induction, whereas mHTT expressing clones displayed impaired proliferative potential, enhanced cell death and altered multi-lineage potential promoting precocious neurogenesis and oligodendrocyte progenitor cell elaboration (Nguyen et al. 2013). Recently, NSC lines generated from a series of heterozygous Hdh CAG knock-in ES with different CAGs expansion were successfully maintained and the lines showed no differences in terms of proliferation rate

and cell cycle distribution. Nevertheless wild-type HTT seems necessary to direct NSC towards a neuronal fate and its absence causes cells to undergo glial differentiation (Conforti et al. 2013). Taken together, all these evidences suggest a role for loss of wild type HTT function in the pathogenesis of the disease.

1.3.2. Misfolding and aggregation of mutant huntingtin

Formation of such aggregates could indicate either an inability to degrade the mHTT or an overall inhibition of cellular trafficking and degradation machinery (Gatchel *et al.* 2005).
Two mechanisms have been hypothesized for aggregate formation of aggregates:
- the **Polar zippers** model refers that aggregation results from multimerization by hydrogen-bonded polar zipper. This was confirmed by the reduction of monomeric fragments upon incubation in concentrated formic acid (Perutz *et al.* 1994). The 40 residues threshold of polyQ has been explained by the fact that the protein sequence forms a helical fiber with 20 residues turn, and that two turns (40 residues) are required for stabilization of the helix and promotion of multimerization (for review, Hoffner *et al.* 2007);
- **Transglutaminase-catalyzed cross-linking**. Transglutaminases are enzymes involved in cross-linking of glutamine residues and, thus, may also participate in the formation of aggregates. Several in vitro studies showed that depending on protein length HTT is a substrate of transglutaminase (Kahlem *et al.* 1998). Transglutaminase activity appears to be elevated in HD brain cortex and cerebellum, regions where HTT aggregates into nuclear inclusions (Karpuj *et al.* 1999). A possible function of brain transglutaminase is stabilization of neuronal aggregates. This is corroborated by its wide distribution and activation in brain and by the occurrence of ε- (γ-glutamyl) lysine cross-linking in normal brain (Karpuj et al. 1999, Hoffner et al. 2007, Gil et al. 2008), Inclusions were found in affected areas of brain (such as cortex and caudate/putamen) but not in unaffected areas (such as cerebellum) (Hoffner *et al.* 2005). Interestingly inclusions observed in affected areas are limited to neurons and are not detected in glial cells. In juvenile form of disease, with large polyQ expansion, inclusion tend to be located in nucleus whilst in patients with the adult onset HD patients (with shorten polyQ expansion) inclusions are mostly cytoplasmatic (DiFiglia *et al.* 1997).

A study using an antibody directed against the 17 most N-terminal amino acids of HTT, showed that the frequency of nuclear inclusions (but not that of cytoplasmic inclusions) is correlated with the severity of disease, suggesting that nuclear aggregation (but not cytoplasmic aggregation) might participate in neuronal death (Hoffner et al. 2005). Another study identified others aggregates located in neuropils, which are likely to correspond to dendrites, and that may contribute to neuronal death, by disturbing dendritic transport (Gutekunst *et al.* 1999).

Several studies demonstrated that HTT fragments are more toxic to cells than full-length mHTT and that such toxicity is proportional to the size of polyQ tract, being also related to the progressive truncation of HTT (Thakur *et al.* 2009). A consequence of HTT cleavage is the release of N-terminal fragments (HTTNT) containing the polyQ tract, which interacts with at least 25 proteins that can be recruited into aggregates of mHTT.

In affected areas of the brain (such as cortex) normal HTT exists as a soluble monomer, but the mHTT is found in fragmented, oligomerized and polymerized forms, which can be either soluble or insoluble in water. The water-soluble forms of cortical mHTT consist of oligomerized and fragmented HTT. Soluble oligomers appear to accumulate in cortex, where they are much more abundant than the normal protein. The water-insoluble mHTT, which is mostly associated with inclusions, consists of oligomeric, polymeric and fragmented protein, establishing bonds with each other via non-covalent bonds since they are released by formic acid. These structures are stabilized by covalent bonds since presents resistant to formic acid (Hoffner et al. 2007). Some evidences have shown that these inclusions could act as neuroprotective through sequestration of toxic N-terminal fragments and oligomers of mHTT and other misfolded proteins, which would be deleterious in the soluble form (for review, Gil et al. 2008).

Accumulation of unfolded or misfolded proteins in endoplasmic reticulum (ER) could induce stress and trigger neuronal death. The apoptosis signal-regulating kinase 1 (Ask1), a MAPK kinase kinase that activates JNK pathway (c-Jun N-terminal kinases), may play a role in this process, since Ask1 is activated by ER stress and that phosphorylated Ask1 interacts with HTT fragments, allowing them to translocate into nucleus more efficiently. This interaction has a positive feedback loop, since it amplifies ER stress and may contribute to potentiate HTT toxicity (Cho *et al.* 2009).

Activity of wild-type and mHTT can be modulated by post –translational modifications. MHTT can change post-tradutional modifications of proteins once they are formed. Several studies indicated that HTT phosphorylation at various sites is neuroprotective, by

preventing cleavage of mHTT and its consequent aggregation. Activation of insulin growth factor 1 (IGF-1)/protein kinase B (Akt) pathway is protective for neurons expressing mHTT, probably due to phosphorylation of HTT on Ser421 (serine 421) (Colin *et al.* 2008).

1.3.3. Intracellular mechanisms of toxicity

The gain of function of mHTT and the loss of function of wild-type HTT are potential contributors to neuronal dysfunction in HD (for review, Landles *et al.* 2004). Several processes may be involved this deregulation, as described in Figure 1.14:

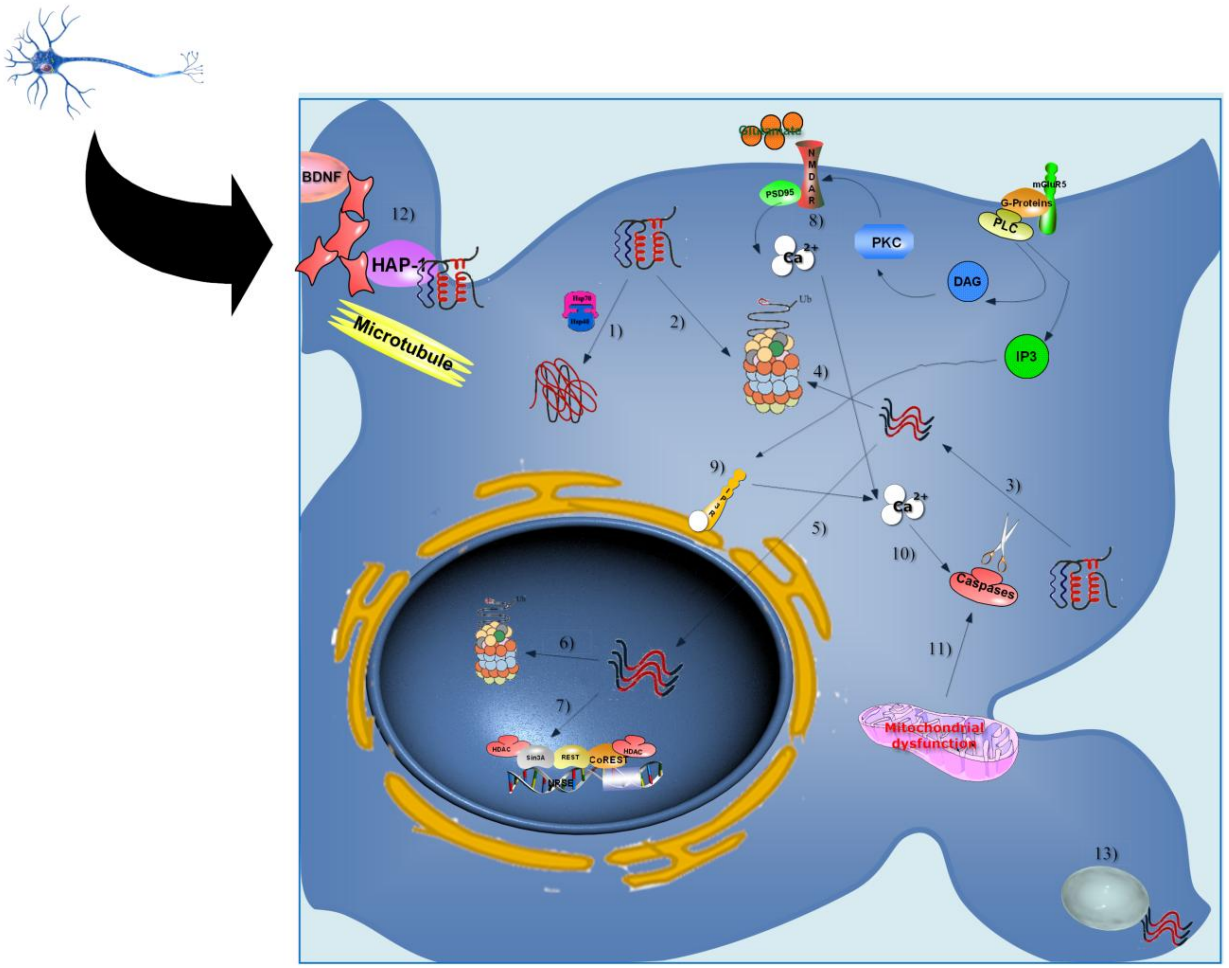

Figure 1.14.- Model for cellular pathogenesis in Huntington's disease. 1) Wild-type HTT is cleaved and stays in the cytoplasm. 3) The mutation causes a conformational change and abnormal folding of the protein, which can be corrected by molecular chaperones. 4) Mutant HTT can undergo proteolytic cleavage, both in the cytoplasm (6) and in the nucleus. 5) HTT complexes also stimulate IP3 (Inositol 1,4,5-Trisphosphate) activation of the calcium release channel IP3R (IP3 Receptor), a key player in intracellular Ca^{2+} signaling. 7) HTT can also associate with transduction proteins and repress transcription. 8) HTT interacts with the NMDAR to increase intracellular Ca2+. 9) Mutant HTT increases the amount of IP3 produced by MGluR5 (Metabotropic Glutamate Receptor-5) stimulation via G-Proteins and PLC (Phospolipase-C). PLC lead to the formation of IP3 and DAG (Diacylglycerol). DAG forms PKC (Protein Kinase-C) which activates NMDAR, whereas IP3 helps in calcium release by binding to IP3R. The combination of these effects increases the intracellular calcium concentration. 10) This leads to overactivation of Caspase3 11) Apoptotic stress induces mitochondrial depolarization and increases the release of Ca^{2+} enhancing the caspases activation and cleavage of HTT. 12) The number of CAG repeats in determines the degree of HTT interaction with HIP1 and HAP1. As repeat numbers increase, HTT binds less to HIP1 and more to HAP1. 12) Huntingtin also enhances vesicular transport of BDNF (Brain-Derived Neurotrophic Factor) along microtubules. Huntingtin-mediated transport involves HAP1 and the $p150^{Glued}$ subunit of Dynactin. The alteration of the HTT/HAP1/p150(Glued) complex due to the presence of mHTT, which cannot bind, correlates with reduced association of motor proteins with microtubules.

1.3.3.1.Protein misfolded and inhibition of protein degradation

Formation of aggregates in nucleus, cytoplasm and neurons all processes is one of the main features of HD, involving sequestration of several proteins by N-terminal fragments of mHTT (for review, Landles et al. 2004) Several components involved in handling and degradation of misfolded proteins (*e.g.* chaperones, ubiquitin, proteasome subunits and autophagy proteins) were found on such aggregates (Mitra *et al.* 2009). Heat shock proteins (HSPs) may play an essential role in folding and assembly of newly synthesized proteins and in re-folding the misfolded ones and aggregation. HSP70, a molecular chaperone, is thought to bind in early stage of HD in order to maintain the protein in a soluble conformation. HSP 70 interacts with a co-chaperone protein that regulates its ATPase activity, the HSP 40 family. These chaperones also bind to misfolded proteins and are able to refold alone (Jana *et al.* 2000). Chaperones can also re-direct these proteins to the ubiquitin-proteasone pathway and increase the expression of HSPs, which has proven to be neuroprotective. These two chaperones were found in cytoplasmic and nuclear aggregates, probably as an attempt to refold the m protein (Jana et al. 2000). Chaperones

were also reported to inhibit caspase-3 and 9 activities and to improve cell viability independently of aggregate formation (Zhou *et al.* 2001).

mHTT was shown to interact with numerous transcriptional factors, such as NF-Y, which has been reported to regulate HSP70 transcription, resulting in an overall reduction of HSP 70 gene expression (Yamanaka *et al.* 2008).The ubiquitin-proteosome system (UPS) is another neuroprotective mechanism that prevents accumulation of misfolded proteins, by degrading them. *In vivo* studies have shown that UPS activity is impaired and some components of proteosome are sequestered into aggregates (Wang *et al.* 2008) . MHTT can be ubiquitinated, itself, which may represent an attempt to eliminate the aggregates (Finkbeiner *et al.* 2008). However, several hypotheses have been proposed to explain such impairment: 1) mHTT could be retained in proteolytic core and impair proteasome activity; 2) mHTT aggregation may impair proteasome or 3) for the proteasome regulatory complex to unfold mHTT and present it to the core catalytic subunits for proteolysis (Finkbeiner et al. 2008). In this regard, it has been suggested that HD could be a proteasomal storage disease (Goellner *et al.* 2003).

A recent study used mass-spectrometry-based methods to quantify polyubiquitin chains from transgenic mouse and knock-in models demonstrating that the abundance of lysine 48-linked polyubiquitin chains could be a faithful endogenous biomarker of UPS function (Bennett *et al.* 2007). These chains where shown to accumulate early in brains of mice and humans with HD showing that UPS dysfunction is a consistent feature of HD pathology (Bennett et al. 2007).

While UPS mainly degrades short nuclear and cytosolic proteins, bulk degradation of cytoplasmic proteins or organelles is largely mediated by macroautophagy (also known as autophagy) (for review, Chu 2006). Increased autophagy was previously found in HD, probably as a response to reduce the toxicity induced by the aggregates (Sapp *et al.* 1997)

1.3.3.2.Caspase activation

Proteases (including caspases, calpains and aspartyl endopeptidades) are involved in cleavage of HTT within the N-terminal domain (Graham et al. 2006). Several studies demonstrated that HTT is a caspase substrate with defined sites for caspase-3 at amino acids 513 and 552, for caspase-2 at amino acid 552, and for caspase-6 at amino acid 586 (Wellington et al. 1998, Wellington et al. 2000). Two caspase-3 consensus sites at amino

acids 530 and 589 that appear to be silent have been also decribed (Graham et al. 2006). HTT is cleaved by caspase 3 and 6 in vitro, and caspase-3-cleaved HTT fragments have been identified in HD brain, prior to the clinical onset. This suggests that N-terminal HTT fragments may play a role in HD pathogenesis (Graham et al. 2006). Both wild-type and mHTT can be cleaved by proteases, but fragments generated from wild-type HTT appear to be more efficiently cleared through the ubiquitin–proteasome pathway (Wellington *et al.* 2002). Such fragments were mainly detected in cytoplasm, which may indicate that this precedes nuclear uptake of N-terminal HTT fragments (Wellington et al. 2002).

MHTT can also reduce the ability of HTT to bind and inhibit active caspase-3 and to bind HIP1 (HTT interaction –protein 1), which is then free to associate with HIPP1 (HIP1-protein interactor) and activate caspase-8, an initiator caspase involved in the apoptotic cascade (for review, Gil et al. 2008). In FVB-YAC128 mice expressing full-length mHTT, the inhibiting of caspase-6 (but not caspase-3) was shown to protect loss against striatal volume and neuronal loss, suggesting that caspase-6-mediated proteolysis of mHTT (586 aa), generating a toxic fragment and mediates excitotoxic stress. Cleavage of HTT could be an ‗initiating' factor for neuronal dysfunction, by generating toxic fragments, altering cellular trafficking and gene expression patterns and activating cell death pathways via altered interaction with HTT-associated proteins. HTT proteolysis could also act as a feed-forward loop, in which cleavage may occur prior to the onset of neurodegeneration in HD, and initiate or exacerbate progression towards activation of cell death proteases and subsequent cell death.

Calpains are a family of Ca^{2+}-dependent intracellular cysteine proteases, activated by elevated intracellular calcium levels, which cleave HTT between amino acids 437 and 540 an area that overlaps with caspase cleavage sites in the protein (amino acids 518–586) (Wellington et al., 2003).

1.3.3.3.Transcription deregulation

It has been proposed that mHTT interacts with several transcriptional factors recruiting them into the aggregates and inhibiting their activity (for review, Bithell *et al.* 2009). Important transcriptional factors (*e.g.* CREB [cyclic-adenosine monophosphate (cAMP) response element (CRE)] binding protein (CBP) (Steffan *et al.* 2000), Nucifora (Nucifora *et al.* 2001), specific protein-1 (SP1) (Li *et al.* 2002), TATA-binding protein (TBP), TBP-associated factor TAFII130 (Dunah *et al.* 2002) and the pro-apoptotic transcription factor

p53) directly interact with mHTT (Steffan et al. 2000). CBP, with a polyQ stretch, is sequestrated into mHTT aggregates, suppressing CREB-mediated CRE transcription (Steffan et al. 2000). TBP, also containing a polyQ stretch, and was shown in an *in vivo* study to be incorporated into mHTT aggregates and to suppress its DNA binding by mHTT (Steffan et al. 2000). SP1, which binds to glutamine-rich region in certain promoters and activates transcription of the corresponding genes and TAFII130 interacts with a soluble form of mHTT, suppressing of SP1 transcriptional activity and finally downregulating dopamine D2 or nerve growth factor receptor (Steffan et al. 2000). p53 is incorporated into mHTT aggregates via its SH3 sequences, leading to repression of p53-mediated transcription (Steffan et al. 2000).

Interaction of mHTT fragments with transcriptional factors is sufficient for transcriptional deregulation *in vivo* suggesting a model whereby mHTT interacts directly with DNA, altering its conformation and transcription factor binding and ultimately leading to transcriptional deregulation (Benn *et al.* 2008). Benn *et al.* (2008) observed that both wild-type and mHTT occupy gene promoters *in vivo* and proposed the enhanced genomic DNA binding by mHTT, (facilitated by its nuclear-localization) alters DNA conformation and subsequent binding of transcription factors, disrupting normal control of mRNA expression at an early time point in HD pathogenesis (Benn et al. 2008). Several transcription factors that interact with the mutant protein have acetyltransferase activity that may impair gene expression, by altering histone acetylation levels. Hypoacetylation has been linked to repression of gene activity (Sadri-Vakili *et al.* 2006).

mHTT can also inhibit gene expression in the cytosol (Zuccato *et al.* 2003). Wild-type HTT was found to interact with the repressor element-1 transcription factor (REST) in cytoplasm. REST associates with neuron restrictive silencer factor (NRSF) to affect nuclear transcription of neuronal genes, including that of BDNF. This interaction REST–NRSF could prevent their entry to nucleus and thus reduce their suppression of gene expression. However, mHTT bind weakly with REST–NRSE, leading to increased accumulation of REST–NRSF in nucleus and subsequent inhibition of BDNF and other genes expression (Zuccato et al. 2003).

1.3.3.4.Disruption of axonal transport

Several HTT-binding cytoplasmic proteins are involved in vesicle trafficking and intracellular transport. A particular protein, HAP 1, was proposed to facilitate the interaction with microtubule motor proteins, forming a complex with kinesin (plus-end directed microtubule motor protein) and with $p150^{Glued}$ subunit of dynactin (Caviston et al. 2007). A study demonstrated a co-precipitation of a complex that includes cytoplasmic dynein, dynactin, HTT, kinesin and HAP1 (Caviston et al. 2007). HAP1 is a multidomain protein with versatile functions that also interacts with HGS, which in turn participates in endocytosis of the epidermal growth factor (EGF) receptor (Gauthier et al. 2004). HAP1 was recently found to interact with the type 1 inositol (1,4,5)-trisphosphate receptor (IP31), forming an IP31–HAP1A–HTT ternary complex in which the mHTT enhances the sensitivity of IP31 to inositol (1,4,5)-trisphosphate (for review, Li et al. 2004). HAP1 interacts with NeuroD (a transcription factor important for neuronal development and survival) and HTT interacts with NeuroD via HAP1 (for review, Gil et al. 2008). HTT has also been linked to actin-based motors through optineurin, a protein that links myosin VI to Golgi membranes (Caviston et al. 2007). A neurotrophic factor essential for neuronal survival, BDNF, is decreased in striatal neurons. BDNF is secreted by cortical neurons, delivered by axonal transport and re-endocyted by striatal neurons (Gauthier et al. 2004). In several studies, it was shown that mHTT plays an important role such depletion, as a consequence of defective axonal trafficking (Gauthier et al. 2004). A study demonstrated an increased association of polyQ-HTT to HAP1 and $p150^{Glued}$, leading to the depletion of HAP1, $p150^{Glued}$, dynein IC (intermediate chain), and kinesin HC from microtubules (Gauthier et al. 2004). This occurs mainly in the early stage of disease, while in later stages neuritic aggregates accumulate and contribute to reduce axonal transport (Gauthier et al. 2004).

1.3.3.5.Synaptic dysfunction

Interactions of mHTT with cytoplasmic proteins have been involved in synaptic dysfunction, either by impairment of axonal transport or sequestration of synaptic vesicles or proteins necessary for endocytosis and recycling (*e.g.* membrane receptors) (Trushina *et al.* 2006). Inhibition of endocytosis occurs through a non-clathrin, caveolar related pathway (Trushina et al. 2006). A recent study revealed that mHTT leads to accumulation

of intracellular cholesterol, which is essential to promote synapse formation and maintenance membrane integrity in CNS (central nervous system) neurons (Trushina et al. 2006)

Another HTT-interacting protein is the neurospecific phosphoprotein PACSIN 1/syndapin, which is located along neurites and within synaptic boutons and has been implicated in synaptic vesicle recycling (Modregger *et al.* 2002). Interaction through C-terminal SH3 domain with mHTT leads to re-localization of PACSIN 1 away from varicosities towards neuronal cell body (Modregger et al. 2002). SH3-containing proteins, binding partners for synaptojanin and dynamin I, play a major role in signal transduction from membrane receptors and in regulation of exo/endocytic cycle of synaptic vesicles (Sittler *et al.* 1998). MHTT was also found to bind to this domain and may contribute to neuronal cell death (Sittler et al. 1998). Another example of loss of function is HIP14 (a neuronal protein that is located mainly in Golgi apparatus and cytoplasmic vesicles) that interacts strongly with wild-type HTT but weakly with the mutant protein and may compromise intracellular traffic (Singaraja *et al.* 2002). Several proteins involved in exocytosis are decreased in HD, including complexin II (Smith *et al.* 2005). Complexin II interacts with the soluble N-ethylmaleimide-sensitive fusion protein attachment protein receptor (SNARE) complex (involved in neurotransmitter release and regulation of membrane fusion between the synaptic vesicle and the presynaptic plasma membrane) (Smith *et al.,* 2005). Another protein whose levels are decrease is rabphilin 3A that is involved in priming and docking of vesicles to the plasma membrane (Smith et al. 2005).

Excitotoxicity induced by glutamate has been implicated as one of the main causes of neuropathology of HD (Fan and Raymond, 2007). R6 transgenic mice have an increased release and a decreased clearance of glutamate by the glial cell glutamate transporter GLT1 with subsequent sustained glutamate stimulation of striatal neurons (Smith et al. 2005). Neurons from mice R6/2 were shown to have increased responses of NMDA and decreased Mg^{2+} sensitivity, suggesting that NMDA receptor alterations may occur very early in development and that constitutively abnormal NMDA receptors with enhanced response may be present (Starling *et al.* 2005). MHTT facilitates activity of NR2B subtype of NMDARs and InsP3R1, causing influx of Ca^{2+} (Tang *et al.* 2005). Activation of glutamatergic receptors alters Ca^{2+} homeostasis, which in turn affects downstream pathways and initiate second messenger cascades (Fan *et al.* 2007). When buffering capacity is compromised, activation of catabolic enzymes (such as nucleases, proteases

and phospholipases) as well as generation of free radicals and induction of mitochondrial damage can occur (Fan et al. 2007).

Metabotropic glutamate receptors (mGluR) (*e.g.* mGluR1, mGluR2 and mGluR3) and ionotropic receptors (3-hydroxy-5-methyl-4-propionate (AMPA) and kainate receptors (KA)) as well as D1 and D2 dopamine (DA) receptors were also found to be decreased or with decreased binding activity in R6/2 mouse model (for review, Gil et al. 2008).

Interestingly, normal HTT associates with postsynaptic density 95 (PSD-95), a scaffold protein that causes clustering and activation of receptors in postsynaptic membrane. Decreased interaction of mHTT with PSD-95 may activate NMDARs (Li et al. 2004).

1.3.3.6.Mitochondrial dysfunction and oxidative stress

Defects in mitochondrial respiratory chain in caudate/putamen of HD patients have been reported include severe reduction in activity of complex II/III and milder decrease of complex IV activity (Sawa *et al.* 1999). Transcriptional impairments produced by mHTT could lead to disruption of Ca^{2+} homeostasis, which may further reduce CREB-dependent expression of mitochondrial oxidative phosphorylation proteins (Gopalakrishnan *et al.* 1994). Mitochondrial respiration and ATP production were found to be significantly impaired in striatal cells expressing mHTT. Moreover, mHTT can also affect mitochondrial function by inhibiting expression of PGC-1α (peroxisome proliferator-activated receptor gamma co-activator 1-alpha), a transcriptional factor required for expression of numerous genes that promote the detoxification of reactive oxygen species (ROS) and prevent oxidative stress (Quintanilla *et al.* 2009). Tang *et al.* (2004) propose that such vulnerability could arise from glutamate released by corticostriatal projection neurons, stimulating NR1/NR2B-composed NMDARs and mGluR5 receptors (Tang et al. 2005). Activation of NR1/NR2B NMDARs leads to Ca2+ influx and activation of mGluR5 receptors through the production of InsP3 and Ca2+ release via InsP3R1. Indeed, mHTT sensitizes InsP3R1 to activation by InsP3, stimulating NR1/NR2B NMDAR activity, and directly destabilizing mitochondrial Ca^{2+} handling. As a result, an abnormal Ca^{2+} response in MSN occurs, leading to an overload in cytosolic Ca^{2+}, which is then taken into mitochondria via Ca^{2+} uniporter/channel. If this occurs continuously, changes storage capacity limit of mitochondrial Ca^{2+} can lead to opening of mPTP (mitochondrial permeability transition pore), release of cytochrome *c* into cytosol, and activation of

caspase-mediated intrinsic apoptotic program (Oliveira *et al.* 2007). MHTT can also interact directly with outer mitochondrial membrane increasing the sensitivity of the mPTP to Ca^{2+} or other apoptotic stimuli and also the aggregates could impair mitochondrial movements along neuronal processes (for review, Damiano *et al.* 2010).

Weydt *et al*. (2006) found a decreased number of functional mitochondria, ATP/ADP and expression of PGC-1α target genes (involved in energy production) in brown adipose tissue from HD mice (N171-82Q mice) (Weydt *et al.* 2006). This suggests that inhibition of PGC-1α (usually involved in adaptive thermogenesis) may cause a global defect in mitochondrial function in HD mice. The authors also showed that these HD mice develop hypothermia associated with impaired activation of brown adipose tissue-mediated thermogenesis, supporting the hypothesis that impaired PGC-1α activity links neurodegeneration-associated mitochondrial dysfunction to thermoregulatory and metabolic defects in HD (Weydt et al. 2006).

1.4. Modeling HD

The most reliable models reproduce neuropathological hallmarks such as degeneration of GABAergic medium spiny neurons at an early stage and cortical loss in advanced conditions and especially the phenotype of the disease (for review, Rubinsztein, 2002). Two categories of animal models were generated: the non-genetic and the genetic ones. Non genetics animal models were the only available before discovery of gene mutation and used excitotoxic mechanisms or mitochondrial dysfunction to induce neurodegeneration, primarily at striatum. Quinolinic acid (QA) and kainic acid (KA) are the most commonly used excitotoxic agents, acting as agonists of NMDA receptors, whereas 3-nitropropionic acid (3-NP) and malonic acid (MA) induce cell death in striatal neurons through inhibition of mitochondrial complex II (succinate dehydrogenase), disrupting mitochondrial electron transport chain with subsequent impairment in ATP synthesis (for review, Ferrante, 2009).

Recently, genetic engineering led to the production of transgenic animals, inserting genetic material in the host genome or into the HTT gene locus, resulting in knock–in models. In HD cases, the material inserted comprised protein-coding region exon -1 (which expresses truncated protein) or the full length HTT gene, expressing the entire protein (for review, Ferrante, 2009). The most widely used animals are rodents and, recently, also non-human primates (Yang *et al.*, 2008), but other non-mammalian animals exist (such as *Caenorhabditis elegans*, *Drosophila melanogaster* and *Zebrafish*) (Fecke *et al*., 2009). These models are simple and have a rapid development, allowing high-throughoutput testing of novel therapeutic compounds and strategies (Fecke *et al*., 2009).

Currently, a wide range of models is available, differing in background, fragment/full-length gene, CAG repeat length, promoter and endogenous expression of transgene. Those particular characteristics of each model influence the disease neuropathology and phenotype (for review, Ferrante, 2009). Frequently there is an inverse correlation between the severity of disease/symptoms, lifespan and mHTT expression and transgenes length (for review, Ferrante, 2009). The full-length models are genetically more accurate, but the fragment models have a rapidly disease progression with a robust phenotype, well-defined behavioural and neuropathological findings and premature death between 13 and 18 weeks of age (*e.g.* Carter *et al*., 2000).

1.4.1. Animal models

The early animal models of HD relied on neurotoxin-mediated striatal lesions. Latter on genetic approaches have prevailed to generate animal models of HD. Several approaches are currently been used to reproduce disease phenotype mostly by insertion of full-length or only a fragment of mutated HTT with a coding region containing only CAG repeats or one containing repeats that are interrupted with one or more CAA codons. The expression of the HD mutation can be from a transgene or knock-in of the mutation into the endogenous HTT locus and can resort to human HTT or the endogenous gene from the animal.

1.4.1.1.N-terminal fragment mouse models

The most common mice models using an insertion of truncated N-terminal fragment of mHTT exon 1 are the R6/1, R6/2 and N171-Q82. R6/1 and R6/2 express mHTT with 116 and 144 CAG repeats, correspondingly, under the control of the human HTT promoter and N171 mice express a truncated HTT cDNA with 82 CAG repeats under the control of the mouse prion protein promoter (Mangiarini *et al.* 1996, Schilling et al. 1999). Common features of truncated forms are the widespread and generalized degenerative phenotype translated in a rapid onset of symptoms, including motor, cognitive and behavioural abnormalities, weight loss and a reduction in lifespan (Dragatsis *et al.* 2009, Cheng *et al.* 2011). The exuberant phenotype exhibited by these mice models however culminates in a minimal neuronal death when compared to human HD patients. The premature death usually occurs into 12-14 weeks for R6/2, 4-5 months of age for R6/1 and 17-20 weeks for N171-Q82 but with HD-like symptoms more similar in the last model (Yu *et al.* 2003, Reiner *et al.* 2007).

Table 1- Rodent models of Huntington's disease

Model	Transgene product	Promoter	CAG repeat length	mHTT expression*
Truncated N-terminal fragment models				
R6/1 mice	67 amino acids of N-terminal fragment (human *HTT*)	1 kb human *HTT* promoter	116	~×0.30
R6/2 mice	67 amino acids of N-terminal fragment (human *HTT*)	1 kb human *HTT* promoter	144‡	~×0.75
N171-Q82 mice	171 amino acids of N-terminal fragment (human *HTT* cDNA)	Mouse *Prp* promoter	82	~×0.10–0.20
HD94 mice	67 amino acids of N-terminal fragment (chimeric human *HTT*:mouse *Htt* exon 1)	*Camklla*	94	Not reported
Shortstop mice	171 amino acids of N-terminal fragment (human *HTT*)	Human *HTT* promoter and regulatory elements (24 kb upstream)	128	~×1.00
N118-82Q mice	118 amino acids of N-terminal fragment (human *HTT* cDNA)	Mouse *Prp* promoter	82	Not reported
N586-82Q mice	586 amino acids of N-terminal fragment (human *HTT* cDNA)	Mouse *Prp* promoter	82	>×1.00
Ubi-G-HTT84Q mice	67 amino acids of N-terminal fragment (human *HTT* cDNA) fused to EGFP	Ubiquitin promoter	84	Not reported
HD150QG mice, HD190QG mice	67 amino acids of N-terminal fragment (human *HTT* cDNA) fused to EGFP	1 kb human *HTT* promoter	150, 190	~×10.00, ~×2.50
HD51 rats	N-terminal fragment (22% of rat *Htt* gene)	Endogenous rat *Htt* promoter	51	<×1.00
Full-length HD models: knock-in models				
CAG140 mice	Full-length chimeric human *HTT* exon 1:mouse *Htt*	Endogenous mouse *Htt* promoter	119, 140	×1.00
HdhQ92 mice	Full-length chimeric human *HTT* exon 1:mouse *Htt*	Endogenous mouse *Htt* promoter	92	×1.00
HdhQ111 mice	Full-length chimeric human *HTT* exon 1:mouse *Htt*	Endogenous mouse *Htt* promoter	111	×1.00
HdhQ150 mice, HdhQ200 mice	Full-length chimeric human *HTT* exon 1:mouse *Htt*	Endogenous mouse *Htt* promoter	150, 200	×1.00
Hdh4/Q72 mice, Hdh4/Q80 mice	Full-length chimeric human *HTT* exon 1:mouse *Htt*	Endogenous mouse *Htt* promoter	72, 80	×1.00
zQ175 mice	Full-length chimeric human *HTT* exon 1:mouse *Htt*	Endogenous mouse *Htt* promoter	188	×1.00
Full-length HD models: transgenic models				
HD48 mice§, HD89 mice§	Full-length human *HTT*	CMV promoter	48, 89	~×1.00–5.00
YAC128 mice	Full-length human *HTT*	Human *HTT* promoter and regulatory elements (24 kb upstream, 117 kb downstream)	128	~×1.00
YAC48 mice	Full-length human *HTT*	Human *HTT* promoter and regulatory elements	48	~×0.30–0.50
YAC72 mice	Full-length human *HTT*	Human *HTT* promoter and regulatory elements	77	~×0.30–0.50 (line 2511), ~×2.00 (line 2498)
BACHD mice	Full-length human *HTT*	Human *HTT* promoter and regulatory elements (20 kb upstream, 50 kb downstream)	97	~×1.36
Hu97/18 mice	Fully humanized mouse model: two full-length human *HTT* alleles, no mouse *Htt* alleles	Human *HTT* promoter and regulatory elements	97	~×1.00‖
iFL148Q mice	Full-length *Htt* (inducible)	*Htt* cDNA	148	×1.00
BACHD rats	Full-length human *HTT*	Human *HTT* promoter and regulatory elements	97	~×2.50–4.50

CamkIIa, calcium/calmodulin-dependent protein kinase IIα; CMV, cyclomegalovirus; EGFP, enhanced green fluorescent protein; HD, Huntington's disease; *HTT*, huntingtin; mHTT, mutant HTT; N, amino; *Prp*, prion protein. *Relative to endogenous levels except where noted otherwise. ‡Unstable, with expansions >250 CAG repeats reported. §These mice are no longer available. ‖Relative to expression of a full-length human *HTT* transgene containing 18 CAG repeats. Adapted from (Pouladi *et al.* 2013).

1.4.1.2.Full-length mouse model

The full-length mHTT rodent models were created using yeast artificial chromosome (YAC) and bacterial artificial chromosome (BAC) technology. Those models targeted the human mHTT transgenes expression, including all the introns and exons as well as the regulatory sequences up to 24 kb upstream and 117 kb downstream of the gene, ensuring adequate symptoms timeline manifestation and tissue-specific expression of mHTT.

In 1999 Hayden and colleagues developed a YAC transgenic mouse using a YAC vector system to express the entire human HTT gene under control of the human HTT promoter. YAC mouse strains contain either 72 or 128 CAG repeats. The mice with 72 expansions show a selective degeneration of medium spiny neurons in the lateral striatum with the translocation of N-terminal HTT generation specifically in the striatum (Hodgson *et al*., 1999). The YAC128 has an increased size of CAG expansion of 128 CAG and in 2003 Slow *et al.* characterize the natural history of disease in these mice. Motor abnormalities and age-dependent brain atrophy were found. In early stages of disease the mice develops a hyperkinetic phenotype manifest at 3 months of age, followed by a progressive motor deficit on the rotarod at 6 months with progression to hypokinesis by 12 months of age. There is a high correlation between motor abnormalities and striatal atrophy, which is evidently at 9 months of age, and develops into cortical atrophy at 12 months and significant decrease (~15%) in striatal neurons accompanied by a decrease in striatal cell surface area.

The motor deficit at 6 months correlates well with evident neuronal loss at 12 months, suggesting that early motor dysfunction might be an indicator of the severity of the extent of dysfunction of striatal neurons YAC128 mice also develop mild cognitive deficits, which precedes the onset of motor abnormalities and progressively deteriorate with age (Van Raamsdonk *et al.*, 2007). HTT inclusions appear latter to behavioral and neuropathological changes associated with neuronal death, at 18-month-old, presupposing that inclusions are not the main cause to neurons loss. Excitotoxicity was described has the most important mechanism responsible for cell death in which disturbed neuronal Ca2+ signaling is involved. An increased NMDAR-mediated current in the MSN cultured from the YAC128 model corroborates this idea (Shehadeh *et al.*, 2006, Van Raamsdonk *et al.*, 2007; Zhang *et al.*, 2008). This susceptibility to neuronal excitability is age-dependent in YAC128 which may be conditioned by background strain since FVB/N WT mice have an age-dependent decrease in susceptibility to excitotoxic stress probably resulting from

morphological changes including decreases in synaptic density, spine density and loss of distal dendritic segments (Graham *et al.,* 2009). Body weight in YAC128 mouse line is increased at 2 month of age (Van Raamsdonk *et al.,* 2007) represented by an increase in both fat mass and fat-free mass influenced by HTT which modulates the IGF-1 pathway (Pouladi *et al.,* 2010). YAC128 mice were initially generated on the FVB/N background strain based on its advantages in generating transgenic mice and its known susceptibility to excitotoxicity (Taketo *et al.,* 1991). This strain has a particular characteristic that makes it attractive to create HD transgenic mice, since it exhibits a high degree of neuronal loss when exposed to excitotoxic stress after injection of kainic acid or quinolinic acid, in an age dependent manner, not experienced in other HD transgenic strains (Schauwecker *et al*., 2002, Graham *et al*., 2009). YAC128 are useful to assess therapeutical interventions, since it reproduces well the phenotype of disease in humans.

1.4.2. Cellular models

1.4.2.1.Characteristics of embryonic and induced pluripotent stem cells

Human embryonic stem (hES) cells are pluripotent cells derived from the inner cell mass of a pre-implantatory blastocyst with the ability to self-renew and differentiate into any tissue of the three germ layers (Thomson et al. 1998).Isolation of mouse ES cells from blastocysts was first described in 1981 (Evans *et al.* 1981, Martin 1981). Based on this paradigm, James Thomson and co-workers (1998) derived human ES cells from blastocysts donated by couples undergoing infertility treatment (Thomson et al. 1998). The authors plated the inner cell mass onto mouse embryonic fibroblasts and after attachment and expansion they were able to replate onto another feeder cell layer with high success (Thomson et al. 1998). These cells had the capacity for self-renewal and grow for long periods without senescence and possessed high telomerase activity, all characteristics of immortalized cell lines. Moreover, structures from all three germ layers, namely mesodermal, ectodermal and endodermal lineages, were observed in the resulting teratomas. ES cells expanded in three-dimensional cultures tended to form aggregates grown in suspension called embryoid bodies (EBs); similarly, spontaneously formed EBs expressed markers representative of the three germ layers (Itskovitz-Eldor *et al.* 2000).

Undifferentiated hES cells exhibit a specific range of proteins involved in several signal pathways that affect their pluripotency and self-renewal. In recent years several cell surface and molecular markers have been shown to characterized ES cells, allowing the distinction with tumour stem cells. Membrane proteins are the most important markers in identifying ES cells; these include the carbohydrate epitopes associated with the lacto- and globo-series glycolipids Stage Specific Embryonic Antigens 1 (SSEA-1), SSEA-3, and SSEA-4 (Kannagi *et al.* 1983, Stewart *et al.* 2006) and the keratin sulfate-related antigens TRA-1-60 and TRA-1-81 (Andrews *et al.* 1984, Pruszak *et al.* 2007). These carbohydrate-associated molecules are involved in controlling cell surface interactions during development. Another hallmark of ES cells is the expression of a specific range of genes that lead to the upregulation of some transcripts, such as Octamer-binding Protein 4 (Oct4), Nanog, and Sox2 (Zhao *et al.* 2012). In humans, elevated levels of alkaline phosphatase are found in the cell membrane, concomitantly with elevated telomerase activity (Stojkovic *et al.* 2004).

Although hES cells have a great potential for disease models and cell therapy application, several ethical questions are associated with the use of human embryos; furthermore, technical issues related with the limited source of ES cells, teratoma formation and graft immune rejection are also evident when using ES cells, thus limiting its potential application in treating human diseases.

Generation of induced pluripotent stem (iPS) cells from somatic cells was one of the major discoveries of the last century. The work of Yamanaka and collaborators (2006, 2007) proved to be a milestone in the field of stem cells due to the possibility of obtaining pluripotent stem cells from almost any somatic cell, without raising ethical or legal objections (Takahashi *et al.* 2006, Takahashi *et al.* 2007). Thus, adult mammalian cells (usually fibroblasts or keratinocytes) can be reprogrammed into a pluripotent, self-renewal state maintaining a multi-lineage differentiation potential. iPS cell technology is based on inducing pluripotency in somatic cells through the retroviral-mediated introduction of four transcription factors, namely octamer-binding transcription factor-3/4 (Oct3/4), SRY-related high-mobility-group (HMG)-box protein-2 (Sox2), c-Myc and Kruppel-like factor-4 (Klf4) – known as the "Yamanaka factors" (Takahashi et al. 2006, Takahashi et al. 2007). These authors selected 24 genes based on their pivotal role in the maintenance of pluripotency in ES cell and in early embryos. The authors differently combined these genes and introduced them into mouse embryonic fibroblasts in order to screen for proper reprogramming factors via the Fbx15-Neo reporter system. To determine which of the 24

candidates were critical, selective withdrawal of individual factors from the pool of transduced candidate genes was performed. The combination of the four transcription factor genes (Oct3/4, Sox2, c-Myc and Klf4) into mouse embryonic fibroblasts was enough to generate ES cell-like colonies. One year later the same transcription factors were transduced into adult human dermal fibroblasts, generating colonies morphologically similar to hES cells that formed teratomas when injected into immunodeficient mice (Takahashi et al. 2007). Resorting to tetraploid complementation, injection of iPS cells into the blastocyst generated live chimeras and germline transmitted mice (Okita *et al.* 2007, Kang *et al.* 2009, Zhao *et al.* 2009).

The protocol of iPS cell generation has been applied to numerous cell types, more commonly mouse and human, and refined to the combination of other factors and methodologies aiming to reduce the risk of insertional mutagenesis (Okita *et al.* 2008, Fusaki *et al.* 2009, Sommer *et al.* 2009, Woltjen *et al.* 2009, Yu *et al.* 2009, Zhou *et al.* 2009, Okita *et al.* 2010, Anokye-Danso *et al.* 2011, Sommer *et al.* 2012).

Several studies have proven that iPS cells are highly similar to ES cells in terms of growth, morphology, gene expression, epigenetic status and the potential for differentiation, but small differences were found at the molecular level (Chin *et al.* 2009, Marchetto *et al.* 2009, Prigione *et al.* 2010, Razak *et al.* 2013). Marchetto and colleagues (2009) performed microarray analysis and concluded that 1,952 Refseq-annotated genes were significantly enriched in iPS *versus* hES cells and that 1,072 genes were enriched in hES *versus* iPS cells. They identified three groups of biologically interesting genes that changed by at least 4-fold compared to hES cells. The first group of iPS cells-expressed genes were proteins important in early embryonic fate, such as Stella, ZFP42 (the same as REX1), CLDN10, LEFTY1 and LEFTY2, which were not sufficiently induced when compared to hES cells. The second group contained iPS cells-expressed genes that were not sufficiently repressed, such as ZIC1, OLIG2, EN2 and PTX3, but were associated with the neuronal lineage. The third group consisted of genes that were upregulated in iPS cells, but silenced in hES cells; these included downstream factors involved in reprogramming to induce pluripotent cells (Marchetto et al. 2009). Chin (2009) showed that late-passaged hiPS cells clustered similarly as hES cells than early-passaged iPS cells, suggesting that some gene expression patterns have not yet been efficiently silenced from the original somatic cell; however, upon passage extension the different gene expression profile of hPS cells appeared to decrease (Chin et al. 2009). Moreover, the expression profiles of miRNAs were also found to be different between ES and iPS cells. For instance, several miRNAs

from the chromosome 19 miRNA cluster were more strongly expressed in iPS cells than in ES cells (Razak et al. 2013).

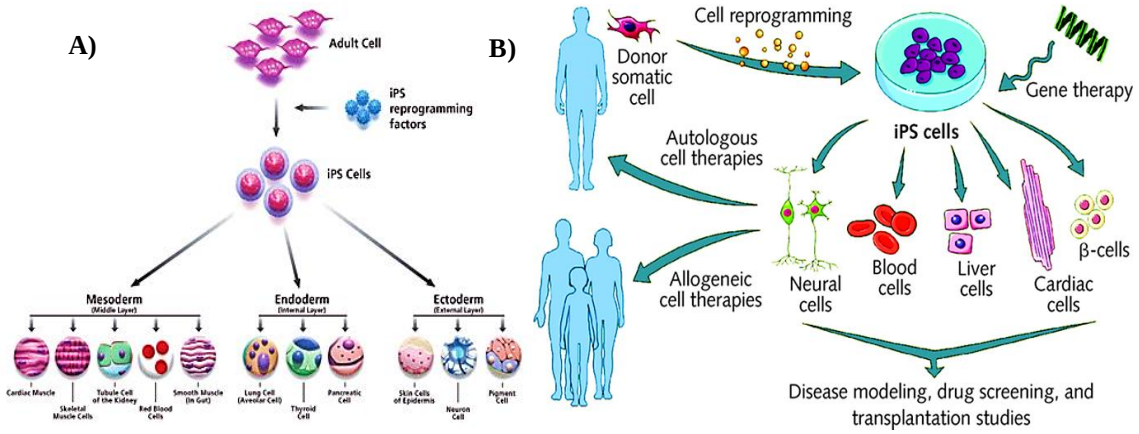

Figure 1.15. – A) Induced Pluripotent Stem Cell (iPS) Pathway. iPS cells are capable of differentiating into cells of the 3 germ layers From *http://www.sigmaaldrich.com/life-science/stem-cell-biology/ipsc.html*. **B) Multiple applications for iPS cells.** Adapted from (Power *et al.* 2011)

1.4.3. Mitochondrial function and metabolism in stem cells

1.4.3.1. Altered metabolic profile and mitochondrial function following reprogramming to pluripotency

Mitochondria are double-membrane organelles, usually referred as the powerhouse of the cell due to its fundamental role in energy production in the form of ATP. Mitochondria are also involved in multiple processes including calcium homeostasis, cell signaling, reactive oxygen species (ROS) formation and apoptosis (Dyall *et al.* 2004). Interestingly, reprogramming somatic cells to a pluripotent state resets genetic and epigenetic landscapes, originating distinct metabolic signatures. Specific metabolic cellular pathways, such as glycolysis, the pentose phosphate pathway (PPP) and mitochondrial function have been reported to be involved in the regulation of stem cell physiology (Varum *et al.* 2009, Chen *et al.* 2010, Liu *et al.* 2013, Son *et al.* 2013).

Highly proliferative cells such as stem cells recur to glycolysis as the main ATP source under aerobic conditions. A high glycolytic flux provides not only ATP, but also anabolic precursors for rapid proliferation, with the associated PPP generating ribose-5-phosphate for nucleotide synthesis and NADPH-reducing power for biosynthetic pathways (e.g. nucleotide and lipid synthesis); furthermore, activation of the PPP decreases intracellular levels of ROS by producing NADPH through the activity of glucose-6-phosphate dehydrogenase, which is essential for the regeneration of reduced glutathione (GSH) by glutathione reductase (Prigione *et al.* 2010). Recent studies revealed that human ES cells obtain most of their ribose from added glucose, with genes in the PPP and lipid biosynthesis pathways highly expressed before their differentiation (Varum et al. 2009, Zhang *et al.* 2011).

During differentiation of pluripotent stem cells (PSC) a significant shift occurs in energy production resulting in a shunt of most of the cytosolic pyruvate into mitochondria, where it is oxidized via the Krebs cycle into acetyl-coenzyme A by pyruvate dehydrogenase, along with stimulation of the electron transport chain to synthesize ATP through oxidative phosphorylation (OXPHOS).

Thus, during reprogramming to pluripotency a few dramatic metabolic changes succeed such as glycolysis being the referential ATP production mechanism over OXPHOS. Rapid proliferative pluripotent stem cells, such as hESC, require a high glycolytic flux to support anabolic metabolism; glycolysis provides intermediate metabolites and, as referred, protects against oxidative stress avoiding the production of high levels of ROS.

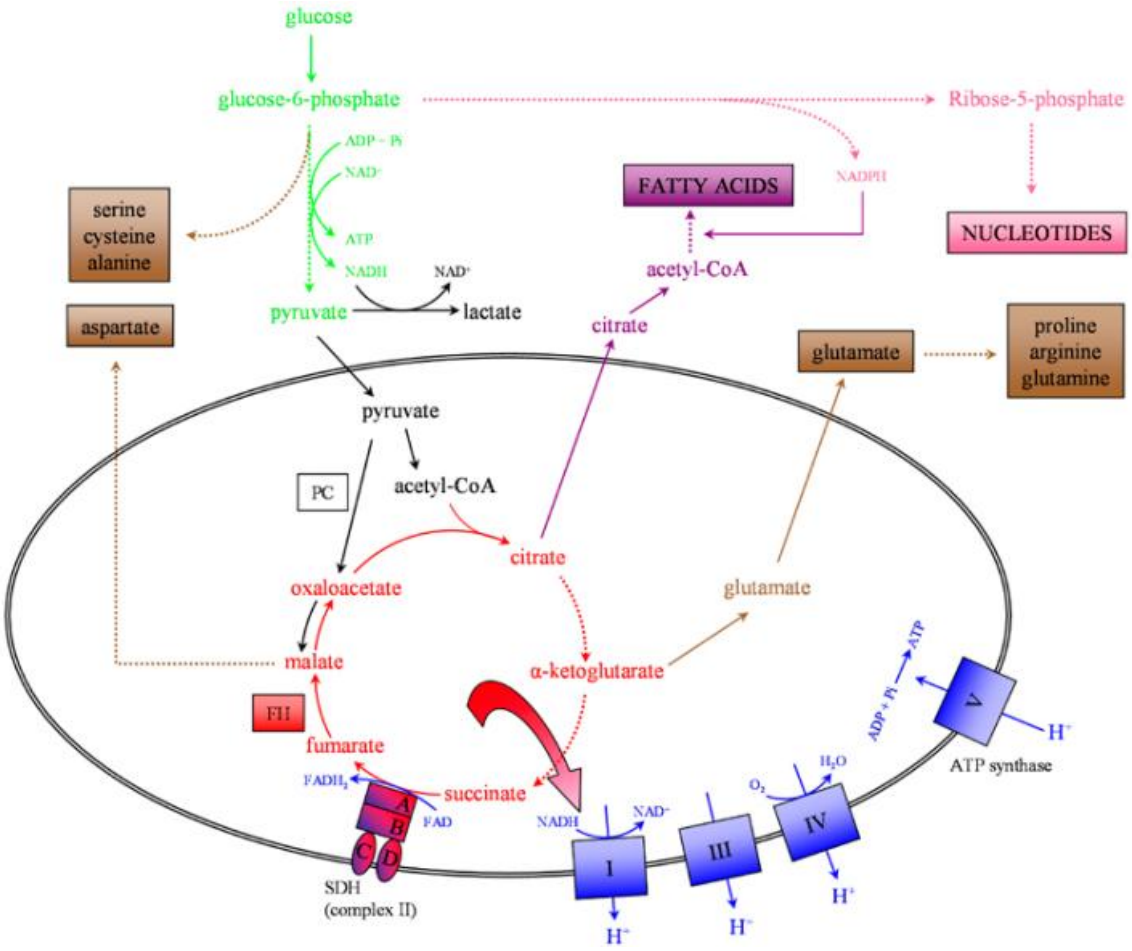

Figure 1.16 - Metabolic pathways Pathways: green – glycolysis; red – tricarboxylic acid (TCA) cycle; blue – oxidative phosphorylation; brown – non-essential amino-acid synthesis; pink – pentose phosphate pathway and nucleotide synthesis; purple – fatty acid synthesis. The SDH complex is involved in both the TCA cycle and oxidative phosphorylation Different complexes of the electron transport chain are represented in this diagram. Solid arrows indicate direct conversion whereas dotted arrows indicate a general pathway (King *et al.* 2006).

Nuclear reprogramming also induces profound morphological and structural changes at mitochondria. This remodelling results in globular or spherical structures with similar minimal and maximal axes lengths and small and undeveloped cristae reflecting a more condensed configuration (dark condensed matrix and expanded translucent cristae), as compared to their differentiated progeny; indeed, more differentiated cells show mitochondria with tightly packed thin cristae within an expanded translucent matrix (Prigione et al. 2010, Suhr *et al.* 2010, Zeuschner *et al.* 2010, Folmes *et al.* 2011). Stem

cells mitochondria usually assume a punctate or fragmented pattern compared with the well-developed filamentous network of somatic cells (Zhang et al. 2011). Mitochondrial localization also suffers significant changes, by transiting from a wide cytosol network to a dominant perinuclear and bipolar localization, most likely to support the vast genetic and epigenetic alterations or probably due to the lack of cytoplasmatic space. Reprogramming induces mitochondria to recede into an immature state observed in ES cells, characterized by low copy number of mitochondrial DNA (mtDNA) and spherical mitochondria with poorly developed cristae (Facucho-Oliveira *et al.* 2007, Kelly *et al.* 2013).

An important parameter of mitochondrial function, membrane integrity, and energy coupling is mitochondrial membrane potential ($\Delta\Psi_m$). Recently it was found that iPS and hES cells have an elevated $\Delta\Psi_m$, which decreases upon differentiation; indeed, increased $\Delta\Psi M$ is observed in mouse embryonic fibroblasts (MEFs) undergoing the reprogramming process. This hyperpolarized-associated mitochondrial state of pluripotent stem cells is most likely related to the reduced ATP consumption, and the preferential glycolysis-based energy metabolism, as described before. Prigione et al (2011) observed that $\Delta\Psi_m$ was low in all fibroblast cells, but increased in iPS cells independently of the age of the donor and in a similar manner as in an hES cell line (Prigione *et al.* 2011). Despite all immature features, mitochondrion is still able to produce ATP from OXPHOS and consume oxygen. Some controversial papers have been published about mitochondria content. Prior studies refer a low content in hES cells (St John *et al*. 2005, Facucho-Oliveira et al. 2007), whereas recent data demonstrated that when mitochondrial mass (measured by mitochondrial proteins, mitochondrial labeling with MitoTracker Red and calcein-AM, and mtDNA copy number) is normalized to total cellular mass, the ratio between these cellular parameters is similar in iPS cells and differentiated cells (Birket *et al.* 2011, Zhang et al. 2011). To maintain the mitochondria hyperpolarized, cells rely on the hydrolysis of glycolytic ATP (described before in this section). Due to a reduced function of the electron transport chain, the F1F0 ATP synthase (complex V) is reversed, hydrolyzing glycolytic ATP to maintain the $\Delta\Psi M$ (Zhang et al. 2011). Studies comparing hES cells and fibroblasts demonstrated higher ATP levels in the last ones and when ATP production by glycolysis was blocked with sodium oxamate, a lactate dehydrogenase inhibitor, the ATP levels dropped dramatically, whereas inhibition of OXPHOS only caused a slight reduction in ATP levels in both hES and IPS cells (Varum *et al.* 2011, Zhang et al. 2011).

A few studies successfully stimulated glycolysis to promote pluripotency. Some submitted hES and iPS lines to hypoxia conditions and verified that activation of transcription factor

hypoxia-inducible factor one alpha (HIF1α) enhanced reprogramming through the upregulation of pyruvate dehydrogenase kinase 3 (PDK3) and pyruvate kinase isoform M2 (PKM2), while the ablation of HIF1α resulted in a dramatic loss of colony formation (Mathieu *et al.* 2013, Mathieu *et al.* 2014, Prigione *et al.* 2014). In early stages of iPS cells generation HIF1α and HIF2α overexpression enhanced the metabolic switch by promoting the kinetics of PDKs. Varum and colleagues (2009) inhibited the mitochondrial respiration chain specifically using antimycin A, a complex III disruptor that blocks the flow of electrons from semiquinone to ubiquinone in the quinone cycle of complex III and disrupts the proton gradient across the inner membrane, prevents O2 consumption at complex IV, as well as ATP formation (Varum et al. 2009). Treatment with antimycin A maintained the cells pluripotent, even after bFGF withdrawal, most likely due to a shift in the metabolism towards glycolysis, as demonstrated by an increase in lactate dehydrogenase (LDH) activity and partially by an increase in ROS production at complex III, leading to upregulating of Nanog expression (Varum et al. 2009). *In vitro,* Nanog, a homeobox transcription factor, is enriched in pluripotent cell lines but not in adult tissues. From the most prominent transcription factors that have been identified to be essential to the ES cell pluripotency more than 90% of the promoter region in the genes bound by Oct4 and Sox2 are also bound by Nanog (Pan *et al.* 2007). Moreover, increasing Nanog levels in ES cells can stimulate pluripotent gene activation from the somatic cell genome (Pan et al. 2007.) A negative loop was described to be formed by Nanog, Oct4 and FoxD3, which allow the maintenance of Oct4 levels. Another study corroborated these results demonstrating that iPS cell lines generated in the presence of rotenone, antimycin A and potassium cyanide showed an increased reprogramming efficiency and exhibited full differentiation potential *in vitro* and *in vivo* (Son et al. 2013). Although these compounds promote efficient iPS cells generation, differentiated cells obtained from these pluripotent cells exhibited a substantial increase in ROS production and growth retardation, most probably as a result of cellular damage after exposure to the mitochondrial inhibitors (Son et al. 2013) Inhibition of the insulin/insulin growth factor-1 signaling pathway also was shown to enhance reprogramming efficiency (Chen *et al.* 2011). On the other hand, when glycolysis was inhibited by sodium oxamate and by 2-deoxyglucose, (which is taken up by the glucose transporters and is phosphorylated in most cells by hexokinase, generating 2-deoxyglucose-6-phosphate, a competitive inhibitor of glucose-6-phosphate isomerase that catalyzes the conversion of glucose-6-phosphate into fructose 6-phosphate in the second step of glycolysis), reprogramming efficiency was significantly reduced (Son et al. 2013).

Moreover, a metabolomic analysis of genes involved in glycolytic and mitochondrial oxidative phosphorylation pathways corroborated these findings and also that bioenergetic status of somatic cells appear to correlate with their reprogramming efficiencies (Panopoulos *et al.* 2012).

Interestingly, gene expression profiles and methylation patterns of iPS cells are influenced by prolonged culture *in vitro*; the higher the passage number, the more closely they genetically and functionally resemble the hES cells (Panopoulos et al. 2012). Varum and collaborators (2011) found that hES cells express high levels of hexokinase II and have an inactive PDH complex, which results in lower levels of acetyl-CoA to enter the TCA cycle (Varum et al. 2011). The authors also observed that hES cells have higher total protein levels of mitochondrial complexes II, III and V subunits when compared with differentiated cells. The upregulation of the TCA cycle could be a reason for these higher levels of mitochondrial electron transport complexes; alternatively, the transcription factor c-Myc, which is important to maintain cell pluripotency and self-renewal, has been related to mitochondrial biogenesis (Li *et al.* 2005). Nevertheless this overall increase in mitochondrial electron transport complexes does not reflect into an increase in mitochondrial activity. This finding suggests a rejuvenation of mitochondrial function and energetic capacity during the process of reprogramming. Recently, Austin Smith's group at Cambridge was able to reprogram adult keratinocytes, fibroblasts or adipose-derived stem cells to "a true ground-state" pluripotency (Takashima *et al.* 2014). The reset of self-renewal requirements and transcription factor complement in human PSC could be achieved by overexpressing Nanog and Klf2 or could be independent of transgene expression by combining two inhibitors of the Erk pathway and of glycogen synthase kinase-3 with LIF (Takashima et al. 2014). Interestingly, human stem cells 'reset' to the earliest developmental pluripotent state resorted more to OXPHOS for ATP production than conventional PS cells, indicating that mitochondrial metabolism might be different in the pristine state. Basal oxygen consumption rate (OCR) and the activity of electron transport chain activity was substantially higher in reset cells, as evidenced by a greater OCR in response to the mitochondrial uncoupler FCCP (carbonyl cyanide-4-(trifluoromethoxy)phenylhydrazone). Mitochondria of reset cells also hadlower mitochondrial membrane potential. Additionally, the cytochrome c oxidase (complex IV) gene family was highly expressed in reset cells than conventional PS cells for 14 out of 17 genes, similarly to ESC. This mitochondrial activation was confirmed by culturing "reset cells" in 2-deoxyglucose to inhibit glycolysis or under reduced glucose concentrations to

increase the dependency on mitochondrial respiration; under these conditions, the cells formed undifferentiated colonies, unlike conventional PS cells. The reset cells where further implanted into mouse preimplantation embryos and successfully incorporated into the ICM and preimplantation epiblast (Takashima et al. 2014).

1.4.4. Metabolic profile of pluripotent stem cells

Metabolomic analysis has demonstrated that iPS cell metabolism is quite different from their progeny source and similar, but not identical, to ES cells. Yanes and collaborators (2010) resorting to liquid chromatography-electrospray ionization mass spectrometry showed that mouse embryonic stem (mES) cells are characterized by the abundant presence of unsaturated lipid metabolites, including fatty acids, whose levels decrease upon differentiation; importantly, the unsaturated metabolome is highly susceptible to pro-oxidative events, which may have a critical role in cell fate (Yanes *et al.* 2010). The most up-regulated metabolites identified are signal transduction molecules such as lipid messengers and inflammatory mediators, namely arachidonic acid, docosapentaenoic acid, eicosapentaenoic acid, linolenic acid, diacylglycerols, glycerophosphocholines, glycerophosphoglycerols, and eicosanoids such as prostaglandin E2 (Yanes et al. 2010). Eicosanoid specific signaling pathway inhibitors where used such as desaturase inhibitors sesamin, a selective inhibitor of 5Δ desaturase; curcumin , an inhibitor of 5Δ and 6Δ desaturase, COX inhibitors (SC236, a selective COX-2 inhibitor; SC560, a selective COX-1 inhibitor, LOX inhibitors AA-861 and BW-A4C, selective 5-LOX inhibitors and a Ca^{2+}-dependent PLA2 inhibitor PTK (palmityl trifluoromethyl ketone) to promote maintenance of pluripotent state in mESCs when cultured in neuronal differentiation conditions (Yanes et al. 2010). Inhibition of these pathways successfully stimulated the pluripotent state of ES cells, delaying the loss of Nanog and Oct4 expression (Yanes et al. 2010). Additionally, the levels of unsaturated fatty acid metabolites were lower in iPS compared to ES cells (Panopoulos, Yanes et al. 2012).

Furthermore, the metabolites involved in the S-adenosyl methionine (SAM) cycle, such as SAM, 5′-methylthioadenosine, hypoxanthine and inosine, important for transmethylation reactions, such as DNA methylation, were all significantly elevated in iPS, compared to ES cells (Panopoulos et al. 2012). Recently, the threonine (Thr) metabolism was also shown to regulate intracellular SAM levels and histone methylation, such that depletion of Thr from the culture medium or knockdown of threonine dehydrogenase (Tdh) in mES

cells decreased SAM accumulation and trimethylation of histone H3 lysine 4 (H3K4me3), leading to slowed growth and increased differentiation (Shyh-Chang *et al.* 2013). Tdh expression levels have been shown to be more abundant in mESCs than in MEFs (Wang *et al.* 2009, Shyh-Chang et al. 2013), and Tdh inhibition was shown to abolish mESC growth. The importance of Tdh consists in converting Thr into both glycine and acetyl-CoA (and also NADH), which appears to optimize the synthesis of SAM to maintain a high SAM/S-adenosylhomocysteine ratio (Shyh-Chang et al. 2013). Moreover, Thr provides glycine for purine biosynthesis to support rapid DNA replication.

SAM is essential for pluripotency maintenance in human ES and iPS cells and their depletion triggers demethylation of H3K4me3, global DNA demethylation, p53 signaling activation, and decreased expression of the pluripotent marker Nanog, but not Oct3/4 (Shiraki *et al.* 2014). Nonetheless, if methionine depletion is prolonged and cells are not submitted to differentiation, human ES/iPS cells undergo apoptosis (Shiraki et al. 2014).

As previously referred, the metabolic profile of ES and iPS cells is very similar, but not exactly the same. This suggests that metabolite levels have a relevant role in regulating the epigenetic changes during reprogramming.

1.4.5. Stem cell differentiation – role of mitochondrial function and ROS

During differentiation stem cells undergo a metabolic switch from glycolysis to oxidative phosphorylation. On differentiation, mitochondria from mouse and human ES cells suffer morphological and functional changes increasing the cristae number and generating an extensive reticular network of tubular structure (Cho *et al.* 2006, St John *et al.* 2006, Facucho-Oliveira et al. 2007) Recently, Zhang *et al* demonstrated that uncoupling proteins (UCP) have an essential role during differentiation. UCP2 is overexpressed in pluripotent stem cells and is repressed during differentiation, allowing the transition from glycolysis to glucose oxidation in mitochondria (Zhang et al. 2011). Ectopic UCP2 expression during early differentiation inhibits differentiation-associated genes expression and embryoid bodies' formation, impairs this metabolic transition and retards ROS accumulation. UCP2 has been postulated to be involved in shunting pyruvate out of mitochondria, blocking pyruvate oxidation in mitochondria and increasing the glycolytic flux (Zhang et al. 2011).

Another mechanism apparently involved in differentiation is ROS formation. Cells in an undifferentiated state produce minimum amounts of ROS, specially due to an uncoupled mitochondrial respiratory chain, low substrate oxidation and high expression of

antioxidant genes UCP2, SOD2 (superoxide dismutase 2) and GPX2 (glutathione peroxidase 2), which are downregulated during differentiation (Saretzki *et al.* 2008, Armstrong *et al.* 2010, Zhang et al. 2011). ROS are known to promote lineage-specific differentiation. Increasing evidences point out that an accurate endogenous ROS control is important for cardiomyocyte formation through the activity of nicotinamide adenine dinucleotide phosphate reduced (NADPH) oxidase system, which triggers for differentiation (Crespo *et al.* 2010). The p38 mitogen-activated protein kinase (MAPK) phosphorelay system seems to control this process (Crespo et al. 2010). The authors found that p38 activation is temporarily upregulated during differentiation in high glucose medium. They also reported that mitochondrial ROS have a major role in p38 activation since p38 activation was not observed during differentiation in ES cells incubated with a mitochondrial-targeted antioxidant (MitoQ). The supraphysiological glucose levels appear to induce the production of mitochondrial ROS, which in turn activates the p38 system via Nox4 downstream pathway (Crespo et al. 2010).

Spitkovsky and collaborators (2004) previously observed that mitochondrial changes are essential for cardiogenic differentiation in mES cells. The enhancement of mitochondrial biogenesis and complex III activity, which are responsible for spontaneous Ca^{2+} oscillations, are main triggers of cardiomyocyte differentiation (Spitkovsky *et al.* 2004).

Differentiation induction leads to profound remodelling of mitochondrial morphology and activity. Some studies have shown that proteins involved in fusion and fission machinery are changed in pluripotent cells compared to their differentiated counterparts. Wang and collaborators (2014) demonstrated that Dynamin-related protein 1 (Drp1, a member of the Dynamin family of large GTPases that controls the final part of mitochondrial fission) is not critical for mitochondrial biogenesis in stem cell proliferation, but is required for neurogenesis, since it delays the reduction of Nanog and Oct4 during differentiation (Wang *et al.* 2014). The authors proved that knockdown of Drp1 has no effect on mitochondrial membrane potential, proliferation nor pluripotency of ES cells (Wang et al. 2014). Similar results were obtained with Drp1 inhibitors to prevent mitochondrial division resulting in an increased differentiation and consequently disruption of the self-renewal of iPS cells (Vazquez-Martin *et al.* 2012). Gene knockdown of the mitochondrial protein growth factor erv1-like (Gfer) in mESCs lead to decreased levels of pluripotent markers (Nanog, Oct4, SSEA), which was associated with an upregulation of Drp1 (Todd *et al.* 2010). Cardiac differentiation of stem cells was also associated with downregulating of genes involved in mitochondrial fission or inhibition of fusion, including Drp1 by

approximately 40%, mitochondrial protein 18 kDa by approximately 66%, optic atrophy type 1 (Opa1) by approximately 34%, while mitofusin2 (Mfn2), linked to mitochondrial fusion, was upregulated by approximately 272% (Chung *et al.* 2007). Although little is known about the impact of mitochondria fusion/fission dynamics on the acquisition and maintenance of stem cell pluripotency, these studies shed some light in this mechanism, highly suggesting that reprogramming and/or differentiation processes are dependent on genes that influence mitochondrial morphology.

A study concerning osteoblasts differentiation from human mesenchymal stem cells found that mitochondrial respiratory function was enhanced in several aspects, including an increase in mtDNA copy number, protein levels of respiratory complexes subunits and oxygen consumption rate (Chen *et al.* 2008). Mitochondrial biogenesis regulators genes such as mitochondrial transcription factor A (TFAM), peroxisome proliferator-activated receptor-c coactivator-1α (PGC-1α) and DNA polymerase γ (POLG) were also upregulated following differentiation (Chen et al. 2008). Nonetheless, when the intracellular ROS levels were examined both superoxide anions and hydrogen peroxide were significantly decreased in the beginning of differentiation though increased aerobic metabolism. Concomitantly, a notorious upregulation of antioxidant enzymes SOD2 and catalase ensured a proper redox environment for cell differentiation by preventing excess ROS and thus oxidative stress (Chen et al. 2008). These mechanisms can be extremely controversial and depend on the type of stem cells, the spontaneous or specific differentiation, as well as the level of differentiation. Prigione and colleagues (2010) found that the expression of biogenesis factors, including POLG, TFAM, and PGC-1α, was induced in undifferentiated iPS cells compared to somatic fibroblasts, in agreement with the array data, and mostly decreased upon differentiation into fibroblast-like cells (Prigione et al. 2010). During spontaneous differentiation the protein expression of TFAM, PGC-1α, and nuclear respiratory factor-1 (NRF-1) was slightly increased in the undifferentiated hES cells, compared to their differentiated counterparts (Cho et al. 2006). The factors essential for mitochondrial biogenesis (TFAM, POLG and NRF1) seem to be upregulated in undifferentiated cells and this may represent a nuclear response to decreased content of mitochondrial DNA, observed before in somatic cells depleted of mtDNA (Holmuhamedov *et al.* 2003, Lloyd *et al.* 2006{Holmuhamedov, 2003 #637)). Concordantly, disruption of mitochondrial function during differentiation by CCCP (carbonyl cyanide m-chlorophenylhydrazone) lead to an abnormal transcription in the expression of HOX genes both in mouse and hES cells (Mandal *et al.* 2011).

Moreover, Schieke and collaborators (2006) demonstrated that there is a link between intrinsic mitochondrial function and stem cell fate. Cells exhibiting low ΔΨm were more prone to undergo mesodermal differentiation and more resistant to teratoma formation, whereas cells retaining high ΔΨm behaved the opposite way (Schieke *et al.* 2008). Regulation of mitochondrial oxidative capacity and function seems to be under the control of the mTOR signaling pathway. Indeed, manipulating mTOR signaling and mitochondrial function affected ES cell differentiation and pointed out to a central role of the mTOR-mitochondria axis in ES cell biology. An interaction between mTOR and PGC-1α was previously described, suggesting that differences in mitochondrial biogenesis might be a potential explanation (Cunningham *et al.* 2007). A common target of mTOR and PGC-1α is the transcription factor yang 1 (YY1) whose function is controlled by mTOR and is recruited to the promoter regions of the genes encoding PGC-1α and cytochrome c (Cunningham et al. 2007). The fact that mitochondria are in a less-functional hyperpolarized state helps to maintain low levels of ROS in stem cells, fundamental for retaining the capacity for self-renewal.

As described before, ES cells have higher expression levels of antioxidant enzymes than differentiated ones, whereas an incremental level of ROS induces differentiation. ES cells also maintain high levels of telomerase activity, protecting telomerase shortening, which is reduced upon differentiation (Saretzki et al. 2008). A high telomerase activity was associated with antioxidant defence and DNA repair in mESC (Saretzki et al. 2008). Telomerase shortening are enhanced by ROS production and surprisingly it started rising only 2 and 3 weeks after the differentiation process, indicating that the fast telomere shortening during the 1st week must be caused by some other mechanism(s), most likely adaptation to telomerase loss (Saretzki et al. 2008).

1.4.6. Mitochondrial modifications and stem cell biology – current knowledge in neurological disorders

The iPS cell technology has an enormous potential and their applications are immense, covering pathological studies, drug screening, and cell-replacement therapy development. Mitochondria have a pivotal role in stem cells reprogramming and during differentiation, as described before in this review. Moreover, mitochondrial dysfunction has been

associated with the pathogenesis of several neurological disorders such as Alzheimer's (AD), Parkinson's (PD) and Huntington's diseases (HD), amyotrophic lateral sclerosis, schizophrenia and bipolar disorder.

Schizophrenia has been defined as a neurodevelopmental disease that causes impairments in several cognitive domains, including memory, executive functions, attention, motor abilities and spatial functions, leading to a mental deterioration (Heinrichs *et al.* 1998). Most individuals with schizophrenia have a disruption of fundamental neural circuits encircling cortical-cerebellar-thalamic-cortical subsystems (Andreasen *et al.* 1998). Altered cell respiration, elevated levels of oxidative stress and an impaired oxidative stress response has been reported in peripheral and central tissues of schizophrenia patients (Yao *et al.* 2004). Recently, several groups reprogrammed skin fibroblasts from schizophrenic patients into IPS cells and successfully differentiated them into neuronal lineages. Robicsek and collaborators (2013) reprogrammed iPS cells from hair follicle keratinocytes, which were then differentiated into β3-tubulin+/tyrosine hydroxylase+/DAT+dopaminergic neurons. Schizophrenia-derived dopaminergic cells showed impaired ability to differentiate, while glutamatergic cells were unable to maturate. Interestingly, abnormalities were found in protein levels of mitochondrial respiration (complex I) and mitochondrial network dynamics (Rosenfeld *et al.* 2011, Robicsek *et al.* 2013). Another group observed that neural precursor cells from schizophrenic patients presented increased levels of ROS, which could be a consequence not only of an aberrant production of ROS, but also of an impaired regulation of antioxidant responses (Paulsen Bda *et al.* 2012). Moreover, other researchers detected that SZ iPS cells NPCs show abnormal gene expression and protein levels related to cytoskeletal remodeling and oxidative stress, leading to aberrant migration and increased oxidative stress (Brennand *et al.* 2014).

Friedreich's ataxia (FRDA), another frequent neurodegenerative disorder, is an autosomal recessive multisystem disorder characterized by neurodegeneration and cardiomyopathy (Gomes *et al.* 2013). The disease is caused by reduced levels of frataxin, an essential mitochondrial protein involved in iron-sulfur cluster synthesis (Campuzano *et al.* 1996). Most patients are homozygous for a GAA triplet repeat expansion within the frataxin (FXN) gene (Campuzano et al. 1996), which leads to partial silencing frataxin transcription. The normal gene has up to 40 GAA repeat, while disease-associated alleles enclose 100–1000 GAA repeats (Campuzano et al. 1996). Depletion of frataxin mainly leads to mitochondrial dysfunction and increased sensitivity to oxidative stress, as well as

impairment of Fe-S cluster-containing proteins and altered cellular iron metabolism, (Schmucker and Puccio, 2010). Recently, iPS cell lines were generated from Friedreich ataxia patients and differentiated into neuronal and cardiac lineages.(Ku *et al.* 2010, Liu *et al.* 2011, Eigentler *et al.* 2013, Hick *et al.* 2013). These cells retained expanded GAA repeats and expressed reduced frataxin levels, epigenetic changes and repeat instability, although no evidence of Fe-S cluster biogenesis defects was observed. IPS cells-derived cardiomyocytes and neurons presented a delay in maturation and lower mitochondrial membrane potential (Ku et al. 2010, Eigentler et al. 2013, Hick et al. 2013).

Several research groups were able to produce patient-specific dopaminergic (DA) neurons from iPS cells derived from patients afflicted by PD, a neurodegenerative disorder characterized by selective degeneration of dopaminergic neurons in the *substantia nigra pars compacta* (Byers *et al.* 2011, Devine *et al.* 2011, Nguyen *et al.* 2011, Seibler *et al.* 2011, Soldner *et al.* 2011, Imaizumi *et al.* 2012, Jiang *et al.* 2012, Sanchez-Danes *et al.* 2012). A study performed in two PARK2 patients carrying parkin mutations has shown abnormal mitochondrial morphology and aberrant tubulovesicular organelle structures adjacent to the Golgi in PARK2 iPS-derived neurons, but not in normal iPS cells (Imaizumi et al. 2012). The authors also found increased oxidative stress and lower levels of GSH in PARK2 iPS cell-derived neurospheres (Imaizumi et al. 2012). Nguyen and collaborators (2011) generated iPS cells that carry the mutation in the leucine-rich repeat kinase-2 (LRRK2) gene and reported increased activation of oxidative stress-response genes and enhanced α-synuclein protein expression, as well as increased sensitivity to caspase-3 activation and cell death following exposure to stress agents (Nguyen, Byers et al. 2011). Cooper and collaborators (2012) generated iPS cells from PD patients carrying mutations in PTEN-induced putative kinase 1 (PINK1) and LRRK2 genes and also observed an increased vulnerability to cellular oxidative stress (Cooper *et al.* 2012).

Folmes et al. (2013) generated iPS cells from a patient with mitochondrial encephalomyopathy with lactic acidosis and stroke-like episodes (MELAS) that represents a prototypical metabolic derangement due to a high heteroplasmy burden at position G13513A (Folmes *et al.* 2013). MELAS fibroblasts demonstrated stable heteroplasmy with 53% wild-type sequence and 47% G13513A sequence, compared to control fibroblasts (Folmes et al. 2013). Cells derived with 50% heteroplasmy and devoided of mutated mtDNA at the disease-causing position in the ND5 subunit of respiratory chain complex I maintained their genotypes throughout lineage specification and differentiation (Folmes et al. 2013).

For HD several iPS cell lines have been specifically generated since the HD iPSC Consortium was created (HTTp://www.ninds.nih.gov/funding/areas/neurodegeneration/iPSC_Executive_Summary.htm). HD patient-derived iPS cell lines exhibited mild instability of the expanded CAG repeat allele with passage or after differentiation. Neural progenitor cells (NPCs) exhibited changes in cytoskeleton, adhesion and energetics that were correlated with the number of CAG repeats. In a cluster formation assay HD NPCs showed significantly decreased cell-cell adhesion properties and reduced intracellular ATP/ADP ratio. Those lines where successfully differentiated into forebrain cell types and DARPP-32-positive neurons presenting disease-associated changes in electrophysiology, metabolism, cell adhesion and cell death for lines with both medium and longer CAG repeat expansions. Higher CAG expansion neural cultures were shown to be more susceptible to acute noxious stimulus. Upon BDNF removal there was increased cell death, as demonstrated by an increase in caspase 3/7 activity; conversely, addition of four times the normal concentration of BDNF could partially rescue this deleterious phenotype. Handling of intracellular Ca^{2+} levels was also impaired following a glutamate stimulus in the higher CAG expanded line. Other toxic stimulus, such as hydrogen peroxide (to induce oxidative stress) and 3-methyladenine (3-MA) (autophagy inhibition) increased cell death in the HD lines. Thus, HD iPS cells are more prone to cell death, as demonstrated after the withdrawal of trophic support, or following the addition of glutamate, or other cell stressors.

Moreover, genetic correction of CAG repeat in iPS cell lines revealed a reversion in disease phenotypes, including a decrease in the susceptibility to cell death and altered mitochondrial bioenergetics. In the genetically corrected-derived NSCs the authors also found normalization in the levels of BDNF. The manipulated HD-iPS cells derived NSCs were transplanted into the striatum of HD mouse model brains; the cells underwent differentiation *in vivo* to DARPP-32-expressing neurons and glial cells two weeks after grafting (An *et al.* 2012). These data suggest that genetically corrected cells are able to efficiently populate the mouse striatum and place us closer to generate autologous cells for cell-replacement therapy (An et al. 2012).

1.5.Therapeutic strategies in HD

1.5.1.Genetic strategies

1.5.1.1.Gene addition

To replace the missing function of a gene a site-specific gene addition into a predetermined endogenous locus in human cells can be performed. Gene insertion methods intent to deliver DNA fragments such as cDNA or shRNA for overexpression. This procedure frequently results in random insertion into the host genome generating, as a consequence, a partial or complete silencing of the transgene suggesting a promoter inactivation or methylation, which has been described for stem cells, or an insertional mutagenesis leading to genome instability and toxicity can also occurs (Cavazza *et al.* 2013). The first successful gene transfer was in SCID-X1 where *ex vivo* retroviral gene transfer of the γc-chain (cytokine receptors) to autologous HSC (CD^{34+} bone marrow cells) was achieved (Cavazzana-Calvo *et al.* 2000). Later, gene engraftment of multipotent hematopoietic stem cells resulted in ADA transgene expression in lymphocytes and red blood cells restoration the immune function (Aiuti *et al.* 2009).

In HD, genetic data, in humans and transgenic animal models, suggest that HTT can act synergistically by conferring deleterious gain-of-function on the target proteins and also by loss-of-function effects secondary to reduction in wtHTT expression. Overexpression of the protein may contribute for ameliorate disease phenotype although evidences are not so convincing (Luo *et al.* 2009, Parsons *et al.* 2014).

1.5.1.2.Silencing

Since the seminal work done by Fire and Mello in 1998 about interfering RNA (RNAi) a lot has been done to improve this technique and use it in clinic applications (Fire *et al.* 1998). RNAi is a double-strand RNA (dsRNA) that induces degradation of a target protein mRNA by activating the RNA-interfering silencing complex (RISC). RNAi can be deliver as short dsRNAs that have complete complementarity to a target mRNA or most frequently introduced in the form of a vector based short hairpin RNA which consists of a sense sequence about 21-23 bases long followed by a six to eight base non-complementary loop and another 21 base sequence complementary to the sense sequence (Brummelkamp *et al.* 2002). This double strand RNA is synthesize in the nucleus of cells, processed by

Drosha, a ribonuclease (RNase) III, and translocated into the cytoplasm where Dicer, a RNase II, chops into short interfering RNA (siRNA). After incorporation into the RISC, the guide strand has to be selected by Ago2, which contains endonuclease activity to cleave the passenger strand, dissociating it from the complex. The activated RISC is then target to the complementary mRNA leading to degradation originating a post-transcriptional gene silencing mechanism (Lee *et al.* 2003, Rand *et al.* 2005, Gonzalez-Alegre 2007). This approach has shown potential applications in neurodegenerative disease, especially in targeting mutant forms of protein that leads to disease phenotype as in HD (Boudreau *et al.* 2009, Drouet *et al.* 2009), Machado–Joseph disease (Alves *et al.* 2010), AD (Nilsson *et al.* 2010) or PD (Sapru *et al.* 2006). In a recent study, RNA interference of mHTT expression mediated by virus vector delivery of short hairpin RNAs (shRNAs) ameliorated early-stage disease phenotypes in transgenic mouse models of HD (Harper *et al.* 2005, Franich *et al.* 2008).

However, siRNA are commonly associated with undesirable side effects which include the effects caused by the activation of the "interferon response", the "saturation effects" and last the "off targeting effect". This latter refers to the possibility of the sh/siRNA interfere with the expression of different other transcripts. siRNA off-targeting seems to be dose dependent, thus a recommendation is to scale down as much as possible the concentration of siRNA or to chemical adjust the synthetic siRNA and its sequence (Scaggiante *et al.* 2011)

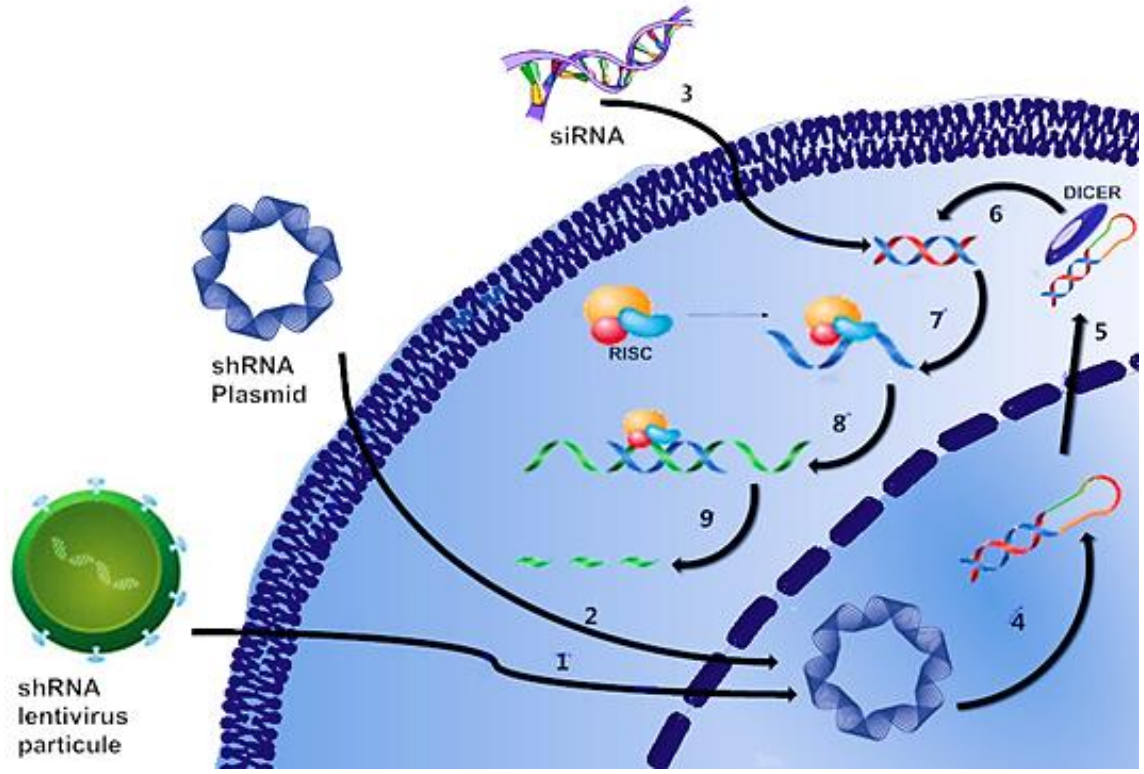

Figure 1.17.- Mechanism of RNAi silencing introduced to cells by different methods.

Another current method of gene silencing or modulation of RNA metabolism employs antisense oligonucleotides (ASOs). ASOs are a 12 to 25-mer chemically modified synthetic nucleic acids that bind and alter RNA function through an array of different mechanisms. Although in nature these sequences are rapidly target to degradation, chemical modifications confers high stability against nuclease degradation and low toxicity to these molecules (Stein *et al.* 1988). RNA manipulation can be either through the recruitment of the enzyme RNaseH for degradation or by non-degradative mechanisms where ASOs binds sterically hampering translation, 5' capping, or splicing (Bennett *et al.* 2010) (Figure 1.17). RNaseH is an enzyme that recognizes RNA–DNA heteroduplexes, cleaves the RNA strand, and releases the DNA. Non-degradative mechanisms don't involve activation of RNaseH enzyme but act by repressing translation, modulating splicing, and inhibiting microRNAs. Almost half of the genetic disorders are due to mutations that alter pre-mRNA splicing (Mills *et al.* 2012). ASOs can be design to bind pre-mRNA structure and modulate splicing, in vitro and in vivo, masking splicing enhancers and repressor sequences, inducing the skipping of one or more additional exons,

restore the transcript reading frame and restore the inclusion of alternatively spliced exons (Aartsma-Rus *et al.* 2007, Siva *et al.* 2014)

To be effective as therapeutic ASOs must reach and hybridize with target RNA without be cleaved by endogenous nucleases. Modifications to the phosphate backbone have been made to reduce the degradation and increase the tissue half-life and in the sugar ring to increase target binding affinity. The earliest changes were performed in the phosphorothioate group, through the substitution of non-bridging oxygen in the phosphate backbone with a sulfur atom. Another strategy is replacing sugar phosphate backbone for a morpholine ring. To increase binding affinity to target RNA some chemical modification of the 2' position of the sugar have been made, specially the 2'-O-methyl and 2'-O-methoxyethyl modification which allows reduce nonspecific protein binding and consequently ASOs toxicity. Locked nucleic acid is an analog of the 2'-O-methyl RNA (Southwell *et al.* 2012). Despite conferring high affinity to RNA, these modifications reduce or even completely obstruct RNaseH enzyme cleavage. To overcome this limitation a "gapmer" design was adopt where a 2'-modified residues region flanks a longer central unmodified region allowing RNaseH cleavage at the central region of the ASO.

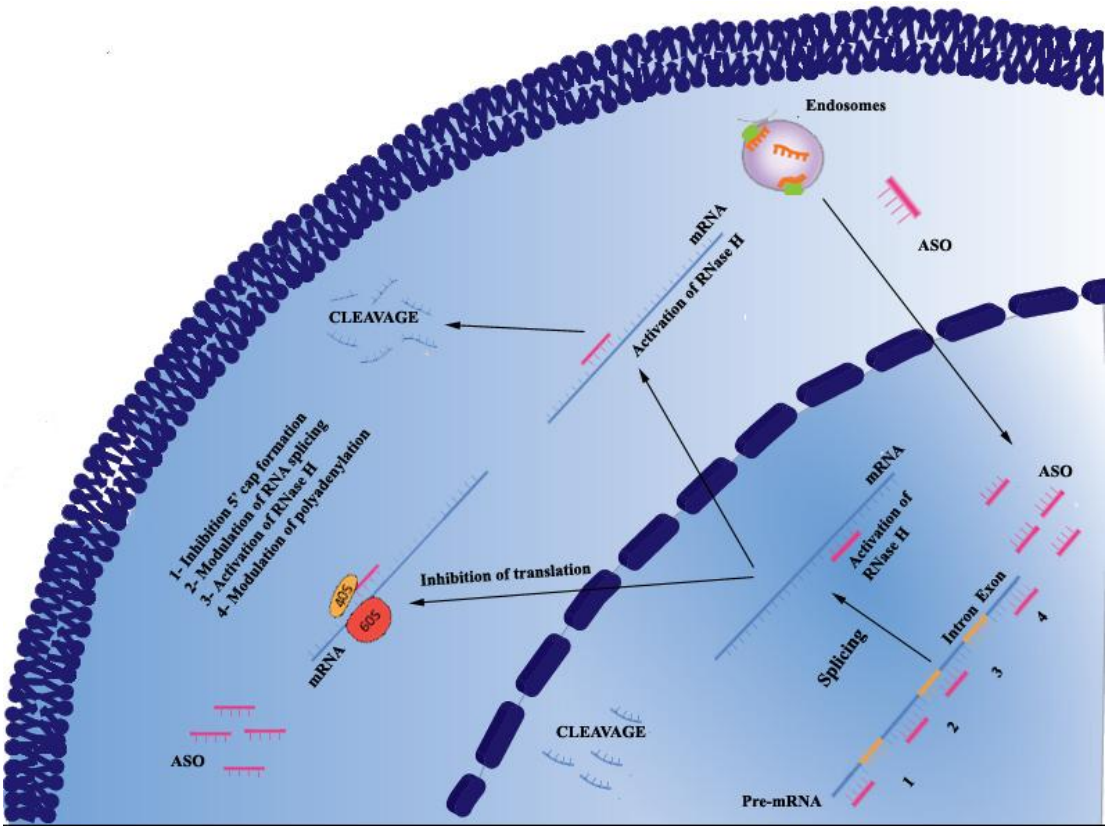

Figure 1.18.- **Antisense oligonucleotide mechanisms of action**. ASOs enter cells through plasma protein receptors on the cell surface, resulting in ASO compartmentalization into endosome. ASOs are released from the vesicles and move into the nucleus. In the nucleus, ASOs can bind directly to mRNA structures and prevent the formation of the 5'-mRNA cap, modulate alternative splicing, dictate the location of the polyadenylation site and recruit RNaseH1 to induce cleavage. In the cytoplasm binds to mRNA and sterically blocks the ribosomal subunits avoiding translation.

Since the major limitation to the systemic delivery of therapeutic AONs to the CNS is the blood-brain barrier (BBB) the most promising studies focus on intramuscular injection with AONs targeting the DMD gene. The method involves exon-skipping treatment that abolish the production of dysfunctional dystrophin in Duchenne muscular dystrophy (Endesfelder *et al.* 2005, Aartsma-Rus et al. 2007, Ferlini *et al.* 2010, Pramono *et al.* 2012). To overcome this drawback animal studies employed alternative routes of administration (intraparenchimal injections in specific brain areas, intracerebroventricular injections, intrathecal injections), sometimes administering the AONs through the use of micro-osmotic pumps (Siva et al. 2014). Assuming AONs treatment for neurogenetic disorders may require administration for a long time and repeated dosing, it would be preferable to have a less invasive administration pathway such as nasal administration that could avoid toxicity due to systemic administration (Dhuria *et al.* 2010) or extracellular

vesicles in the form of exosomes capable of crossing the BBB (Lee *et al.* 2012). Nevertheless a wide range of neurodegenerative disorders could potentially benefit from a knockdown therapeutic strategy. Theoretically all the diseases secondary to single aberrant protein can be treated with ASO. ASOs can be used in human neurodegeneration to decrease total protein, increase total protein, modulate splicing or inhibit miRNAs to modulate genes expression.

A promising treatment for a CNS-neurodegenerative disorder using ASOs targets the human SOD1 transgene in the transgenic rat model of amyotrophic lateral sclerosis (ALS) (Smith *et al.* 2006). A clinical trial is currently ongoing in ALS patients with SOD1 mutations (ClinicalTrials.gov 2009).

For HD, nonselective HTT silencing and allele-specific mHTT silencing strategies are being pursued with ASOs. Evers et cols (2011) observed a significant reduction on protein and RNA levels of HTT in patient-derived fibroblast cell lines with a preferential allele specific reduction of mutant HTT and this allele specificity was improved ASOs dose-dependent (Evers *et al.* 2011). In a recent study Østergaard et cols (2013) using RNase H active ASOs to target an SNP in the HTT gene achieved a high allele-selective downregulation of mHTT mRNA and protein in HD patient-derived fibroblasts and in the CNS of a fully humanized mouse model of HD (Ostergaard *et al.* 2013). Also a transient infusion of a human-specific HTT ASO into cerebrospinal fluid of symptomatic HD mouse models and nonhuman primates resulted in broad distribution throughout the brain. A selective 60–75% reduction of the human mHTT transgene up to 12 weeks post-infusion termination and amelioration of HD like phenotype was observed (Kordasiewicz *et al.* 2012). In BACHD mice, another full length human mHTT transgenic model, a total knockdown of HTT mRNA and protein was attained with 14 days of intracerebroventricular (ICV) infusion of ASOs. The treatment resulted in a partial recovery of motor deficits and a halting of disease progression albeit at 16 weeks post-treatment both mRNA and protein levels had returned to nearly basal levels. The therapeutic benefits extended to an additional 5 months period (Carroll *et al.* 2011). For AD, ASOs directed against the Aβ region of APP were injected intracerebroventricular or systemically in the tail vein. A decrease in Aβ APP expression and Aβ production was observed proceeded of a phenotype improvement (Chauhan *et al.* 2007, Fiorini *et al.* 2013, Farr *et al.* 2014, Farr *et al.* 2014). Another study showed that suppressing Glycogen synthase kinase 3, in 12-month-old SAMP8 mice, an AD model, with ASOs treatment, improved learning and memory, reduced oxidative stress and decreased tau

phosphorylation. (Farr, Ripley et al. 2014). RNA processing manipulation through ASOs is a particularly attractive method with great potential for treating many diseases.

RNA reprogramming can also be achieved by spliceosome-mediated RNA trans-splicing (SMaRT®) (Puttaraju *et al.* 1999, Mansfield *et al.* 2000).

The process where introns are removed from the mRNA and exons are join together to form mature mRNA is called cis-splicing and is catalyzed by the spliceosome, an enzymatic complex of many proteins and four small ribonucleoprotein particles (snRNPs): U1 snRNP, U2 snRNP, U5 snRNP and U4/U6 snRNP (Lim *et al.* 2001). A less common splicing process is trans-splicing, which occurs between two independently transcribed RNA precursors to form a composite mRNA and was suggested as a mechanism to generate new genes by retrotransposition (Bruzik *et al.* 1992). The SMaRT® approach uses constructs called pre-trans-splicing molecules (PTMs) that are engineered to bind to specific pre-mRNAs in the nucleus and generate a trans-splicing event mediated by the spliceosome. PTMs comprise three domains: (i) A binding domain, complementary to the target intron and serves to tether the PTM to a specific location within the target; (ii) a splicing domain, which contains splicing elements that are equivalent to those found in cis-splicing precursors; and (iii) a coding domain, consisting of an exon or exons that are trans-spliced to the target. The splicing domain has the purpose of maximize trans-splicing activity and usually contais potent branchpoint sequence (UACUAAC) and a long pyrimidine-rich tract. The coding sequence can be one or more, few exons or the entire coding sequence. SMaRT® act in three different ways: (i) 3' exon replacement (Puttaraju et al. 1999, Dallinger *et al.* 2003), (ii) 5' exon replacement and (Mansfield *et al.* 2003, Wally *et al.* 2008, Rindt *et al.* 2012) (iii) internal exon replacement. SMaRT® as an RNA-repair technology has been proven in a variety of models *in vitro*, *ex vivo* and *in vivo* (Liu *et al.* 2002, Chao *et al.* 2003, Pergolizzi *et al.* 2003). Recently Rindt et at (2012) demonstrate that 5' exon replacement of HTT by spliceosome mediated pre-mRNA trans-splicing can be achieved in cultured cells using a binary transfection system consisting of a HTT minigene and a pre-mRNA trans-splicing module (Rindt et al. 2012). Importantly, trans-splicing was also detected in endogenous HTT by the PTM lentivirus in fibroblasts of HD patients in the absence of minigene. Since an important part of Huntington pathology is accumulation of mutant protein, trans-splicing can effectively reduce the load by converting the mutant allele to wild-type and increasing the level of the wild-type form. The excision of an exon 1 with expanded polyQ tract results in a truncated RNA species lacking a polyadenylation signal susceptible to degradation in the nucleus.

1.5.2. Repair

1.5.2.1. Homologous recombination

As DNA is continuously exposed to damage agents, cells created their how endogenous mechanism to repair DNA double strand breaks (DSB). When complementary stands of the DNA helix breaks at sites close enough from each other that base-pairing and chromatin structure are insufficient to keep the two DNA ends juxtaposed and DSB are generated. Two main largely distinct and complementary pathways for DNA DSB repair coexist in cells —homologous recombination (HR) and non-homologous end-joining (NHEJ) (Jackson 2002). During HR, the damaged chromosome enters into synapsis with an undamaged DNA molecule with which it shares extensive sequence homology and will be used as template. This method can be used to manipulate the human genome, replace or modify specific chromosomal regions, or insert reporters and genes in specific promoter locations (Capecchi 1989). Spontaneous DSBs often occur, whereas artificial DSBs are introduced by irradiation or site-specific endonucleases (Yajima *et al.* 2013). The efficiency of HR is extremely low in mammalian around 10^{-6} to 10^{-7} and this process can only allow efficient correction of mutations within a ≈200-bp window surrounding the break. To improve efficiency and reproducibility of this technique reporter cell lines can be generated with the help of gene-editing technology as engineered nucleases, chimeric restriction endonucleases, homing endonucleases and 'chemical' nucleases.

1.5.2.2. Zinc finger nucleases

Restriction endonucleases and modification methylases are simple bacterial enzymes that recognize specific sequences in duplex DNA. Zinc-finger nucleases (ZFNs) are hybrid restriction enzymes that cut DNA at any preferred site and result of the fusion of zinc finger proteins (ZFP) to the cleavage domain of *Fok I* endonuclease (Kim *et al.* 1996). These chimeric endonucleases are inactive as monomers and interact through their cleavage domains (Figure 1.19).

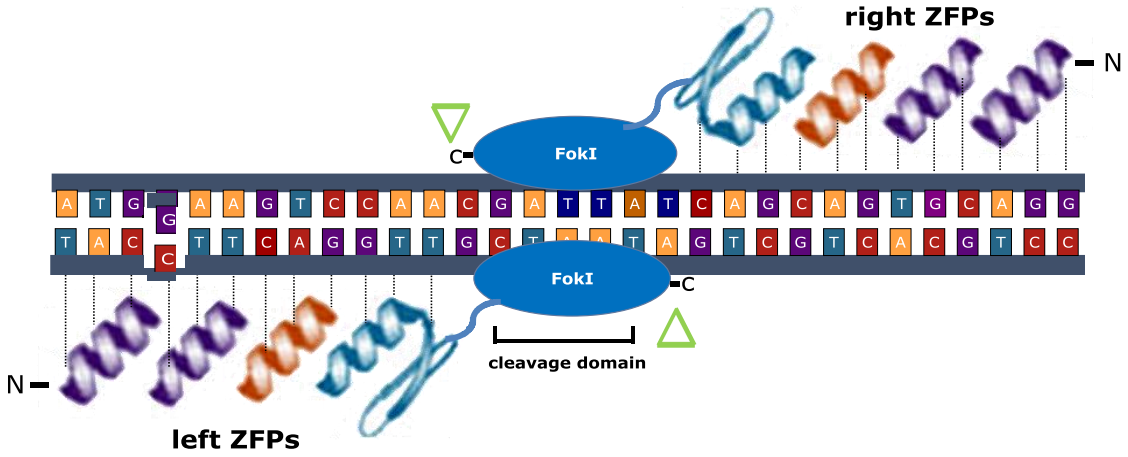

Figure 1.19. - DNA cleavage site recognition by zinc-finger nucleases (ZFNs). ZFN dimer is bound to a DNA target. Each ZFN is a synthetic protein consisting of an engineered zinc finger DNA-binding domain fused to the cleavage domain of the FokI restriction endonuclease.

Cys2His2 zinc fingers ("zinc fingers") define the most common transcription factor family in organisms ranging from yeast to humans (Razin *et al.* 2012). The DNA-binding domain is derived from the C2H2 motif of ZFP, holding 28 amino acids length including an α helix that can specifically bind 3 DNA nucleotides. Each ZF motifs recognizes 3–4 base pairs and binds via the α-helix into the major groove of the DNA double helix. These modules are rearranged in a specific order necessary to recognize a given sequence in a target locus. Each individual ZFN contains three-finger modules recognizing up to 18 bp binding site specific enough to just bind a single location in the genome (Liu *et al.* 1997). The complete target sequence thus consists of two 9-18 bp binding sites in opposite orientation separated by a 6-bp spacer (Liu et al. 1997). More recently a two DNA-binding domains, each containing four zinc-finger motifs and thus recognizing a total of 24 bp was assembled and proved to be highly specific in DNA cleavage and exhibited decreased cytotoxicity (Urnov *et al.* 2005). The construction of 'artificial' DNA-binding proteins that can bind the 64 possible DNA triplets would allow the selection of zinc finger that could be linked in tandem to target DNA sequences. Theoretically this system can increase the efficiency of gene targeting at a specific locus. This approach can be useful for gene disruption in model organisms for generate knockout animals or in mammalian somatic cell genetics, particularly in human ES cells, in which the ZFN can be transiently expressed. Also associated to HR can be a powerful tool for genome editing and further correction or for specific and stable ZFN-mediated gene addition (Urnov *et al.* 2010). A major concern about the therapeutic approach with technique is its specificity. In general

'off-target' cleavage – in which ZFNs might destroy or injure unexpected regions in the human genome without detection- can lead to reduced efficiency of on-target modification and cytotoxicity (Olsen *et al.* 2010).

This method was efficiently used to target three genes in human pluripotent cells (Hockemeyer *et al.* 2009). Two reporter genes were successfully added to hiPSCs and hESCs (OCT4, PITX3) and a transgenes was inserted into the AAVS1 locus to generate a robust drug-inducible overexpression system (Hockemeyer et al. 2009). Reinhardt et al also resorting to this technique reprogrammed iPSCs from PD patients where a correction vector was cotransfected with ZFNs designed to introduce a double-strand break adjacent to the G2019S mutation of the LRRK2 gene (Reinhardt *et al.* 2013).

1.5.2.3.TAL effectors

Transcription activator-like effector nucleases (TALEN) are artificial design nucleases targeting specific DNA and like ZFN capable of creating DSBs in the genome. These nucleases result from the fusions of the *FokI* cleavage domain and DNA-binding domains derived from TALE proteins. TALEs contain multiple 33–35-aminoacid repeat domains that each recognizes a single base pair. Different repeat types recognize different DNA base pairs. The repeats can be ordered to yield TALEs with desired DNA specificity. Members of this effector family are highly conserved and differ mainly in the amino acid sequence and number of repeats. As TALEs are large molecules, Miller et al. designed and synthesized truncated forms of the protein. Concluded that the most active combination of 63-bp C terminus and a 14–18-bp spacing allows higher cleavage efficiency (27%) comparable to ZFN (Miller *et al.* 2011) (Figure 1.20).

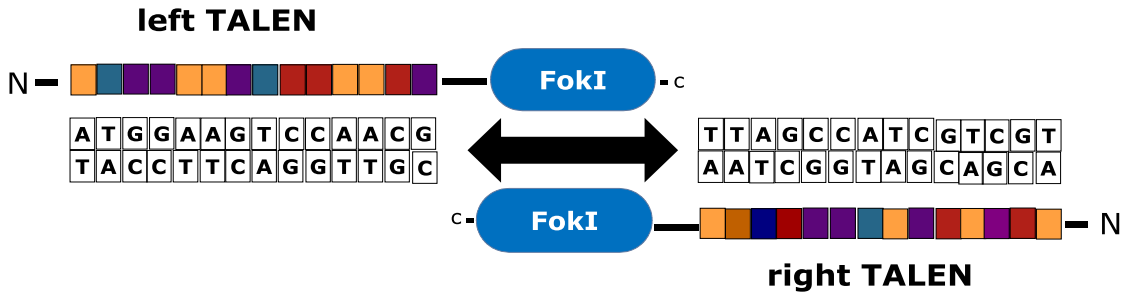

Figure 1.20. - TALE nuclease with 63 or 28 amino acids in C terminus and FokI endonuclease domain. TALE nuclease dimer bound to DNA and upon FokI dimerization DNA cleaveage occurs.

As TALENs function as dimers, pairs can recognize 32- to 40-bp DNA sequences. Recently, Hockemeyer et al generated hESC and iPSC single-cell-derived clones carrying transgenic cassettes solely at the TALEN-specified location with similar efficiency and precision as do zinc-finger nucleases (Hockemeyer *et al.* 2011). Resorting to TALENs, modification of livestock embryos genome was achieved, more precisely KO of genes and large chromosomal rearrangements (Carlson *et al.* 2012).

1.5.2.4.Crispr/CAS

The type II prokaryotic CRISPR was first discovered in 1987 in Escherichia coli (Ishino *et al.* 1987). This bacterial adaptive immune systems known as clustered regularly interspaced short palindromic repeats (CRISPR) and CRISPR associated (Cas) systems uses a combination of proteins and short guide RNAs to recognize and cleave complementary DNA sequences and works as a mechanism to defend against viruses and foreign DNA. CRISPR are found in most archaeal (~90%) and bacterial (~40%) genomes (Horvath *et al.* 2010). Are clusters of short DNA noncontiguous repeats separated by nonhomologous variable sequences called spacers found at regular intervals and are often adjacent to Cas genes. CRISPR in combination with Cas proteins, forms the CRISPR/Cas systems. In type II systems consist of just four Cas genes, where Cas9 is always present. Cas9 is a large protein that includes two nuclease domains and provides the enzymatic machinery required for the acquisition of new spacers from invading elements and posterior destruction. The integration of those short sequences (usually 23 and 47 bp in length) from foreign genetic elements into repetitive genetic elements provides resistance to bacteria. This process comprises three stages. The first is adaptation, where foreign DNA is recognized, and a fragment of this DNA inserted as a new spacer into a host CRISPR array. A short conserved sequence called the protospacer adjacent motif (PAM), flanks the spacer sequence in the viral genome and determines the targets of most CRISPR/Cas systems. In the second occurs the transcription of a CRISPR cluster into a long precursor-crRNA (pre-crRNA). This process is dependent on a trans-activating crRNA (tracrRNA), a 25 nt long stretch complementary to the crRNA repeat, encoded in the environs of CRISPR loci. Cas9 binds to tracrRNA:crRNA complex, which forms a RNA duplex that are substrates for endonuclease RNase III. Cleavage of this duplex generates short CRISPR RNAs (crRNAs). Transcription is controlled by promoter located within the

leader sequence that contains promoter elements and possible binding sites for regulatory proteins. In the final stage, the interference reaction, Cas protein complex use these mature crRNAs to target the viral foreign RNA by complementarity and degrade (Garneau *et al.* 2010, Richter *et al.* 2012, Richter *et al.* 2013) (Figure 1.21).

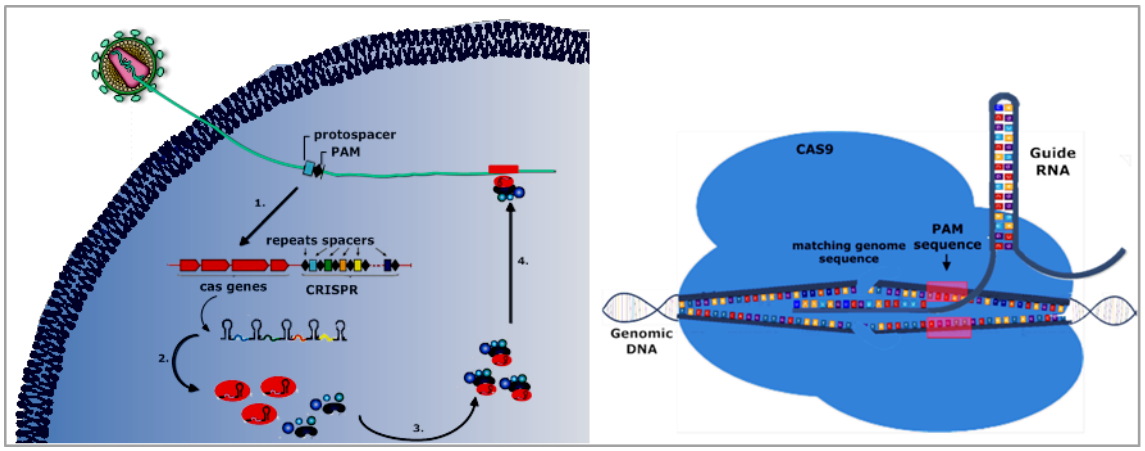

Figure 1.21.- A) The CRISPR/Cas system proteins can target and cleave invading DNA in a sequence-specific manner. CRISPR–Cas systems function in three steps: adaptation or immunization (involving the acquisition of spacers), biogenesis of CRISPR RNA (crRNA; encoded by the repeat–spacer regions) and interference (cleavage of invading nucleic acid). **B) RNA-guided gene targeting in human cells involves a C terminus nuclear localization signal with guide RNAs (gRNAs) expressed from the human polymerase III promoter.** The protospacer-adjacent motif (PAM) targets the correct genomic sequence.

Cas9 is an essential player in the CRISPR system as genome editing tool. To engineer the type II bacterial CRISPR system a specific small guide RNA (sgRNA), which is designed to resemble crRNA:tracrRNA sequence, is fused to Cas9 as well as an eukaryotic nuclear localization signal (NLS) and a promoter. The sgRNA expression plasmid contains the PAM sequence. The resulting ribonucleoproteins are termed RNA Cas9 guided endonucleases (RGENs) and can target single genes or multiple genes enabling efficiently and site-specific editing of the DNA sequence (Jiang et al. 2012, Wiedenheft *et al.* 2012, Mali *et al.* 2013, Richter et al. 2013). This system generates a DSB in the target DNA which can be repaired by HR or NHEJ, being the first process preferential for gene repair.

Subsequent studies used this process to generate disease models by introducing precise point mutations in two target genes allowing to generate, in one-step process, animals with multiple gene mutations (Li *et al.* 2013, Wang *et al.* 2013).

The advantageous of this system is that only by changing the sgRNA and maintain the CAS9 protein unchanged several targets can be aimed. A single vector can also accommodate multiple sgRNAs that will be processed as individual RNAs targeting different sites in the genome (Cong *et al.* 2013).

A few studies revealed that gene- editing tools can be useful to creating wild-type versus mutant cell lines. Some monogenic disease iPSCs lines were "cured" and hence the reverse of phenotype when compared to "non corrected" cells. A HD iPSCs cell line mentioned previously with 72 polyglutamine was genetic corrected by HR resulting in a 21 polyglutamine repeats carrier (An et al. 2012). These cells were successfully differentiated into DARPP-32-expressing striatal neurons as well as some of the HD-iPSCs features described previously (Zhang *et al*. 2010) were corrected, such as altered mitochondrial deficits, lower levels of BDNF, altered cadherin and TGF-β signaling (An et al. 2012).

1.5.3. IGF-1 as a potential therapeutic drug

The insulin-like growth factors, including IGF-1, IGF-2, and insulin, belong to the insulin-like peptide hormone superfamily which are single-chain polypeptides that share a similar secondary structure, with three α-helixes and three disulphide bonds. IGF-1 exerts its action through interaction with the IGF-1 receptor (IGF1-R) although may interact with insulin and hybrid receptors. IGF-1-triggered cellular responses are essential for the regulation of tissue formation and remodeling, bone growth, prenatal growth, brain development, and muscle metabolism (Laviola et al. 2008).

IGF1-R is highly expressed within the brain and is essential for normal brain development. In the rat brain, a widespread localization with distinct distribution patterns was found. The higher concentration is in regions related to olfaction, autonomy, and sensory processing, as well as in the pituitary gland, where they are involved in the regulation of growth hormone release (Werther et al. 1989). IGF-1 appear to be involved in enhancing nerve cell metabolism (Bondy *et al.* 2002) and modulate neuronal excitability (Carro *et al.*

2000) promoting antiapoptotic actions, and protect nerve cells against insults (Carro *et al.* 2003).

Upon IGF-1 binding, tyrosine kinase of the IGF-IR is activated, resulting in autophosphorylation of tyrosines on the intracellular portion of the β-subunit including tyrosine residues in the juxtamembrane and COOH-terminal domains. The phosphorylated tyrosine 950, in the juxtamembrane domain, acts as docking site for several receptor substrates, including the insulin receptor substrates and Shc proteins thus initiating phosphorylation cascades. Phosphorylated IRS-1 can activate the p85 regulatory subunit of PI3K, leading to activation of several downstream substrates, including Akt. Subsequently the protein synthesis is enhanced through mTOR and p70 S6 kinase activation and triggers the antiapoptotic effects of IGF-IR through phosphorylation and inactivation of Bad. Another downstream pathway that can be activated is through the recruitment of Grb2/SOS by phosphorylated IRS-1 or Shc. It recruits Ras and activates the Raf-1/MEK/ERK pathway and downstream nuclear factors, resulting in the induction of cell proliferation (for review, (Laviola et al. 2008) (Figure 1.22).

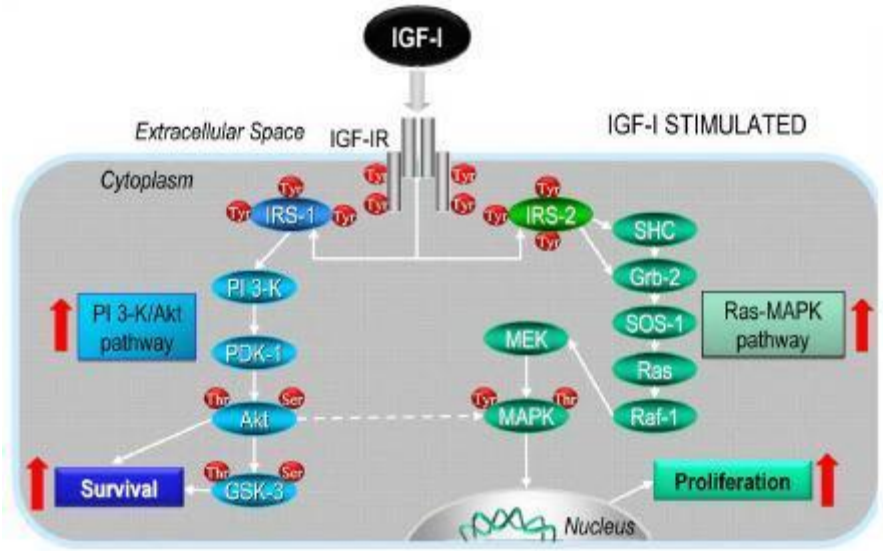

Figure 1.22.- Transduction of signals and biological actions induced by insulin or IGF-1 through their receptor. Adapted from (Laviola *et al.* 2008).

The downstream phosphorylation of Akt by IGF-1 appears to be involved in the regulation of glucose transport via the facilitative GLUT4 and glycogen synthesis in peripheral tissues and nerve process membranes in the normal developing brain (Cheng et al. 2000). Another target of insulin/IGF signaling via Akt in the brain is GSK3 since it was a major colocalization of its phosphorylated form with abundant glycogen stores specifically in IGF-I-expressing neurons suggesting that IGF-I acts in an autocrine manner to promote glucose uptake and storage as glycogen in developing projection neuron (Cheng et al. 2000).

Modifications in IGF-1/Akt pathways were described in HD. Recent evidences demonstrate that Akt is cleaved into an inactive form by caspase-3 leading to a downregulation of this survival pathway (Colin *et al.* 2005). Previously, was shown that HTT is phosphorylated on serine-421 by Akt and this exerts a protective effect against the toxicity of polyglutamine-expanded huntingtin (Humbert *et al.* 2002, Pardo *et al.* 2006). Furthermore phosphorylation at S421 was reported to reduce the nuclear accumulation of huntingtin. The nuclear fragments of mutant huntingtin depend on cleavage at amino acid 586 by caspase-6 and thus phosphorylation at S421 reduces its cleavage and consequently its nuclear targeting and also the total cellular level of full-length huntingtin (Warby *et al.* 2009). Those evidences lead to an increase attention of IGF-1 role in preventing and rescuing the damage of striatal neurons. Duarte et al (2011) demonstrated that peritoneal infusion of IGF-1 partially restored plasmatic levels of IGF-1 in R6/2 mice and reverse metabolic defects (weight loss and impaired glucose tolerance) and improved animal behavior, reflected on paw clasping scores (Duarte *et al.* 2011). Although these data suggests a favourable role for IGF-1 in HD, conflicting results were published. Pouladi et al (2010) showed that YAC128 mice have increased levels of IGF-1 and correlate directly with increased body weight (Pouladi *et al.* 2010). Moreover, in HD patients high plasma IGF-1 was associated with cognitive decline (Saleh *et al.* 2010) and additionally, in R6/2 mice, higher levels of insulin receptor substrate 2 was related with reduced lifespan and increased neuronal oxidative stress and mitochondrial dysfunction (Sadagurski *et al.* 2011). However, activation of IRS2 in mutated exon1-expressing cell lines induced the clearance of accumulated mHTT through a mTOR-independent macroautophagy pathway (Yamamoto *et al.* 2006).

More evidences were reported in other medical conditions. IGF-1 has been suggested to exert protective role against stroke in rats when administered intracerebroventricularly (Lin *et al.* 2009, Liu *et al.* 2009), intranasal administration in spinocerebellar ataxia-1 mice

rescues motor phenotype (Vig *et al.* 2006) and was shown to down regulate glial activation and induces expression of endogenous growth factor with anti-depressant activity therefore reducing depressive-like behavior (Park *et al.* 2011)

1.6. Hypothesis and specific aims of the present work

HTT, a large and ubiquitously expressed protein, when mutated, is responsible for the appearance of a devastating neurodegenerative disease - HD. Although recent findings have enlightened the pathophysiological pathways surrounding its mechanisms and clinical features much is still unknown about the trigger event(s). This thesis focuses on clarify some pathological mechanisms involved in the disease development but also identify possible therapeutic targets and therapeutic approaches aiming to rescue MSN from neurodegeneration and death *in vivo* and *in vitro.*

We divide this study in three approaches. The first aimed to evaluate the possible protective role of IGF-1 pathways against behavior impairment in HD and mechanisms of action. For this purpose, we used animal models expressing full length mHTT and tested a novel methodology for administration of IGF-1 into the HD brain. Indeed, BBB is one major limitations of therapeutic success for peripheral administrated compounds and this technique can overcame this.

The second approach aimed to identify the role of HTT mutation on human neural progenitors division and reverse the phenotype through an allele specific silencing approach. For this purpose, we combined the use of neural stem cells derived from WT and adult-onset HD-hESC and SNP-targeting allele specific HTT mRNA interference.

The third approach aimed to elucidate the pathological mechanisms surrounding the timeline of mitochondrial and metabolic dysfunction as well as the role of oxidative stress as a trigger factor. For this purpose, we used human iPSCs-HD, which most possible represent initial stages of the disease, and characterized their proliferative and neuronal differentiation potential.

Thus, the overall aim of this study is to validate possible therapeutic strategies focusing either in neurotropic factors involving protective intracellular signaling pathways activated by IGF-1 or in silencing specifically the allele responsible for mHTT expression, always targeting to ameliorate HD phenotype.
Moreover, a combination of therapeutic approaches seems necessary to offset the multiple effects of mHTT. Additionally, cells reprogrammed from patients with a genetic

neurodegenerative disease, such as HD, have an enormous therapeutic potential but the possibility of genetic damage during reprogramming exists. Thus, molecular regulatory mechanisms of pluripotent cells carrying mHTT still need to be assessed as this could affect both the safety and function of differentiated cells.

CHAPTER II - IGF-1 INTRANASAL ADMINISTRATION RESCUES HUNTINGTON'S DISEASE PHENOTYPES IN YAC128 MICE

2.1. Introduction

Huntington's disease is a rare genetic neurodegenerative disease that mainly affects striatal (caudate nucleus and putamen) medium spiny neurons (mostly composed by GABAergic neurons) and cortical neurons. HD pathophysiological features have been linked to the accumulation of mutant huntingtin (mHTT) forming soluble oligomeric or insoluble inclusions (mainly nuclear) (Vonsattel et al. 1998, MacDonald *et al.* 2003). mHTT can sequester several proteins, leading to cellular dysfunction, which involves transcription deregulation, synaptic and mitochondrial dysfunction and energy deregulation (for review; Landles et al. 2004, Ramaswamy *et al.* 2007). Indeed, mitochondrial dysfunction and altered mitochondrial dynamics due to expression of mHTT may occur through dysregulation of mitochondrial-related nuclear transcription and calcium dyshomeostasis and/or a direct interaction of N-terminal polyglutamine expanded tract with mitochondria (Panov *et al.* 2004, Orr *et al.* 2008, Weydt *et al.* 2009). This has been closely related with impairment in energy metabolism and apoptotic features occurring both in the central nervous system (CNS) and in peripheral tissues, such as the human HD muscle (Ciammola *et al.* 2006) and cybrid lines derived from HD patient peripheral blood platelets (Ferreira *et al.* 2010, Ferreira *et al.* 2011). In a previous study, glucose metabolism was found to be significantly decreased in the striatum, and temporal and frontal cortical lobes, in both preclinical and affected HD patients (Ma et al. 2007). Furthermore, increased brain lactate levels found in HD patients and human HD cybrids, largely suggest altered mitochondrial function and bioenergetics accompanying the HD phenotype (Koroshetz et al. 1997, Ferreira et al. 2011). Hence, metabolic abnormalities are common features of the disease, with controversial descriptions of HD patients featuring a higher risk of developing diabetes (Farrer 1985) and even normoglycemic patients showing impaired insulin secretion, with a simultaneous decrease in insulin sensitivity and an increase in insulin resistance (Lalic et al. 2008). Some of these features have been replicated in the R6/2 mouse line, a model recapitulating early/juvenile onset HD (Bjorkqvist et al. 2005). Accordingly, we previously showed that diabetic features in R6/2 can be rescued upon treatment with insulin growth factor-1 (IGF-1). Continuous peripheral IGF-1 therapy was capable of partially restoring plasma IGF-1 levels in R6/2 mice and consequently reverse metabolic abnormalities such as weight loss and

impaired glucose tolerance, as well as animal behavior, such as paw clasping scores (Duarte et al. 2011).

HD is also associated with altered intracellular signaling pathways essential for the control of neuronal survival. Decreased levels of cyclic adenosine monophosphate (cAMP) were found in the striatum, which compromise protein kinase A (PKA)/cAMP response element-binding (CREB)-binding protein (CBP)/CREB-mediated signaling and transcription, with reduced expression of target genes such as brain-derived neurotrophic factor (BDNF) (Gines *et al.* 2003, Zuccato et al. 2003). Indeed, mHTT leads to aberrant accumulation in the nucleus of repressor element-1 transcription factor/neuron restrictive silencer factor (REST/NRSF), which activates activation the repressor element 1/neuron-restrictive silencer element (RE1/NRSE) located within the BDNF promoter, resulting in reduced BDNF transcription in HD (Zuccato et al. 2003).

Another pro-survival signaling molecule, Akt (or protein kinase B) was downregulated during neuronal dysfunction in a rat model of HD and in human peripheral tissues (Colin et al. 2005)**.** In this respect IGF-1 has received much attention due to its role in preventing and rescuing the damage of striatal neurons (Alexi *et al.* 1999, Humbert et al. 2002). Two main well known signaling pathways can be activated through the IGF-1 receptor, the phosphatidylinositol-3-kinase (PI3K)/Akt/mammalian target of rapamycin (mTOR) and the Ras/mitogen-activated protein kinase (MAPK) pathway (Vincent *et al.* 2002). Importantly, activated Akt plays a key role in the prevention of program cell death through phosphorylation and inactivation of caspase 9 (Kermer *et al.* 2000). Moreover, the IGF-1/Akt pathway was recognized to counteract the toxic properties of mHTT. This appears to be mediated by the direct phosphorylation of HTT by Akt at serine 421 (S421) (Humbert et al. 2002), which can also restore HTT function in microtubule-based anterograde and retrograde transport of trophic factors, namely BDNF-containing vesicles (Colin et al. 2008, Zala et al. 2008).

IGF-1 mRNA was previously shown to be decreased in the striatum and skin fibroblasts of HD patients, which appears to correlate with data in striatal cells from HD knock-in mice and in the R6/2 mice (Pouladi et al. 2010). In contrast with these animal models, increased levels of IGF-1 were observed in YAC128 mice, expressing human full-length mHTT, and correlated with increased body weight (Pouladi et al. 2010). High plasma IGF-1 was also associated with greater cognitive decline in HD patients (Saleh et al. 2010); moreover, increasing levels of insulin receptor substrate 2 (IRS2,

which mediates the signaling cascades of insulin and IGF-1) in the brains of R6/2 mice reduced lifespan and increased neuronal oxidative stress and mitochondrial dysfunction (Sadagurski et al. 2011). Nevertheless, activation of IRS2 in cell lines inducibly expressing exon1 of mHTT induced the clearance of accumulated mHTT through a mTOR-independent macroautophagy pathway (Yamamoto et al. 2006). Additionally, activation of the IGF-1/Akt pathway can also inhibit mHTT-induced striatal cell death and formation of nuclear inclusions (Humbert et al. 2002). Such conflicting results regarding the role of IGF-1 led us to test the influence of enhancing the brain levels of this neurotrophic factor in HD mice. The YAC128 HD mouse model recapitulates several disease signs and symptoms, including the expression of full-length mHTT, age-dependent motor deficits and selective striatal degeneration (Van Raamsdonk *et al.* 2007, Barker *et al.* 2013), as well as increased susceptibility of striatal neurons to excitotoxicity and apoptosis (Zhang *et al.* 2008, Barker et al. 2013) . In early stages of the disease, mice develop a hyperkinetic phenotype, followed by progressive motor deficit on the rotarod at 6 months, with progression to hypokinesia by 12 months of age (Van Raamsdonk et al. 2007, Barker et al. 2013). A correlation between rotarod performance at 6 and 9 months and neuronal loss at 12 months of age, as well as the appearance of nuclear HTT staining, was previously established in this mouse model (Slow *et al.* 2003). Although YAC128 mice are well characterized in terms of neuronal loss and disease progression, few studies have focused on peripheral and cerebral metabolism, as well as on the possible benefits of IGF-1 administration. Taking into account that neuronal dysfunction occurs before striatal atrophy and neurodegeneration, and that motor deficits are evident in 6 month-old YAC128 mice, we hypothesized that brain IGF-1 supplementation could trigger IGF-1 receptor signaling pathways and ameliorate metabolic function, thus rescuing HD phenotype in YAC128 mice prior to major symptomatic features. In order to promote IGF-1 delivery in the brain, the peptide was administered through intranasal (i.n.) infusion. The i.n. delivery constitutes a method to target therapeutics to the CNS; indeed, this represents an alternative to invasive methods and exhibits benefits in the treatment of neurologic disorders, since compounds easily overcome the blood-brain barrier, reducing systemic exposure and side effects (Liu et al. 2002, Thorne *et al.* 2004, Hanson *et al.* 2008). Administration of IGF-1 through this route was previously demonstrated to deliver the neurotrophic factor to multiple areas of the CNS, where it can activate IGF-1 signaling pathways (Thorne et al. 2004). The present work presents a novel methodology for therapeutic administration

of IGF-1 into the HD brain. Indeed, effective amelioration of HD motor phenotype, intracellular signaling pathways and energy metabolism are accomplished following IGF-1 i.n. administration in YAC128 mice.

2.2.Materials and methods

2.2.1.Materials

Haemoglobin A_{1C} kit was purchased to Biosystems S.A. (Barcelona, Spain). PCR reagents, such as MasterMix, Taq polymerase, proteinase K, primers, DNA ladder (100 bp) and DNA loading dye were acquired from Invitrogen® (Carlsbad, CA, USA). D-glucose and human insulin recombinant were from Sigma-Aldrich Co (St. Luis, MO, USA). Recombinant human IGF-1 (rhIGF-1) was supplied by BioVision® (Mountain View, CA, USA). Insulin (mouse) Elisa kit was obtained from ALPCO (Salem, USA). Quantikine® mouse/rat IGF-1 immunoassay was purchased from R&D Systems, Inc. (Minneapolis, USA). Pyruvate and Lactate colorimetric assay kits were obtained from Abcam (Cambridge, U.K.). Antibodies against P(Ser473)-Akt, Akt, P(Thr202/Thr204)- Erk(42/44), Erk(42/44), P(Ser2448)-mTor and mTor were obtained from Cell Signaling (Beverly, MA, USA); anti-HTT (MAB1266) and anti-α-tubulin were obtained from Chemicon (Hampshire, U.K.). Anti-P(Ser421)-HTT was produced at Institut Curie, Orsay, France.

2.2.2.Experimental animals

In this study we used male HD transgenic hemizygous YAC128 (line 53), expressing full-length human mHTT with ~128 CAG repeats, and non-transgenic wild-type (WT) littermate mice with 6 months of age. All animals were generated from our local colony, with breeding couples gently provided by Dr. Michael Hayden (University of British Columbia, Vancouver, Canada). The YAC128 mice were maintained on FVB/N background and compared with WT littermate mice (FVB/N strain). Mice were housed in groups with *ad libitum* access to chow food and water under standard conditions (12 h light/dark cycle, 22ºC). All animal studies were performed according to the Helsinki Declaration and EU guidelines (86/609/EEC). Painful procedures were performed under anesthesia with Avertin® (12 µl/g body weight).

2.2.2.1.Genotyping

Three week-old mice were genotyped by using a tail-tip DNA Polymerase Chain Reaction (PCR) standard procedure. Primers used were: LyA1 (CCT GCT CGC TTC GCT ACT TGG AGC), LyA2 (GTC TTG CGC CTT AAA CCA ACT TGG), RyA1 (CTT GAG ATC GGG CGT TCG ACT CGC), RyA2 (CCG CAC CTG TGG CGC CGG TGA TGC), Actin Foward (GGA GAC GGG GTC ACC CAC AC) and Actin Reverse (AGC CTC AGG GCA TCG GAA CC). PCR protocol consisted in 35 cycles, with the following temperatures and times for each step: denaturation – 94ºC for 30 s; annealing – 63ºC for 30 s; elongation – 72ºC for 30 s. At the end of the cycles, DNA was left at 70ºC for 10 min. PCR products were analyzed on 1.7% agarose gels followed by staining with ethidium bromide and visualized under a UV trans-illuminator, *Gel Doc* XR *system* (BioRad®, Hercules, USA). A 100-bp ladder (Invitrogen®) was used as a size marker.

2.2.2.2.Intranasal administration of IGF-1

All experiments used rhIGF-1 (molecular weight 7.6 kDa), which was reconstituted in water to a concentration of 1.0 mg/ml, according to manufacturer's instructions and stored at –20º C until used. Prior to intranasal administration, animals were anesthetized with Avertin® (12 µl/g body weight). Intranasal administration was performed as described previously (Liu et al. 2002), with slight modifications. Mice were placed in supine position and a heated pad was inserted under the dorsal neck to induce a hyperextension of the head back. A total of 35 µl rhIGF-1 (35 µg) or vehicle solution (0.9% NaCl) was given as nose drops (3.5 µl/drop in each nostril corresponding to 7 µl/administration), alternating between the left and right nostrils for 5 times, at intervals of 4 minutes. Subsequent doses were given each 48 h, for 2 weeks (Figure 2.1.). Animals were divided into 4 groups: 1) WT+vehicle; 2) YAC128+vehicle; 3) WT+IGF-1; 4) YAC128+IGF-1.

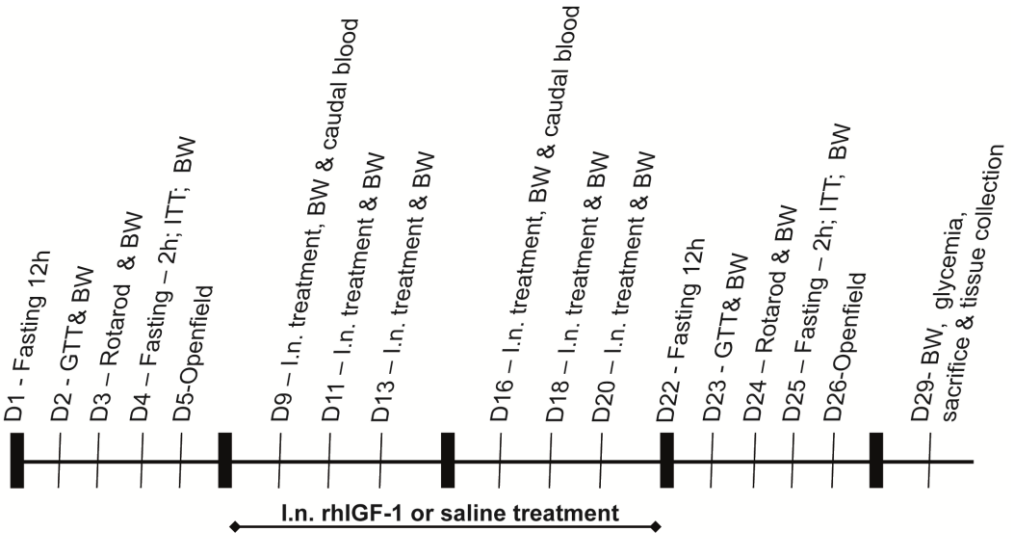

Figure 2.1. - Experimental protocol. One week prior and after treatment animals were subjected to several tests. Six-month-old YAC128 or wild-type mice were subjected to intranasal (i.n.) rhIGF-1 (35 µg every 2 days) or vehicle (0.9 % NaCl) treatment for 2 weeks. D day, GTT glucose tolerance test, BW body weight, ITT insulin tolerance test

2.2.2.3.Body weight

Body weight was measured using a high precision electronic weighing scale, Kern 440-47 N®, from Kern & Sohn GmbH (Balingen, Germany) and assessed in early afternoon, before and after behaviour tests, glucose/insulin tolerance tests, or every two days during IGF-1/saline treatment, from the age of 26 weeks (pre-treatment) to 29 week-old mice (post-treatment) (Figure 2.1.). Results were expressed as body weight (g).

2.2.2.4.Blood collection and plasma isolation

Blood was collected either from caudal vein (in living, anesthetized mice), twice/week (before, during and after treatment), or directly from the heart by transcardial punction (immediately after animal's sacrifice) with a heparinized syringe (100 U/ml heparin). Plasma was obtained by centrifugation at 5 000 xg, for 2 min, at 4 °C, in an Eppendorf Centrifuge 5415 C, to determine glucose, insulin and IGF-1 levels.

2.2.2.5.Blood glucose levels, glucose tolerance test and insulin tolerance test

Blood glucose levels were determined twice/week by a digital glucometer (Johnson & Johnson Company, Milpitas, CA, USA). Glucose Tolerance Test (GTT) and

Insulin tolerance test (ITT) were performed the week prior and three and five days after treatment, respectively (Figure 1).

GTT analyses the rate of glucose clearance from blood (2009). 12h before GTT test, mice were kept fasted. Then, 2 mg *D*-glucose/g body weight were given intraperitoneally and glycemia was determined after 0, 15, 30, 60 and 120 min. Results were expressed as mg glucose/dl blood and as the area under the curve (AUC).

ITT analyses the capacity of glucose transporters to uptake glucose, as a response to an increase in plasma insulin levels (Bruning *et al.* 1997). Before the test, mice were kept fasted for two hours (from noon to 2 p.m.) in their cages. Basal glycemia was measured before insulin injection, corresponding to time 0. Then, an intraperitoneal injection of 1 μU human recombinant insulin/g body weight was given to mice and glycemia was monitored at

15, 30, 60 and 90 min. Results were expressed as mg glucose/dl blood and as AUC. AUC was calculated using trapezoidal integration. Trapezoidal rule is a numerical integration method used to approximate the integral or the area under a curve. Animals were allowed to recover for two days before further testing.

2.2.2.6.Measurement of glycated haemoglobin

After the sacrifice, 100 μl of total blood was isolated to measure glycated haemoglobin (HbA_{1c}). We used the Haemoglobin A_{1C} kit (Biosystems S.A.) consisting of an ion exchange chromatographic-spectrophotometric method. Briefly, a hemolysate was prepared from total blood, where the labile fraction was eliminated and haemoglobins were retained by a cationic exchange resin. Haemoglobin A_{1c} was specifically eluted after washing away the haemoglobin A_{1a+b} fraction and quantified by direct spectrophotometric reading, at 415 nm. The % of HbA_{1c} was obtained by calculating: $\%\mathrm{HbA1c} = \frac{A_{HbA1c} \times V_{HbA1c}}{A_{Hbtotal} \times V_{Hbtotal}}$. Results were expressed as % of total haemoglobin.

2.2.2.7.Behaviour analysis

To measure motor ability, exploratory capacity and anxiety in mice, two behavioural test paradigms were performed, the rotarod and the openfield tests (Figure 1). Mice were allowed to adapt to test room for at least 1 h before behaviour studies.

Procedures were consistently performed for all animals, between 12 p.m. and 18 p.m., with tests made in lit room, temperature of 25^0C and at minimum noise levels. The two tests were performed the week prior and after treatment and with 24 h interval between them. Behaviour equipment was cleaned thoroughly with 30% ethanol before each animal trial.

Rotarod test- performed in a Rotarod apparatus, model LE8200 from Panlab®, (Barcelona, Spain). Animals were tested before and six days after treatment, at 26 and 29 weeks of age, respectively. Mice were gently grabbed by the tail and placed on the roller lane of the rotarod. The rotarod unit was composed of Perspex base with 362 (wide)×240 (diameter)×400 (high) mm with an integrated drum (250 mm diameter) containing a rod (30 mm diameter) and 5 lines (50 mm wide). Before the test, mice were allowed to train for 40 s, at a constant speed of 4 rpm, to allow familiarization with the equipment. After a two hour resting, each mouse was tested for 4 sessions on the rod, with a gradual acceleration rate from 4-40 rpm during 5 min, each one separated by a 30 min resting period (Carter *et al.* 2001). When the animal fell off the rod, the time latency to fall and rotation speed were automatically recorded. Results were expressed as latency to fall off rotarod, in seconds (s).

Open Field exploration test (shown as supplementary data) - Animals were tested before and seven days after treatment in an Open Field apparatus from Panlab®, (Barcelona, Spain). The system is composed by 2 square frames with 22 x 22 cm size, a frame support and a control unit. Chamber walls and floor are made of transparent Plexiglass. Open field arena is divided into a grid of equally-sized areas by infrared photocell beams or lines drawn on the chamber floor, for visual scoring of activity by the experimenter. A central square (18 cm x 18 cm) is drawn in the middle of the open field. The discrimination of central square is relevant because some mouse strains have high locomotor activity and cross the lines of the test chamber many times during a test session. The number of central square entries and the duration of time spent in the central square are measures of exploratory behaviour and anxiety. A high frequency/duration of these behaviours indicates high exploratory behaviour and low anxiety levels (Carrey *et al.* 2000). FRAMES (photo beam sensors) are equipped with 32 infrared photocells, 16 placed in axis X and 16 placed in axis Y. Photocell works at a wavelength of 950 nm and its information is multiplexed at a rate of 40Hz. System gives data about fast (5 cm/s) and slow (2 cm/s) movements, fast and slow stereotypes, number of fast and slow rearing and number of fast and slow nose-pokes in the hole-

board test. During the test, which lasted for 30 min, lights were on, with the same illumination levels as the holding room, and the test recorded with a digital camera. The test started with the mouse placed in the center of the chamber and the experimenter left the testing room after this procedure, since sudden motion or noise could affect exploratory activity. Mice were allowed to freely explore the chamber for 30 min and each line crossed or photocell beam break was scored as one unit of activity. Defecation and grooming activities were also scored. At the end of the test, the mouse returned to home cage and allowed to rest for two days before further testing. Results were expressed as the maximal and mean velocity (cm/s), distance travelled, slow and fast movements (%), time spending in central square (s), and rearing and resting time (s).

2.2.2.8.Brain tissue preparation and total blood collection

At the end of the study (one week after the last i.n. administration, in 30 week-old mice), the animals were anesthetized with 30 µl/g body weight Avertin® and tissues and blood were collected. Blood was collected by transcardial punction, as described above. Mice were perfused with 1% PBS (phosphate buffered saline) to eliminate blood clots from tissues, and the brain was removed and dissected into striatum and cortex (in ice, at 0-4ºC), which were frozen at -80ºC for posterior analysis. Afterwards, the brain tissues were thawed and homogenized in PBS or lysis buffer, supplemented with protease and phosphatase inhibitors, with a Potter-Elvejhem homogenizer with a Teflon pestle, at 300 rpm. The homogenates were then frozen/thawed 3 times in liquid nitrogen and stored at -80ºC for later use. Buffered solution contained (in mM): 250 sucrose, 20 Hepes, 10 KCl, 1.5 $MgCl_2$, 1 EDTA, and 1 EGTA, pH 7.4, supplemented with 1 mM DTT, 100 □M PMSF and 1:1000 of a broad spectrum protease inhibitor cocktail containing chymostatin, pepstatin A, leupeptin, and antipain (1 mg/mL). For the analysis of phosphorylated proteins, the supplemented solution also included 1% SDS, 50 mM NaF, 1 mM sodium *o*-vanadate and 0.1 □M okadaic acid. Protein concentration was determined with Bradford® assay (Bio-Rad Laboratories, Hercules, CA, USA).

2.2.2.9.Assessment of plasma and brain levels of insulin and IGF-1

Using the previously described plasma and brain tissue homogenates, insulin and IGF-1 levels were measured with Insulin (mouse) Elisa kit (ALPCO) and Quantikine mouse/rat IGF-1 Immunoassay (R&D systems), respectively, according to manufacturer's instructions. For insulin, the optical density was measured using a microplate reader (SpectraMax Plus 384 spectrophotometer, Molecular Devices, Winnersh, UK) at 450 nm with a reference wavelength of 620 nm. For IGF-1, the optical density of each well was measured at 450 nm, with a correction set to 540 nm using the same apparatus. Results were obtained as pictograms per milliliter, normalized to the amount of protein per sample, and thus expressed as pictograms/milliliter protein or nanogram//milligram protein.

2.2.2.10.Analysis of adenine nucleotides

Levels of adenine nucleotides (ATP, ADP and AMP) were determined from brain homogenates in PBS, which were maintained at -20ºC until the analysis. The samples were assayed by separation in a reverse-phase high-performance liquid chromatography (HPLC), using a Lichrospher 100 RP-18 (5 µm) HPLC column from Merck (Darmstadt, Germany), upon an isocratic elution with 100 mM phosphate buffer (KH_2PO_4, pH 6.5) and 1% methanol, with a flow rate of 1 ml/min and detection at 254 nm, as previously described (Stocchi *et al.* 1985). The required time for each analysis was 6 min. The chromatographic apparatus used was a Beckman-System Gold, consisting of a 126 Binary Pump Model and 166 Variable UV detector. Peak identity was determined by following the retention time of standards. Cellular energy charge was calculated using the formula: ([ATP] + 0.5 [ADP])/([ATP] + [ADP] + [AMP]) (Rego *et al.* 1997).

2.2.2.11.Assessment of brain levels of pyruvate and lactate

Pyruvate and lactate levels were measured colorimetrically, by using Pyruvate Assay kit and Lactate Assay Kit (from Abcam®), according to manufacturer's instructions. In the pyruvate assay, pyruvate is oxidized by pyruvate oxidase, generating a product detected by spectrophotometry at 570 nm. In the lactate assay, lactate is oxidized by

lactate dehydrogenase to generate a product detected at 450 nm using a SpectraMax Plus 384 spectrophotometer. Results were expressed as nmol/mg protein.

2.2.2.12.Western blotting

Dissected cortical and striatal tissues were homogenized in a supplemented lysis buffer containing phosphatase and protease inhibitors (as described before). The samples were denatured with SDS sample buffer (50 mM Tris-HCl, pH 6.8, 2% sodium dodecyl sulphate, 5% glycerol, 0.01% bromophenol blue and 100 mM DTT), at 95ºC, for 5 min. Samples containing the denatured proteins (100 μg) were subjected to SDS/PAGE and transferred onto polyvinylidene difluoride (PVDF) Hybond-P membranes. Then, membranes were blocked for 2 h at room temperature in Tris-buffered saline (TBS; pH 7.4) plus 5% nonfat dry milk and 0.1% Tween 20, and incubated with antibodies against phosphorylated proteins such as P(Ser473)-Akt (1:1000), P(Thr202/Tyr204)-Erk(42/44) (1:1000), P(Ser2448)-mTor (1:1000) or P(Ser421)-HTT (1:200), overnight, at 4ºC, with gentle shaking. The membranes were reprobed for total protein with the antibodies for anti- Akt (1:1000), Erk(42/44) (1:1000), mTor (1:1000) or HTT (MAB2166) (1:250), and for total protein loading control with anti-α-tubulin (1:20000). Membranes were further incubated with anti-rabbit IgG and anti-mouse IgG+IgM secondary antibodies (1:20000), for 90 min, at room temperature, and developed using ECF fluorescent reagent. Fluorescence signal was analyzed using the QuantityOne software and the results were given as fluorescence intensity (INT)/mm2. Data were presented as the ratio of phosphorylated protein/total protein or protein levels/α-tubulin. Immunoreactive bands were visualized with VersaDoc Imaging System (BioRad®, Hercules, USA).

2.2.2.13.Data analysis and statistics

Results are the mean±SEM of the indicated number of independent experiments in figure and table legends. The F test was performed to analyze the interaction term, as described in the figure and table legends. Statistical significance was analyzed using parametric tests, namely two-way ANOVA, followed by Bonferroni post-test. Data that do not meet the assumptions of normality were submitted to rank transformation

method followed by parametric analysis of ranks (Mitchell *et al.* 1994). $P<0.05$ was considered significant.

2.3.Results

2.3.1.Intranasal treatment with rhIGF-1 increases cortical but not plasma or striatal levels of IGF-1 in WT and YAC128 mice

Intranasal (i.n.) administration was previously proven to be an effective method to deliver IGF-1 into most caudal brain regions and peripheral tissues (Thorne et al. 2004) . Plasma and brain (cortex and striatum) tissue levels of IGF-1 were assessed after two weeks of i.n. administration, in both WT and hemizygous YAC128 mice. No changes were observed in plasma IGF-1 levels between saline-treated YAC128 and WT mice (Fig. 2.2.A), which may account for the fact that WT mice were as overweighed as YAC128 mice (Table 1). The plasma levels of IGF-1 slightly increased, although non-significantly, in rhIGF-1-treated YAC128 and WT mice, compared to saline-treated animals (Fig. 2.2.A), possibly reflecting some absorption of IGF-1 from the nasal passages through the cervical lymph nodes (Rosen *et al.* 1999). In striatal samples from IGF-1-treated YAC128 mice we also observed a slight tendency for an increase in IGF-1 levels, although this was not significant when compared to saline-treated HD mice (Fig. 2.2.B). Importantly, a significant increment in IGF-1 levels was observed in cortical tissue of IGF-1-treated wild-type and YAC128 mice (Fig. 2.2.C). These data show that this method is efficient in delivering IGF-1 to the brain tissue (particularly the cortex) and that enhanced levels can still be detected one week after the administration has ended.

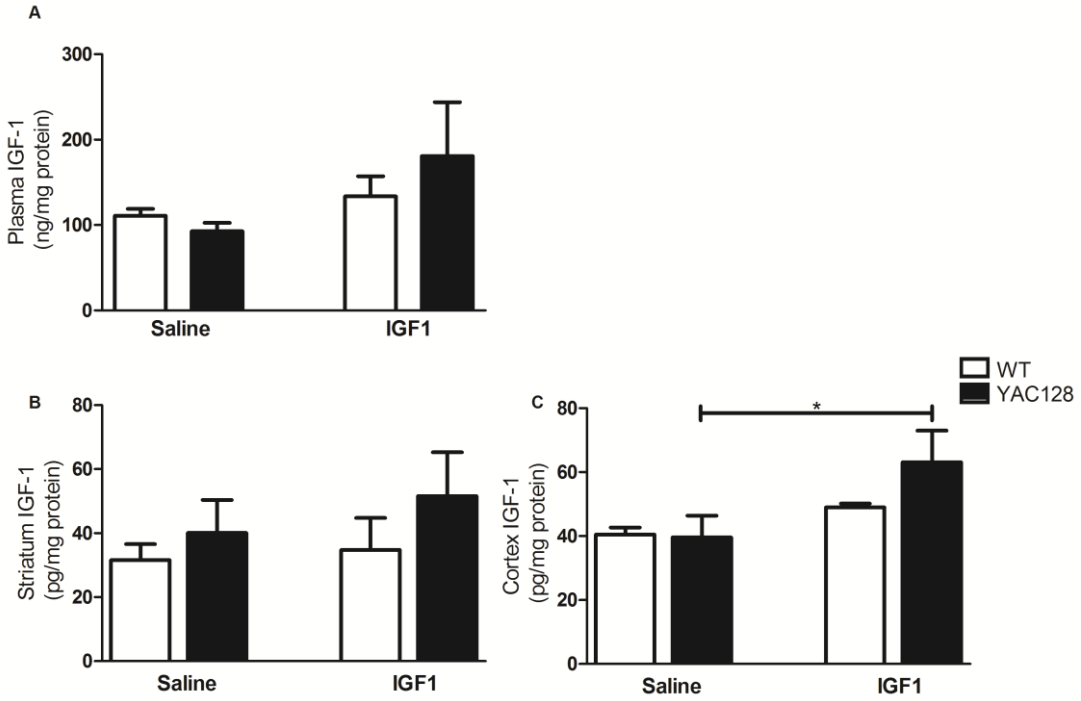

Figure 2.2 - Effect of intranasal rhIGF-1 treatment on plasma and brain levels of IGF-1 in WT and YAC128 mice. Six month-old WT and YAC128 mice were treated for 2 weeks with intranasal rhIGF-1 (35 µg every two days) or saline (0.9% NaCl), as described in Materials and Methods. Blood and brain samples were collected from animals one week after treatment. (A) shows plasma IGF-1 levels in saline and rhIGF-1 treated mice; no interaction between genotype and treatment was found ($F(1,29)=0.95$, p=ns) (n=8-9 mice per treatment and genotype). For the striatal IGF-1 levels (B) no significant interaction was found either ($F(1,10)=0.84$, p=ns) (n=3-6 brain samples per treatment and genotype). Two-way ANOVA analyses revealed a significant effect of treatment on IGF-1 levels in the cortex ($F(1,9)=6,36$, $p<0.05$), but no interaction between genotype and treatment ($F(1,9)=1.38$, p=ns) (C) (n=3-6 brain samples per treatment group and genotype). IGF-1 levels were determined in duplicates by the Quantikine Mouse/Rat IGF-1 Immunoassay. Data are the mean ± SEM of the indicated number of animal samples. Multiple comparisons using two-way ANOVA followed by Bonferroni correction (*$p< 0.05$).

2.3.2.IGF-1 administration influences blood metabolic parameters

A correlation between plasma IGF-1 levels, body weight and HTT levels was previously described in YAC128 mice expressing full-length human HTT. Increased plasma IGF-1 levels were shown to regulate body weight in YAC128 mice (Pouladi et al. 2010). Thus, we also measured body weight before and after IGF-1 i.n. treatment (Table 1). All mice were shown to be overweight, since a normal weight for FVB/N mouse strain is between 25-30 g (Pouladi et al. 2010) , whereas both WT and YAC128 mice body weight largely exceeded those values, ranging from 28 to 45 g. Moreover, i.n.

treatment with IGF-1 did not produce any changes in body weight (Table 1), despite the rise in plasma IGF-1 levels (Fig. 2.2.A). YAC128 mice under a FVB/N background start to gain weight, compared to WT mice, after 2 months of age, which has been related with the background strain in which they were developed (Van Raamsdonk et al. 2007). High body weight in both WT and YAC128 mice was not due to the diet; in a subgroup of animals the diet was changed during a month to a less caloric diet without access restriction, but no significant differences were detected on body weight or plasma glucose levels (not shown).

Table 2 - Effect of rhIGF-1 treatment on body weight, plasma glucose and HbA1c in WT and YAC128 mice

			Body weight (g)	Plasma glucose levels (mg/dl)	HbA1c (% of total hemoglobin)
Saline	WT	PRE	35.1 ± 1.7 (10)	181.7 ± 11.9 (10)	n.d.
		POST	33.4 ± 1.5 (10)	179.8 ± 17.4 (8)	9.9 ± 1.2 (3)
	YAC128	PRE	36.4 ± 1.9 (9)	183.3 ± 10.73 (9)	n.d.
		POST	33.0 ± 1.5 (9)	190.3 ± 20.71 (9)	10.2 ± 1.1 (3)
IGF-1	WT	PRE	33.4 ± 0.4 (9)	227.2 ± 24.6 (6)	n.d.
		POST	32.5 ± 0.7 (9)	202.2 ± 11.2 (6)	9.9 ± 1.3 (4)
	YAC128	PRE	35.1 ± 1.1 (10)	258.8 ± 25.9 (6)	n.d.
		POST	34.0 ± 1.1 (9)	242.5 ± 30.0 (6)	9.8 ± 1.4 (4)

Body weight and plasma glucose levels were measured the week before (pre) treatment and after (post) the treatment. Plasma glucose and glycated hemoglobin (HbA1c) levels were measured under fed conditions, using a glucometer and a kit for analysis of glycosylated hemoglobin, respectively. Data are mean±SEM of the indicated number of animals/group (n). Repeated measures ANOVAwas performed for body weight and plasma glucose levels. Two-way ANOVA analyses shows no difference effect of genotype or treatment on HbA1c levels [F(1,10)=0.02, p =ns] n.d. not determined

We further examined the changes in glycemia, since there is some controversy regarding the prevalence of diabetes in HD. Data in Table 1 show similar, although high, glycemia levels in all groups of animals, under fed conditions, which were not altered after IGF-1 treatment. A more reliable method to characterize a diabetic phenotype is the measurement of glycated haemoglobin (HbA_{1c}), which reflects average glycemia over the preceding 6 weeks (Bennett et al. 2007). All animals exhibited values above 9.1% of HbA_{1c} determined by the BioSystem method, which correspond to pathological values reported by The International Federation of Clinical Chemistry Working Group (NGSP), over 6.4%, and the National Glycohaemoglobin Standardization Program (NGSP), over 8.0%. These results suggest that FVB strand

mice have basal hyperglycemia, which is likely to progress to diabetes, although this is apparently independent of the genotype.

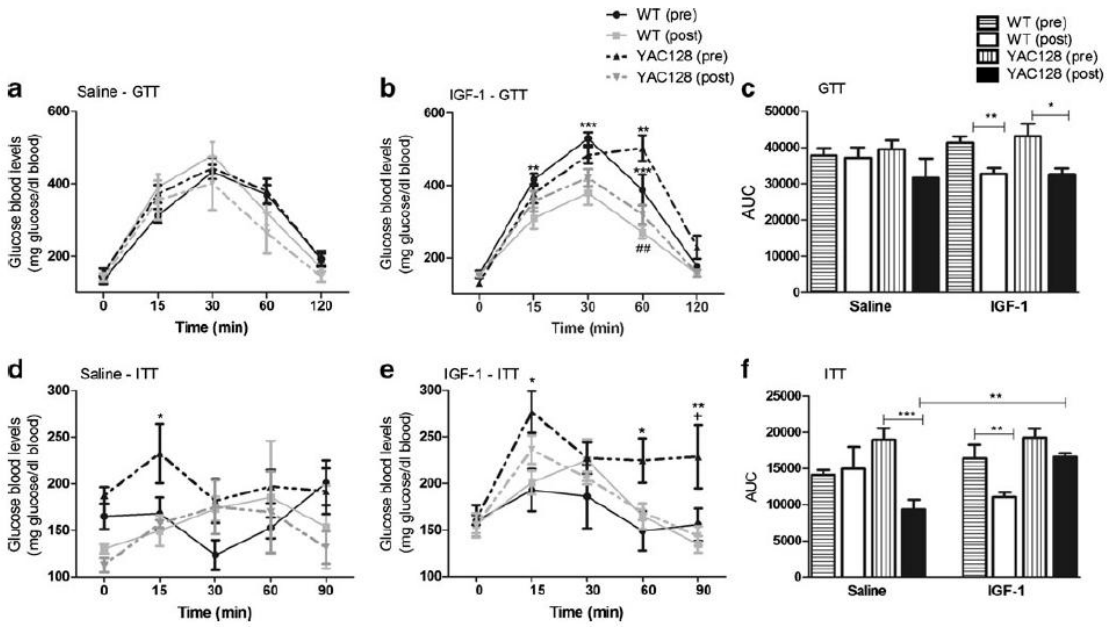

Figure 2.3 - Effect of intranasal rhIGF-1 treatment on glucose and insulin tolerance tests in YAC128 and WT mice. For glucose tolerance test (GTT) (a–c), glucose (2 mg/g body weight) was intraperitoneally administered following 12 h fasting and blood collected for measurement of glucose levels after 0, 15, 30, 60, and 120 min. For insulin tolerance test (ITT) (d–f), mice were fasted for 2 h following intraperitoneal administration of insulin (1 μU/g body weight) and blood glucose levels determined at 0, 15, 30, 60, and 90 min. The area under the curve (AUC) for GTT (in c) was calculated from data in graphs a and b, and the AUC for ITT (in f) from graphs d and e, using the trapezoidal rule. In a, two-way ANOVA for repeated measures showed that there was no interaction of genotype and saline treatment [$F(12,108)=1.75$, $p=0.06$], but there was a significant effect of time [$F(4,108)=124.91$, $p<0.001$] onGTT values. In b, a significant interaction between time×genotype×treatment was found [$F(12,209)=3.38$, $p<0.0001$]. A difference was found (determined by two-way ANOVA for repeated measures after Bonferroni correction) on pretreated YAC128 mice at 60min, showing higher levels of glucose than WT mice, which was ameliorated following i.n. IGF-1 treatment. IGF-1 treatment significantly reduced glucose levels in WT and YAC128 mice (c). In d and e, pretreated YAC128 mice exhibited higher glucose levels at 15 min, compared to WT mice. In e, a significant interaction between time×genotype×treatment was found [$F(12,88)=3.38$, $p<0.01$]. Pretreated YAC128 mice showed increased glucose levels at 60 and 90 min, compared to WT mice; i.n. administration of IGF-1 in YAC128 mice reduced significantly glucose plasma levels at 90 min. Data are the mean±SEM of n =4–7 mice per treatment group and per genotype). Statistical significance: *$p<0.05$, **$p<0.01$, or ***$p<0.001$ by two way ANOVA for repeated measures followed by Bonferroni correction, for comparison between pretreated YAC128 and WT mice; and +$p<0.01$ using two-way ANOVA for comparison between pre- and posttreated YAC128 mice.

The GTT assesses the ability of WT and YAC128 mice to deal with an acute glucose load. In the IGF-1 treated group, pre-treated YAC128 mice showed higher levels of glucose at 60 min, compared to WT mice (Fig. 2.3.B). WT mice treated with IGF-1 exhibited a better response in GTT with a significant reduction in glucose levels at several time points (Fig. 2.3.B). Moreover, the AUC values for the GTT showed a reduction in glucose values after treatment with IGF-1 in both WT and YAC128 mice (Fig. 2.3.C).

The ITT is used to evaluate insulin sensitivity and/or insulin resistance. YAC128 mice showed a lower capacity to regulate blood glucose concentrations 15 min after a bolus of intraperitoneal injection of insulin since the levels detected were significantly higher compared with the WT group before treatment (Fig. 2.3.D,E). After 2 weeks of i.n. treatment with IGF-1, YAC128 mice significantly reduced plasma glucose levels after 120 minutes, compared to values prior to IGF-1 administration (Fig. 2.3.E). Analysis of AUC for the ITT showed a significant reduction in both WT and YAC128 glucose values after IGF-1 treatment (Fig. 2.3.F), which may be accounted for by the treatment procedure since a decrease in AUC values in the ITT were also observed in saline- treated YAC128 mice. Nevertheless, these data suggest that YAC128 mice bear some systemic insulin resistance, while IGF-1 can partially restore the uptake of glucose.

Table 3 - Effect of rhIGF-1 treatment on plasma and brain insulin levels in WT and YAC128 mice

		Plasma (pg/mg protein)	Total brain (pg/mg protein)
Saline	WT	27.0±8.7 (3)	22.8±4.7 (3)
	YAC128	34.4±4.8 (3)	19.9±11.4 (3)
IGF-1	WT	33.8±9.2 (5)	17.1±5.3 (5)
	YAC128	51.0±3.5 (4)	14.6±2.7 (5)

Insulin levels were determined in plasma and brain homogenates. Insulin was quantified by an ELISA Assay. YAC128 mice showed similar brain levels of insulin compared to WT. IGF-1 i.n. treatment slightly increased plasma insulin levels in YAC128 mice. Data are the mean±SEM of the indicated number of animals/group (n). Two-way ANOVA analyses shows no effect of genotype or treatment on levels of plasma [$F(1,11)= 0.39$, p =ns] and total brain [$F(1,12)=0.81$, p =ns] insulin levels

Because administering IGF-1 in R6/2 mice enhanced plasma insulin levels (Duarte et al. 2011), we also measured insulin in plasma and brain in YAC128 and WT mice. No significant differences in plasma or brain insulin levels were found between the animals before treatment (Table 2). Following IGF-1 administration there was a slight, although not significant, increase in plasma insulin levels in YAC128 mice (Table 2), suggesting that changes in ITT do not reflect significant modifications in plasma insulin levels. No significant differences in insulin levels were found in total brain samples after i.n. IGF-1 treatment in WT or YAC128 mice (Table 2).

2.3.3.IGF-1 treatment ameliorates motor impairment in YAC128 mice

In accordance with prior motor impairment described in YAC128 mice (Slow et al. 2003), we observed that 6 month-old YAC128 mice exhibited impairment in motor coordination and balance, compared to WT littermates (Fig. 2.4.). Considering all pre-treated WT and YAC128 mice (in saline and IGF-1 groups) a very significant decrease in the latency to fall off the rotarod was observed in WT mice compared to YAC128 littermates (respectively 50.80 ± 4.34 s; n=18 versus 31.36 ± 2.62 s; n=21, $p<0.001$). IGF-1 i.n. administration significantly improved motor impairment in YAC128 mice, with a significant increase on time spent on the rotarod apparatus (Fig. 2.4.).

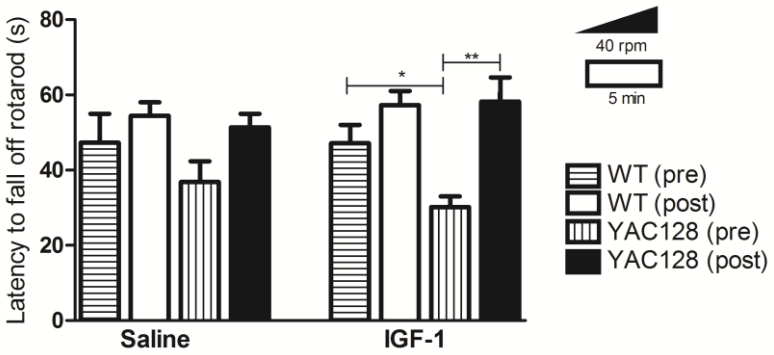

Figure 2.4 - Effect of rhIGF-1 intranasal administration on rotarod test in YAC128 and WT mice. YAC128 andWT mice littermates were allowed to adapt to the behavior test room and procedures before tested in four trials on an accelerating rotarod (4–40 rpm), for 5 min. A significant interaction between genotype and treatment [$F(3,68)=3.79$, $p<0.05$] was found. Data are the mean±SEM of 9–12 mice per treatment group and genotype. Statistical significance: *$p<0.05$, **$p<0.01$, by repeated-measures

Mice locomotor activity was further measured using an openfield apparatus. YAC128 mice showed similar locomotion and exploration behavior profiles as their WT littermates (Fig. 2.5.). Moreover, IGF-1 treatment did not affect most of the parameters analyzed, except for the maximal velocity, which increased in YAC128 mice, compared to untreated mice (Fig. 2.5.).

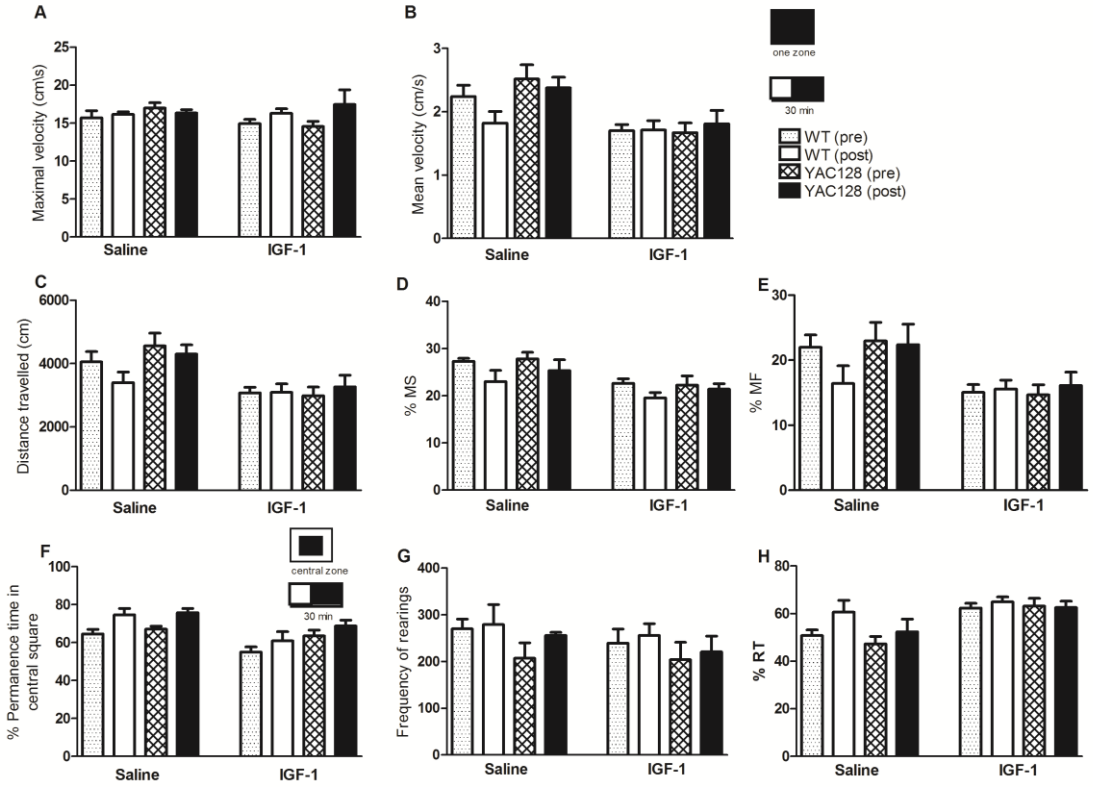

Figure 2.5 - Influence of IGF-1 intranasal administration on openfield exploration on YAC128 and WT mice. YAC128 and WT littermates (n=5-10 mice for treatment group and for genotype) were tested in an openfield activity box over a period of 30 min as described in Material and Methods. Locomotor horizontal activity was recorded and analyzed for maximal (A) and mean velocity (B) (cm/s), distance travelled (cm) (C), slow movements (MS) (D) and fast movements (MF) (E) (% of total movement), time spent in central square (s) (F), rearing (G) and resting time (RT) (s) (H). There was no effect of genotype or treatment on openfield performance, except maximal velocity which increased in the YAC128 mice IGF-1 treated ($F(7,50)=9.27$, $p<0.01$). Data are the mean ± SEM of the indicated number of animals. Statistical significance: ttp< 0.01 by Student's t-test.

2.3.4.IGF-1 administration promotes cortical and striatal intracellular signaling pathways

IGF-1 is one of the most important activators of PI3K/Akt/mTOR signaling pathway, a stimulator of cell growth and proliferation (Latres *et al.* 2005).. In HD, there is clear evidence that IGF-1/Akt neuroprotective pathway is altered (Humbert et al. 2002, Colin et al. 2005). In order to examine whether IGF-1 i.n. delivery involves activation of Akt, Erk or mTOR signaling pathways, we analyzed the activation of these proteins in cortical and striatal lysates from IGF-1- *versus* saline- treated WT and YAC128 mice.

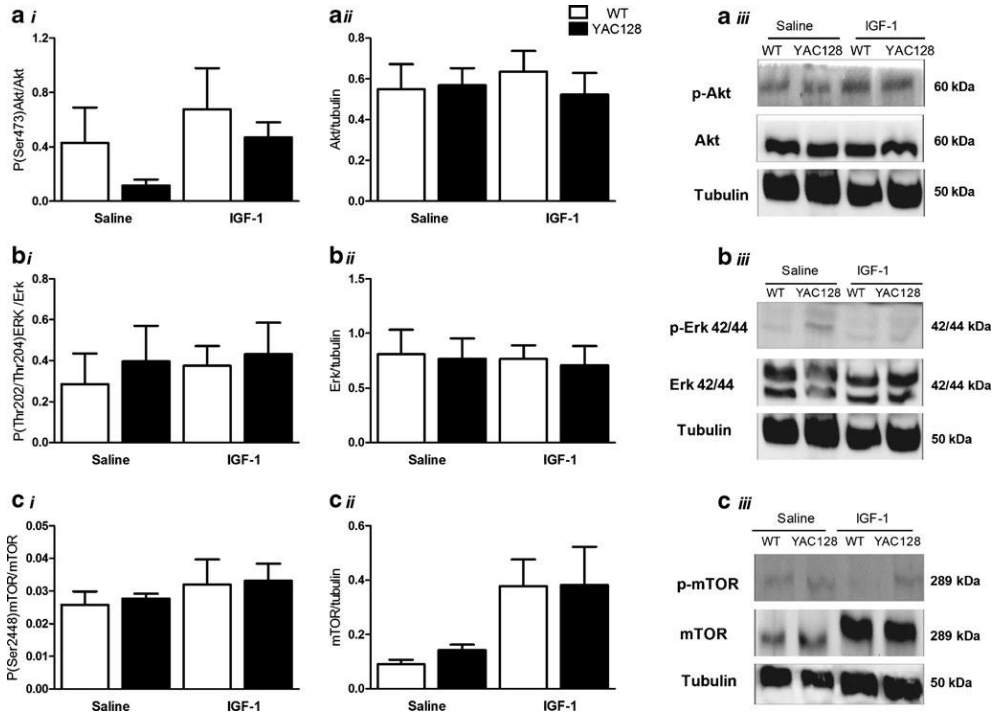

Figure 2.6. Influence of rhIGF-1 intranasal administration on Akt, Erk, and mTOR phosphorylation in the striatum of YAC128 mice. Striatal tissue was isolated 1 week following i.n. treatment with rhIGF-1 or saline and lysates were submitted to SDS-PAGE gel electrophoresis. No interaction between genotype and treatment occurred for all proteins analyzed. Two way ANOVA analyses revealed that there is a significant effect of genotype on levels of anti-P(Ser473)Akt (A.i) [$F(1,13)=6$, $p<0.05$], and levels tended to be higher in YAC128 IGF-1-treated mice. For the relative levels of other downstream IGF-1 effectors Akt (B.i) [$F(1,19)= 0.40$, p =ns], Erk (B.ii) [$F(1,20)=0.0003$, p =ns] and their activated (phosphorylated) forms, anti-P(Thr202/Thr204)Erk (B.i) [$F(1,16)=0.45$, p =ns] and anti-P(Ser2448)mTOR (C.i) [$F(1,10)=0.004$, p =ns], there was no significant effect of genotype or treatment. When considering mTOR (C.ii), there was a significant effect of the treatment [$F(1,17)= 7.64$, $p<0.05$]. Data are the mean±SEM of 3–4 mice per genotype and treatment, performed in duplicates. The bar graphs represent the quantitative analysis of the blot images shown in A.iii, B.iii, and C.iii. In order to use two-way ANOVA test, we performed a rank transformation of the data

In striatal tissue a decrease in Akt activation (P-(Ser473)Akt) was observed in saline-treated YAC128 mice, which was partially rescued after treatment with IGF-1 (Fig.2.6A.*i*). Conversely, no significant changes were observed on Erk or mTOR phosphorylation due to expression of full-length mHTT, and IGF-1 failed to further activate Erk or mTOR (Fig. 2.6.B-C). Nevertheless, IGF-1 promoted protein expression levels of mTOR, as observed in Fig. 2.6.C.*ii-iii*.

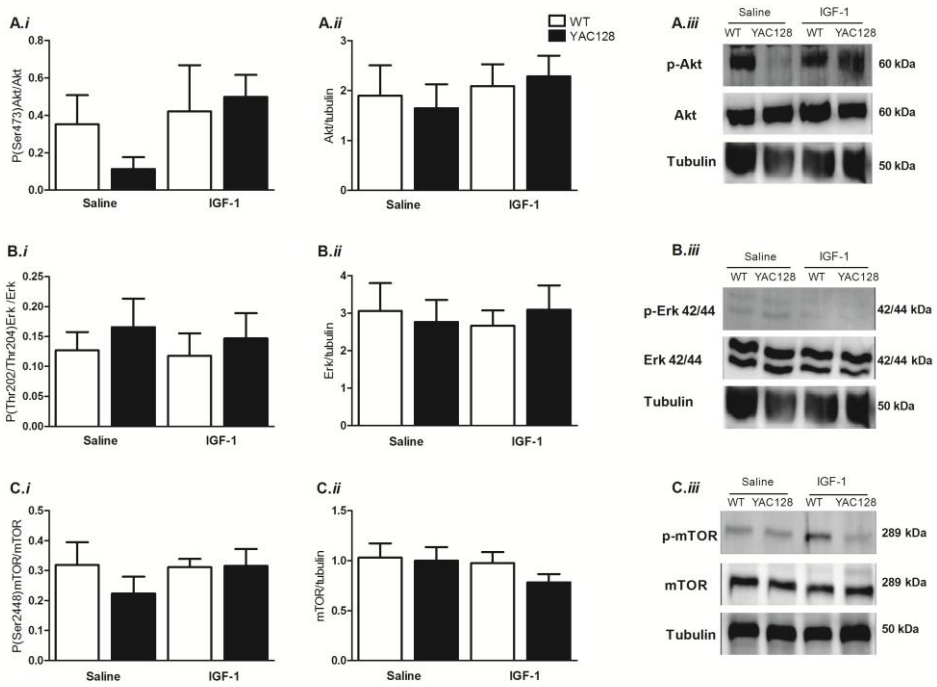

Figure 2.7. Influence of rhIGF-1 intranasal treatment on Akt, Erk, and mTOR phosphorylation in the cortex of YAC128 mice. Cortical tissue was isolated `1 week following i.n. treatment with rhIGF-1 or saline and lysates were submitted to SDS-PAGE gel electrophoresis. No interaction between genotype and treatment occurred for all proteins analyzed. Two-ANOVA analyses revealed that the levels of anti-P(Ser473)Akt (A.i) tend to be higher in YAC128 IGF-1-treated mice [$F(1,22)=3.20$, $p=0.084$]. For the relative levels of other downstream IGF-1 effectors Akt (B.i) [$F(1,26)=0.2$, p =ns], Erk (B.ii) [$F(1,19)=0.32$, p =ns], and mTOR (C.ii) [$F(1,14)=0.46$, p =ns], and their activated/phosphorylated forms anti-P(Thr202/Thr204)Erk (B.i) [$F(1,26)=0.02$, p =ns] and anti-P(Ser2448)mTOR (C.i) [$F(1,23)=0.02$, p =ns] no significant effect of genotype×treatment interaction was observed. Data are the mean±SEM of 3–4 mice per genotype and treatment, performed in duplicates. The bar graphs represent the quantitative analysis of the blot images shown in A.iii, B.iii, and C.iii . In order to use two-way ANOVA test, we performed a rank transformation of the data

HD mice also showed decreased activation of Akt in cortical samples, as compared to WT littermates (Fig. 2.7.A.*i*). After treatment with IGF-1, YAC128 mice exhibited an increase in Akt phosphorylation (Fig. 2.7.A.*i*). However, no differences inactivation or expression levels of Erk or mTOR were found between WT and YAC128 cortical tissue before or after treatment with IGF-1 (Fig. 2.7.B-C). Data obtained in brain striatal and cortical samples from IGF-1-treated YAC128 mice largely suggest that IGF-1 activates Akt intracellular signaling.

2.3.5.Phosphorylation of mHTT at S421 is increased following IGF-1 i.n. treatment

Activation of IGF-1/Akt pathway was previously shown to be protective in neurons expressing mHTT, as a result of increased phosphorylation of HTT on Ser421 by Akt (Humbert et al. 2002). The IGF-1/Akt pathway is downregulated in HD (Humbert et al. 2002, Colin et al. 2005) and phosphorylation of HTT at P(Ser421)-HTT progressively declines in the striatum of YAC128 mice (Metzler *et al.* 2010). Thus, we further examined the changes in Ser421 phosphorylation and differential protein levels of wild-type HTT (wtHTT) and mHTT in saline- and rhIGF-1-treated WT and YAC128 mice. In the striatum, the levels of P(Ser421)-mHTT increased approximately 3-fold in YAC128 mice after IGF-1 treatment (Fig. 7A.i), whereas wtHTT in WT or YAC128 mice failed to be activated (Fig. 2.8.A.*i*). Interestingly, the levels of wtHTT in the striatum of YAC128 mice were enhanced after IGF-1 treatment (Fig. 2.8.A.*ii*), suggesting that IGF-1 levels may regulate the expression of wtHTT in the striatum. In cortical tissue we observed an increase in P(Ser421)-wtHTT (by 2.4-fold) and in P(Ser421)-mHTT (by 2.3 fold) in YAC128 mice treated with IGF-1, although this was not significant (Fig. 2.8.B.*i*). No major differences were seen in the expression levels of wtHTT and mHTT in cortex following IGF-1 administration (Fig. 2.8.B*ii*). These data support that IGF-1 treatment increases the phosphorylation of mHTT on Ser421.

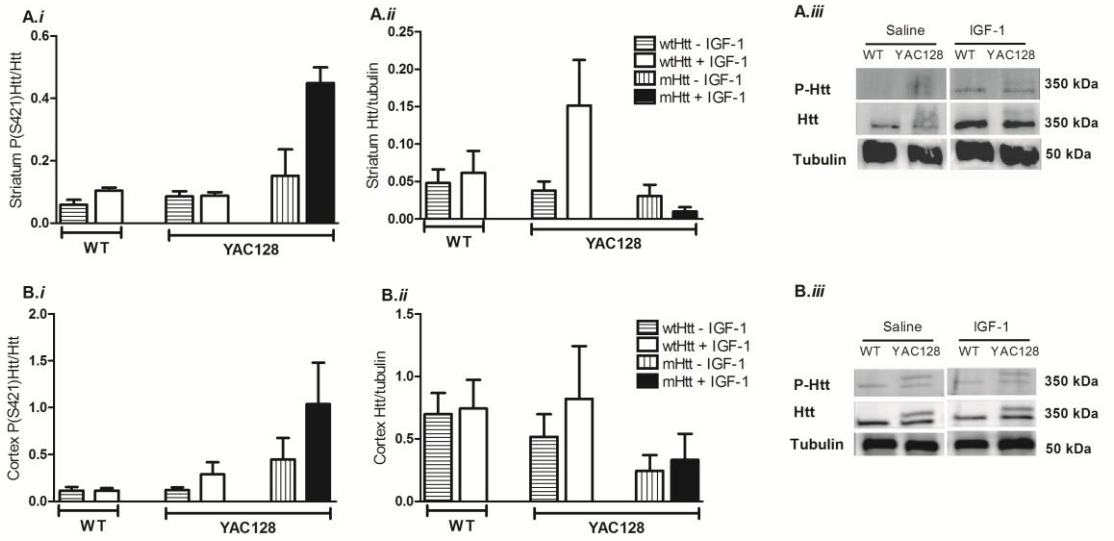

Figure 2.8. - Phosphorylation of wild-type and mutant HTT at Ser421 following intranasal IGF-1 treatment in WT and YAC128 mice. Brain tissue was isolated and striatal and cortical lysates were electrophoresed on 6 % SDSPAGE and probed with anti-P(S421)HTT (A.i, B.i) selective antibody, followed by reprobing with anti-HTT (MAB2166) (A.ii, B.ii). The ratio between the levels of wt pS421-wtHTT and total wtHTT and pS421-mHTT and total mHTT were analyzed for WT and YAC128 mice in striatal (A) or cortical (B) brain samples. wtHTT-IGF-1 wild-type huntingtin in saline-treated mice; wtHTT+IGF-1 wild-type huntingtin in rhIGF-1-treated mice; mHTT-IGF-1 mutant huntingtin in saline-treated mice; mHTT+IGF-1 mutant huntingtin in rhIGF-1-treated mice. IGF-1 i.n. administration increased pS421-mHTT/mHTT in striatum of YAC128 mice. Data are the mean±SEM of 3–4 mice per genotype and treatment, run in duplicates. In order to use two-way ANOVA test, we performed a rank transformation of the data

2.3.6.rhIGF-1 improves energy deficits in YAC128 mice brain

It is widely recognized the relationship between mHTT and energy deficits, which may be accounted for by mitochondrial dysfunction, namely by interfering with oxidative phosphorylation (Browne *et al.* 2004, Bossy-Wetzel *et al.* 2008). Energy deficiencies have been described early in the pathogenic process, and precede pathological and symptomatic markers of disease onset (Gil et al. 2008). Previously, IGF-1 was suggested to have a primordial role on glucose metabolism (Petersson *et al.* 2009). Since bioenergetic abnormalities affect different areas of the brain, we examined the effect of IGF-1 administration on total brain energy metabolic parameters.

Metabolic abnormalities in HD YAC128 mice were ascribed to a reduction in YAC128 mice brain energy charge (Fig. 2.9.A). According to Atkinson's hypothesis the cell stabilizes its energy charge and the normal brain value is between 0.85 and 0.95, exhibiting little circadian variation (Ataullakhanov *et al.* 2002). In our study, WT mice exhibited a value of energy charge approximate to the normal range. Interestingly, treatment with IGF-1 was able to recover the energy levels in YAC128 mice (Fig. 2.9.A).

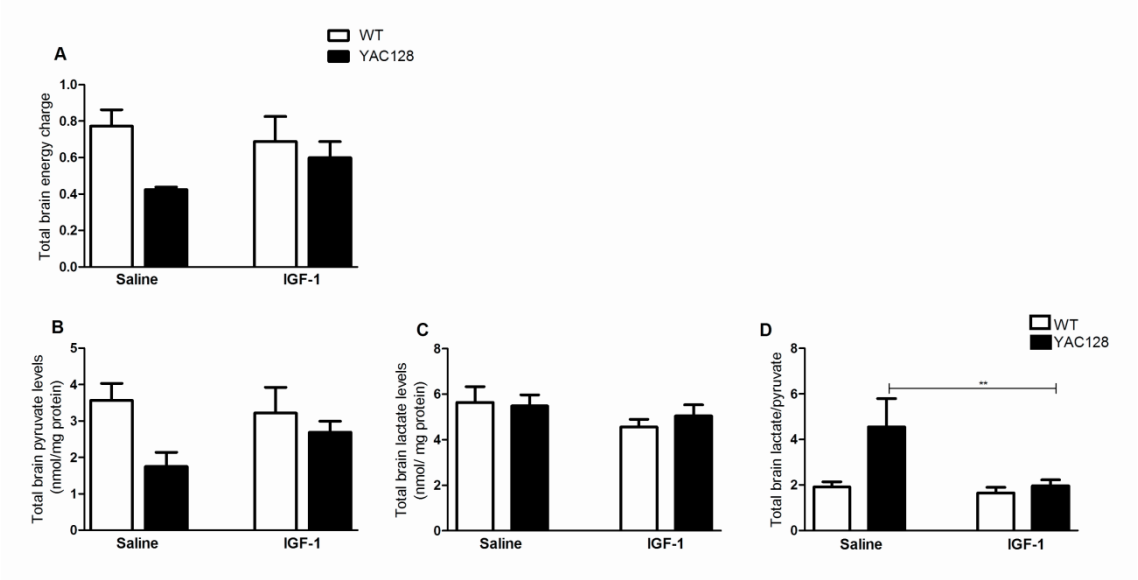

Figure 2.9. - Effect of rhIGF-1 intranasal administration on brain energy charge and pyruvate and lactate levels of YAC128 mice. Brain energy charge (a) was determined in YAC128 and WT littermates as ([ATP]+0.5 [ADP])/([ATP]+[ADP]+[AMP]). The tissue lysates were assayed for ATP, ADP, and AMP by separation in a reverse-phase HPLC with detection at 254 nm. There was a significant effect of genotype on YAC128 mice brain energy charge [$F(1,12)=6.12$, $p<0.05$], which was ameliorated after i.n. treatment with IGF-1. Pyruvate (b), lactate (c), and lactate/ pyruvate ratio (L/P) (d) were determined in total brain samples from

To determine whether decreased adenine nucleotides and energy balance was a consequence of altered pyruvate and/or lactate levels, as determined previously (Koroshetz et al. 1997), brain levels of pyruvate, lactate and lactate/pyruvate (L/P) ratio were also assessed. In total brain samples, YAC128 mice showed lower pyruvate levels (Fig. 2.9.B). Consequently, YAC128 mice brain also exhibited higher L/P ratio, compared to WT mice ($p=0.059$) (Fig. 2.9.D); importantly, rhIGF-1 i.n. administration

was able to significantly reduce this ratio (Fig. 8D), in agreement with the improvement in energy parameters.

In summary, YAC128 mice show impaired total brain energy metabolism, with lower brain energy change, lower pyruvate levels and higher L/P ratio. Importantly, i.n. administration of rhIGF-1 partially recovered energy metabolism through increased pyruvate levels and thus glycolytic metabolism in the brain of HD mice.

2.4. Discussion

Our results show that exogenous rhIGF-1 given through i.n. administration can alleviate motor impairment and brain metabolic dysfunction, two characteristic features of HD. Interestingly, this occurred concomitantly with the restoration of Akt activity and increased phosphorylation of mHTT.

A major limitation in developing potential therapeutic agents to treat neurodegenerative disorders is the blood-brain barrier, which restricts the delivery of several compounds and peptides to the brain. Indeed, very little IGF-1 can cross the blood brain barrier following systemic administration (Thorne et al. 2004, Laviola et al. 2008). In our study IGF-1 brain cortical levels increased following i.n. treatment, largely suggesting that IGF-1 can reach the CNS. Concordantly, this method has been successfully applied in the treatment of brain injured conditions and neurodegenerative diseases, such as lipopolysaccharide- induced brain injury, focal cerebral ischemia, and spinocerebellar ataxia type 1 (Liu et al. 2002, Vig et al. 2006, Cai *et al.* 2011). Intranasally administered compounds and peptides can reach the CNS via the olfactory and trigeminal neural pathways, which enervate the nasal cavity, providing a direct connection with the CNS (Thorne et al. 2004). The results of our study are in accordance with another study that confirmed that i.n. delivery of IGF-1 to the CNS was accompanied by activation of signalling pathways in several areas that express high levels of the IGF-1 receptor, demonstrating that IGF-1 can reach deeper areas in the brain (Thorne et al. 2004). Intranasal administration also resulted in slightly rising the plasma concentration (although non-significantly), possibly reflecting continual absorption of IGF-1 from the nasal passages (Thorne et al. 2004).

A condition often found in HD patients is weight loss and muscle wasting, which is recapitulated in the R6/2 transgenic mice (Gaba et al. 2005, Goodman et al. 2008). In these mice, we have recently shown restoration of body weight after IGF-1

peripheral treatment (Duarte et al. 2011). In contrast, the YAC128 transgenic mice are overweight, largely exceeding the typical weight for these mice; nevertheless, IGF-1 treatment failed to produce any change in YAC mice weight. Transgenic mice expressing full-length human mHTT, such as BACHD and FVB- YAC128 mice, start to gain weight, compared to WT mice, after 2 months of age, which seems to be due to the background strain (Van Raamsdonk et al. 2007). Comparing the backcrossing of YAC128 mice from the FVB/N strain onto the C57BL/6 strain and the 129 strain, the FVB-YAC128 mice were the only that presented an increase in body weight and reduced lifespan (Van Raamsdonk et al. 2007). A positive correlation was previously found between plasma levels of IGF-1, modulated by full-length HTT, and body weight in YAC128 mice; interestingly, YAC18 mice exhibited higher HTT and plasma IGF-1 levels and increased body weight than YAC128 mice (Pouladi et al. 2010). The mRNA expression of IGF-1 in striatal tissue of YAC128 mice was higher than that of WT control, but in cortical tissues IGF-1 mRNA did not change; conversely, in R6/2 mice with 11 weeks of age IGF-1 plasma levels were largely reduced, which were related with decreased body weight and depletion of endogenous full-length HTT (Pouladi et al. 2010) IGF-1 is an essential modulator of GH action, acting as a neurotrophic and anabolic factor (Juul 2003). Our study failed to reproduce a large increase in plasma and brain IGF-1 levels in non-treated YAC128 compared to WT mice. This difference may be accounted for by considerable high body weights of our WT mice (which are similar to YAC128 mice), as well as for a lower number of animals used compared to Pouladi's study.

HD has been associated with endocrine abnormalities, glucose intolerance and insulin resistance, even in normoglycemic patients (Podolsky et al. 1977, Farrer 1985, Lalic et al. 2008). These metabolic changes have been reproduced in R6/2, R6/1 and N171-82Q mice, which may culminate, in the later stages, in a diabetic state (Schilling et al. 1999, Bjorkqvist et al. 2005, Josefsen et al. 2008). Nevertheless, a previous study highly suggested that adult-onset HD patients do not have an increased risk of developing diabetes (Boesgaard et al. 2009). Our data reflect hyperglycemic features in FVB background. Both WT and YAC128 transgenic mice exhibited elevated glycemia under fed conditions (180-260 mg/dl) and pathological values of glycated haemoglobin (>9% of total haemoglobin), compatible with diabetes mellitus. Interestingly, significant differences were observed between WT and YAC128 before IGF-1 treatment in the ITT, which could be related with altered insulin sensitivity to regulate plasma glucose.

Following IGF-1 treatment, both groups showed a significant reduction of the ITT-AUC. Decreased insulin resistance in IGF-1 treated YAC128 mice may be related with slightly higher plasma insulin levels and/or possible higher sensitivity to insulin, as plasma glucose uptake tend to increase as evaluated by GTT and ITT. Conversely, hyperglycemia in R6/2 mice may be a consequence of pathogenic mechanisms occurring due to polyglutamine inclusions in pancreatic β-cells, impairing insulin secretion (Bjorkqvist et al. 2005). In the R6/2 mice, IGF-1 appears to have a protective role against HD-associated peripheral impairment of glucose tolerance, namely through increased blood insulin levels, as shown by us (Duarte et al. 2011). Another possible explanation for this improvement involves the IGF-1-induced Akt phosphorylation which appears to be linked to both production and translocation of glucose transporter 4 (GLUT4) from intracellular pools to the membranes in the normal developing brain and in regulation of brain hexokinase activity in astrocytes (Laviola et al. 2008).

Indeed, we found reduced activation of Akt in YAC128 mice in cortical and striatal tissue, corroborating a previous study where the levels of Akt and its activated form were diminished before neuronal loss in a rat model of HD (Colin et al. 2005). In peripheral tissues from HD patients, Akt specific activity was also found to be reduced, and in final stages of the disease lower Akt levels were observed in postmortem brain samples (Colin et al. 2005). These observations demonstrate a linear progressive alteration of Akt activation and disease progression (Colin et al. 2005, Warby et al. 2009). In IGF-1-treated YAC128 mice Akt phosphorylation was increased; under these conditions we also observed motor improvement and amelioration of brain metabolic deficits. Mild recovery of motor impairment in YAC128 mice seems to be related with the increase in IGF-1 levels in cortical areas. Indeed, restricted motor outcome may be related with non-significant IGF-1 levels in the sub- cortical areas, i.e. the striatum. In agreement with our study, in spinocerebellar ataxia type 1 transgenic model, i.n. administration of IGF-1 was able to improve motor coordination on the rotarod behavior test (Vig et al. 2006). Nevertheless, in HD patients Saleh and co-authors (Saleh et al. 2010) established a negative correlation between plasma IGF-1 levels and the degree of cognitive deterioration, contradicting another study where IGF-1 was described to delay cognitive impairment in healthy elderly (Arwert *et al.* 2005). The present data suggest that i.n. IGF-1 can be properly delivered to the brain, positively influencing the phenotype of the disease.

One putative mechanism proposed for this phenotype rescue involves phosphorylation of HTT at Ser421 by Akt. Indeed, HTT is a substrate of Akt and its phosphorylation is crucial to mediate the neuroprotective effects of IGF-1 (Humbert et al. 2002). Importantly, our results show a large increase in the phosphorylation of mHTT at Ser421 upon IGF-1 treatment in striatal and cortical tissue in YAC128, compared to saline-treated mice, concomitantly with increased phosphorylation of Akt. Recent studies demonstrated that phosphorylation of HTT at S421 restores HTT function in microtubule-based transport (Colin et al. 2008, Zala et al. 2008). We verified that P-wtHTT and P-mHTT was lower in striatum (approximately 2- fold less) in saline-treated mice. This regional difference in the endogenous pattern of HTT phosphorylation, being lower in the striatum relatively to the cortex of wild-type mice, may predispose the striatum to degeneration (Warby et al. 2009). Decreased HTT phosphorylation was seen prior to overt neuropathology in the YAC128 mice and may contribute to HD-related pathogenesis, since a correlation exists between the decline in the level of pS421-HTT in the striatum of YAC128 mice and the aged phenotype (Metzler et al. 2010). In the present study we demonstrate that IGF-1 promotes the activation of cortical and striatal intracellular signaling pathways in YAC128 mice and the phosphorylation of mutant HTT at S421.

Another hallmark of HD is the impairment in energy metabolism. Glucose metabolism was found to be significantly decreased in striatum and temporal and frontal cortical lobes, in both preclinical and affected HD patients, with marked striatal hypometabolism reflecting neuronal atrophy (Ma *et al.* 2007). The relationship between mHTT and mitochondrial dysfunction is widely recognized, resulting in bioenergetic failure (Bossy-Wetzel et al. 2008, Rosenstock *et al.* 2010). This interaction occurs with proteins of the respiratory chain, reducing their activity and compromising energy metabolism (Milakovic *et al.* 2005, Rosenstock et al. 2010). Thus, L/P ratio is typically elevated due to increased regional brain lactate production (Martin et al. 2007) as a result of mitochondrial dysfunction and/or reduced mitochondrial usage of pyruvate, as we showed recently (Ferreira et al. 2011) or due to decreased pyruvate levels accompanying glycolysis inhibition. In this perspective, mHTT is known to interact and decrease the activity of GAPDH (glyceraldehyde-3-phosphate dehydrogenase), which is fundamental for the glycolytic pathway (Wu et al. 2007). In the present study, YAC128 mice brain exhibited lower levels of pyruvate and increased L/P ratio. Our results are in agreement with the results obtained by other studies (Martin et al. 2007, Olah *et al.*

2008) since saline-treated YAC128 mice showed a higher L/P ratio, compared to WT littermates in brain tissue. This may result from altered glucose metabolism in neurons and/or glial cells. A major finding of this study is that IGF-1 ameliorates energy deficits in YAC128 mice brain. Treatment with rhIGF-1 was capable of decreasing L/P ratio in YAC128 mice brain by increasing pyruvate levels, suggesting the improvement of glycolytic function. IGF-1 in the brain can modulate energy metabolism and its decline is associated with loss of energy metabolism (Cheng et al. 2000, Pruszak et al. 2007). A possible mechanism for IGF-1- induced glycolysis upregulation may occur through IGF-1-induced Akt phosphorylation, which may regulate GLUT4 translocation and thus increase glucose uptake. In the rat hippocampus, insulin (applied through intracerebroventricular administration)- stimulated phosphorylation of Akt was localized to neurons and was linked to the translocation of GLUT4 to the plasma membrane (Grillo *et al.* 2009), similarly as described in peripheral tissues. Thus, IGF-1 may act in an insulin-like manner to promote glucose uptake and possible storage of glycogen in non-neuronal cells.

In conclusion, we demonstrate that the non-invasive route of administration of IGF-1 through i.n. can be efficient in increasing the levels of the neurotrophic factor in the brain, with an important outcome of rescuing motor deficits and glucose metabolic dysfunction in HD, even in the YAC128 mice exhibiting slightly increased levels of IGF-1 in the striatum. These data provide an experimental basis for establishing intranasal administration as an important therapeutic route for the administration of neurotrophic factors, such as IGF-1, in HD and in other neurodegenerative diseases. A successful therapy approach for HD patients implies that it has to efficiently cross the blood brain barrier (BBB) and reach the specific brain area to which it is directed. Indeed, i.n. administration can effectively overcome some of the major limitations described for other technical approaches (such as transient BBB opening, drug delivery vehicles as viral vectors or nanoparticles), since it reduces systemic toxicity and increases tissue- specific concentrations. In humans, insulin administration was shown to improve cognitive function in patients with early Alzheimer's disease (Reger *et al.* 2008) without overall changing blood glucose or insulin levels (Born *et al.* 2002). Given the promising results in recent animal studies, the clinical potential of such neuropeptide/growth factor delivery method in patients suffering from neurodegenerative diseases is very significant.

CHAPTER III - Dominant-negative effects of adult onset mutant Huntingtin leads to an altered division of human embryonic stem cells derived neural cells

3.1. Introduction

Huntington's disease is a dominant neurodegenerative disorder caused by abnormal extension of a CAG repeat tract in the first exon of at least one of the two alleles of the *HTT* gene (Group 1993); when mutated the huntingtin protein contains an extended stretch of glutamine (poly-Q) near its NH_2 terminus that is encoded by this tract (Persichetti *et al.* 1995). While in the general population the average CAG expansion is 18 repeats, patient with HD carry expansion exceeding 35. In most patient with HD, the longest CAG expansion of the two HTT alleles range from 41 to 48 with an average 44 repeats (Andrew *et al.* 1993, Snell *et al.* 1993, Rubinsztein et al. 1996, Killoran *et al.* 2013). In these patients characteristic psychiatric, cognitive and motor disturbances emerge usually between 35 and 50 year old; HD is then inexorably fatal within 10 to 15 years. Early onset of symptoms, increased severity and more rapid progression of the disease is associated with higher CAGs repeat numbers (Andrew et al. 1993). Fewer than 10% of patients develop symptoms before age 20. This juvenile variant of the disease is characterized by a more widespread and rapidly progressing pattern of brain degeneration that cause very different symptoms than adult-onset HD. Patient with juvenile-HD carry expansion with usually more than 60 CAGs (Nance et al. 1999, Nance et al. 2001, Seneca et al. 2004)

Huntingtin is a large scaffold protein involve in diverse cellular functions in multiple cellular compartments (Li et al. 2004, Fiorini et al. 2013). Among hundreds of protein partners, HTT protein interacts with microtubules (MTs), directly with dynein and indirectly with dynactin through huntingtin-associated protein 1 (HAP-1) which binds to its $p150^{Glued}$ subunit to form the dynein/dynactin complex. This complex regulates the microtubule-dependent transport of organelles in neurons (Gauthier et al. 2004, Caviston et al. 2007, Colin et al. 2008, Zala et al. 2008), ciliogenesis (Keryer *et al.* 2011) and ensure a proper mitotic spindle orientation thus contributing to the regulation by HTT of cell fate (Godin et al. 2010, Elias et al. 2014). Current knowledge on pathological processes suggested that neuronal loss in HD is caused both by a loss of wild-type (wtHTT) functions and the gain of new toxic functions by mutant HTT (mutHTT) likely acting both cell and non-cell autonomously (Landles et al. 2004, Biagioli *et al.* 2015).

Genetic mice and cellular models most often used to study the impact of HTT mutations express fragments or full length mHTT with exacerbated poly-Q stretch encoded by

expansion over 100 (or even 140) CAG repeats. The capacity of such acute models to accurately replicate the decade long pathological processes, originating from the most common form of HD mutations (41-48 CAGs), observed in the brain of patient is difficult to ascertain.

Technologies providing access to human pluripotent stem cells (hPSC) (hESCs: (Thomson et al. 1998) & hiPSCs: (Takahashi et al. 2007, Yu *et al.* 2007) have allowed the development of a new disease model based on hPSC derivatives that may help bridge the gap between our current understanding of HD, based on the wealth of existing HD genetic models, and the actual pathological processes occurring in patient. A number of disease-specific (i.e mutant) hPSC lines derived from embryos characterized as mutant-gene carriers during a pre-implantation genetic diagnosis procedure or derived from patient fibroblasts have been obtained. Several of these lines (all in the case of HD-human embryonic stem cells (hESC)) carry triplet repeats with common lengths for the adult-onset form of the disease (Mateizel *et al.* 2006, Park *et al.* 2008, Zeuschner et al. 2010, Bradley *et al.* 2011, Consortium 2012). Such HD-hPSC lines has just started to be used to decipher the impact of adult or juvenile-onset HTT mutation in human cells (Camnasio *et al.* 2012, Feyeux *et al.* 2012, Drouet *et al.* 2014, Farr et al. 2014).

Recently the consequence of *HTT* mutation for cell division has been deciphered in context of cortical development (Molina-Calavita et al. 2014) and mammary carcinoma progression using mouse genetic model carrying *HTT* mutation with expansion over 100 CAG repeats (Carroll et al. 2011). In the present study we combined the use of neural derivatives of wild type and adult-onset HD-hESC and SNP-targeting allele specific HTT mRNA interference to address the consequence of adult-onset HTT mutation on human neural progenitors division.

3.2.Materials and methods

3.2.1.Cell culture

Neural cells were derived from H9 (WT XX, passages 40–60, WiCell Research Institute) (Thomson et al. 1998), SIVF018 (XX, 46 CAG, passage 18-30, Sydney IVF Stem Cells, Australia) (Bradley et al. 2011) and SA01 (WT XY, passages 12, CellArtis AB, Göteborg, Sweden) (Heins *et al.* 2004) embryonic stem cell lines, as previously described in (Nicoleau *et al.* 2013). Neural Stem Cells obtained were maintained on poly-L-ornithine and laminin (Sigma, St. Louis, Missouri, United States) coated plates until passage 29 and then discarded. Cells were harvested with 0.05% trypsin (Invitrogen, Cergy Pontoise, France) and seeded at 100.10^3 cells/cm^2 in culture plates. NSCs were cultured in 1:1 ratio of Neurobasal: DMEM/Hams's F-12 (Invitrogen, Cergy Pontoise, France), supplemented with 0.1% penicillin/streptomycin, 0.1% β-mercaptoethanol (Sigma-Aldrich), 1% B27 (Invitrogen, Cergy Pontoise, France), 0.5% N_2 (Invitrogen, Cergy Pontoise, France), 10 ng/mL FGF_2 (Invitrogen, Cergy Pontoise, France) and 10 ng/mL EGF (R&D systems, Minneapolis, USA). The medium was changed every 2 days or when needed. Cells were plated in multi-well plates 54 hr before synchronization using RO-3306 (18hr, 10µM) (Enzo Life Sciences, France). The population was released from the G2 block by three washes with pre-warmed drug-free media and incubation with fresh media (30 min).

3.2.2.DNA constructs and siRNA

Genotypes on exon 50 for SNP rs362331 of H9 and SIVF018 NSC lines were analyzed by sequencing the PCR product encompassing this SNP generated using the following primers: 5'-CCCCAAACGAAGGTACACGA-3' and 5'-CCTGTTGGCCATCTCTCACC-3'. SIVF018 NSC line is heterozygous at SNP rs362331 (C/T) while H9 is homozygous (T/T). shRNAs targeting these SNP (si50C, si50T) were designed as previously described (Drouet et al 2014). The SIN-CWP-GFP-LTR(N)-TRE-si1.1 (complete knock-down, shHTT), SIN-CWP-GFP-LTR(N)-TRE-si50T (50T allele specific, sh50T), SIN-CWP-GFP-LTR(N)-TRE-si50C (50C allele specific, sh50C) and SIN-CWP-GFP-LTR(N)-TRE-siUNIV (shcontrol) plasmids were previously described (Drouet et al. 2014). The plasmids encoding N-terminal fragments of wild-type (23Q; mCherry-HTT-N586-23Q) and poly-Q HTT (100Q; mCherry-HTT-

N586-100Q) constructs, were generated by the cleavage of pARIS-HTT encoding full-length HTT (Myers et al. 1991).

.

3.2.3.Transfection

Prior to nucleofection, cells were harvested with trypsin. $5x10^6$ cells were nucleofected using the Amaxa® Rat NSC Nucleofector® Kit (Lonza) according to the manufacturer's protocol. NSCs were resuspended in 100 µL of nucleofection solution with 5 µg of DNA and 0.5 µg pmaxGFP® Vector and electroporated with an Amaxa Nucleofector Program A-033 (Lonza) before plating on poly-ornithine/laminin coated dishes. For shRNA nucleofection, Five million NSCs resuspended in 100 µL of nucleofection solution of the Amaxa® Rat NSC Nucleofector® Kit (Lonza) with 5µg of shRNA (1µM) were electroporated with an Amaxa Nucleofector Program A-033 (Lonza) before plating on poly-ornithine/laminin coated dishes. All cells were incubated in humidified 37°C/5% CO_2 incubator and medium was changed after 24 hr.

3.2.4.RNA extraction and quantitative RT-PCR

Total RNA from NSC cells was extracted using RNeasy® Mini Spin Columns (Qiagen, Courtaboeuf, France). The purified RNA was then quantified with NanoDropR ND-1000A spectrophotometer (A260/A280 ratio 1.9–2.1; 28S:18S rRNA ratio on agarose gels 2:1). Reverse transcription was performed on 500 ng of RNA using Cloned AMV First-Strand cDNA Synthesis Kit (Invitrogen, Cergy Pontoise, France). cDNA synthesis was performed using total RNA primed with oligo(dT) (50 µM) mixed with Random Hexamers (50 ng/µL) according to manufacturer's protoco. Quantitative real time-polymerase chain reactions (QRT-PCRs) are performed with Power SYBR Green PCR Mix (ROCHE) and a LC480 system (Roche). Quantification was performed at a threshold detection line (Ct value). The Ct of each target gene was normalized to the 18S housekeeping gene. For primer sequences see Supporting Information Table 4.
HTT mRNA allelic ratio analysis was performed using "TaqMan® SNP Genotyping Assays" (Hs00918153_m1: Applied Biosystems, Foster City, CA, USA) on cDNA used for QRT-PCR. The mean of difference of Ct of each target allele (3 technological replicate) was used to calculate the HTT allelic ratio expressed in % of SNP 50C and

SNP50T in all HTT mRNA (Genomic DNA was used a control sample with 50%/50% HTT allelic ratio).

For the CAG repeats size analysis, a PCR was performed using TaKaRa LA Taq DNA Polymerase with GC Buffers (Takara Bio, Madison, USA), according to manufacturer protocol, on cDNAs obtained from allele specific cDNA synthesis using specific primers for HTT exon 1 5´-AAGGCCTTCGAGTCCCTCAA-3' and 5'-CACACGGTCTTTCTTGGTAGC-3'. The expected amplicon size for a normal allele with 23 CAG repeats is 281bp. The PCR products were analyzed by the Bioanalyser 2100 (Agilent, CA, USA) using microfluidic chips which were prepared according to manufacturer's instructions. Analysis of the data was performed using Data Review software version A.01.20 Sl211 and presented in the form of electropherograms or alternatively as a list of calculated band sizes.

Table 4- Sequences of the oligonucleotides used to generate the shRNA targeting the SNP and the control. In bold are the sense and anti-sense strands of the shRNA. In red is the position of the SNP (Drouet et al. 2014).

NAME	SEQUENCE
siHTT	CTAGTTTCCAAAAA**AAGAACTTTCAGCTACCAA**TCTCTTGAA**TTGGTAGCT GAAAGTTCTT**GGGGATCTGTGGTCTCATACAGAAC
siscramble	CTAGTTTCCAAAAA**GTATCGATCACGAGACTAG**TGACAGGAAG**CTAGTCT CGTGATCGATAC**GGGGATCTGTGGTCTCATACAGAAC
si50C	CTAGTTTCCAAAAA**CCCTCATCCACTGTGTGCA**TGACAGGAAG**TGCACACA GTGGATGAGGG**GGGGATCTGTGGTCTCATACAGAAC
si50T	CTAGTTTCCAAAAA**CCCTCATCTACTGTGTGCA**TGACAGGAAG**TGCACACA GTAGATGAGGG**GGGGATCTGTGGTCTCATACAGAAC

3.2.5.Immunofluorescence

To visualize spindles, cells were permeabilized with PHEM/0.5% Triton X-100 for 30 sec then fixed with 4% PAF/PHEM (20 min at RT) and then with -20ºC methanol (5 min). Cells were rehydrated with PBS/0.1% Triton X-100 (3 washes), blocked in 10% Normal Goat Serum (NGS)/PBS (30 min) and incubated with the following antibodies: anti γ- tubulin (1:500, T3320 or 1:100, 6557; Sigma-Aldrich); anti-P150^{Glued} (1:100,

610474; BD Transduction Laboratories), anti-736-HTT (1:300; polyclonal (Arning *et al.* 2007)), anti-NUMA (1:500; Novus biological)

For dynein intermediate chain (DIC) staining (1:200; mAB 1618 Chemicon) the fixation procedure was as followed: cells were immersed in microtubule stabilizing buffer (MTSB: 4M glycerol, 100 mM PIPES, pH6.8, 1 mM EGTA, 5mM $MgCl_2$) for 2 min, followed by extraction for 2 min in MTSB/0.5% Triton X-100. Cells were then fixed 3 min with -20ºC methanol.

For all immunostainings, the slides were counterstained with DAPI (Roche) and mounted in Mowiol. The pictures were captured either with a three-dimensional deconvolution imaging system as previously described (Gauthier et al. 2004) or with a Leica DM RXA microscope equipped with a 63x oil-immersion objective coupled to a piezzo and a Micromax RTE/CDD-1300-Y/HS camera controlled by Methamorph software (Molecular Devices). Z-stack steps were of 0.3 µm. Images were treated with ImageJ (HTTp://rsb.info.nih.gov/ij/, NIH, USA).

3.2.6. Spindle Orientation Quantification and Image Analyses

Spindle orientation in metaphase cells stained for γ-tubulin and DAPI to visualize the spindle poles and chromatin was quantified using ImageJ software (HTTp://rsb.info.nih.gov/ij/, NIH, USA). A line crossing both spindle poles was drawn on the Z projection pictures and repositioned along the Z-axis using the stack of Z-sections. The angle between the pole-pole and the substratum plane was calculated by the ImageJ Plug-in. Spindle lengths and cell lengths were quantified along the line that crosses both spindle poles.

The quantification of $P150^{Glued}$ and DIC at spindle poles was achieved with 3D object counter plugin (Bolte *et al.* 2006),; HTTp://imagej.nih.gov/ij/plugins/track/objects.html. A circle (radius equal to half of pole-pole distance) was drawn around the pole position, and image was cleared outside the circle. Total volume and intensity of the particles were retrieved for further analysis.

Quantification of NUMA at spindle pole was performed on the resulting z-stacks (one for each pole) using JACoP plugin (HTTp://imagej.nih.gov/ij/plugins/track/jacop.html) which determines the localization of NUMA at spindle poles given by γ-tubulin. Manders' overlap coefficient corresponds to the co-localization between both images.

Numb distribution at the membrane was done on the resulting z stack by drawing a scanline around the cells outline followed by profile plot and analyses of the distribution (symmetric vs. asymmetric).

3.2.7.Immunoblotting

Cells were lysed 72h after transfection (lysis buffer: 50 mM Tris-HCl pH 7.5, 0.1% Triton X-100 2 mM EDTA, 2 mM EGTA, 50 mM NaF, 10 mM β-glycerophosphate, 5 mM sodium pyrophosphate, 1 mM sodium orthovanadate, 0.1% (v/v) β-mercaptoethanol, 250 µM PMSF, and 10 mg/ml aprotinin and leupeptin). Twenty five □g of protein was loaded in 6% gel, subjected to SDS-PAGE and electrophoretically transferred to Protran nitrocellulose membranes from Whatman. Blots were blocked in 5% BSA/TBST buffer (20 mM TrisHCl, 0.15 M NaCl, 0.1% Tween 20) and incubated with anti-HTT D7F7 (1:1000; Cell Signaling Technology, Danvers, USA), anti-polyQ 1C2 (1:5000; Euromedex, France) and anti α- tubulin (1:1000; Sigma) antibodies for 1hr.

3.2.8.Statistical analyses

GraphPad Prism 5.0 software (San Diego, CA) was used for statistical analysis. Data are expressed as mean ± SEM of the indicated number of independent experiments. Statistical significance was analyzed using parametric tests, namely Student's t-test and one way-ANOVA. Complete statistical analyses with number of measures are detailed in Supplemental Information.

3.3. Results

3.3.1. Human HTT regulates spindle orientation in dividing neural stem cell derived from human embryonic stem cells

We previously showed that HTT modulates spindle orientation in mouse neural and HeLa cells, and in cortical progenitors *in vivo* (Godin et al. 2010). To address whether human HTT has the same function, we used neural stem cells (NSC) differentiated from wild-type human embryonic stem cells (hESC) (H9 line) and used plasmids encoding a short hairpin RNA (shRNA) directed against HTT (sh*HTT1.1*) or a control shRNA (shControl) to study the effect of the knock-down of HTT expression (Figures 3.1A). HTT protein level measured by western blot was reduced by 70%+/- 16.18 (n=3) in H9-derived WT-NSCs 72 hours after transfection with the sh*HTT1.1* plasmid (Figure 3.1B). During mitosis, the polyclonal mAb763 antibody labelled HTT at the spindle poles as previously described (Godin et al. 2010) (Figure 3.1D). We also observed HTT localizing at the cell cortex. Treatment with shHTT led to a statistically significant reduction of signal intensity at the spindle pole and to a dispersion of HTT from its cortical localization.

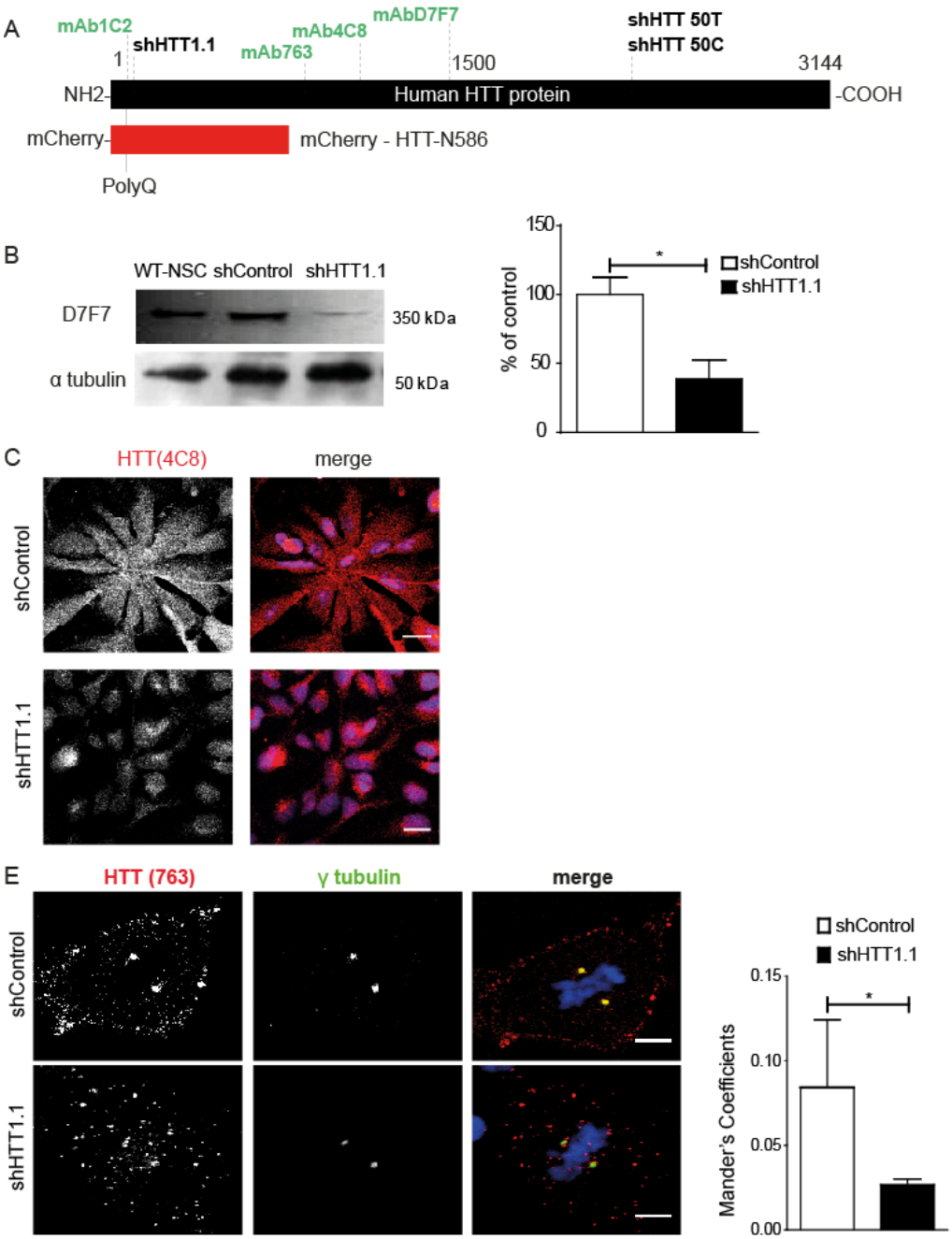

Figure 3.1. Silencing of HTT in wild-type neural stem cells.

(A) Schematic representation of HTT. **(B)** Immunoblotting with anti-HTT and anti-α-tubulin antibody of lysates of H9 cells treated with shcontrol and shHTT. The graph represents the quantitative assessments of the ratio of HTT over tubulin in each conditions.**(C)** Immunostainings of shcontrol and shHTT-treated cells with anti-γ-tubulin and anti-HTT (4C8) antibodies and DAPI counterstaining. **(D)** Immunostainings of metaphasic shcontrol and shHTT-treated cells with anti-γ-tubulin and anti-HTT antibodies and DAPI counterstaining. Quantification of anti-HTT signal at the spindle poles (p=15-20, n=13 cells).

Results are shown as mean values ± SEM. *p<0.01.

We next immunostained with an anti-γ-tubulin antibody, H9-derived WT-NSCs transfected with shControl or sh*HTT1.1* plasmids to analyse in Z-series stacks (ΔZ > 1.8 µm) the position of the spindle poles with respect to the substratum plane (Figures 3.2A and 3.2B). Spindle orientation was quantified in metaphasic cells by determining the angle between the pole-pole axis (axis of the metaphase spindle) and the substratum plane. Non-transfected and WT-NSCs transfected with shControl plasmid showed a significantly lower mean angle (7.6º ± 0.7, n=86; 8.1º± 0.9, n=65) compared to sh*HTT1.1*-treated cells (18.9º± 2.1, n=74) (Figure 3.2B). In sh*HTT1.1*-transfected WT-NSCs there was more metaphasic cells with an angle superior to 10º (79.5%) compared to control cells (non-transfected 28%; shcontrol 30%;). In particular, there was a significant proportion of cells (30.1%) having spindle angles greater than 20º in sh*HTT1.1* condition.

We confirmed these results using an alternative RNA interference plasmid targeting the SNP rs362331 in exon 50 of the *HTT* gene in the H9 genome. Genotyping of H9 cells (supplementary data) revealed that the H9 WT-hESC line is homozygous for the SNP rs362331 in exon 50 (T/T). We therefore transfected H9-derived WT-NSCs with a plasmid encoding an allele-specific shRNA targeting SNP rs362331 –T in exon 50 of the HTT gene (sh*HTT50T*) i.e targeting both allele of the HTT in H9-hESC derivatives (Feyeux et al. 2012). H9-derived WT-NSCs treated with shControl had mean spindle angles below 10º (8.9º ± 0.7, n=129; 7.4º± 0.6, n=106), while the mean angle in sh*HTT50T*-treated WT-NSCs was above 20° (22.4º± 2.3, n=32) (Figure 3.2C). In sh*HTT50T*-treated cells, the spindle angles were randomized with more than 33% of the metaphasic cells with an angle superior to 20º.

Next we introduced in WT-NSCs an 586 amino acid N-terminal fragment of human HTT (HTT-N586-23Q) that recapitulates HTT function during microtubule-based transport (Colin et al. 2008). The nucleotide sequence encoding this fragment was modified in order not to be targeted by the sh*HTT1.1* which specifically targets endogenous human HTT (Pardo *et al.* 2010). HTT-586-23Q/ *HTT-N586-Q23* rescued the spindle orientation defect observed when silencing HTT in WT-NSCs (Figure 3.2D).

Finally, we also analyzed the distribution of cells across mitotic phases based on chromosome configurations. HTT-depleted and control WT-NSCs had similar distribution of cells across mitotic phases (Figure 3.2E; (Godin et al. 2010)). These

findings support that human HTT regulates spindle orientation with no effect on the progression through the cell cycle in human neural stem cells.

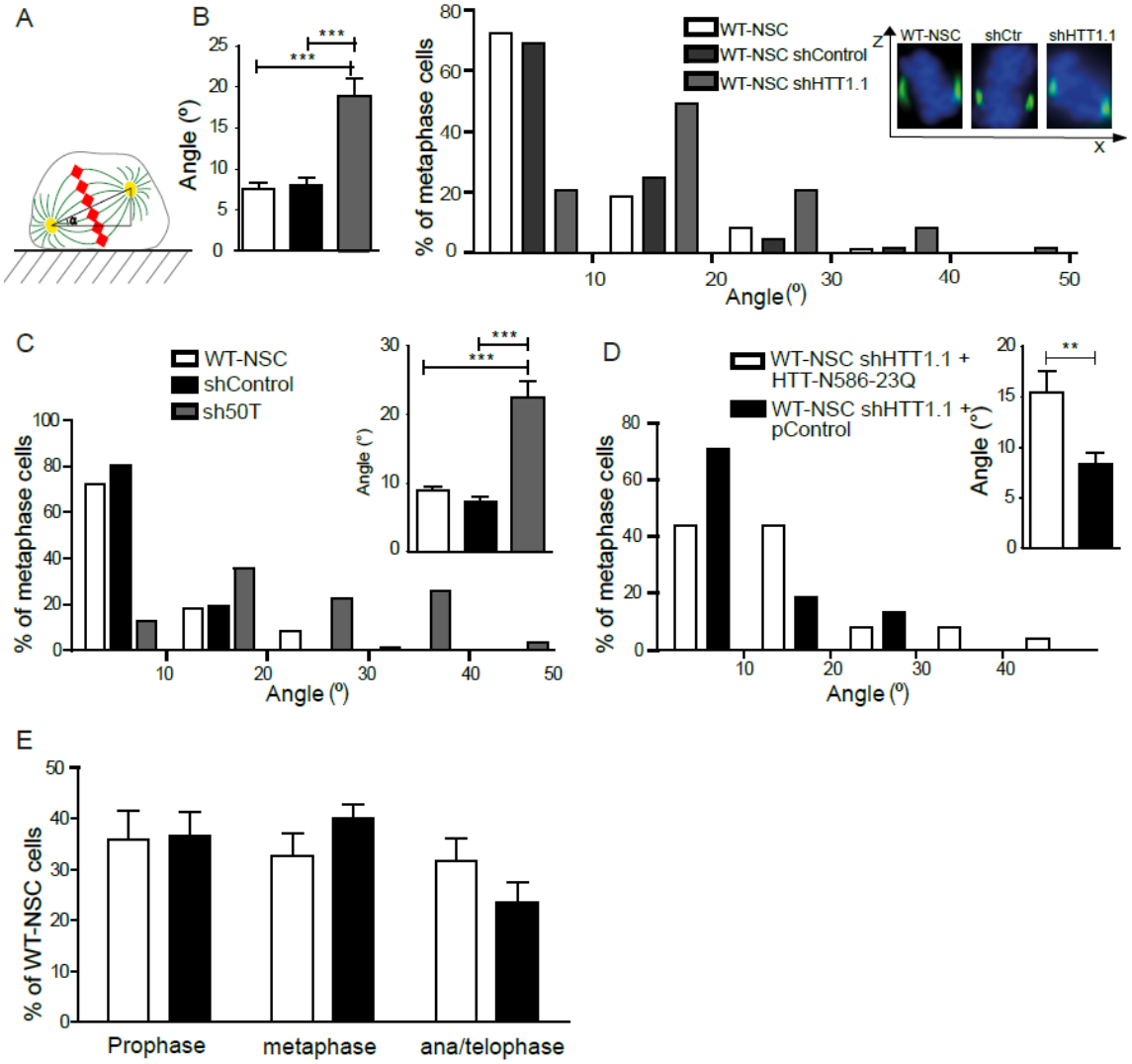

Figure 3.2.- Silencing of human HTT induces spindle misorientation.

(A) Schematic illustration of spindle angle measurement. **(B-D)** H9 neuronal stem cells were either non-treated or treated with shcontrol, shHTT, sh50T or shHTT + N586-HTT-Q23 as indicated. Distribution and average of spindle angles of metaphase cells are shown. (**B**) Cells were stained with anti-γ-tubulin and DAPI and Z-X projections are shown. **(E)** Distribution of H9 cells transfected with shcontrol and shHTT in prophase, metaphase and ana/telophase of cell cycle. Results are shown as mean values ± SEM. ***p<0.001; **p<0.01.

3.3.2.HTT is required for the mitotic localization of dynein, dynactin and NUMA in human NSCs

HTT associates with dynein/dynactin to stimulate axonal transport in neurons (Gauthier et al. 2004, Colin et al. 2005). Silencing of mouse HTT in neuronal cells mislocalizes the $P150^{Glued}$ subunit of dynactin, dynein and the large Nuclear Mitotic Apparatus protein NUMA at the spindle poles suggesting that HTT could scaffold these proteins to ensure correct spindle orientation (Godin et al. 2010). We immunostained H9-derived NSCs for HTT during mitosis and observed a strong HTT labelling at the spindle poles (Figure 3.3A). To a lesser extent, HTT also localized at the spindle and microtubules plus ends. Dynein, the $P150^{Glued}$ subunit of dynactin and NUMA were present at the spindle poles and spindle, along astral microtubules and at cortical sites (Figures 3.3B-D). We analyzed whether these localizations depend on HTT by silencing endogenous human HTT (Figures 3.3E). Silencing of HTT in WT-NSC using shHTT1.1 plasmid resulted in partial mislocalization of dynein and $P150^{Glue}$d from the spindle poles (Figures 3.3B-D). In contrast, NUMA accumulated at the spindle poles when HTT levels were lowered. In HTT depleted human NSC, the astral microtubules and cortical localization of dynein, $P150^{Glued}$ and NUMA was reduced. We thus propose that human HTT controls the proper localization of several key mitotic proteins and that this may, as a consequence, influence spindle orientation in human WT-NSCs.

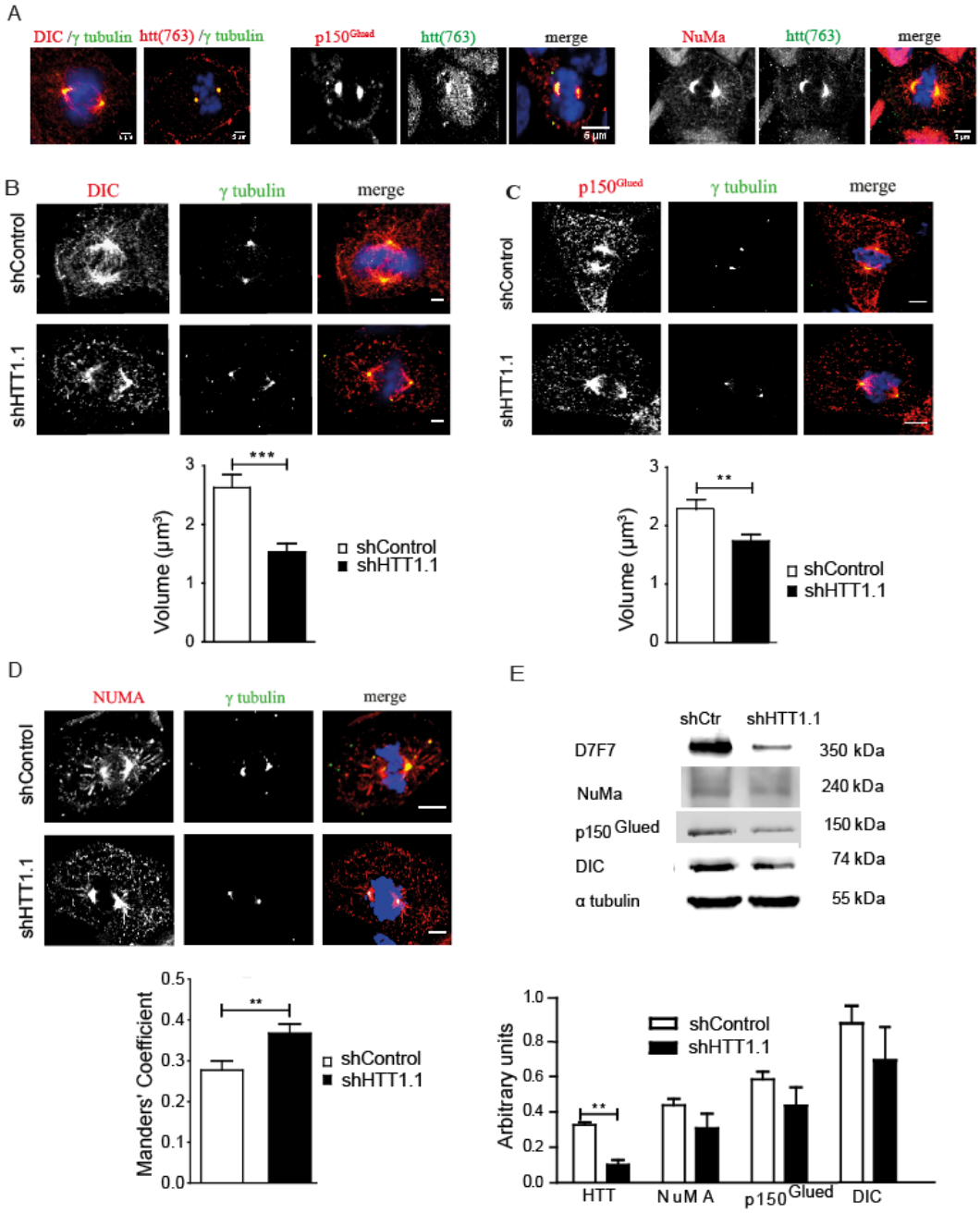

Figure 3.3. - Loss of HTT alters P150^{Glued}, dynein and NUMA localization

(A, B, C) Immunostaining of metaphasic neural stem cells with anti-DIC and anti-HTT (**A**), anti-P150^{Glue} and anti-HTT **(B),** anti-NUMA and anti-HTT **(C). (D, E, F)** Immunostaining of metaphasic neural stem cells with anti-DIC (**D**), anti-P150^{Glue} **(E),** anti-NUMA **(F)** and anti-γ-tubulin antibodies and DAPI counterstaining. Graphs represent the quantification of n=52 and n=60 for D; n=57 and n=60 for E, n=22 for F. **(E)** Immunoblotting of extracts of H9 cells treated with shcontrol and shHTT for the presence of the indicated proteins. Results are shown as mean values ± SEM. ***p<0.001; **p<0.01.

3.3.3.Human adult-onset mutant HTT exerts a dominant negative effect on spindle orientation in HD-hESC derived NSCs

We next addressed the effect of HD mutations on the role of HTT during spindle orientation in dividing NSCs derived from hESCs. We first expressed a mutant 586 amino acid N-terminal fragment of HTT with an expanded polyglutamine stretch of 100 residues (HTT-N586-100Q) in WT-NSCs derived from H9-hESCs. In WT-NSCs expressing HTT-N586-Q100, we observed a significant increase in the mean angle compared to controls (16.9º± 1.3; n=51 versus non-treated cells: 7.6º± 0.7, n= 86 and WT-NSC expressing an empty plasmid: 8.3º ±1, n=38) (Figure 3.4A). In particular, 78.4% of metaphasic cells expressing mutant HTT had a spindle angle with an angle superior to 10º.

We then used NSCs differentiated from a hESC lines characterized as carriers of one *HTT* allele with an adult onset mutant-gene during a pre-implantation genetic diagnosis procedure (SIVF018 line). In this cell line, the longest CAG expansion size is 46 CAGs; the size of CAG expansions and the link between the mutated allele was and the SNP rs362331 at exon 50 (50T) was confirmed (Supplementary Figure 1A). Allelic ratio of *HTT* allele using Taqman probe specific for SNP rs362331-T and -C in HD-NSCs nucleofected with siRNA targeting SNP rs362331-T(siHTT4) and SNP rs362331-C (siHTT5) showed that SNP-targeting RNA interference could discriminate both alellele as previously shown (Drouet et al 2014).

As expression of a mutant HTT fragment leads to a defect in spindle orientation that is similar to the loss of function in WT-NSC (Figures 3.2B and 3.4A), we assessed whether the allele specific silencing of mutant HTT was associated to a functional recovery. Treatment of SIVF018 HD-NSCs with sh50T had no effect on the progression through the cell cycle (Figure 3.4C). We compared spindle angles in non-treated, and shcontrol- or sh50T-treated SIVF108 cells. Non-treated and shcontrol-treated SIVF108 HD-NSCs had spindle angles distribution and mean spindle angles comparable to that of loss of function situation (19º± 1.2, n=83; 16.8± 1.5, n=61) (Figure 3.4D and see Figure 3.2). In contrast, in SIVF018 cells treated with sh50T, most of the cells divided with an angle below 10° and the mean spindle angle was comparable to that of wild-type situation (9.5º±1, n=68). We also expressed a wild-type HTT fragment (N586-HTT-Q23) in mutant cells and found no effect on the distribution and mean spindle angles observed in mutant situation (Figure 3.4E).

Taken together, these results indicate that a limited expansion in HTT similar to that found in most patients with HD is sufficient to induce a dominant negative effect on spindle orientation. Furthermore, an allele-specific silencing of mutant HTT in HD cells is associated with a functional recovery during spindle orientation.

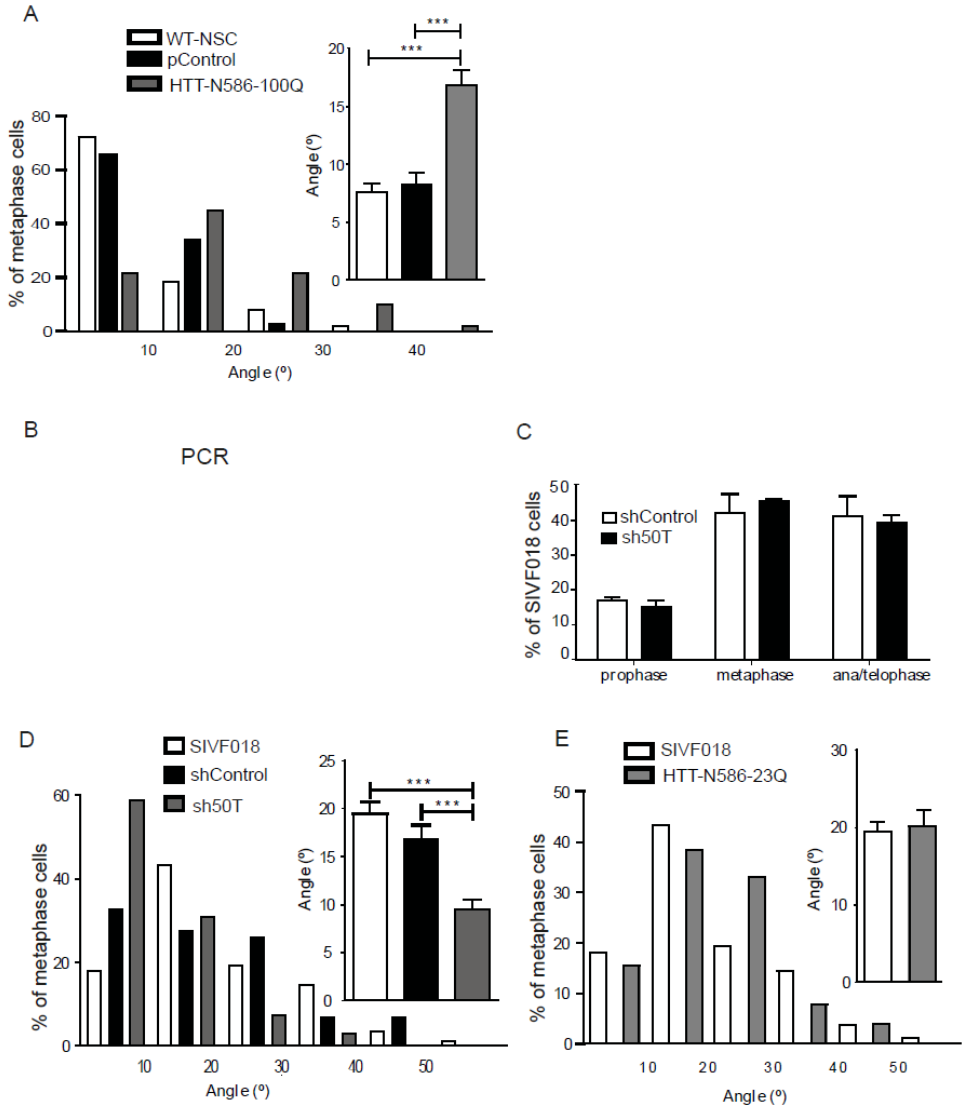

Figure 3.4.-Allele specific silencing rescues spindle misorientation in NSC derived from HD patients

(A) H9 neural stem cells were either non-electroporated or electroporated with empty plasmid and N586-HTT-Q23 as indicated. Distribution and average of spindle angles of metaphase cells are shown.

(B) PCR (C) Distribution of shcontrol and sh50T SIVF018 cells in prophase, metaphase and ana/telophase of cell cycle. **(D,E)** SIVF018 cells were either non-electroporated or electroporated with shcontrol, sh50T and N586-HTT-Q23 as indicated. Distribution and average of spindle angles of metaphase cells are shown. Results are shown as mean values ± SEM. ***p<0.001.

3.3.4.Recovery of dynein, P150^{Glued} and NUMA localization after mutant HTT allele-specific silencing

We then asked whether, the functional rescue on spindle orientation induced by sh50T treatment of SIVF018 HD-NSCs would impact on the localization of dynein, P150^{Glued} and NUMA. Cells were treated with shcontrol and sh50T and immunolabelled for these proteins (Figures 3.5). In control mutant conditions, the patterns of staining for dynein, P150^{Glued} and NUMA were similar to that observed in wild-type cells silenced for HTT (compare Figures 3.3 and 3.5). In sh50T cells, the localization of these proteins was restored. Indeed, there was more dynein and P150^{Glued} at spindle poles and along astral microtubules in SIVF018 HD-NSCs transfected with sh50T as compared to the shControl situation (Figures 3.5B and 3.5C). Upon treatment of SIVF018 HD-NSCs with sh50T, the spindle pole signal of NUMA was less dispersed than in shcontrol cells (Figures 3.5C).

Our results show that allele-specific silencing of *mHTT* selectively rescues the displacement of dynein, dynactin and NUMA whose correct localization is required for spindle positioning. Together, we thus suggest that allele specific silencing rescues the phenotype observed in HD cells by restoring HTT function.

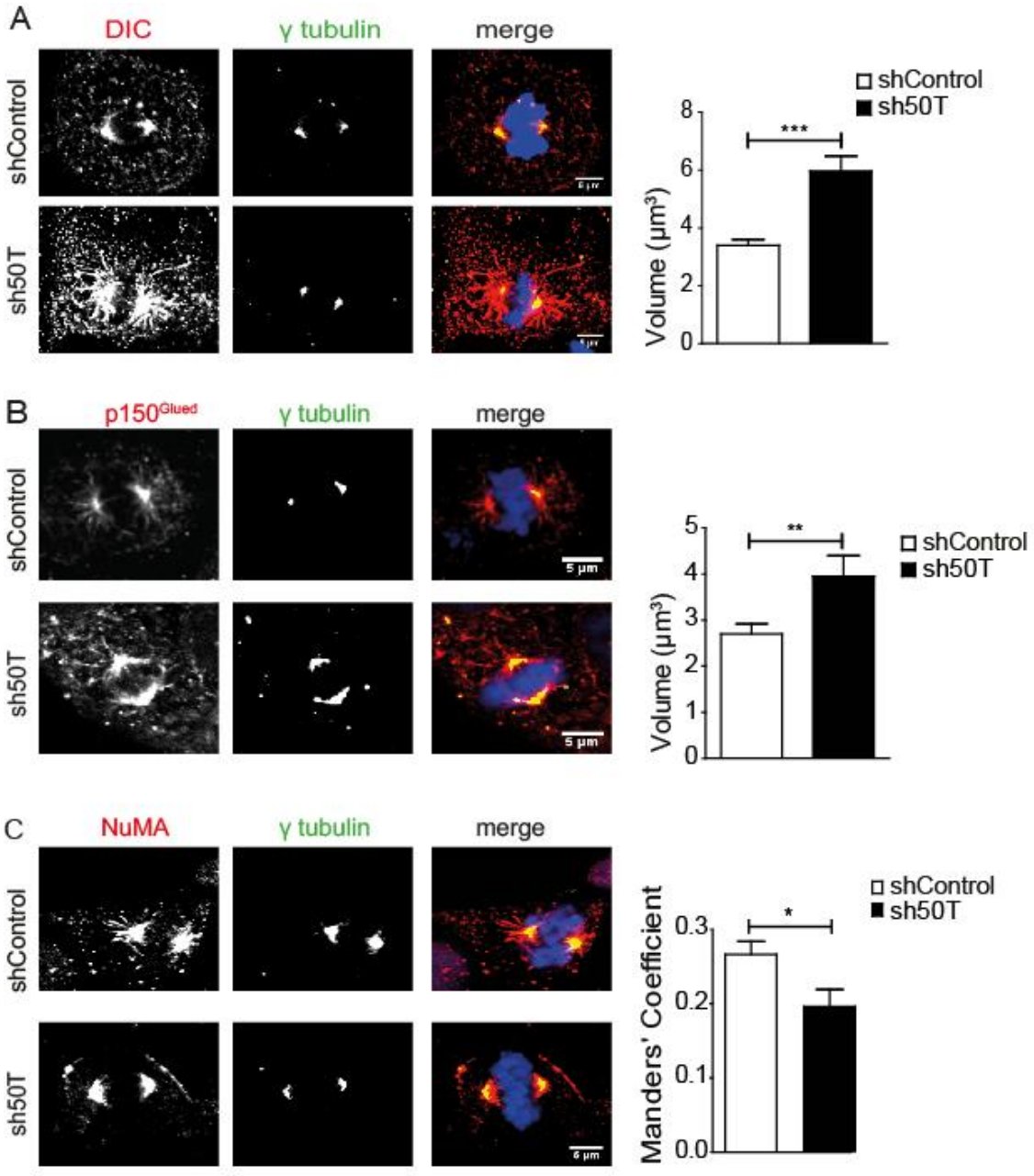

Figure 3.5. - Allele specific silencing of mutant HTT rescues dynein, dynactin and NUMA mislocalization

(A, B, C) Immunostaining of metaphasic neural stem cells with anti-DIC and anti-HTT (**A**), anti-P150^{Glue} and anti-HTT **(B),** anti-NUMA and anti-HTT **(C). (D, E, F)** Immunostaining of metaphasic neural stem cells with anti-DIC (**D**), anti-P150^{Glue} **(E),** anti-NUMA **(F)** and anti-γ-tubulin antibodies and DAPI counterstaining. Graphs represent the quantification of n=46 for D; n=54 and n=45 for E, n=16 and n=28 for F. Results are shown as mean values ± SEM. ***p<0.001; **p<0.01, *p<0.05.

3.4.Discussion

Previous studies have established a role for HTT in formation and maintenance of the dynein/dynactin complex in neurons (Waterman-Storer *et al.* 1997, Caviston et al. 2007). These microtubules associated proteins are essential for microtubule-dependent vesicular transport in axons (Gauthier et al. 2004, Caviston et al. 2007, Colin et al. 2008, Zala et al. 2008). Recently was proven that this complex is critical for spindle assembly and maintenance (Godin et al. 2010) as well as for the cell cortex to exert pulling forces on astral microtubules (Fink *et al.* 2006, Laan et al. 2012, Zheng *et al.* 2013). HTT seems to be an important key in the recruitment of dynein and dynactin to the complex and on distribution of this complex at the cell cortex.

In our study we found that depleting HTT induces spindle misorientation as well as the localization of proteins involved in spindle assembly. More precisely $p150^{Glued}$ subunit of dynactin and dynein were drastically reduced at spindle poles and the opposite effect was observed with NuMA, an accumulation at the spindles. In fact NuMA–LGN–Gα form a complex known to be involved in regulation of spindle orientation (Zheng et al. 2010, Zheng et al. 2013) and HTT seems to interfere with this recruitment. The mitotic spindle orientation dictates the cleavage plane of the mother cell and subsequent inherence of cytoplasmic structures by one or both of the two daughter cells (Siller et al. 2009, Godin et al. 2010, Bornens 2012). During asymmetric division the two daughter cells have different sizes and cellular components are preferentially segregated into only one cell. This differential inheritance of cell fate determinants is an important process for cell fate determination and morphogenesis during development (Kosodo et al. 2004, Noatynska *et al.* 2012). *In vivo* planar divisions generates two identical cell fates and apical/basal spindle orientation generates two different cell types (Willardsen *et al.* 2011). The well characterized canonical Notch signaling pathway is a key regulator of NSC maintenance in the developing nervous system maintaining the neural precursors in an undifferentiated self-renewing state (Borghese *et al.* 2010). Numb, an endocytic adaptor protein that acts as a Notch pathway inhibitor has been associated with neuronal differentiation. In later stages of development the differentiated neuronal daughter cell inherits Numb (Shen *et al.* 2002, Wirtz-Peitz *et al.* 2008). It was reported recently that wild-type HTT seems necessary to direct NS cells towards a neuronal fate, and its absence causes cells to undergo glial differentiation (Conforti et al. 2013, Nguyen et al.

2013). In our study we found that cells lacking HTT tend to divide asymmetrically as was shown by heterogeneous inherence of Numb in dividing cells.

Theoretically treating HD patients should be easy, it only would be necessary to suppress mHTT expression, as shown previously in mice models (Yamamoto *et al.* 2000). In clinical practice turn off the expression of an autosomal dominant gene in the brain is not yet feasible. An interesting approach, which has been explored in the past years, is using RNA interference to specific target brain HTT mRNA. Several studies have addressed this question, unfortunately using a non-allele specific silencing of HTT that cannot distinguish between normal and CAG-repeat expanded transcripts resulting in the reduction of both types. Nonetheless, those studies have shown that total knockdown of HTT is well tolerated for up to 9 months in rodents and improved HD-associated abnormalities (Harper et al. 2005, Wang *et al.* 2005, Franich et al. 2008, Boudreau et al. 2009, Drouet et al. 2009). However the prominent question has not yet been answered: which are the deleterious effects in long term reduction of endogenous wild-type HTT expression and for how long could be tolerated in adult post mitotic neurons. An alternative and more safe strategy would be the allele specific silencing of mHTT by targeting heterozygous SNPs. Warby and colleagues demonstrated that a large percentage of HD European patients belong to a single haplotype with a specific set of SNPs (Warby *et al.* 2009) and two other recent studies confirmed that HD patients share polymorphic sites and that a reduced number of siRNA targeting mHTT allele can treat up to 75% of HD patients (Lombardi *et al.* 2009, Pfister *et al.* 2009). Promising results were obtained so far *in vitro* with HD patient-derived fibroblasts (van Bilsen *et al.* 2008) and NSCs derived from HD patients (Drouet et al. 2014) and *in vivo* using animal models for Machado-Joseph disease (Alves *et al.* 2008) and of dominant inherited ALS (Xia *et al.* 2006). In cultured cells siRNA have successfully silence the mutant HD allele, whereas preserving expression of its wild-type counterpart and in NSCs a functional recovery was observed by restoring the mean velocity of BDNF vesicles (Drouet et al. 2014). Recently, Carroll and colleagues developed antisense oligonucleotides (ASO) able to target both exonic and intronic SNP sites, and were able to specifically and potently reduce mHTT levels at in primary human cells, cultured primary neurons and the adult CNS of YAC18 and BACHD mice (Carroll et al. 2011). In our study in NSC derived from HD patiens we found spindle abnormalities both in the cleavage plane (spindle angle) and in location of key proteins for proper spindle assembly that could not be rescued by overexpressing wild type HTT. In agreement

with aforementioned studies we demonstrate that allele specific silencing can be an efficient therapeutic approach *in vitro* by reversing the phenotype observed in NSC derived from HD patients. These data suggest that is feasible to use this therapeutic approach to reduce mHTT levels and support the continued development toward using RNA-based therapeutics to treat HD.

SUPPLEMENTAL INFORMATION

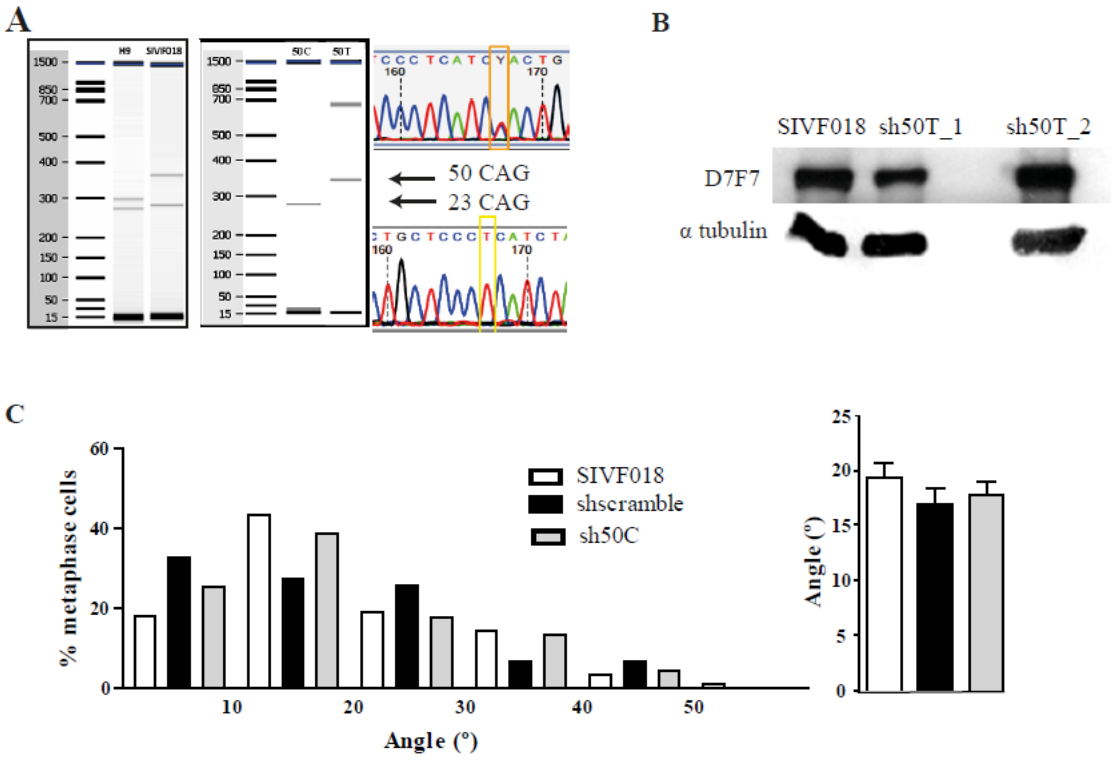

Figure 3.6. Supplementary data. A) H9 neural cells have 2 normal alleles while SIVF018 have a normal allele with 23 CAG repeats and an expanded with 50 CAGs and is heterozygous for SNP rs362331 at exon 50. CAG repeats size detection was obtained using a microfluidic chip from Agilent®. (B) Immunoblotting of extracts from SIVF018 scramble and SIVF018 treated with sh50T_1 for 3 days and sh50T_2 for 5 days using anti-htt targeting CAG repeats (D7F7) and α-tubulin antibodies and respective quantification. C) Distribution and average of spindle angles of metaphase cells in shcontrol and sh50C SIVF018 cells.

CHAPTER IV - Induced pluripotent stem cells derived from Huntington´s disease patients unravel early mitochondrial dysfunction and metabolic disturbances

4.1. Introduction

Huntington's disease is an autosomal dominant disease caused by an expansion of CAG repeats in the gene encoding for huntingtin (Group 1993). The known prevalence of the mutation is 4–10 cases per 100,000 but presumably in Caucasian populations is highly underestimates (Morrison 2010, Morrison 2012). The mutant huntingtin abnormal interactions results in cellular alterations, including abnormal vesicle recycling, disturbance in Ca^{2+} signaling, loss of BDNF, excitotoxicity, decreases in intracellular ATP levels, alterations of gene transcription, inhibition of protein clearance pathways, mitochondrial and metabolic disturbances inducing neurodegeneration and cell death (Zuccato *et al.* 2010). Several pathological mechanisms have been proposed for neurodegeneration, including mitochondrial dysfunction and oxidative stress (Horton *et al.* 1995, Cantuti-Castelvetri *et al.* 2005, Ferreira et al. 2011, Ribeiro *et al.* 2014). An increase susceptibility of HD striatal medium spiny neurons to ROS was documented but the underlying pathogenesis mechanisms are not fully understood (Vonsattel *et al.* 2008, Ribeiro et al. 2014). In genetically complex diseases, revealing the mechanisms underlying the pathology has not been easy and usually is based on cell or animal model that not always reproduce the disease mechanistic in the target cells. Important tools to disease modeling have emerged in the last few years with the reprogramming of somatic human cells into human induced pluripotent stem cells (hiPSCs) (Takahashi et al. 2007) and the use of human embryonic stem cells (hESCs) (Thomson et al. 1998). The differentiation capacity into various neuronal lineages has been explored and a few novel iPSCs models have been created. These advances allow generating patient-specific iPSCs and differentiation into cell types affected in disease providing a powerful new tool to recapitulate the neuropathologic phenotype in a developmental stage. The new iPSC-based disease models reproduce some of the main features of the pathology providing important insights into disease biology but not always exhibit the neuronal maturation and network defects that are observed *in vivo*. The first report on patient-specific iPSCs was in 2008 when Park and colleagues successfully reprogrammed fibroblasts from one patient with Huntington chorea with 72/19 CAGs (Park et al. 2008). Further characterization was done by Zhang (2010) showing that these cells can differentiate into HD specific neural stem cells (HD-NSCs) and neurons with striatal characteristics. Other study found, in lower repeat lengths lines, altered lysosomal content that was maintained during proliferation and in hiPS-derived neurons

(Camnasio et al. 2012) More recently the HD iPSC Consortium generated iPSC lines from HD patients and controls with early onset and late onset HD-iPSC lines (Consortium 2012). Those lines where successfully differentiated into neurons with striatal phenotype that presented disease-associated changes in electrophysiology, metabolism, cell adhesion and cell death for lines with both medium and longer CAG repeat expansions. Indeed, HD-iPSC and their differentiated counterparts can help to reveal the role of mitochondrial and metabolic dysfunction in early stages of HD.

More recently 72 polyglutamine iPSC line was genetic corrected and cells were successfully differentiated into DARPP-32-expressing striatal neuron reverting some of the classical hallmarks of HD (An et al. 2012). In this study, we show that HD-iPSCs have altered mitochondria dynamics presenting more negative membrane potential and increased intracellular basal Ca^{2+} levels, but reduced Ca^{2+} mitochondrial storage capacity. We report a metabolic deficit and a shift favoring glycolysis for ATP production in HD-iPSC. Moreover, increased levels of mitochondrial superoxide anion and hydrogen peroxide production were observed in HD-iPSCs *versus* control iPSC. Overall, our study suggests that mitochondrial dysfunction occurs in early HD pathogenesis.

4.2.Materials and methods

4.2.1.Materials

Mitotically inactivated murine embryonic fibroblasts (MEFs) were acquired at AMSBIO® (Abingdon, U.K.). Matrigel was purchase from Corning® (Amsterdam, The Netherlands). Geltrex, MitoSOX® Red Mitochondrial Superoxide Indicator analyses, Neurobasal medium, Hoechst 33342, acetoxy-methyl-ester Fura-2 (Fura-2AM), Accutase, N-2 Supplement (100X) and B-27® Supplement (50X) were obtained from Life Technologies (Eugene, OR, USA). Lipofectamine 3000, MitoTracker Red CMXRos, DMEM/F12 and knockout serum replacement were from Invitrogen (Carlsbad, CA, USA). L-glutamine, nonessential amino acids, 2-mercaptoethanol, XAV939, Y-27632, 2-deoxy-D-glucose, oligomycin, FCCP, 4Br-A23187, ionomycin, antimycin A, 3-nitropropionic acid, Mitochondria peroxy yellow 1, SOD Assay Kit, decyl-ubiquinone, acetyl-CoA, cytochrome c, nicotinamide adenine dinucleotide (NADH), DL-dithiothreitol (DTT), hydrogen peroxide (H_2O_2), PMSF (phenylmethanesulfonyl fluoride), protease inhibitors (chymostatin, pepstatin, A, leupeptin and antipain), pyruvate, Rhodamine 123, etomoxir sodium salt hydrate, Sodium palmitate and L carnitina were purchase at Sigma-Aldrich Corporation (St. Louis, MO, USA). Human FGF2, human EGF, MITOMYCIN C and Dorsomorphin were from Tebu-bio (Yvelines, France). SB431542 was from from Tocris Bioscience (Bristol, United Kingdom). Dulbecco's Modified Eagle's Medium (DMEM) culture medium, Fetal Bovine Serum (FBS), penicillin/streptomycin and geneticin were purchased by GIBCO (Paisley, UK). Amplite Colorimetric Pyruvate and Amplite Colorimetric L-Lactate kits were from AAT Bioquest's (Sunnyvale, CA, USA). Pyruvate dehydrogenase (PDH) Enzyme Activity Microplate Assay Kit was from MitoSciences (Oregon, USA). Secondary antibodies conjugated to alkaline phosphatase (anti-mouse and anti-rabbit) were purchased from Amersham Biosciences (Buckinghamshire, UK). Enhanced ChemiFluorescence reagent (ECF), anti-rabbit IgG (from goat), anti-mouse IgG+IgM (from goat) were from GE Healthcare (Little Chalfort, UK). Antibodies used were anti-OCT4 (Cell Signaling Technology), anti-SOX2 (Cell Signaling Technology), D7F7 anti-HTT (Cell Signaling Technology); anti-nestin (), anti-OPA1 (Santa Cruz), anti-DRP1 (BD bioscience), anti-MFN2 (Sigma), anti-Fis1 (Novus Biologicals), anti-polyglutamine stretch (1C2) (Millipore), anti-PDK1

(Cell Signalling), anti-acetyl SOD2 (Abcam), anti-SOD2 (Abcam) and anti-α-tubulin (Sigma).

4.2.2. Human ES cell culture

Wild-type iPS cell line used was AMS4-iPS (XY, passages 7-30) and HD-iPS4 (XY, passage 4-30) with one normal (<35 repeats) and one expanded allele (72 repeats) generated by Park and colleagues (Park et al. 2008). Cells were maintained on a layer of mitotically inactivated murine embryonic fibroblasts (MEFs) for a variable number of passages or allowed to grown under feeder-free conditions on Matrigel® or Geltrex®. MEFs were acquired from AMSBIO® inactivated or to expand and were inactivated with mitomycin C after 3 passages. Manual dissection was routinely used to passage the cells rather than enzymatic methods.

The iPS cells were cultured in DMEM/F12 supplemented with 20% knockout serum replacement, 2 mM glutamine, 1 mM nonessential amino acids, 1% penicillin/streptomycin, 100 μM 2-mercaptoethanol and 10 ng/ml recombinant human FGF2. Cultures were fed daily and passaged at least once a week. When cells were grown in matrigel, medium was conditioned for 24h in mouse embryonic fibroblasts and filtered. Neural differentiation was based on dual SMAD inhibition (Chambers *et al.* 2009, Delli Carri *et al.* 2013, Nicoleau et al. 2013). Colonies were grown on 6-well plate in matrigel until reach 100% confluence. Neural induction medium consisted of DMEM/F12, Neurobasal, N2 (100x), 2 mM l-glutamine, 100 μm nonessential amino acids, 100 μM 2-mercaptoethanol, 1% penicillin/streptomycin and B-27 (50x). Neural induction occurred between day 0 and day 10-12. For day 0 to day 5 cells were maintained in KSR medium without FGF and incubated with Dorsomorphin 5 μM (BMP inhibitor), SB431542 10 μM (TGF-β inhibitor) and XAV939 1 μM (β-catenin-transcription inhibitor and axin stabilizing agent). Medium was change every day. From day 5 to 10-12 medium was gradually replaced by 75 % KSR + 25 % N2 Medium, 50 % KSR + 50 % N2 Medium until reach 100 % N2 Medium plus Dorsomorphin 5 μM, SB431542 10 μM and XAV939 1 μM (Mak *et al.* 2012, Delli Carri et al. 2013, Nicoleau et al. 2013). Between days 10 and 12, fields full of rosettes become morphologically visible. To allow the cells to differentiate, they were replated in matrigel coated 12-well plate. For detaching, cells were incubated with Accutase at 37 °C in 5 % CO2 for 15–20 min. Accutase was diluted in DEM/F12 medium prewarmed

at 37 °C. Cells were collected and spin 3 min at 1000 rpm at RT and resuspend in 200 µl into a well of a 12-well plate. Cells were allowed to adhere for 30 min and then more 300 µl of N2 medium was added supplemented with Y-27632 10 µM, FGF 10 ng/ml and EGF 10 ng/ml. Dishes were carefully transferred in a 37 °C, 5 % CO_2 incubator and leaved overnight. Cells were maintained in the same medium and passaged every 2-3 days for no more than 10 passages.

4.2.3.Mitochondrial staining

MitoTracker Red CMXRos is a red-fluorescent dye (ex-578/em-599) that stains mitochondria in live cells and its accumulation is dependent upon membrane potential. The MitoTracker probe contains a mildly thiol-reactive chloromethyl moiety that keeps the dye associated with the mitochondria after fixation. Into the cell medium was added 400nM of CMXRos for 20 minutes and incubated at 37°C in a humidified atmosphere at 95% O2 and 5% CO2. MitoTracker probe passively diffuses across the plasma membrane and accumulates in active mitochondria. After removing the media with CMXRos, the cells were fixed with 4% paraformaldehyde (pH 7.4) for 10 minutes and immunocytochemistry continued as described ahead.

Mitochondrial morphology was examined with pDsRed2-Mito which encodes a fusion of Discosoma sp. red fluorescent protein (DsRed2) and a mitochondrial targeting sequence of human cytochrome c oxidase subunit VIII (Mito). The targeting sequence is fused to the 5'-end of DsRed2, which is human codon-optimized for high expression in mammalian cells. Cells were plated in a 24-well plate and when 70% confluence was achieved transfection was performed according to the instructed procedures of Lipofectamine™ 3000.

4.2.4.Immunocytochemistry

Cells were washed with warmed PBS 1x followed by permeabilization with PHEM (5 mM HEPES, 60 mM PIPES, 10 mM EGTA, 2 mM MgCl2, pH 7.0 with KOH)/0.1% Triton X-100 for 30 sec then fixed with 4% PAF/PHEM (20 min at RT). Cells were rehydrated with PBS/0.1% Triton X-100 (3 washes), blocked in 3% BSA/PBS (30 min) and incubated with the following primary antibody overnight at 4°C: anti-OCT4 (1.200), anti-sox2 (1:200), anti-nestin (1:200), anti-OPA1 (1:100), anti-DRP1 (1:100),

anti-MFN2 (1:300) and anti-Fis1 (1:100). Secondary antibodies and DAPI counterstain were applied for 1 h at room temperature. Confocal analysis was performed on a Leica TCS SP2 microscope (Leica Microsystems).

4.2.5.Immunoblotting

Cells were lysed in lysis buffer (50 mM Tris-HCl pH 7.5, 0.1% Triton X-100, 2 mM EDTA, 2 mM EGTA, 50 mM NaF, 10 mM β-glycerophosphate, 5 mM sodium pyrophosphate, 1 mM sodium orthovanadate, 0.1% (v/v) β-mercaptoethanol, 250 µM PMSF, and 10 mg/ml aprotinin and leupeptin). The samples were denatured with SDS sample buffer (50 mM Tris-HCl, pH 6.8, 2% sodium dodecyl sulphate, 5% glycerol, 0.01% bromophenol blue and 100 mM DTT), at 95ºC, for 5 min. Twenty five µg or seventy of protein µg was loaded in 6% and 12% gel, subjected to SDS-PAGE and electrophoretically transferred onto polyvinylidene difluoride (PVDF) Hybond-P membranes. Blots were blocked in 5% BSA/TBST buffer (20 mM TrisHCl, 0.15 M NaCl, 0.1% Tween 20) and incubated with anti-HTT (D7F7) (1:1000) and polyglutamine stretch (1C2) (1:5000), anti-OCT4 (1:500), anti-PDK1 (1:1000), anti-acetyl SOD2 (1:500) and SOD2 (1:5000) and α-tubulin (1:10000). Membranes were further incubated with anti-rabbit and anti-mouse secondary antibodies (1:10000), for 90 min, at room temperature, and developed using ECF fluorescent reagent. Fluorescence signal was analyzed using the QuantityOne software and the results were given as fluorescence intensity (INT)/mm2. Data were presented as the ratio of phosphorylated protein/total protein or protein levels/α-tubulin. Immunoreactive bands were visualized with VersaDoc Imaging System (BioRad®, Hercules, USA).

4.2.6.Assessment of intracellular pyruvate and lactate

Cells were washed with ice-cold PBS and extracted with 0.6 M perchloric acid supplemented with 25mM EDTA-Na^+ for pyruvate and PBS for lactate. Cell extracts were centrifuged at 14 000 rpm for 5min at 4 °C in order to remove cell debris. Lactate and pyruvate were determined in the supernatant by using kits from Amplite Colorimetric Pyruvate and Amplite Colorimetric L-Lactate from AAT Bioquest's (Sunnyvale, CA, USA) respectively. Results of lactate and pyruvate content were obtained in µg/mg protein and expressed as a ratio of lactate/pyruvate

4.2.7.Measurement of ATP

In experiments targeting to inhibit glycolysis, the culture medium was replaced by DMEM with glucose (GLUC) or supplemented with 2-deoxy-D-glucose (2-DOG) a competitive inhibitor of glucose metabolism (Wick *et al.* 1957) for 2 hours (Ferreira et al. 2011). To further inhibit mitochondrial ATP synthesis 2 μg/ml of oligomycin was added to glucose-containing medium or supplemented with 2-DOG. Additionally to analyze the glycolytic metabolism in cell bioenergetics status, medium without glucose plus 2-DOG was supplemented with 10 mM pyruvate (2-DOG+Pyr) to directly feed the mitochondria (Ferreira et al. 2011).

For ATP measurement, cells were washed with ice-cold PBS, scraped, and extracted with 0.6 M perchloric acid, supplemented with 25 mM EDTA-Na^+, and centrifuged at 14 000 rpm for 2 min at 4 °C. Pellet was discarded and supernatant was neutralized with 10M KOH, samples were then centrifuged at 14 000 rpm for more 2 min at 4 °C. The resulting supernatants were assayed for ATP determination by separation in a reverse-phase high-performance liquid chromatography (HPLC), with detection at 254 nm, as described previously (Stocchi et al. 1985). The samples were assayed by separation in a reverse-phase high-performance liquid chromatography (HPLC), using a Lichrospher 100 RP-18 (5 μm) HPLC column from Merck (Darmstadt, Germany), upon an isocratic elution with 100 mM phosphate buffer (KH_2PO4, pH 6.5) and 1% methanol, with a flow rate of 1 ml/min and detection at 254 nm, as previously described (Stocchi et al. 1985). The required time for each analysis was 6 min. The chromatographic apparatus used was a Beckman-System Gold, consisting of a 126 Binary Pump Model and 166 Variable UV detector. Peak identity was determined by following the retention time of standards. Cellular energy charge was calculated using the formula: ([ATP] + 0.5 [ADP])/([ATP] + [ADP] + [AMP]).

4.2.8.Determination of pyuvate dehydrogenase (PDH) E1α subunit protein levels and phosphorylation

PDH expression and phosphorylation were assessed using Pyruvate dehydrogenase (PDH) Enzyme Activity Microplate Assay Kit from MitoSciences (Oregon, USA) following the manufacturer instructions and using the solutions provided in the kit. Briefly, cells were plated at confluent density, allowed to adhere, and fixed with 3.7%

formaldehyde/4% sucrose. Cells were permeabilized, blocked and incubated with total PDH E1α combined with another antibody against the phosphorylated forms of PDH E1α at pSer 232, pSer293 or pSer 300, and developed by dual colorimetric detection. Cell density was normalized after Janus Green staining. Absorbance was monitored using a microplate reader Spectra Max Plus 384 (Molecular Devices, USA).

4.2.9.Mitochondrial membrane potential (ΔΨm) determination and intracellular Ca^{2+} (Ca^{2+i}) by fluorimeter

The ΔΨm was determined using the cationic fluorescent probe Rhodamine 123 (Rhod123). This positively charged molecule will accumulate within mitochondria in inverse proportion to ΔΨm according to the Nernst equation. More polarized mitochondria (interior is more negative) will accumulate more cationic dye, and depolarized mitochondria (interior is less negative) accumulate less dye. Fluorescent dye accumulation in mitochondria is then optically detected by fluorescent plate reader (Scaduto *et al.* 1999). Briefly, iPS cells were cultured in a 6-well plate and NSC in 96-well plate until reach confluence. For iPS cells, detachment was required previously to incubation with the probes. Therefore cells were incubated with Accutase at 37 °C in 5 % CO2 for 15–20 min. Accutase was diluted in KSR medium prewarmed at 37 °C and left for 30 min to minimize the enzyme stress on cells. Then, iPS cells were washed twice in Krebs medium and incubated at 37ºC for 30 min with 8 µM Rhod123 and 1.5 µM acetoxy-methyl-ester Fura-2 (Fura-2AM).

NSC were incubated in the 96-wells plates directly following the same protocol. After incubation, cells were washed once and the basal fluorescence was taken during 5 min using a Microplate Spectrofluorometer Gemini EM (Molecular Devices, USA). Fluorescence spectra for Rhod123 are 510 nm excitation and 590 nm emission. For Fura-2AM, the excitation spectra are at 380 nm (calcium free) and 340 nm (calcium complex) with fixed emission at 540 nm. Oligomycin (2 µg/ml) and p-trifluoromethoxy carbonyl cyanide phenyl hydrazone (FCCP) (2 µM), (separately or together), which produces maximal mitochondrial depolarization, were added to cells and the fluorescence was taken during another 5 min. Cells were also challenged with 5 µM of a Ca^{2+} ionophore - 4Br-A23187- which is highly selective for Ca^{2+} and increases its levels. Furthermore to directly evaluate the role of mitochondria, glycolysis was inhibited by adding 2-deoxy-D-glucose (2 mM) and by replacing glucose with pyruvate

(10 mM) for 2 hours (pyruvate-based medium) (Rego *et al.* 2001, Oliveira *et al.* 2006). Results were expressed as the difference between the increase in Rhod123 or FURA-2 AM fluorescence and upon addition of oligomycin and FCCP or oligomycin/FCCP and basal fluorescence values.

4.2.10.Monitoring dynamic changes intracellular Ca2+ and mitochondrial membrane potential by single cell microscope

IPS cells were plated on glass coverslips coated with matrigel and allowed to form colonies. When colonies were visible iPS cells were washed with Krebs medium containing (in millimolar) 132 NaCl, 4 KCl, 1 CaCl2, 1.2 mM KH_2PO4 1.4 $MgCl_2$, 6 glucose, 10 HEPES, and pH 7.4. Subsequently, glass coverslips were transferred to Krebs medium containing 0.2% (w/v) pluoronic acid, 0.1% (w/v) BSA, 1.5 µM Rh123, and 8 µM Fura-2AM for 30 minutes in a 37 °C, 5 % CO2 incubator. Cells were rinsed with fresh buffer and coverslips assembled in a nonperfused chamber filled with 500µl of Krebs medium containing 1.5 µM Rh123. Simultaneous Ca^{2+} levels and Rh123 fluorescence were acquired by using an inverted fluorescence microscope Axiovert200 (Zeiss, Jena, Germany) equipped with a dual-band path emission filter (510/40 and 600/60 nm) and a Lambda DG4 apparatus (Sutter Instruments Company, Novato, CA, USA). Oligomycin (2 µg/ml) was added and fluorescence was registered for 3 min followed by FCCP addiction, to induce maximal mitochondrial depolarization. Calibration of Ca^{2+}i responses was performed at the end of the experiment by adding 2 µM ionomycin ($\Delta\Psi$m collapse).

The determinations of fluorescence time courses were calculated on the basis of 1 microscopic field per coverslip, containing 50 cells. Moreover, individual whole cells were identified as regions of interest (ROI). Each experimental condition was assayed at least in three different coverslips from three independent culture preparations.

4.2.11.Measurement of ROS (superoxide and hydrogen peroxide)

For MitoSOX® Red Mitochondrial Superoxide Indicator analyses iPS cells were detached by Accutase, collected and allowed to rest for 30 min in KSR medium. Subsequently were centrifuged 3 min, 1000 rpm at RT and washed with Krebs medium. Cells were incubated at 37ºC with 5 µM MitoSOX® for 30 min, washed with Krebs and

the resultant fluorescence analyzed on a Microplate Spectrofluorometer Gemini EM for 5 min after which were treated with the stressor compounds H_2O_2 (1 mM), antimycin A (1 µM) and 3-nitropropionic acid (3-NP) (300 nM) and fluorescence was measured for more 5 min. at

NSCs were cultured for 24 hr at 37°C in 96-well assay plates coated with matrigel. Cells were washed with HBSS (in millimolar: 1.3 CaCl2, 0.5 $MgCl_2$-6H2O 0.4 MgSO4-7H2O, 5.3 KCl, 0.4 KH2PO4, 4.2 NaHCO3, 137.9 NaCl, 0.3 Na2HPO4, 5.6 D-Glucose at pH 7.4) and incubated for 30 min with 5 µM MitoSOX® Red Mitochondrial Superoxide Indicator in HBSS and proceed as above described.

To test the antioxidant response capacity, iPSC were challenged for 2 hr with 300 nM 3-NP, 100 µM H_2O_2, 1 µM antimycin A or medium replaced for DMEM without glucose and supplemented with 2-DOG. Fluorescence was measure for 5 min, as described, after which cells were treated with the stressor compounds cited. Results were obtained with excitation at 510 nm and collection at 580 nm.

Mitochondria peroxy yellow 1 (MitoPY1) is a fluorescent probe that selectively tracks to the mitochondria and detects fluxes of H_2O_2 (Dickinson *et al.* 2013). Briefly, iPS cells were detached by Accutase, collected and allowed to rest for 30 min in KSR medium. Subsequently were centrifuged 3 min, 1000 rpm at RT and washed with PBS. Cells were incubated at 37ºC with10 µM of MitoPY1 for 30 min.

After, the cells were washed by removing the MitoPY1 solution and replacing it with warm DPBS. As a positive control, stimulation with 100 µM H_2O_2 was carried out for 30 min. Fluorescence was measure for 15 min, as described, after which cells were treated with the stressor compounds mentioned above. Resultant fluorescence was analyzed on a Microplate Spectrofluorometer Gemini EM with excitation at 500 nm and collection at 538 nm.

Differences in the fluorescence was quantified and presented as mean +/-SEM. The results were calculated as RFU per mg protein for NSC or per 300.00 cells for iPSC.

4.2.12.Measurement of SOD activity

Determination of SOD activity was performed accordingly to the SOD Assay Kit (Sigma). In order to measure SOD2 activity, 2 mM potassium cyanide (KCN) (which inhibits SOD1) was added. SOD2 activity can be measured in the presence of potassium cyanide (KCN), since it inhibits SOD1 activity.

4.2.13.Preparation of mitochondrial-enriched fractions from iPSC

In brief, the medium was removed and cells washed once with ice-cold PBS. Afterwards were scraped, collected in homogenization buffer (250 mM sucrose, 20 mM HEPES, 10 mM KCl, 1.5 mM $MgCl_2$, 1 mM EDTA, 1 mM EGTA at pH 7.4) and homogenize with a 2-ml glass/Teflon tissue grinder with a tight clearance kept on ice with 100 slow up-down strokes. Subsequently the homogenized was submitted to centrifugation at 2300 rpm for 12 min at 4 °C. The mitochondria-enriched supernatant was collected immediately and kept at −80 °C until analysis.

4.2.14.Measurement of mitochondrial respiratory chain complexes activities

The mitochondria-enriched fraction was assayed for the activity of mitochondrial complexes (Cx) I–III by spectrophotometry.

Complex I: NADH–ubiquinone oxidoreductase assay

Briefly, in a 1 ml cuvette was added 800 µl of K_2HPO_4 buffer (0.25 M, pH 7.2), 50 µl of fatty acid–free BSA (50 mg/ml), 10 µl of KCN (100 mM) and 30 µl of NADH (5 mM). After sample quantification 100 µg of protein was added and the final volume adjusted to 990 µl with distilled water. In parallel, a separate cuvette was prepared, containing the same quantity of reagents and sample but with the addition of 10 µl of 1 mM rotenone solution (blank). To start the reaction 10 µl of ubiquinone-1 (5 mM) was added and read for 5 min until the reaction was stopped with 10 µl rotenone (1 mM). Cx-I activity, measured at 30°C, was determined at 340 nm by following the decrease in NADH absorbance due to ubiquinone (50 µM) reduction to ubiquinol (Ragan 1987). Cx-I activity expressed in nanomoles per minute per milligram of protein was normalized for citrate synthase activity and corresponds to the rotenone (1 µM) sensitive rate.

Complex II: Succinate–ubiquinone oxidoreductase assay

Briefly, in a 1 ml cuvette was added 500 µl of K_2HPO_4 buffer (0.1 M, pH 7.4), 10 µl of KCN (100 mM), 40 µl of succinate (500 mM), 40 µl of DCPIP (1.5 mM), 40 µM of EDTA-K2 (5 mg/5ml) and 10 µl rotenone (1 mM). After sample quantification 150 µg of protein was added and the final volume adjusted to 990 µl with distilled water. In

parallel, a separate cuvette was prepared, containing the same quantity of reagents and sample but with the addition of 10 µl of 50 mM TTFA before solution (blank). To start the reaction 10 µl of decylubiquinone (50 mM) was added and read for 3 min until the reaction was stopped with 10 µl of TTFA (100 mM). Cx-II activity, measured at 37°C, was monitored at 600 nm by following the reduction of 6,6-dichlorophenolindophenol (DCPIP) (600 µM) by ubiquinol resulting from this reaction (Hatefi *et al.* 1978) . Cx-II activity expressed in nanomoles per minute per milligram of protein was normalized for citrate synthase activity and corresponds to complex II inhibitor, thenoyltrifluoroacetone (TTFA), sensitive rate.

Complex III: Ubiquinol–cytochrome c reductase assay

Briefly, in a 1 ml cuvette was added 620 µl of K_2HPO_4 buffer (0.056 M, pH 7.2), 150 µl of reduced cytochrome c (100 µM), 10 µl of KCN (100 mM), 50 µl of EDTA-K_2 (20 mM, pH 7.2), 50 µl $MgCl_2.6H_2O$ (100 mM) and 10 µl rotenone (0.5 mM). After sample quantification 50 µg of protein was added and the final volume adjusted to 998 µl with distilled water. In parallel, a separate cuvette was prepared, containing the same quantity of reagents and sample (blank). To start the reaction 2 µl of 10 mM ubiquinol was added and read for 5 min until. Cx-III activity was monitored at 550 nm by following the ubiquinol reduction of cytochrome c at 30 °C. Cx-III activity expressed in nanomoles per minute per milligram of protein was normalized for citrate synthase activity.

Complex I+III: NADH cytochrome c oxidoreductase

Briefly, in a 1 ml cuvette was added 200 µl of Tris-HCl (0.05 M, pH 8.0) medium supplemented with 50 µl BSA (5 mg/ml), 150 µl oxidized cytochrome c (0.267 mM) and 10 µl KCN (0.024 M) left to incubate for 4 min. After sample quantification 50 µg of protein was added and the final volume adjusted to 990 µl with distilled water. In parallel, a separate cuvette was prepared, containing the same quantity of reagents and sample but with the addition of 10 µl of rotenona solution (blank). To start the reaction 0.8 mM NADH (26.7 mM) was added and read for 3 min until the reaction was stopped with 10 µl rotenone (0.4 mM). The activity of complex I+III was measured at 30°C by the change in absorbance at 550 nm (ε = 19.1 mM−1cm−1) due to the reduction of oxidized ferricytochrome c (Hagopian *et al.* 2010). The activity of complex I+III

expressed in nanomoles per minute per milligram of protein was normalized for citrate synthase activity

Citrate synthase (CS) assay

Briefly, in a 1 ml cuvette was added 500 µl of Tris (200 mM, pH 8.0) with Triton X-100 (0.1% (vol/vol)), 20 µl of DTNB (10 mM), 20 µl of AcetylCoA (10 mM) and 50 µg of sample. The volume was adjusted to 90 µl with distilled water. The reaction started by adding 10 µl of oxaloacetic acid (10 mM). CS activity was performed at 412 nm following the reduction of 5,5′-dithio-bis(2-nitrobenzoic acid) (DTNB) (200 µM) in the presence of acetyl-CoA (200 µM) and oxaloacetate (100 µM) (Coore *et al.* 1971). CS activity was expressed in nanomoles per minute per milligram of protein.

4.2.15.XF24 extracellular flux analyser

iPSCs were seeded onto an XF24 Cell Culture Microplate coated with matrigel (Seahorse Bioscience) (Zhang *et al.* 2012) and incubated at 37ºC until confluent. One ml of XF Calibrant Solution was placed into each well of the sensor hydration microplate and the sensor cartridge placed onto the microplate. The plate was incubated with immersed sensors in a non-CO2 incubator at 37 °C for ~16 h (overnight). Fifty ml of XF assay medium was supplemented with 17.5 mM glucose, 1 mM pyruvate and 2 mM glutamine and pH Adjusted to 7.4 at 37 °C. The cell medium was aspirated from each iPSC- or NSC–containing XF24 V7 cell culture microplate without disturbing the cell monolayers attached on the well bottoms. Gently each well was washed with 0.5 ml of XF assay medium at 37 °C. Then, 450 µl of XF assay medium at 37 °C was added to each well and the plate putted into a non-CO2 incubator at 37 °C for 1 hour. The final additive concentrations of the inhibitors added into injection ports A, B or C was 1 µM oligomycin, 0.3 µM FCCP, 1 µM rotenone and 1 µM antimycin. This method allows to measure mitochondrial oxygen consumption rate (OCR) and acess the mitochondrial function in their native intracellular environment. Glycolysis converts glucose to lactate resulting in production of protons released into the extracellular medium following acidification of the medium surrounding the cells. This can be measured directly by the XF Analyzer and outputted as the Extracellular Acidification Rate (ECAR). Firstly, cells were incubated in the glycolysis stress test medium (DMEM D (5030 Sigma), NaCl 143mM, Phenol Red 3mg) without glucose for 1 hour a 37°C incubator without

CO_2. The port A injects a saturating concentration of glucose (10mM) leading to ATP and protons production through the glycolytic pathway pyruvate to lactate. The second injection is oligomycin, which inhibits mitochondrial ATP production and thus shifts the energy production to glycolysis, with the subsequent increase in ECAR. The last injection is 2-DOG, which inhibits glycolysis through competitive binding to glucose hexokinase. The resulting decrease in ECAR further confirms that the ECAR produced in the experiment is due to glycolysis.

For fatty acid oxidation measurements for hPSCs and NSC KHB assay medium (111 mM NaCl, 4.7 mM KCl, 2 mM $MgSO_4$ Na_2, 1.2 mM HPO_4, 2.5 mM Glucose) supplemented with 500 mM L-carnitine was used. The exogenous free fatty acid palmitate (200 µM), which can be internalized by intact cells, was added into injection ports A, B followed by the addition of etomoxir at port C. The component of OCR due to palmitate oxidation is determined by the addition of etomoxir, which freely diffuses into cells and is an inhibitor of carnitine palmitoyltransferase 1 (CPT1), an enzyme that transports long-chain fatty acids across the mitochondrial inner membrane, thereby effectively inhibiting fatty acid oxidation. The design a study protocol in the XF24 Extracellular Flux Analyzer software for analyzing iPSCs and NSC was to set the time to mix for 2 min, wait for 2 min and measure for 4 min. OCR and ECAR were normalized to protein concentration using the Protein Assay reagent (Bio-Rad) in all experiments.

4.3.Results

4.3.1.HD- iPSCs and differentiated Neural Stem Cells express mutant HTT and display specific protein expression patterns

To confirm that mHTT was still expressed by HD cells immunoblots of protein extracts were performed. An antibody that recognizes normal and mutant HTT (D7F7) and other that only detects the polyglutamine expansion (1C2) revealed that HD-iPSC and HD-NSCs express both proteins (Figure 4.1A). The AMS4-iPSC cell line expresses only wild type HTT and the HD –iPSC, as described by Park (2008), has one normal (<35 repeats) and one expanded allele (72 repeats) (Park et al. 2008).

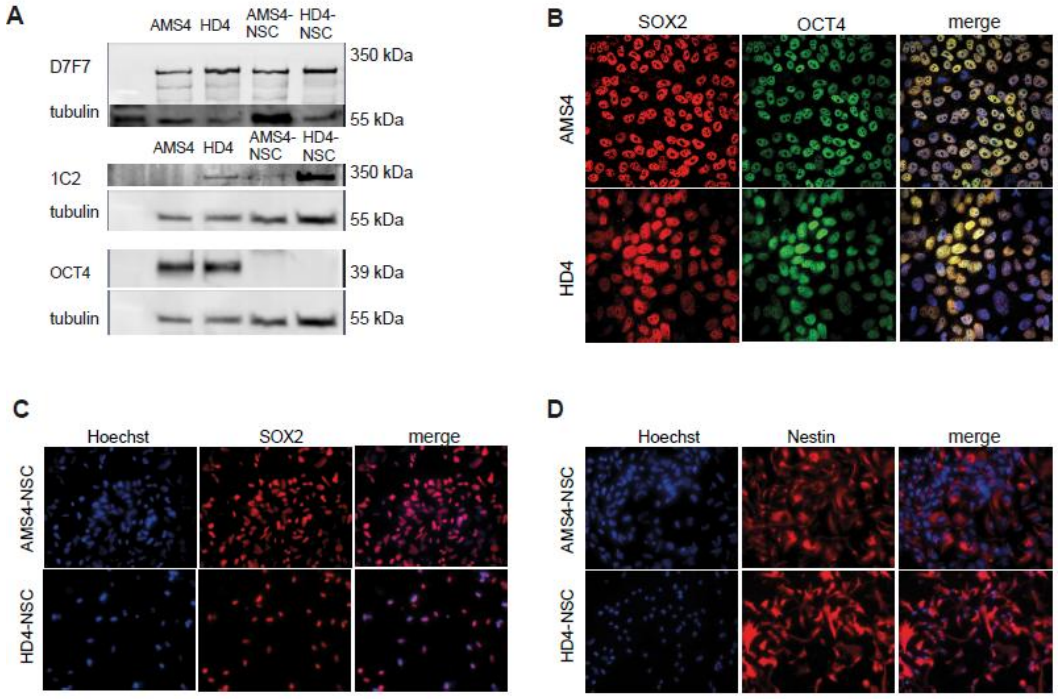

Figure 4.1.- Characterization of iPS and NS cell lines. (A) Western blots of HTT expression in iPSC and iPSC-derived NSC with the HTT antibody D7F7 and 1C2 demonstrate normal and mutant HTT expression. Also the pluripotency marker OCT4 was present in iPSC. (B-D) Expression of pluripotency markers OCT4 and SOX2 by induced pluripotent stem cells (iPSC) and Nestin and SOX2 by neural stem cells (NSC).

The pluripotency of HD-iPSC was confirmed by the detection of specific markers. The HD- iPS affected cell lines expressed the markers OCT4 and SOX2 as well as AMS4-iPSC line (Figure 4.1A, 4.1B). The neural stem cells were generated from the HD and wild type iPS cell lines by neural induction protocol. The blockade of SMAD signalling was achieved by SB431542 (inhibits the Lefty/Activin/TGFβ), dorsomorphin (BMP inhibitor) and XAV-939 (β-catenin-mediated transcription inhibitor) factors. The successfully differentiation was confirmed by the expression of Nestin and SOX2 (Figure 4.1C, 4.1D). HD-NSC grew in defined medium with epidermal growth factor (EGF) and fibroblast growth factor-2 (FGF-2) and were expandable for 10 passages and could be frozen and thaw very efficiently.

4.3.2.Mitochondrial dysfunction and calcium dyshomeostasis in HD-iPSC

Mitochondrial is an important key player in Ca^{2+} regulation acting as a Ca^{2+} buffer thus controlling the impact on cytosolic Ca^{2+} signals and on the activity of Ca^{2+}-dependent proteins. Ca^{2+} also controls numerous functions on mitochondria and its uptake is dependent on mitochondrial membrane potential ($\Delta\Psi$) (for review, Demaurex *et al.* 2009). The $\Delta\Psi$ was explored with the fluorescent lipophilic cationic dye Rhodamine 123 which selectively accumulates within mitochondria (Perry *et al.* 2011). When HD-iPSC where exposed to ATP synthase inhibitor (2 µg/ml oligomycin) and a mitochondria uncoupler FCCP (2 µM) ensemble, released more probe than controls (Figure 2A*i*). To further confirm this data we incubated the drugs at different time points. Results found are consistent with a more negative $\Delta\Psi$ in HD-iPSC since when challenged with oligomycin more probe is release to cytoplasm (AMS4 vs HD - 0.43 ± 0.28 vs 3.00 ± 0.71, $p<0.05$) (Figure 4.2A*ii-iii*). Finally, $\Delta\Psi$ was quantified on a single cell based on incorporation of specific fluorescent dyes and similar results were obtained (Figure 4.2C*i-ii*). Although in somatic cells the $\Delta\Psi$ is maintained by the proton gradient through the electron transport chain, in iPSC $\Delta\Psi$ appears to be maintained by glycolysis. Hydrolysis of glycolytic ATP due to the conversion of ATP synthase to hydrolase activity seems to be essential for maintaining the $\Delta\Psi$, proliferation, and viability of iPSCs (Cho et al. 2006). Our results are consistent with data from other studies since oligomycin induced a completely depolarization and loss of $\Delta\Psi$.

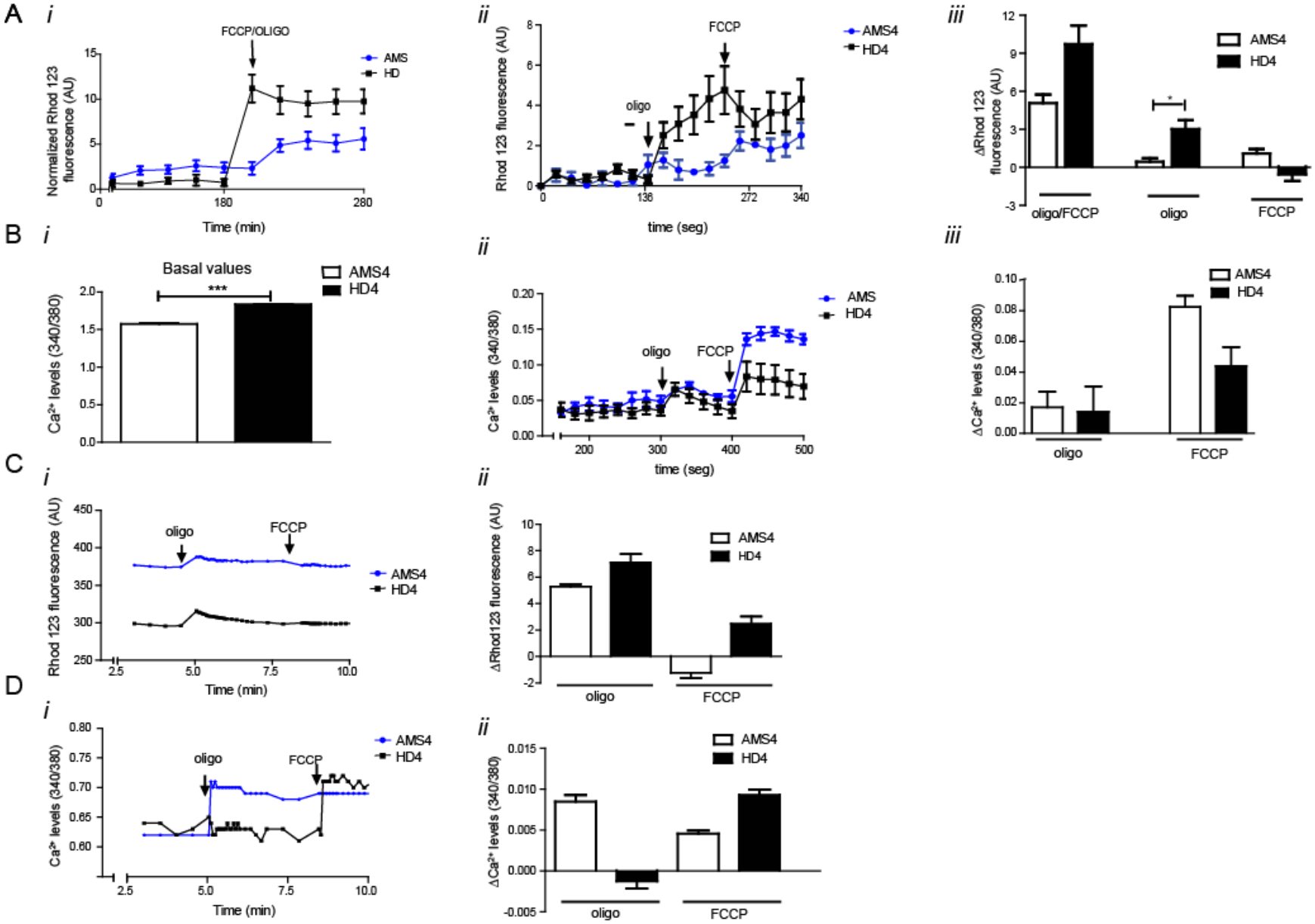
A
i
FCCP/OLIGO
AMS
HD
Normalized Rhod 123 fluorescence (AU)
Time (min)
ii
FCCP
oligo
AMS4
HD4
Rhod 123 fluorescence (AU)
time (seg)
iii
AMS4
HD4
ΔRhod 123 fluorescence (AU)
oligo/FCCP
oligo
FCCP
B
i
Basal values
***
AMS4
HD4
Ca2+ levels (340/380)
ii
oligo
FCCP
AMS
HD4
Ca2+ levels (340/380)
time (seg)
iii
AMS4
HD4
ΔCa2+ levels (340/380)
oligo
FCCP
C
i
oligo
FCCP
AMS4
HD4
Rhod 123 fluorescence (AU)
Time (min)
ii
AMS4
HD4
ΔRhod123 fluorescence (AU)
oligo
FCCP
D
i
oligo
FCCP
AMS4
HD4
Ca2+ levels (340/380)
Time (min)
ii
AMS4
HD4
ΔCa2+ levels (340/380)
oligo
FCCP

Figure 4.2. - Mitochondrial membrane potential measured with the fluorescent lipophilic cationic dye Rhodamine 123 and representative Fura-2 analysis of intracellular Ca^{2+}. (A) (*i*) After 30 minutes incubation with Rhod123, fluorescence was measure in the fluorimeter. iPSC were exposed to 2 µg/ml oligomycin FCCP ensemble or (*ii)* separately at the times indicated by the arrows, which respectively caused the characteristic quenching (hyperpolarization of ψm) and unquenching (depolarization of ψm) (B)(i) iPSC were incubated for 30 minutes with Fura-2AM and basal fluorescence was measured in the fluorimeter (ii) followed by the response to oligomycin and FCCP at the times indicated by the arrows. (C-D) (i-ii) Time course of iPSC mitochondrial membrane potential and of cytosolic Ca^{2+} change following oligo and FCCP addition measured in the single cell microscope. The results are expressed as the mean±S.E.M. from 3 independent experiments. Statistical analysis was performed by one way ANOVA, followed by Bonferroni post test. **p<0.01

An association between Ca^{2+} homeostasis dysfunction and ΔΨ abnormalities was described in several studies with mitochondria showing an interaction with mHTT and mitochondria (Lim *et al.* 2008, Sommer et al. 2012). The Ca^{2+} basal levels measured by Fura- 2AM probe fluorescence intensity were significantly increased in HD-iPSC (1.57 ± 0.01 vs 1.83 ± 0.003, p<0.0001) (Figure 4.2B*i*). After, we tested for functional differences in Ca^{2+} handling due to dynamics of mitochondrial Ca^{2+} pool by challenging cells with ATP synthase inhibition (2 µg/ml oligomycin) and ΔΨ collapse with FCCP (2 µM). Figure 4.2B*i-iii* shows that after the uncoupler addition the mitochondria in HD-iPSC released less Ca^{2+} indicating a lower uptake by mutant cells than in controls. Single-cell calcium imaging for quantification of changes in Ca^{2+} were also analyzed. When cells are analyzed individually Ca^{2+} levels measured show an increased release when mitochondria are totally depolarized with FCCP in AMS4-iPSC (0.08 ± 0.007 vs 0.04 ± 0.01, p=ns) (Figure 4.2D*i-ii*).

Furthermore to elucidate the mitochondrial role in Ca^{2+} handling, we reduced glucose levels to 2mM and replaced with pyruvate (10 mM). Removal of glucose leads to suppression of glycolysis but increasing pyruvate levels, a mitochondrial energy substrate, stimulates mitochondrial energy production and forces the electron transport chain to work (Oliveira et al. 2006, Ferreira et al. 2011). Mitochondria from iPSC cultures exposed to those conditions became more hyperpolarized as shown in Figure 4.3A*i*. Both HD and AMS4-iPSC released more quenched Rhod123 when stimulated with oligomycin, although the dye uptake was significantly higher in HD cells (p<0.01).

Mitochondria from iPSC cultures exposed to low levels of glucose have increased basal Ca^{2+} levels. For AMS4-iPSC the Ca^{2+} levels increased by 0.42 RFU ($p<0.001$) and for HD-iPSC the increased in Ca^{2+} levels was of 0.79 RFU ($p<0.001$) suggesting an increased accumulation of Ca^{2+} (Figure 4.3B*i*). When the low glucose medium iPSC cultures are completely depolarized by FCCP a significant magnification of Ca^{2+} release was observed (Figure 4.3B*ii*).

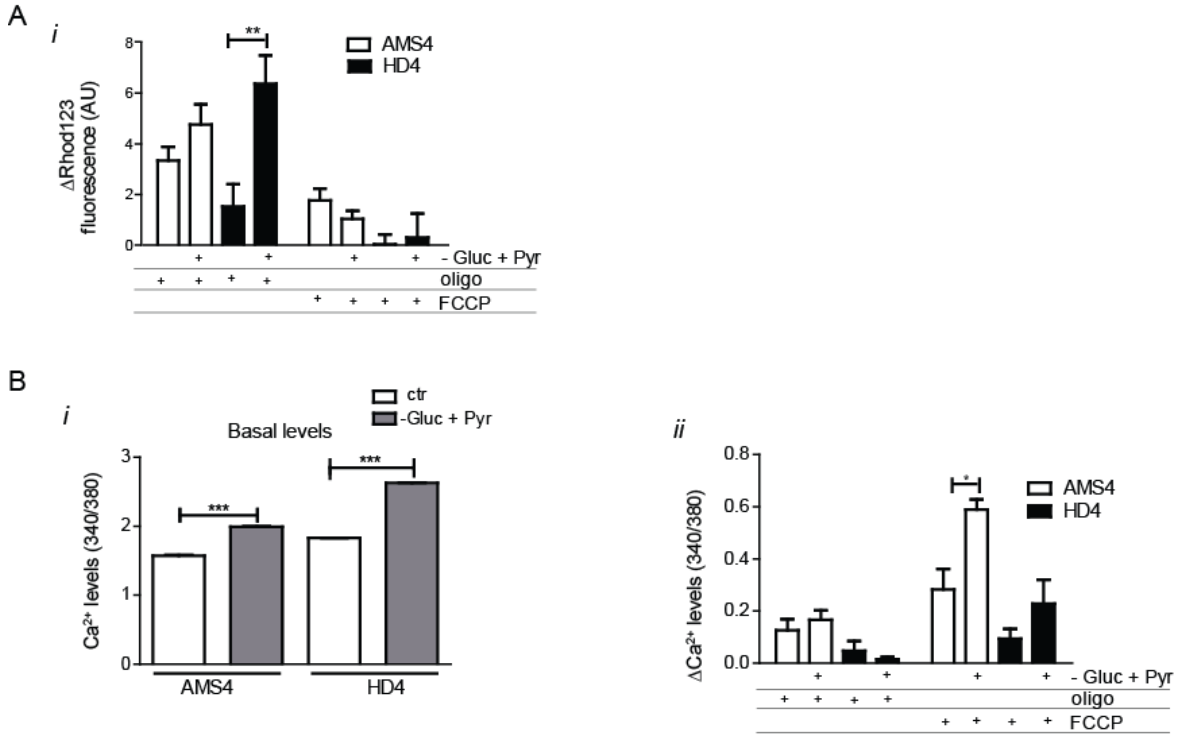

Figure 4.3. iPSC were loaded with Rhod123 and Fura-2AM and assayed in low glucose medium containing 10 mM pyruvate. The results are expressed as the mean±S.E.M. from 3 independent experiments. Statistical analysis was performed by one way ANOVA, followed by Bonferroni post test. ***$p<0.001$, **$p<0.01$, *$p<0.05$.

4.3.3.Abnormal mitochondrial dynamics in HD-iPSC

Next, in order to evaluate mitochondria dynamics we incubated cells with MitoTracker Red or transfected with pDsRed2-Mito for mitochondrial staining. We observed that HD-iPSC stained for MitoTracker Red and pDsRed2-Mito contain mitochondria with more elongated and less globular shape than AMS4-IPSC cells and the localization is not strictly perinuclear but more disperse in cell cytosol (Figure 4.4). AMS4-iPSC

mitochondria assume a bipolar clustering at the two sides of the nuclei not seem in HD-iPSC. MitoTracker Red is sensitive to mitochondrial membrane potential and in HD-iPSC culture it accumulates more in some cells (Figure 4.4*i*).

Mitochondrial dynamics is maintained by 2 divergent forces: mitochondrial fusion and mitochondrial fission - that balances equally to constantly shape the mitochondrial network. More fission results in over-fragmented networks while more fusion leads to over-connected networks. Fission is regulated by the dynamin-related protein (Drp1) and mitochondrial fission 1 (Fis1). Fis1 is localized to the outer-membrane of mitochondria and Drp1 protein is localized in the cytoplasm. Mitochondrial fusion is controlled by 3 GTPase proteins: two outer-membrane localized proteins Mfn1 and Mfn2, and one innermembrane localized protein Opa1. The GTPases to become active have to be recruited to the mitochondria. Immunostainings for those proteins reveal reduced overlap with mitochondria particularly for OPA1 and Mfn2 and slight more for DRP1 (Figure 4.4A*i-v*, 4.4B). Fis1 highly colocalize with the mitochondria (Figure 4.4B). The levels of fusion/fission markers associated with mitochondria were similar for AMS4 and HD-iPSC.

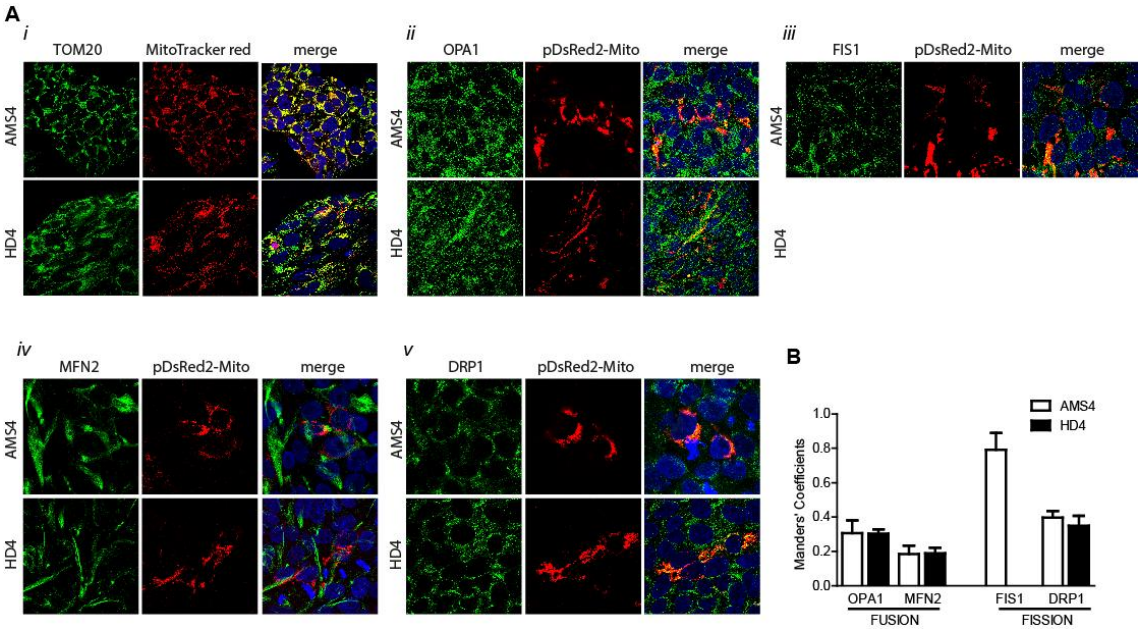

Figure 4.4. – Mitochondrial dynamics. (A) (i)Immunofluorescence analysis of mitochondrial proteins TOM20 and MitoTracker red and (ii-v) Opa1, Fis1, Mfn2 and Drp1 fusion and fission molecules and pDsRed2-Mito. Fusion molecules Mfn is a mitochondrial outer membrane protein with a cytosolic GTPase domain and OPA1 is a GTPase in the intermembrane space. Fission molecules Fis1 is localized uniformly to the mitochondrial outer membrane, whereas Drp1 is localized to the cytosol and punctate spots on mitochondria. (B) Western blot analysis of mitochondrial fission and fusion proteins in HD-iPSC and controls. Images were photographed at ×63. The results are expressed as the mean±S.E.M. from 3 independent experiments. Statistical analysis was performed by one way ANOVA, followed by Bonferroni post test. ***p<0.001, **p<0.01, *p<0.05

4.3.4.Energetic metabolism is impaired in HD-iPSC and HD-NSC

The metabolic profile of iPSC is quite different upon differentiation (Schieke et al. 2008, Prigione et al. 2010, Folmes et al. 2011). The bioenergetics processes for ATP production, OXPHOS and glycolysis, were examined in iPSC and NSC. Thus the oxygen consumption rate (OCR) and the extracellular acidification rate (ECAR), which can approximate glycolysis from lactate production, were determined using a XF24 Extracellular (Figure 4.5). The ratio of OCR to ECAR indicates cellular preference for OXPHOS versus glycolysis when mitochondria are coupled for oxygen consumption and energy generation. The OCR response to oligomycin A, FCCP and rotenone + antimycin A indicate (1) basal mitochondrial and (5) nonmitochondrial components of cellular oxygen consumption, (2) oxygen consumed for ATP generation through the

complex V versus (3) oxygen consumed with passive proton leakage across the mitochondrial inner membrane, which reduces the mitochondrial membrane potential, and (4) maximal respiratory capacity in coupled and completely uncoupled conditions. OCR studies showed that HD-iPSC consume less oxygen than control, at room air OCR was 282.9 ± 15.78 pmol/min/mg protein for control and 234.7 ± 7.63 pmol/min/mg protein for HD –iPSC ($p<0.05$) (Figure 4.5A1). The component of OCR used to generate ATP (94.87 ± 28.36 vs 67.69 ± 7.04, p=ns) was slightly although not significantly lower as the maximal respiratory capacity (174.3 ± 53.72 vs 137.2 ± 19.72, p=ns) (Figure 4.5A2, A4). Proton leakage can have several functions (1) production of heat to maintain body temperature, (2) endowment of increased sensitivity of metabolic reactions to effectors (3) reduction of harmful free radical production and (4) regulation of carbon flux (Buttgereit *et al.* 2000, Serviddio *et al.* 2010). HD-iPSC have increased OCR proton leaks (34.0 ± 9.24 vs 49.3 ± 3.34; p=ns). OXPHOS was inhibited with oligomycin and HD-iPSC showed lower reduction in oxygen consumption suggesting that are less dependent on OXPHOS than control.

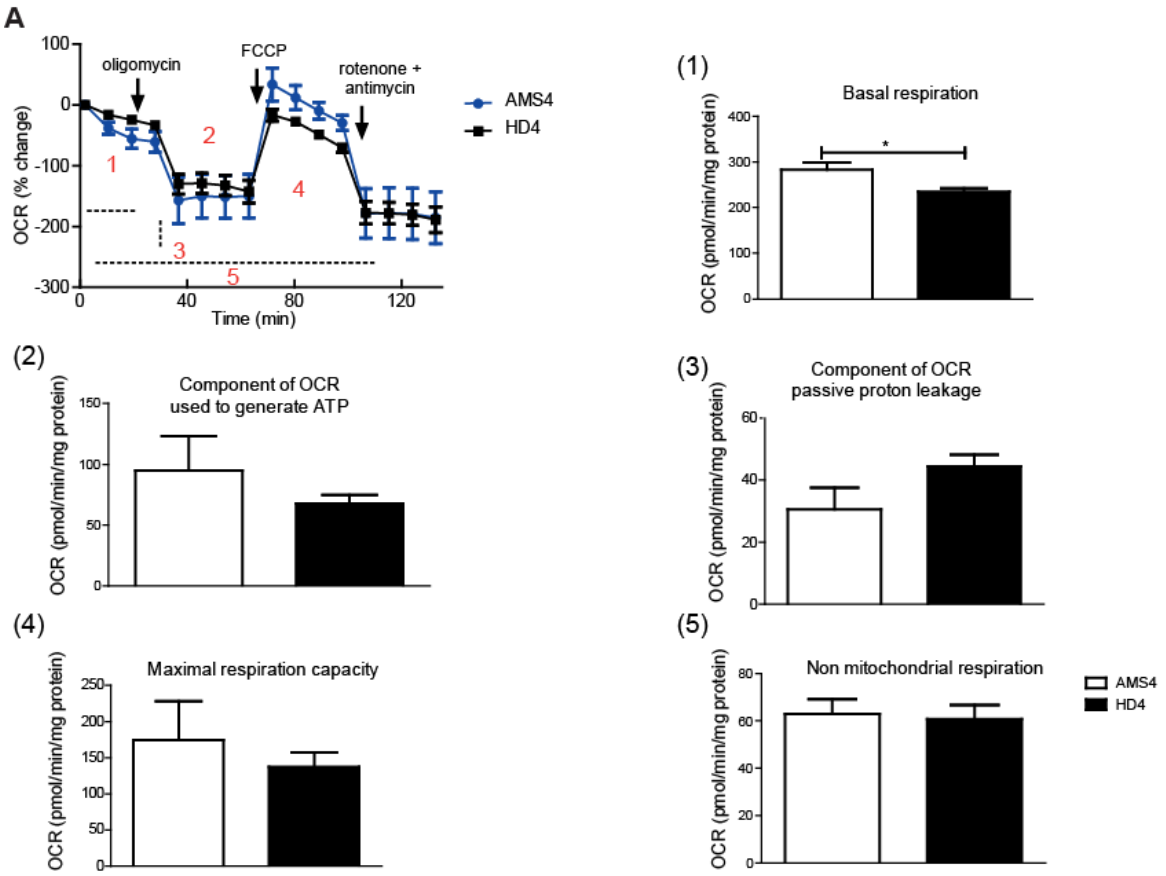

Figure 4.5 - Oxygen consumption rate (OCR) and extracellular acidification rate (ECAR) was determined by Seahorse XF24 analyzer in iPSC. (A) The mitochondrial inhibitors were sequentially injected into different ports and the final concentrations of each were: 1 µM oligomycin, 0.3 µM FCCP, 1 µM rotenone and 1 µM antimycin A. 1) basal OCR (represents the mean of the first four measurements); 2) oxygen consumed for ATP generation through the complex V (mean of basal values minus mean of measurements after oligomycin A); 3) component of OCR representing passive proton leakage across the mitochondrial inner membrane (mean of measurements after oligomycin A minus mean of measurements after rotenone + antimycin A) 4) the maximal respiration capacity (mean of measurements after fccp minus mean of measurements after rotenona antimycin A; 5) non mitochondrial respiration (mean of measurements after rotenona antimycin A minus zero). The results are expressed as the mean±S.E.M.. Statistical analysis was performed by t-student test *p<0.05

Upon differentiation a marked decrease in mitochondrial oxygen consumption was documented in HD-NSC (Figure 4.6A). HD-NSC showed a reduced basal OCR compared to control (104.1 ± 2.56 pmol/min/mg protein vs 68.70 ± 0.49 pmol/min/mg protein) ($p<0.0001$) (Figure 4.6A1). All the components evaluated for OXPHOS such as the component of OCR used to generate ATP (28.93 ± 2.09 vs 15.25 ± 1.35, $p<0.0001$), the maximal respiratory capacity (148.2 ± 12.47 vs 59.99 ± 5.16, $p<0.0001$), component of OCR passive proton leakage (11.34 ± 0.76 vs 5.99 ± 1.78, $p=<0.01$) were diminished in HD-NSC compared to AMS4-NSC (Figure 4.6A2-5).

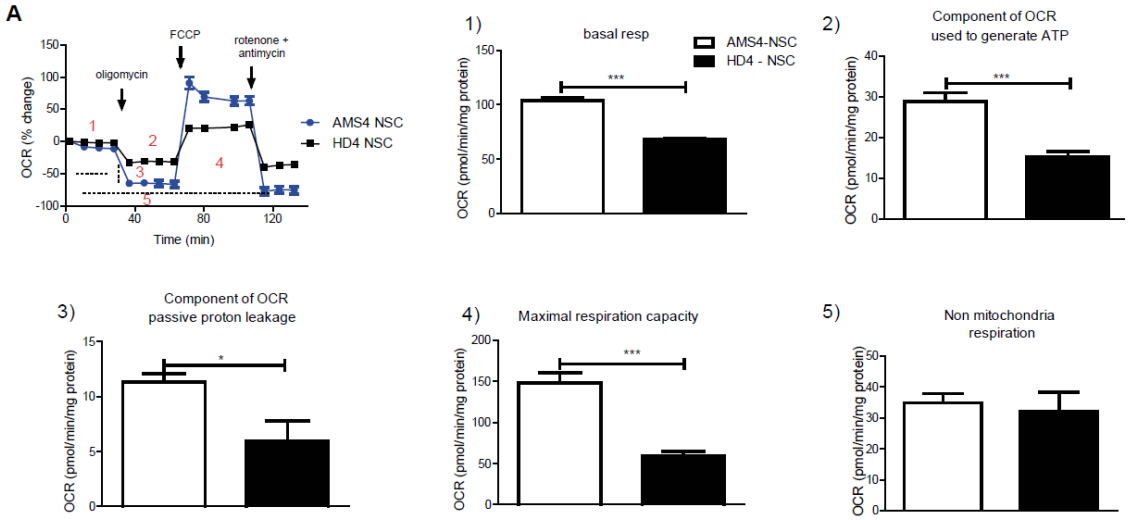

Figure 4.6. - Oxygen consumption rate (OCR) was determined by Seahorse XF24 analyzer in neural stem cells derived from iPSC. (A) The mitochondrial inhibitors were sequentially injected into different ports and the final concentrations of each were: 1 µM oligomycin, 0.3 µM FCCP, 1 µM rotenone and 1 µM antimycin A. 1) basal OCR (represents the mean of the first four measurements); 2) oxygen consumed for ATP generation through the complex V (mean of basal values minus mean of measurements after oligomycin A); 3) component of OCR representing passive proton leakage across the mitochondrial inner membrane (mean of measurements after oligomycin A minus mean of measurements after rotenone + antimycin A) 4) the maximal respiration capacity (mean of measurements after fccp minus mean of measurements after rotenona antimycin A; 5) non mitochondrial respiration (mean of measurements after rotenona antimycin A minus zero). The results are expressed as the mean±S.E.M.. Statistical analysis was performed by t-student test *p<0.05; **p<0.01; ***p<0.001.

To further understand mitochondrial respiratory chain alterations we analyzed the enzymatic activities of respiratory complexes I, II, III and I+III by spectrophotometry. Results were normalized to the protein content and the activity of citrate synthase (CS), a mitochondrial matrix enzyme. According to our data, Cx-I and Cx-II present no significant differences while the activity was significantly reduced in Cx I+III (211.7 ± 52.78 vs 40.57 ± 21.44, $p<0.05$) (Figure 4.7A).

Taking into account the alterations detected in mitochondrial Cx activities, we further determined the complex subunits mitochondrial expression.

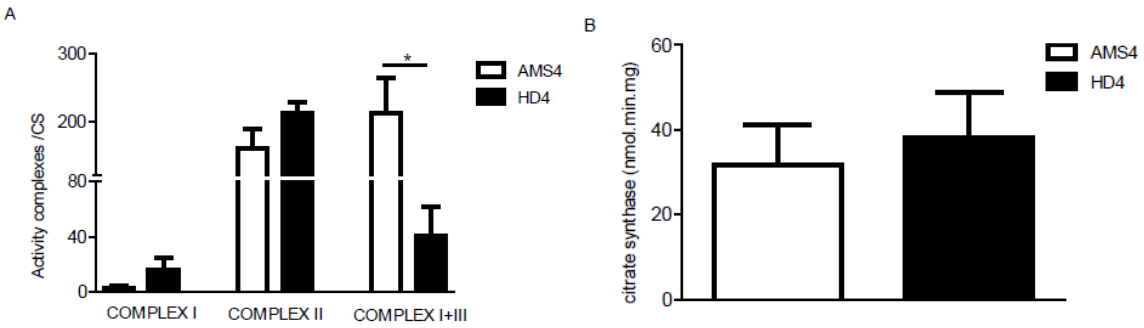

Figure 4.7 Activity of mitochondrial respiratory chain complexes I–III and citrate synthase. Mitochondrial respiratory chain complexes (Cxs) and citrate synthase (CS) activities were determined in mitochondrial fractions isolated from iPSC. Data are the mean ± S.E.M. of 5 independent samples, normalized for protein content and citrate synthase activity. Statistical analysis: The results are expressed as the mean±S.E.M.. Statistical analysis was performed by t-student test *p<0.05; **p<0.01; ***p<0.001.

The lower dependence on OXPHOS demonstrated by HD-iPSC is consistent with the decrease in mitochondrial enzymatic activity found.

Another major energy production pathway is glycolysis. Cells with a more glycolytic phenotype exhibit significantly higher rates of proton production due to the conversion of glucose to lactate, independent of oxygen (extracellular acidification rate) (Ferrick *et al.* 2008). To analyze ECAR, cells were incubated with a high dose of glucose to evaluate the glycolysis rate followed by addition of 2-deoxy-glucose that inhibits glycolysis, lowering ECAR. The maximum glycolytic capacity of the cells is achieved when oligomycin is added, inhibiting mitochondrial ATP production, and therefore shifts the energy production to glycolysis increasing in ECAR (Ferrick et al. 2008)..

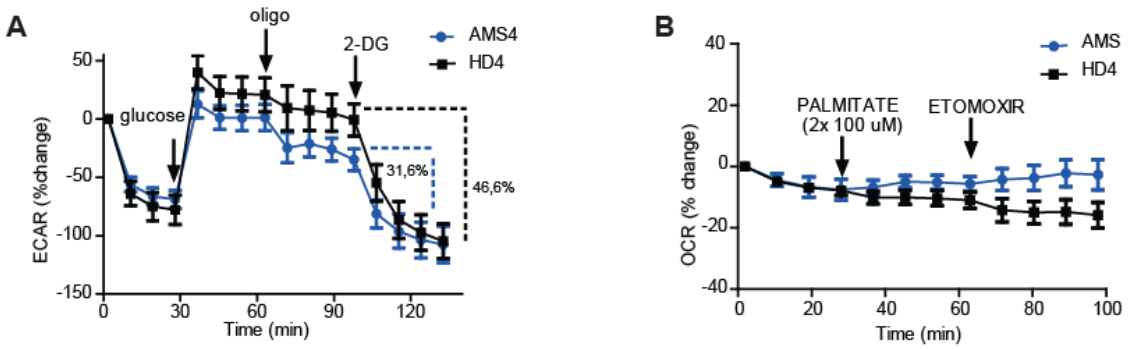

Figure 4.8. Extracellular acidification rate (ECAR) and fatty acid oxidation was determined by Seahorse XF24 analyzer in iPSC. (A) Cells were cultured in assay medium with 2.5mM glucose. ECAR changes with glucose (25mM final), oligomycin A (1µM) and 2-DG (100mM final) additions is shown. (B) oxygen consumption rate (OCR) following exposure to palmitate, as a direct indicator of fatty acid oxidation. The results are expressed as the mean±S.E.M.. Statistical analysis was performed by t-student test *p<0.05

Additional glucose (from 2.5 mM to 25 mM) maximized ECAR, with 80% increase in HD-iPSC whereas AMS4-iPSC ECAR increased by a more modest 52% indicating that controls are closer to their maximal glycolytic capacity compared with HD-iPSC. Subsequent addition of 2-DOG, which competes for uptake with glucose, HD-iPSC glycolysis was repressed 47% from the ECAR maximum whereas AMS4-iPSC glycolysis change only 32% from the ECAR maximum (Figure 4.8A), indicating that the HD-iPSC glycolysis level is greater than in AMS4-iPSC. Combined, the data indicate that HD-iPSC are less sensitive to OXPHOS inhibition but more sensitive to glycolysis disruption and AMS4-iPSC functions closer to their maximum glycolytic capacity.

Alternative carbon fuels can be used by cells for ATP production such as fatty acids oxidation (Zaugg *et al.* 2011). Palmitate, a fatty acid, can be internalized at cells by carnitine palmitoyltransferase 1 (CPT1), an enzyme that transports long-chain fatty acids across the mitochondrial inner membrane, and the component of OCR attributed to palmitate oxidation is determined by the addition of etomoxir an inhibitor of the transporter. When 200 µM palmitate is added to iPSC no variation in OCR level was observed (supplementary data) suggesting that iPSC do not use exogenous fatty acids as a carbon source for OXPHOS (Figure 4.8B).

Pyruvate dehydrogenase (PDH) complex catalyzes the oxidative decarboxylation of pyruvate linking glycolysis to the tricarboxylic acid cycle. Three components that catalyze the conversion of pyruvate to acetyl-CoA (pyruvate dehydrogenase (E1), dihydrolipoamide acetyltransferase (E2), and dihydrolipoamide dehydrogenase (E3)) are regulated by the enzymes pyruvate dehydrogenase kinases (PDK) and pyruvate dehydrogenase phosphate phosphatase (PDP). PDK and PDP catalyze a phosphorylation-dephosphorylation cycle involving specific serine residues on the subunitof E1. In our data PDH E1α subunit was significantly increased in HD-iPSC (Figure 4.9A*i*). We also observed that PDK1 protein levels are up regulated in HD-iPSC when compared to control and its expression increases dramatically in AMS4-NSC (Figure 4.9B*i*). Consistent with upregulated PDK1 expression displayed by HD-iPSC higher phospho PDH (PDH E1α serines 232, 293 and 300) levels were found when compared to AMS4-iPSC indicative of devoid activity (Figure 4.9A*ii*).

Cellular energy can be obtained either by aerobic respiration resulting in greater amount of ATP or by anaerobic respiration followed by lactic acid formation. To test energy generation in undifferentiated and differentiated iPS cells, ATP content and pyruvate/ lactate generation were measured. HD-iPSC exhibited similar production of pyruvate/ lactate in comparison to AMS4-iPSC (Figure 4.9C). Differentiated HD cells displayed higher amounts of pyruvate as well as lactate than AMS4-NSC. Upon differentiation pyruvate levels decrease in both cells lines and lactate production increases for HD-NSC as long as the ratios lactate/pyruvate. A significantly lower content of cellular ATP and ATP/ADP was detected in HD-iPSC (Figure 4.10). Taken together, the results suggest that HD-iPSC seems to rely less on mitochondrial respiration and mainly produce energy by anaerobic glycolysis followed by lactate production.

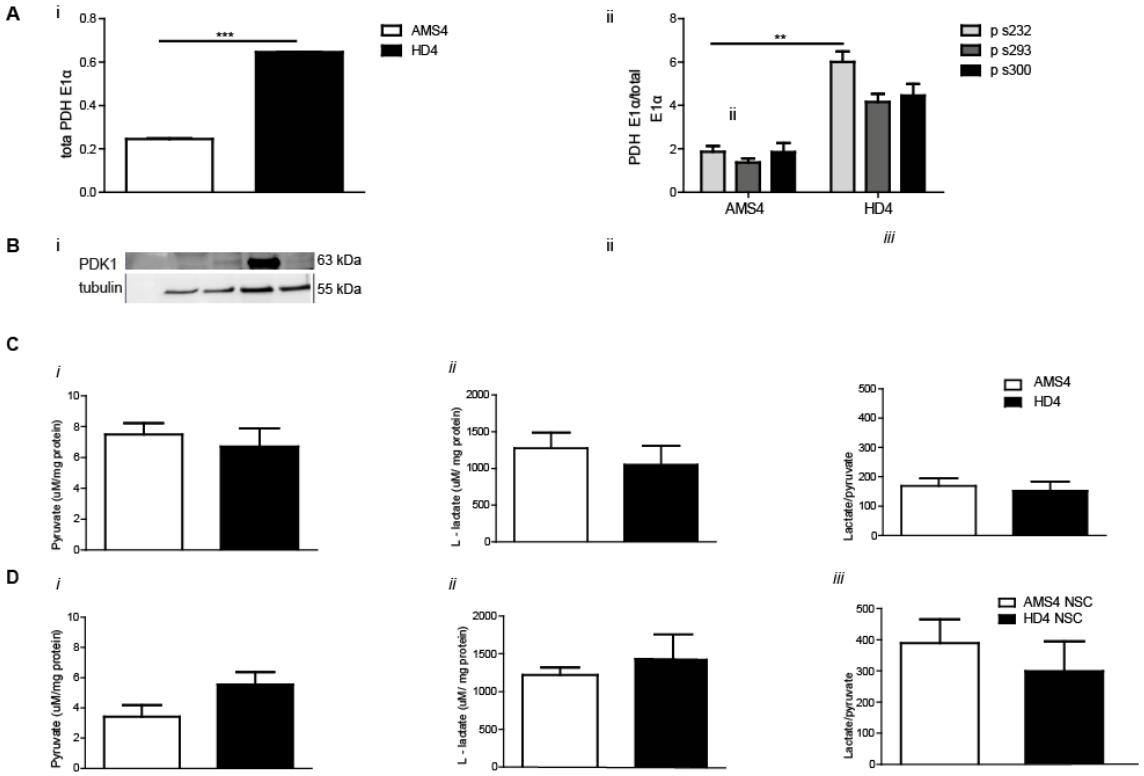

Figure 4. 9.- (A) (*i*) Determination of the total PDH levels in iPSC and (*ii*) activity levels of phospho-PDH (Ser 232, 293, 300 of the E1-*α* subunit). (B) (*i*) Western blotting analysis of PDK1 protein levels. (C) Pyruvate and lactate levels on iPSC and their differentiated counterparts. Tubulin was used as a loading control. Two way ANOVA analyses revealed that there is a significant effect of genotype on levels of phospho-PDH [$F(1,44)=98.96$, $p < 0.001$]. The results are expressed as the mean±S.E.M. Statistical analysis was performed by t-student test and two way ANOVA followed Bonferroni analysis *p<0.05; **p<0.01; ***p<0.001. Abbreviations: PDK1, pyruvate dehydrogenase kinase one; pPDH: phospho pyruvate dehydrogenase subunit E1a; PDH: pyruvate dehydrogenase.

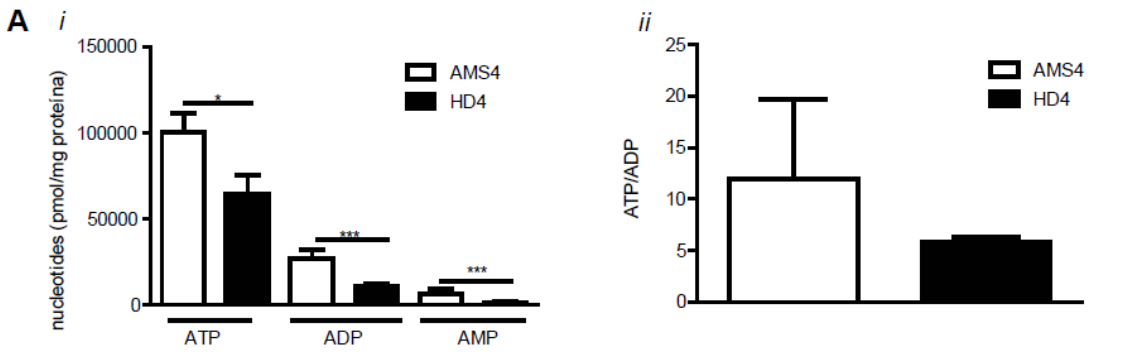

Figure 4.10 - (A) – Intracellular iPSC levels of adenine nucleotides ATP, ADP and AMP. The cell lysates were assayed for ATP, ADP, and AMP by separation in a reverse-phase HPLC with detection at 254 nm Statistical analysis was performed by one way ANOVA followed Bonferroni analysis *p<0.05; **p<0.01; ***p<0.001.

4.3.5.HD-iPSC exhibit mitochondrial dysfunction associated with increased oxidative stress

Mitochondria abnormalities and oxidative stress have been suggested to play a critical role in HD neurodegeneration. Previously data of our lab as reported increase susceptibility of HD striatal cells to ROS (Ribeiro et al. 2014) . Moreover proteomic analysis of HD-iPSC showed that oxidative stress- related proteins such as SOD1 and peroxiredoxin (Prx) are affected (Chae *et al.* 2012). ROS are mitochondrial respiration by-products that cause oxidative damage to proteins, lipids, and DNA. Varun and colleagues revealed that ROS production increase with iPSC differentiation and it seems that a ROS-dependent pathway influences pluripotency (Mandal et al. 2011).

To better understand if the changes we found in Ca^{2+} handling were related with ROS production we further analyze superoxide and hydrogen peroxide production, sub-products of OXPHOS. To determine the mitochondrial superoxide anion and hydrogen peroxide production in iPSC, we used MitoSox Red and MitoPY1 and exposed cells to 1 µM Antimycin A (AA). AA acts by inhibiting the flow of electrons from cytochrome b to cytochrome c1 in complex III. It displaces coenzyme Q, the primary electron carrier, thus disrupting the proton gradient across the inner membrane of mitochondria and preventing O_2 consumption at complex IV as well as ATP formation. Our results indicate that HD-iPSCs and HD-NSC are highly susceptible to oxidative stress showing

increased basal levels of superoxide anion and hydrogen peroxide ($p<0.005$) (Figure 4.11*i*, Figure 4.12*i-ii*, Figure 13A*i*). When exposed to acute AA, H_2O_2, 3NP or oligo/FCCP stimulus a higher amount of ROS were produced in iPSC and NSC compared to control demonstrating a lower capacity to neutralize the produced ROS (Figure 4.11A*ii*, 4.12B*i*,*ii*,4.12C*i*, Figure 4.13B*i-ii*, 4.13C*i-ii*).

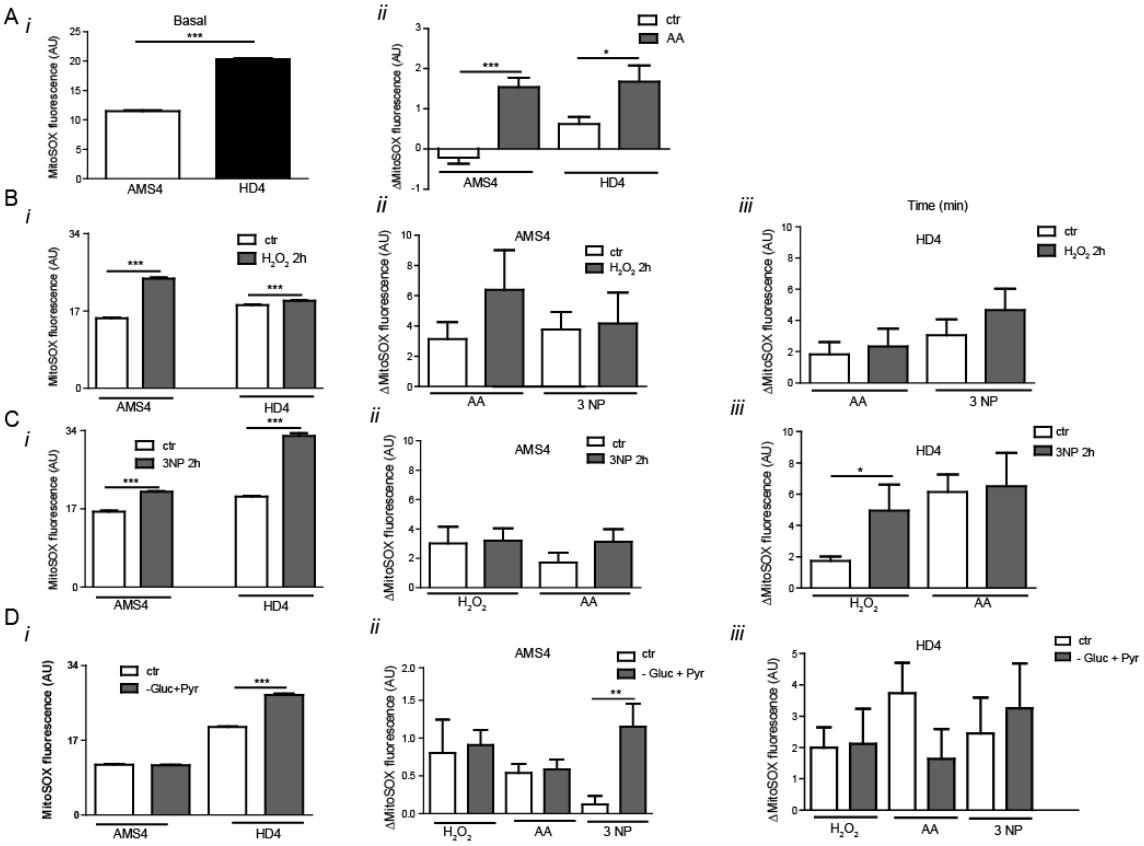

Figure 4.11.- Characterization of intracellular basal superoxide levels and induction after acute incubation with noxious stimulus (A) (i) Intracellular basal superoxide levels measure with Mitosox probe. (ii-iii) Generation of superoxide after acute exposure to 1 µM antimycin A. (B) (C) (i-iii) iPSC were treated for 2 hours with 100 µM H_2O_2 or 300 nM 3NP after which basal superoxide was measure for 5 minutes and exposed to acute stimulus with 1µM antimycin A, 300nM 3NP or 1 mM H_2O_2 for more 5 minutes. (D) iPSC were maintained for 30 minutes in low glucose medium containing 10 mM pyruvate followed by superoxide measure for 5 minutes and exposition to acute stimulus with 1µM antimycin A, 300nM 3NP or 1 mM H_2O_2 and fluorescence acquisition for more 5 minutes. The results are expressed as the mean±S.E.M. Statistical analysis was performed by t-student test *$p<0.05$; ***$p<0.001$.

To evaluate if anti-oxidative stress long term response was also impaired in HD-iPSC we incubated cells for 2h with H_2O_2 100 μM or 3NP 300 nM followed an acute stimulus with AA, 3NP and/or H_2O_2. Basal levels of ROS significantly increased in cells incubated for 2 h with the noxious agents (Figure 4.11B*i*, C*i*). As expected both AMS4 and HD-iPSC treated with H_2O_2 for 2h produced more ROS when challenged acutely with AA and 3 NP (Figure 4.11B*ii-iii*, 4.11Ci*i-iii*). In AMS4-iPSC, AA induced an enormous production of ROS but 3 NP only resulted in a small change. Incubation of 3 NP for 2h resulted in higher predisposition of AMS4-iPSC for ROS production when exposed to AA but no changes were found for H_2O_2. For HD-iPSC H_2O_2 also led to an increased production of ROS subsequently to 3 NP exposure. Consistently, as previously described iPSC medium was changed to deplete glucose-medium supplemented with 10 mM pyruvate to inhibited glycolysis and promote OXPHOS, this way stimulating ATP production by mitochondria. No increase in superoxide anion production was found except for AMS4-iPSC stimulated with 3 NP (Figure 4.11D*ii*). The lack of augmentation on ROS was most likely due to the short period maintained in the depleted medium.

SOD1 is located in the cytosol and mitochondrion and is extremely important to reduce cellular ROS and promote oxidative stress resistance. The total SOD activity and particularly the SOD1 activity was found to be extremely reduced in HD-iPSC (SOD2 12.47±4.31 vs 9.79±3.65; SOD1 9.69±4.42 vs 3.48±0.69) (Figure 4.12D*i*). In the western blotting analysis we observed that SOD is more acetylated in HD-iPSC lines, thus more inactive and the expression increases strongly in differentiated cells (Figure 4.12D*ii*). The increase amount of ROS found in HD cells is most likely related to increased inactivation of SOD2 by acetylation and upon differentiation in total SOD expression.

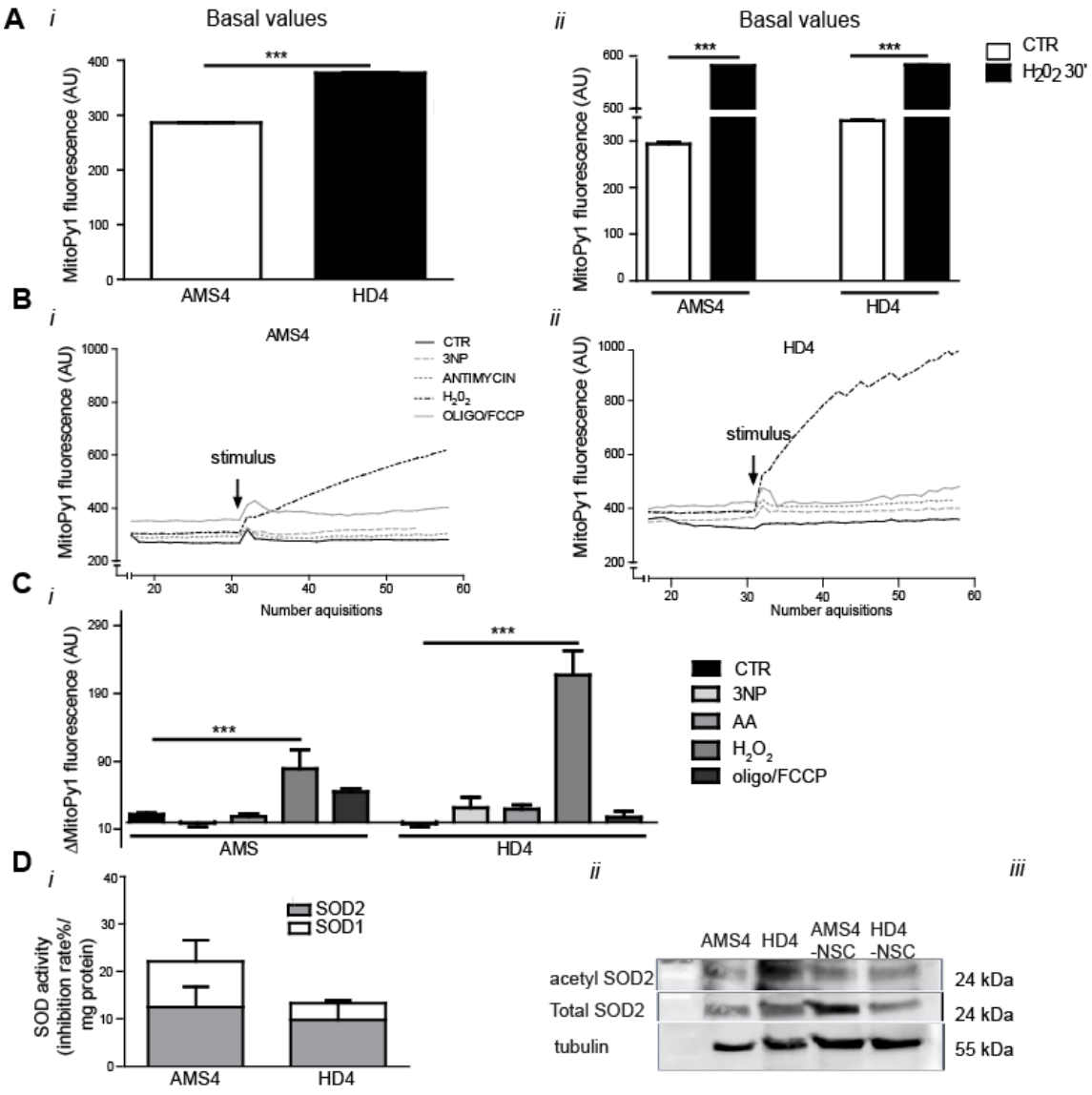

Figure 4.12- Characterization of intracellular H_2O_2 levels in iPSC. (A) (i) MitoPY1 was used to measure basal mitochondrial H_2O_2 levels (ii) iPSC were incubated for 30 minutes with 100 µM H_2O_2 for probe positive control. (B)(i-ii) (C)(i) Generation of H_2O_2 after acute exposure to 300nM 3NP, 1µM antimycin A, 1 mM H_2O_2 or 2g/ml oligomycin/ 2µM FCCP for 15 minutes. (D) (i) Superoxide dismutase (SOD) activity in iPSC. Parallel experiments were conducted in the presence of KCN (2 mM) to inhibit SOD1. (ii) Acetylated and total Superoxide dismutase 2 protein levels in iPSC and NSC cell lysates. The results are expressed as the mean±S.E.M. Statistical analysis was performed by t-student test and two way ANOVA followed Bonferroni analysis *p<0.05; **p<0.01; ***p<0.001. ***p<0.001.

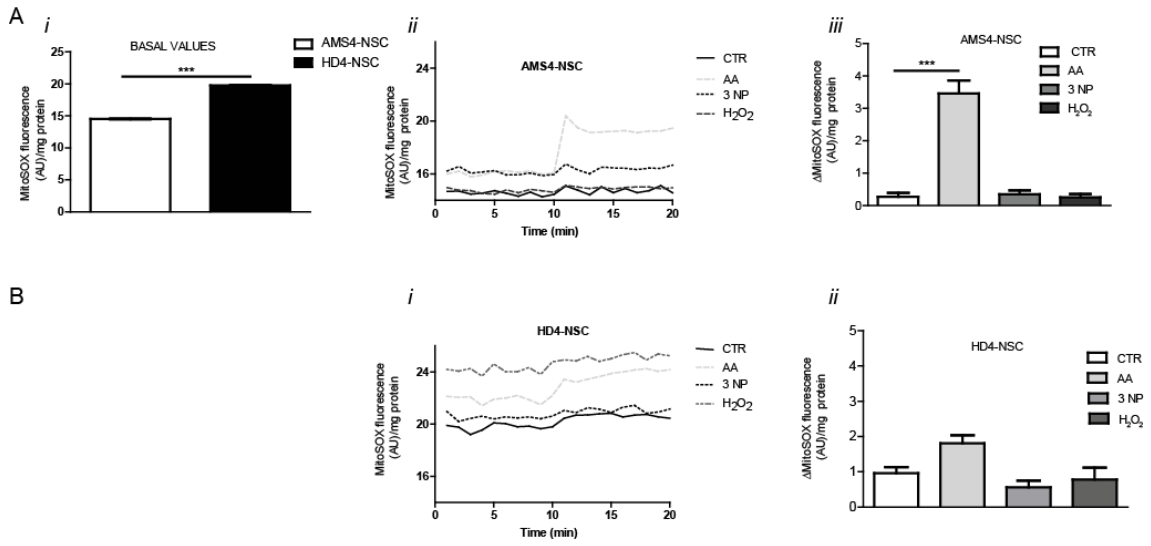

Figure 4.13- Characterization of intracellular basal superoxide levels and induction after acute incubation with noxious stimulus in NSC (A) (i) Intracellular basal superoxide levels measure with Mitosox probe. (ii-iii) Generation of superoxide in AMS4-NSC after acute exposure to 1 µM antimycin A, 300 nM 3NP and 1 mM H_2O_2 (B) (*i-ii*) and in HD4-NSC. The results are expressed as the mean±S.E.M. Statistical analysis was performed by t-student test *p<0.05; ***p<0.001.

4.4.Discussion

This study characterizes a 74 CAG-repeat-expansion iPSC and neural cells derived from HD-iPSC line. The correlation between the length of CAG expansion and HD phenotype is well known (Andrew et al. 1993, Henley *et al.* 2009). Recently,iPSC lines derived from HD patient fibroblasts (Takahashi et al. 2007, Yu et al. 2007) and human embryonic stem cell lines donated mutant embryos were generated (Thomson et al. 1998) showed great promise in the study of HD mechanisms of disease. In our study we directly differentiate iPSC into NSC successfully resorting the combined and specific application of a few morphogens, as was previously described (Chambers et al. 2009, Delli Carri et al. 2013, Nicoleau et al. 2013).

In recent years mitochondrial dysfunction has assume a great importance in clarifying the link between disease phenotype and upstream mitochondrial pathways that can be involved in the initiation phase. Numerous studies suggest that alterations in mitochondrial respiration are responsible for the bioenergetics defects found in HD. Biochemical studies from HD patients tissue and HD cells and animal models revealed decreased activity of several enzymes involved in oxidative phosphorylation such as complex I, II, III, and IV (Powers *et al.* 2007, Browne 2008, Lim et al. 2008, Kim *et al.* 2010, Silva *et al.* 2013). Despite, data from early HD patients do not support major deficits in the activity of striatal mitochondrial respiratory complexes sustaining the evidence that respiratory chain impairment could be a late secondary event and not the pathology trigger (Guidetti *et al.* 2001, Powers et al. 2007, Powers *et al.* 2011).

The work described here has shown that HD-iPSC and NSC demonstrate early signs of mitochondrial dysfunction and calcium dyshomeostasis. HD-iPSC seems to be more hyperpolarized than wild type since it releases more Rhod123 when exposed to oligo/FCCP. Also the basal levels of Ca^{2+} were increased but when mitochondria were challenged with oligo/FCCP HD-iPSC released less Ca^{2+} indicating a lower uptake. The single cell imaging allow to measure in the same cell $\Delta\Psi$ and Ca^{2+} handling providing complementary information to the previous results. The data obtained confirmed a more negative $\Delta\Psi$ for HD-iPSC, consistent with a higher release of probe after oligomycin addition and a lower uptake of Ca^{2+} since when mitochondria depolarizes less Ca^{2+} was release. Although in the majority of cells oligomycin administration induces hyperpolarization our data reveals an immediate depolarization. The ATP synthase in iPSC seems to have hydrolase activity of glycolytic ATP for maintaining the $\Delta\Psi$ more

negative. Previous studies have shown that ATP synthase (complex V) is reversed in iPSC hydrolyzing glycolytic ATP to maintain the $\Delta\Psi$ (Cho et al. 2006, Zhang et al. 2011). The authors blocked ATP production by glycolysis resulting in a strong decrease in ATP levels, whereas inhibition of OXPHOS only caused a slight reduction in ATP levels in both hES and iPS cells (Varum et al. 2011, Zhang et al. 2011). Disturbances in calcium homeostasis, due to excitotoxicity and/or mitochondrial dysfunction are well known features of HD. Is known that intracellular Ca^{2+} concentration is elevated in striatal neurons from symptomatic HD in basal condition and after exposure to NMDA. In our study iPSC revealed a higher Ca^{2+} concentration but a low mitochondrial Ca^{2+} storage capacity.

Glutamate receptors stimulation activates the IP3 signaling pathway increasing Ca^{2+} release from InsP3R1 in cells expressing mutant huntingtin. Similar results were observed by HD Consortium in HD-iPSC where there was a clear CAG-repeat-expansion-associated phenotype with Ca^{2+} dyshomeostatis after acute pulses and chronic exposure to glutamate (Consortium 2012).

Moreover, in this study replacing pyruvate by glucose in the medium we accentuated the cellular bioenergetic consequences of mitochondrial dysfunction as previously described in cultured striatal neurons (Oliveira et al. 2006, Ferreira et al. 2011). Recent studies showed that mitochondrial fission and fusion may be altered in HD (Wang *et al.* 2009, Kim et al. 2010, Shirendeb *et al.* 2011, Shirendeb *et al.* 2012). Accordingly, we found abnormal mitochondrial structure and functional dynamics in HD-iPSC. Unlike previous reports, were mitochondria assume a globular or spherical morphology with a dominant perinuclear localization (Facucho-Oliveira et al. 2007, Prigione et al. 2010, Zhang et al. 2011, Kelly et al. 2013), HD-iPSC revealed a more elongated and less globular shape and the localization is not exactingly perinuclear but more disperse in cell cytosol contrasting to control cells data. As well-known mitochondrial fission and fusion proteins regulate the morphology, function, integrity and topographic distribution of mitochondria. A tight balance between mitochondrial fission and fusion is required to maintain ESC pluripotency and regulate the localization of mitochondria (Todd et al. 2010, Todd *et al.* 2010, Harvey *et al.* 2011). Recently Todd et al (2010) demonstrated that growth factor erv1-like (Gfer), an inner mitochondrial membrane protein, is involved in preserving mouse ESC mitochondrial morphology and function and the KD led to a decrease of pluripotency marker expression, impair embryoid body (EB) formation and reduce cell survival associated with loss of mitochondrial function.

Levels of Drp1 were increased in Gfer-KD ESCs and treating ESC with a specific inhibitor of Drp1 rescued mitochondrial function and apoptosis. Moreover, overexpression of Gfer resulted in elongation of mitochondria, upregulation of Oct4 and Nanog and downregulation of the fission protein Drp1 (Todd et al. 2010, Todd et al. 2010). Herein immunofluorescent staining of iPSC demonstrates lower mitochondrial localization of fusion proteins Mfn2 and OPA1 and higher for fission proteins Fis1 and Drp1. Since iPSC are rapidly dividing cells our results suggest that iPSC have impaired fusion and enhanced fission to promote proliferation. A recent report described that human cancer cell lines exhibit an imbalance of Drp-1/Mfn-2 expression, which promotes a state of impaired fusion and enhanced fission contributing fundamentally to the proliferation/apoptosis imbalance in cancer pointing to potential commonalities in mitochondrial dynamics (Rehman *et al.* 2012). Kim et al (2010) similarly demonstrated elevated levels of Drp1 and reduced levels of Mfn1 in HD caudate nucleus lysates consisting with alterations in the expression pattern of mitochondrial fission/fusion proteins (Kim et al. 2010).

Mitochondrial dynamics has been shown to regulate mitochondrial metabolism (Bach *et al.* 2003, Pich *et al.* 2005). Previous studies using allelic series of heterozygous CAG knock-in mouse ES cell lines show energy metabolism dependency on CAG length (Jacobsen *et al.* 2011). Additionally the HD consortium revealed that human-derived HD-NPCs have significantly decrease intracellular ATP and decreased ATP/ADP ratios suggesting that energy metabolism is compromised in higher CAG length cell lines (Consortium 2012) Our study similarly describes an impaired energetic metabolism in HD-iPSC and HD-NSC. We show that HD-iPSC have functional respiratory complexes however consume less oxygen than controls while are able to consume O_2 at maximal capacity. Moreover, upon differentiation a marked decrease in mitochondrial oxygen consumption was observed. Those findings are in agreement with a reduced mitochondrial electron transport chain complexes activity. Furthermore, HD-iPSC seems to rely more on glycolysis for supplying ATP demands since they function closer to their maximum glycolytic capacity and fatty acids it is not a carbon source for OXPHOS. Overall HD-iPSC seems to have lower OXPHOS activity. Surprisingly the decrease in OXPHOS dependence was not expected although a recent study showed that hESCs have a high mitochondrial activity that declines disproportionately, alongside several related parameters of mitochondrial biogenesis, with differentiation into NSC and that this is coupled to a decrease in overall ATP turnover (Birket et al. 2011). The

authors reported that hESCs maintain a high rate of mitochondrial oxidative phosphorylation compared with hESC-derived NSC, but without increased glycolysis. Concomitantly high levels of expression of the mRNA encoding coactivators PGC-1α and PGC-1β was observed in hESCs, and upon hESC and iPSC differentiation many genes involved in mitochondrial biogenesis, including those encoding the mtDNA transcription factor TFAM and the mitochondrial RNA polymerase POLRMT are downregulated (Armstrong et al. 2010, Prigione et al. 2010). ATP in hESCs and NSCs is mainly directed to protein and nucleic acid synthesis.

A key metabolic regulator favoring glycolysis versus OXPHOS involves the PDH complex (Varum et al. 2011). Varum et al (2011) found that hESC express high levels of hexokinase II and have an inactive PDH complex. Tellingly PDH E1α subunit was significantly increased in HD-iPSC but serines 232, 293 and 300 residues were more phosphorylated. Since phosphorylation of PDH complex can be carried out by four PDKs we analyzed PDK1 expression levels. PDK1 levels were up regulated in HD-iPSC consistent with the inactivation of PDH found. These data confirm that HD-iPSC have a greater reliance on glycolysis than controls. Unexpectedly no changes in pyruvate/ lactate production were observed in iPSC although afterward differentiation HD-NSC cells displayed higher amounts of pyruvate as well as lactate. Moreover, HD-iPSC disclosed reduced ATP levels. Thus, the results suggest that glycolysis is the main energetic pathway in HD-iPSC. During reprogramming to pluripotency metabolic changes succeed favoring glycolysis as the referential ATP production mechanism over OXPHOS (Varum et al. 2009, Chen et al. 2010, Liu et al. 2013, Son et al. 2013). Importantly the hyperpolarized-associated mitochondrial state of HD-iPSC found can be related to the reduced ATP consumption and the preferential glycolysis-based energy metabolism, as reported formerly (Prigione et al. 2011).

Insights on the pathogenesis and neurodegeneration of HD exposes mutant huntingtin as crucial agent in mitochondrial energy impaired production and cellular respiration, thus promoting apoptosis, oxidative stress, and susceptibility to excitotoxicity. Mitochondria are both a target and an important source of ROS since superoxide anion is generated in a constant manner by the mitochondria. The semiquinone (coenzyme Q) is an important electron leakage in the inner mitochondrial membrane. Our results indicate that HD-iPSCs are highly susceptible to mitochondrial dysfunction associated with increased oxidative stress. The increased basal levels of superoxide anion and hydrogen peroxide are consistent with the decreased activity of antioxidant enzyme Cu/Zn SOD1 and

acetylation of SOD2 and the expression increases strongly in differentiated cells. Effectively, HD-iPSC and HD-NSC showed increased vulnerability to the addition of exogenous stressors. Preceding studies described an increased amount of cell death in the HD lines in response to toxic stressors showing that HD-iPSC are associated with increased reactive oxygen species (Consortium 2012). Chae et al (2012) shed some light in protein expression profiles that are key regulators in oxidative stress, DNA damage and expression of cytoskeleton associated proteins (Chae et al. 2012). Lower levels of SOD1, GST and Gpx1 were found in HD-iPSC lines compared to hESC in contrast with the upregulation of Prx family members, including Prx1, Prx2 and Prx6 which have been implicated as important indicators for cellular ROS signals (Chae et al. 2012).

In summary, we have carried out a comparative study of HD-PSC line and their differentiated counterparts to better identify the abnormalities and pathways that triggers neurodegeneration and to distinguish them from the ones that are secondary responses. This study takes the advantage of using a model system to elucidate the role of mHTT in *in vitro* differentiation of HD-affected iPSC and it is remarkable that significant changes are detected in very early *in vitro* stage. Considering the significance of iPSC research, in particular from disease-specific iPSC lines, brings some important insights on the pathogenesis and extended studies should be made with lower CAG carrying HD-iPSC lines to draw generalized conclusions. Moreover a valuable approach would be genetic correction of the mutated cells to better understand the role of mHTT in the early onset of HD phenotypes

5. LIST OF ABBREVIATIONS

3-NP, 3-nitropropionic acid

Aa, amino acids

ADP, adenosine diphosphate

Akt, protein kinase B

AMP, adenosine monophosphate

AMPA, 3-hydroxy-5-methyl-4-propionate

Ask1, apoptosis signal-regulating kinase 1

ATP, adenosine triphosphate

AUC, area under the curve

BDNF, brain-derived neurotrophic factor

CAG, cytosine-adenine-guanine

cAMP, cyclic-adenosine monophosphate

CGG, cytosine-adenine-guanine

CNS, central nervous system

CREB - cyclic-adenosine monophosphate response element binding protein

CTG, cytosine- thymine-guanine

D1, subtype 1 dopamine receptor

D2, subtype 2 dopamine receptor

DA, dopamine

EGF, Epidermal growth factor

ELISA- Enzyme Linked Immuno Sorbent Assay

EMG, electromyography

ER, endoplasmic reticulum

GAA, guanine–adenine-adenine

GABA, γ–aminobutyric acid

GAD, glutamic acid decarboxylase

GAPDH, glyceraldehyde-3-phosphate dehydrogenase

GCC, guanine-cytosine-cytosine

GLUT, glucose transporter

GPe, external segment of the globus pallidus

GPi, internal segment of the globus pallidus

GTT, Glucose Tolerance Test

HAP1, Huntingtin associated protein 1

HD, Huntington‘s disease

HIP1, huntingtin-interacting protein 1

HIP2, huntingtin-interacting protein 2

HIPPI, HIP1-protein interactor

HSPs, Heat shock proteins

HTT, huntingtin

HTTNT, N-terminal fragments

IGF-1, insulin growth factor 1

InsP3R1, inositol 1,4,5-trisphosphate receptors

iPSC -Induced Pluripotent Stem Cell

IP31, inositol (1,4,5)-trisphosphate type 1

IT15, Interesting Transcript 15 gene

ITT, Insulin Tolerance Test

KA, Kainic acid

L/P ratio, lactate/pyruvate ratio

MA, malonic acid

mGluR, metabotropic glutamate receptors

mHTT, mutant huntingtin

mPTP, mitochondrial permeability transition pore

MSN, medium spiny neurons

NAD+, nicotinamide-adenine dinucleotide

NSC, neural stem cells

NMDAR, N-methyl-D-aspartate receptor

NR2, NMDA receptor subunit

NTL, nucleus tuberalis lateralis

PBS, phosphate buffered saline

PCR, polymerase chain reaction

PGC-1α, peroxisome proliferator-activated receptor gamma coactivator 1-alpha

polyQ, polyglutamine(s)

QA, Quinolinic acid

REST, repressor element-1 transcription factor

ROS, reactive oxygen species

SBMA, Spinal and Bulbar Muscular Atrophy

SDH, succinate dehydrogenase

SNARE, ethylmaleimide-sensitive fusion protein attachment protein receptor

SNpc, substantia nigra pars compacta

SNr, substantia nigra pars reticulata

SP1, specific protein-1

STN, subthalamic nucleus

TAFII, TATA-associated factors

TBP, TATA-binding protein

UK, United Kingdom

UPS, ubiquitin–proteasome system

UPS, ubiquitin–proteasome system

VA/VL complex, ventral anterior and ventral lateral thalamic nuclei

WHO, World Health Organization

YAC, yeast artificial chromosome

6. References

(2009). "Standards of medical care in diabetes--2009." Diabetes Care 32 Suppl 1: S13-61.

Aartsma-Rus, A. and G. J. van Ommen (2007). "Antisense-mediated exon skipping: a versatile tool with therapeutic and research applications." RNA 13(10): 1609-1624.

Aiuti, A., F. Cattaneo, S. Galimberti, U. Benninghoff, B. Cassani, L. Callegaro, S. Scaramuzza, G. Andolfi, M. Mirolo, I. Brigida, A. Tabucchi, F. Carlucci, M. Eibl, M. Aker, S. Slavin, H. Al-Mousa, A. Al Ghonaium, A. Ferster, A. Duppenthaler, L. Notarangelo, U. Wintergerst, R. H. Buckley, M. Bregni, S. Marktel, M. G. Valsecchi, P. Rossi, F. Ciceri, R. Miniero, C. Bordignon and M. G. Roncarolo (2009). "Gene therapy for immunodeficiency due to adenosine deaminase deficiency." N Engl J Med 360(5): 447-458.

Alders, J., M. Smits, B. Kremer and P. Naarding (2009). "The role of melatonin in sleep disturbances in end-stage Huntington's disease." J Neuropsychiatry Clin Neurosci 21(2): 226-227.

Alexi, T., P. E. Hughes, W. M. van Roon-Mom, R. L. Faull, C. E. Williams, R. G. Clark and P. D. Gluckman (1999). "The IGF-I amino-terminal tripeptide glycine-proline-glutamate (GPE) is neuroprotective to striatum in the quinolinic acid lesion animal model of Huntington's disease." Exp Neurol 159(1): 84-97.

Alves, S., I. Nascimento-Ferreira, G. Auregan, R. Hassig, N. Dufour, E. Brouillet, M. C. Pedroso de Lima, P. Hantraye, L. Pereira de Almeida and N. Deglon (2008). "Allele-specific RNA silencing of mutant ataxin-3 mediates neuroprotection in a rat model of Machado-Joseph disease." PLoS One 3(10): e3341.

Alves, S., I. Nascimento-Ferreira, N. Dufour, R. Hassig, G. Auregan, C. Nobrega, E. Brouillet, P. Hantraye, M. C. Pedroso de Lima, N. Deglon and L. P. de Almeida (2010). "Silencing ataxin-3 mitigates degeneration in a rat model of Machado-Joseph disease: no role for wild-type ataxin-3?" Hum Mol Genet 19(12): 2380-2394.

An, M. C., N. Zhang, G. Scott, D. Montoro, T. Wittkop, S. Mooney, S. Melov and L. M. Ellerby (2012). "Genetic correction of Huntington's disease phenotypes in induced pluripotent stem cells." Cell Stem Cell 11(2): 253-263.

Andreasen, N. C., S. Paradiso and D. S. O'Leary (1998). ""Cognitive dysmetria" as an integrative theory of schizophrenia: a dysfunction in cortical-subcortical-cerebellar circuitry?" Schizophr Bull 24(2): 203-218.

Andreassen, O. A., A. Dedeoglu, V. Stanojevic, D. B. Hughes, S. E. Browne, C. A. Leech, R. J. Ferrante, J. F. Habener, M. F. Beal and M. K. Thomas (2002). "Huntington's disease of the endocrine pancreas: insulin deficiency and diabetes mellitus due to impaired insulin gene expression." Neurobiol Dis 11(3): 410-424.

Andrew, S., J. Theilmann, E. Almqvist, A. Norremolle, G. Lucotte, M. Anvret, S. A. Sorensen, J. C. Turpin and M. R. Hayden (1993). "DNA analysis of distinct populations suggests multiple origins for the mutation causing Huntington disease." Clin Genet 43(6): 286-294.

Andrew, S. E., Y. P. Goldberg, B. Kremer, H. Telenius, J. Theilmann, S. Adam, E. Starr, F. Squitieri, B. Lin, M. A. Kalchman and et al. (1993). "The relationship between trinucleotide (CAG) repeat length and clinical features of Huntington's disease." Nat Genet 4(4): 398-403.

Andrews, P. W., G. Banting, I. Damjanov, D. Arnaud and P. Avner (1984). "Three monoclonal antibodies defining distinct differentiation antigens associated with different high molecular weight polypeptides on the surface of human embryonal carcinoma cells." Hybridoma 3(4): 347-361.

Anokye-Danso, F., C. M. Trivedi, D. Juhr, M. Gupta, Z. Cui, Y. Tian, Y. Zhang, W. Yang, P. J. Gruber, J. A. Epstein and E. E. Morrisey (2011). "Highly efficient miRNA-mediated reprogramming of mouse and human somatic cells to pluripotency." Cell Stem Cell 8(4): 376-388.
Armstrong, L., K. Tilgner, G. Saretzki, S. P. Atkinson, M. Stojkovic, R. Moreno, S. Przyborski and M. Lako (2010). "Human induced pluripotent stem cell lines show stress defense mechanisms and mitochondrial regulation similar to those of human embryonic stem cells." Stem Cells 28(4): 661-673.
Arning, L., C. Saft, S. Wieczorek, J. Andrich, P. H. Kraus and J. T. Epplen (2007). "NR2A and NR2B receptor gene variations modify age at onset in Huntington disease in a sex-specific manner." Hum Genet 122(2): 175-182.
Arwert, L. I., J. B. Deijen, M. Muller and M. L. Drent (2005). "Long-term growth hormone treatment preserves GH-induced memory and mood improvements: a 10-year follow-up study in GH-deficient adult men." Horm Behav 47(3): 343-349.
Ataullakhanov, F. I. and V. M. Vitvitsky (2002). "What determines the intracellular ATP concentration." Biosci Rep 22(5-6): 501-511.
Aziz, N. A., C. K. Jurgens, G. B. Landwehrmeyer, W. M. van Roon-Mom, G. J. van Ommen, T. Stijnen and R. A. Roos (2009). "Normal and mutant HTT interact to affect clinical severity and progression in Huntington disease." Neurology 73(16): 1280-1285.
Aziz, N. A., H. Pijl, M. Frolich, M. Snel, T. C. Streefland, F. Roelfsema and R. A. Roos (2010). "Systemic energy homeostasis in Huntington's disease patients." J Neurol Neurosurg Psychiatry 81(11): 1233-1237.
Aziz, N. A., J. M. van der Burg, G. B. Landwehrmeyer, P. Brundin, T. Stijnen and R. A. Roos (2008). "Weight loss in Huntington disease increases with higher CAG repeat number." Neurology 71(19): 1506-1513.
Bach, D., S. Pich, F. X. Soriano, N. Vega, B. Baumgartner, J. Oriola, J. R. Daugaard, J. Lloberas, M. Camps, J. R. Zierath, R. Rabasa-Lhoret, H. Wallberg-Henriksson, M. Laville, M. Palacin, H. Vidal, F. Rivera, M. Brand and A. Zorzano (2003). "Mitofusin-2 determines mitochondrial network architecture and mitochondrial metabolism. A novel regulatory mechanism altered in obesity." J Biol Chem 278(19): 17190-17197.
Bacos, K., M. Bjorkqvist, A. Petersen, L. Luts, M. L. Maat-Schieman, R. A. Roos, F. Sundler, P. Brundin, H. Mulder and N. Wierup (2008). "Islet beta-cell area and hormone expression are unaltered in Huntington's disease." Histochem Cell Biol 129(5): 623-629.
Bae, B. I., M. R. Hara, M. B. Cascio, C. L. Wellington, M. R. Hayden, C. A. Ross, H. C. Ha, X. J. Li, S. H. Snyder and A. Sawa (2006). "Mutant huntingtin: nuclear translocation and cytotoxicity mediated by GAPDH." Proc Natl Acad Sci U S A 103(9): 3405-3409.
Barker, R. A., S. L. Mason, T. P. Harrower, R. A. Swain, A. K. Ho, B. J. Sahakian, R. Mathur, S. Elneil, S. Thornton, C. Hurrelbrink, R. J. Armstrong, P. Tyers, E. Smith, A. Carpenter, P. Piccini, Y. F. Tai, D. J. Brooks, N. Pavese, C. Watts, J. D. Pickard, A. E. Rosser and S. B. Dunnett (2013). "The long-term safety and efficacy of bilateral transplantation of human fetal striatal tissue in patients with mild to moderate Huntington's disease." J Neurol Neurosurg Psychiatry 84(6): 657-665.
Bates, G. P. (2005). "History of genetic disease: the molecular genetics of Huntington disease - a history." Nat Rev Genet 6(10): 766-773.
Becker, K. A., P. N. Ghule, J. A. Therrien, J. B. Lian, J. L. Stein, A. J. van Wijnen and G. S. Stein (2006). "Self-renewal of human embryonic stem cells is supported by a shortened G1 cell cycle phase." J Cell Physiol 209(3): 883-893.
Benchoua, A., Y. Trioulier, D. Zala, M. C. Gaillard, N. Lefort, N. Dufour, F. Saudou, J. M. Elalouf, E. Hirsch, P. Hantraye, N. Deglon and E. Brouillet (2006). "Involvement of

mitochondrial complex II defects in neuronal death produced by N-terminus fragment of mutated huntingtin." Mol Biol Cell 17(4): 1652-1663.
Benn, C. L., T. Sun, G. Sadri-Vakili, K. N. McFarland, D. P. DiRocco, G. J. Yohrling, T. W. Clark, B. Bouzou and J. H. Cha (2008). "Huntingtin modulates transcription, occupies gene promoters in vivo, and binds directly to DNA in a polyglutamine-dependent manner." J Neurosci 28(42): 10720-10733.
Bennett, C. F. and E. E. Swayze (2010). "RNA targeting therapeutics: molecular mechanisms of antisense oligonucleotides as a therapeutic platform." Annu Rev Pharmacol Toxicol 50: 259-293.
Bennett, C. M., M. Guo and S. C. Dharmage (2007). "HbA(1c) as a screening tool for detection of Type 2 diabetes: a systematic review." Diabet Med 24(4): 333-343.
Bhide, P. G., M. Day, E. Sapp, C. Schwarz, A. Sheth, J. Kim, A. B. Young, J. Penney, J. Golden, N. Aronin and M. DiFiglia (1996). "Expression of normal and mutant huntingtin in the developing brain." J Neurosci 16(17): 5523-5535.
Biagioli, M., F. Ferrari, E. M. Mendenhall, Y. Zhang, S. Erdin, R. Vijayvargia, S. M. Vallabh, N. Solomos, P. Manavalan, A. Ragavendran, F. Ozsolak, J. M. Lee, M. E. Talkowski, J. F. Gusella, M. E. MacDonald, P. J. Park and I. S. Seong (2015). "Htt CAG repeat expansion confers pleiotropic gains of mutant huntingtin function in chromatin regulation." Hum Mol Genet.
Birket, M. J., A. L. Orr, A. A. Gerencser, D. T. Madden, C. Vitelli, A. Swistowski, M. D. Brand and X. Zeng (2011). "A reduction in ATP demand and mitochondrial activity with neural differentiation of human embryonic stem cells." J Cell Sci 124(Pt 3): 348-358.
Bithell, A., R. Johnson and N. J. Buckley (2009). "Transcriptional dysregulation of coding and non-coding genes in cellular models of Huntington's disease." Biochem Soc Trans 37(Pt 6): 1270-1275.
Bjorkqvist, M., M. Fex, E. Renstrom, N. Wierup, A. Petersen, J. Gil, K. Bacos, N. Popovic, J. Y. Li, F. Sundler, P. Brundin and H. Mulder (2005). "The R6/2 transgenic mouse model of Huntington's disease develops diabetes due to deficient beta-cell mass and exocytosis." Hum Mol Genet 14(5): 565-574.
Boesgaard, T. W., T. T. Nielsen, K. Josefsen, T. Hansen, T. Jorgensen, O. Pedersen, A. Norremolle, J. E. Nielsen and L. Hasholt (2009). "Huntington's disease does not appear to increase the risk of diabetes mellitus." J Neuroendocrinol 21(9): 770-776.
Bolte, S. and F. P. Cordelieres (2006). "A guided tour into subcellular colocalization analysis in light microscopy." J Microsc 224(Pt 3): 213-232.
Bondy, C. A. and C. M. Cheng (2002). "Insulin-like growth factor-1 promotes neuronal glucose utilization during brain development and repair processes." Int Rev Neurobiol 51: 189-217.
Borghese, L., D. Dolezalova, T. Opitz, S. Haupt, A. Leinhaas, B. Steinfarz, P. Koch, F. Edenhofer, A. Hampl and O. Brustle (2010). "Inhibition of notch signaling in human embryonic stem cell-derived neural stem cells delays G1/S phase transition and accelerates neuronal differentiation in vitro and in vivo." Stem Cells 28(5): 955-964.
Born, J., T. Lange, W. Kern, G. P. McGregor, U. Bickel and H. L. Fehm (2002). "Sniffing neuropeptides: a transnasal approach to the human brain." Nat Neurosci 5(6): 514-516.
Bornens, M. (2012). "The centrosome in cells and organisms." Science 335(6067): 422-426.
Bossy-Wetzel, E., A. Petrilli and A. B. Knott (2008). "Mutant huntingtin and mitochondrial dysfunction." Trends Neurosci 31(12): 609-616.

Boudreau, R. L., J. L. McBride, I. Martins, S. Shen, Y. Xing, B. J. Carter and B. L. Davidson (2009). "Nonallele-specific silencing of mutant and wild-type huntingtin demonstrates therapeutic efficacy in Huntington's disease mice." Mol Ther 17(6): 1053-1063.
Boumezbeur, F., K. F. Petersen, G. W. Cline, G. F. Mason, K. L. Behar, G. I. Shulman and D. L. Rothman (2010). "The contribution of blood lactate to brain energy metabolism in humans measured by dynamic 13C nuclear magnetic resonance spectroscopy." J Neurosci 30(42): 13983-13991.
Bradley, C. K., H. A. Scott, O. Chami, T. T. Peura, B. Dumevska, U. Schmidt and T. Stojanov (2011). "Derivation of Huntington's disease-affected human embryonic stem cell lines." Stem Cells Dev 20(3): 495-502.
Brennand, K., J. N. Savas, Y. Kim, N. Tran, A. Simone, K. Hashimoto-Torii, K. G. Beaumont, H. J. Kim, A. Topol, I. Ladran, M. Abdelrahim, B. Matikainen-Ankney, S. H. Chao, M. Mrksich, P. Rakic, G. Fang, B. Zhang, J. R. Yates, 3rd and F. H. Gage (2014). "Phenotypic differences in hiPSC NPCs derived from patients with schizophrenia." Mol Psychiatry.
Brinkman, R. R., M. M. Mezei, J. Theilmann, E. Almqvist and M. R. Hayden (1997). "The likelihood of being affected with Huntington disease by a particular age, for a specific CAG size." Am J Hum Genet 60(5): 1202-1210.
Browne, G. J., S. G. Finn and C. G. Proud (2004). "Stimulation of the AMP-activated protein kinase leads to activation of eukaryotic elongation factor 2 kinase and to its phosphorylation at a novel site, serine 398." J Biol Chem 279(13): 12220-12231.
Browne, S. E. (2008). "Mitochondria and Huntington's disease pathogenesis: insight from genetic and chemical models." Ann N Y Acad Sci 1147: 358-382.
Brummelkamp, T. R., R. Bernards and R. Agami (2002). "A system for stable expression of short interfering RNAs in mammalian cells." Science 296(5567): 550-553.
Bruning, J. C., J. Winnay, S. Bonner-Weir, S. I. Taylor, D. Accili and C. R. Kahn (1997). "Development of a novel polygenic model of NIDDM in mice heterozygous for IR and IRS-1 null alleles." Cell 88(4): 561-572.
Bruzik, J. P. and T. Maniatis (1992). "Spliced leader RNAs from lower eukaryotes are trans-spliced in mammalian cells." Nature 360(6405): 692-695.
Burke, J. R., J. J. Enghild, M. E. Martin, Y. S. Jou, R. M. Myers, A. D. Roses, J. M. Vance and W. J. Strittmatter (1996). "Huntingtin and DRPLA proteins selectively interact with the enzyme GAPDH." Nat Med 2(3): 347-350.
Buttgereit, F., G. R. Burmester and M. D. Brand (2000). "Bioenergetics of immune functions: fundamental and therapeutic aspects." Immunol Today 21(4): 192-199.
Byers, B., B. Cord, H. N. Nguyen, B. Schule, L. Fenno, P. C. Lee, K. Deisseroth, J. W. Langston, R. R. Pera and T. D. Palmer (2011). "SNCA triplication Parkinson's patient's iPSC-derived DA neurons accumulate alpha-synuclein and are susceptible to oxidative stress." PLoS One 6(11): e26159.
Cai, Z., L. W. Fan, S. Lin, Y. Pang and P. G. Rhodes (2011). "Intranasal administration of insulin-like growth factor-1 protects against lipopolysaccharide-induced injury in the developing rat brain." Neuroscience 194: 195-207.
Camnasio, S., A. Delli Carri, A. Lombardo, I. Grad, C. Mariotti, A. Castucci, B. Rozell, P. Lo Riso, V. Castiglioni, C. Zuccato, C. Rochon, Y. Takashima, G. Diaferia, I. Biunno, C. Gellera, M. Jaconi, A. Smith, O. Hovatta, L. Naldini, S. Di Donato, A. Feki and E. Cattaneo (2012). "The first reported generation of several induced pluripotent stem cell lines from homozygous and heterozygous Huntington's disease patients

demonstrates mutation related enhanced lysosomal activity." Neurobiol Dis 46(1): 41-51.
Campuzano, V., L. Montermini, M. D. Molto, L. Pianese, M. Cossee, F. Cavalcanti, E. Monros, F. Rodius, F. Duclos, A. Monticelli, F. Zara, J. Canizares, H. Koutnikova, S. I. Bidichandani, C. Gellera, A. Brice, P. Trouillas, G. De Michele, A. Filla, R. De Frutos, F. Palau, P. I. Patel, S. Di Donato, J. L. Mandel, S. Cocozza, M. Koenig and M. Pandolfo (1996). "Friedreich's ataxia: autosomal recessive disease caused by an intronic GAA triplet repeat expansion." Science 271(5254): 1423-1427.
Cantuti-Castelvetri, I., M. T. Lin, K. Zheng, C. E. Keller-McGandy, R. A. Betensky, D. R. Johns, M. F. Beal, D. G. Standaert and D. K. Simon (2005). "Somatic mitochondrial DNA mutations in single neurons and glia." Neurobiol Aging 26(10): 1343-1355.
Capecchi, M. R. (1989). "Altering the genome by homologous recombination." Science 244(4910): 1288-1292.
Carlson, D. F., W. Tan, S. G. Lillico, D. Stverakova, C. Proudfoot, M. Christian, D. F. Voytas, C. R. Long, C. B. Whitelaw and S. C. Fahrenkrug (2012). "Efficient TALEN-mediated gene knockout in livestock." Proc Natl Acad Sci U S A 109(43): 17382-17387.
Carrey, N., M. P. McFadyen and R. E. Brown (2000). "Effects of subchronic methylphenidate hydrochloride administration on the locomotor and exploratory behavior of prepubertal mice." J Child Adolesc Psychopharmacol 10(4): 277-286.
Carro, E., A. Nunez, S. Busiguina and I. Torres-Aleman (2000). "Circulating insulin-like growth factor I mediates effects of exercise on the brain." J Neurosci 20(8): 2926-2933.
Carro, E., J. L. Trejo, A. Nunez and I. Torres-Aleman (2003). "Brain repair and neuroprotection by serum insulin-like growth factor I." Mol Neurobiol 27(2): 153-162.
Carroll, J. B., S. C. Warby, A. L. Southwell, C. N. Doty, S. Greenlee, N. Skotte, G. Hung, C. F. Bennett, S. M. Freier and M. R. Hayden (2011). "Potent and selective antisense oligonucleotides targeting single-nucleotide polymorphisms in the Huntington disease gene / allele-specific silencing of mutant huntingtin." Mol Ther 19(12): 2178-2185.
Carter, R. J., J. Morton and S. B. Dunnett (2001). "Motor coordination and balance in rodents." Curr Protoc Neurosci Chapter 8: Unit 8 12.
Cavazza, A., A. Moiani and F. Mavilio (2013). "Mechanisms of retroviral integration and mutagenesis." Hum Gene Ther 24(2): 119-131.
Cavazzana-Calvo, M., S. Hacein-Bey, G. de Saint Basile, F. Gross, E. Yvon, P. Nusbaum, F. Selz, C. Hue, S. Certain, J. L. Casanova, P. Bousso, F. L. Deist and A. Fischer (2000). "Gene therapy of human severe combined immunodeficiency (SCID)-X1 disease." Science 288(5466): 669-672.
Caviston, J. P. and E. L. Holzbaur (2009). "Huntingtin as an essential integrator of intracellular vesicular trafficking." Trends Cell Biol 19(4): 147-155.
Caviston, J. P., J. L. Ross, S. M. Antony, M. Tokito and E. L. Holzbaur (2007). "Huntingtin facilitates dynein/dynactin-mediated vesicle transport." Proc Natl Acad Sci U S A 104(24): 10045-10050.
Chae, J. I., D. W. Kim, N. Lee, Y. J. Jeon, I. Jeon, J. Kwon, J. Kim, Y. Soh, D. S. Lee, K. S. Seo, N. J. Choi, B. C. Park, S. H. Kang, J. Ryu, S. H. Oh, D. A. Shin, D. R. Lee, J. T. Do, I. H. Park, G. Q. Daley and J. Song (2012). "Quantitative proteomic analysis of induced pluripotent stem cells derived from a human Huntington's disease patient." Biochem J 446(3): 359-371.

Chambers, S. M., C. A. Fasano, E. P. Papapetrou, M. Tomishima, M. Sadelain and L. Studer (2009). "Highly efficient neural conversion of human ES and iPS cells by dual inhibition of SMAD signaling." Nat Biotechnol 27(3): 275-280.
Chao, H., S. G. Mansfield, R. C. Bartel, S. Hiriyanna, L. G. Mitchell, M. A. Garcia-Blanco and C. E. Walsh (2003). "Phenotype correction of hemophilia A mice by spliceosome-mediated RNA trans-splicing." Nat Med 9(8): 1015-1019.
Chauhan, N. B. and G. J. Siegel (2007). "Antisense inhibition at the beta-secretase-site of beta-amyloid precursor protein reduces cerebral amyloid and acetyl cholinesterase activity in Tg2576." Neuroscience 146(1): 143-151.
Chen, C. T., S. H. Hsu and Y. H. Wei (2010). "Upregulation of mitochondrial function and antioxidant defense in the differentiation of stem cells." Biochim Biophys Acta 1800(3): 257-263.
Chen, C. T., Y. R. Shih, T. K. Kuo, O. K. Lee and Y. H. Wei (2008). "Coordinated changes of mitochondrial biogenesis and antioxidant enzymes during osteogenic differentiation of human mesenchymal stem cells." Stem Cells 26(4): 960-968.
Chen, T., L. Shen, J. Yu, H. Wan, A. Guo, J. Chen, Y. Long, J. Zhao and G. Pei (2011). "Rapamycin and other longevity-promoting compounds enhance the generation of mouse induced pluripotent stem cells." Aging Cell 10(5): 908-911.
Cheng, C. M., R. R. Reinhardt, W. H. Lee, G. Joncas, S. C. Patel and C. A. Bondy (2000). "Insulin-like growth factor 1 regulates developing brain glucose metabolism." Proc Natl Acad Sci U S A 97(18): 10236-10241.
Cheng, Y., Q. Peng, Z. Hou, M. Aggarwal, J. Zhang, S. Mori, C. A. Ross and W. Duan (2011). "Structural MRI detects progressive regional brain atrophy and neuroprotective effects in N171-82Q Huntington's disease mouse model." Neuroimage 56(3): 1027-1034.
Chenn, A. and S. K. McConnell (1995). "Cleavage orientation and the asymmetric inheritance of Notch1 immunoreactivity in mammalian neurogenesis." Cell 82(4): 631-641.
Chin, M. H., M. J. Mason, W. Xie, S. Volinia, M. Singer, C. Peterson, G. Ambartsumyan, O. Aimiuwu, L. Richter, J. Zhang, I. Khvorostov, V. Ott, M. Grunstein, N. Lavon, N. Benvenisty, C. M. Croce, A. T. Clark, T. Baxter, A. D. Pyle, M. A. Teitell, M. Pelegrini, K. Plath and W. E. Lowry (2009). "Induced pluripotent stem cells and embryonic stem cells are distinguished by gene expression signatures." Cell Stem Cell 5(1): 111-123.
Cho, K. J., B. I. Lee, S. Y. Cheon, H. W. Kim, H. J. Kim and G. W. Kim (2009). "Inhibition of apoptosis signal-regulating kinase 1 reduces endoplasmic reticulum stress and nuclear huntingtin fragments in a mouse model of Huntington disease." Neuroscience 163(4): 1128-1134.
Cho, Y. M., S. Kwon, Y. K. Pak, H. W. Seol, Y. M. Choi, J. Park do, K. S. Park and H. K. Lee (2006). "Dynamic changes in mitochondrial biogenesis and antioxidant enzymes during the spontaneous differentiation of human embryonic stem cells." Biochem Biophys Res Commun 348(4): 1472-1478.
Chu, C. T. (2006). "Autophagic stress in neuronal injury and disease." J Neuropathol Exp Neurol 65(5): 423-432.
Chung, S., P. P. Dzeja, R. S. Faustino, C. Perez-Terzic, A. Behfar and A. Terzic (2007). "Mitochondrial oxidative metabolism is required for the cardiac differentiation of stem cells." Nat Clin Pract Cardiovasc Med 4 Suppl 1: S60-67.
Ciammola, A., J. Sassone, L. Alberti, G. Meola, E. Mancinelli, M. A. Russo, F. Squitieri and V. Silani (2006). "Increased apoptosis, Huntingtin inclusions and altered

differentiation in muscle cell cultures from Huntington's disease subjects." Cell Death Differ 13(12): 2068-2078.
Cicchetti, F., L. Prensa, Y. Wu and A. Parent (2000). "Chemical anatomy of striatal interneurons in normal individuals and in patients with Huntington's disease." Brain Res Brain Res Rev 34(1-2): 80-101.
ClinicalTrials.gov (2009). "Safety,tolerability,and activity study of ISIS SOD1Rx to treat familial Amyotrophic Lateral Sclerosis (ALS) caused by SOD1 gene mutations (SOD-1)." NCT01041222.
Colin, E., E. Regulier, V. Perrin, A. Durr, A. Brice, P. Aebischer, N. Deglon, S. Humbert and F. Saudou (2005). "Akt is altered in an animal model of Huntington's disease and in patients." Eur J Neurosci 21(6): 1478-1488.
Colin, E., D. Zala, G. Liot, H. Rangone, M. Borrell-Pages, X. J. Li, F. Saudou and S. Humbert (2008). "Huntingtin phosphorylation acts as a molecular switch for anterograde/retrograde transport in neurons." EMBO J 27(15): 2124-2134.
Collins, E. S., S. K. Balchand, J. L. Faraci, P. Wadsworth and W. L. Lee (2012). "Cell cycle-regulated cortical dynein/dynactin promotes symmetric cell division by differential pole motion in anaphase." Mol Biol Cell 23(17): 3380-3390.
Conforti, P., S. Camnasio, C. Mutti, M. Valenza, M. Thompson, E. Fossale, S. Zeitlin, M. E. MacDonald, C. Zuccato and E. Cattaneo (2013). "Lack of huntingtin promotes neural stem cells differentiation into glial cells while neurons expressing huntingtin with expanded polyglutamine tracts undergo cell death." Neurobiol Dis 50: 160-170.
Cong, L., F. A. Ran, D. Cox, S. Lin, R. Barretto, N. Habib, P. D. Hsu, X. Wu, W. Jiang, L. A. Marraffini and F. Zhang (2013). "Multiplex genome engineering using CRISPR/Cas systems." Science 339(6121): 819-823.
Conneally, P. M. (1984). "Huntington disease: genetics and epidemiology." Am J Hum Genet 36(3): 506-526.
Consortium, H. i. (2012). "Induced pluripotent stem cells from patients with Huntington's disease show CAG-repeat-expansion-associated phenotypes." Cell Stem Cell 11(2): 264-278.
Cooper, O., H. Seo, S. Andrabi, C. Guardia-Laguarta, J. Graziotto, M. Sundberg, J. R. McLean, L. Carrillo-Reid, Z. Xie, T. Osborn, G. Hargus, M. Deleidi, T. Lawson, H. Bogetofte, E. Perez-Torres, L. Clark, C. Moskowitz, J. Mazzulli, L. Chen, L. Volpicelli-Daley, N. Romero, H. Jiang, R. J. Uitti, Z. Huang, G. Opala, L. A. Scarffe, V. L. Dawson, C. Klein, J. Feng, O. A. Ross, J. Q. Trojanowski, V. M. Lee, K. Marder, D. J. Surmeier, Z. K. Wszolek, S. Przedborski, D. Krainc, T. M. Dawson and O. Isacson (2012). "Pharmacological rescue of mitochondrial deficits in iPSC-derived neural cells from patients with familial Parkinson's disease." Sci Transl Med 4(141): 141ra190.
Coore, H. G., R. M. Denton, B. R. Martin and P. J. Randle (1971). "Regulation of adipose tissue pyruvate dehydrogenase by insulin and other hormones." Biochem J 125(1): 115-127.
Costa, M. C., P. Magalhaes, F. Ferreirinha, L. Guimaraes, C. Januario, I. Gaspar, L. Loureiro, J. Vale, C. Garrett, F. Regateiro, M. Magalhaes, A. Sousa, P. Maciel and J. Sequeiros (2003). "Molecular diagnosis of Huntington disease in Portugal: implications for genetic counselling and clinical practice." Eur J Hum Genet 11(11): 872-878.
Couturier, L., N. Vodovar and F. Schweisguth (2012). "Endocytosis by Numb breaks Notch symmetry at cytokinesis." Nat Cell Biol 14(2): 131-139.
Crespo, F. L., V. R. Sobrado, L. Gomez, A. M. Cervera and K. J. McCreath (2010). "Mitochondrial reactive oxygen species mediate cardiomyocyte formation from embryonic stem cells in high glucose." Stem Cells 28(7): 1132-1142.

Cunningham, J. T., J. T. Rodgers, D. H. Arlow, F. Vazquez, V. K. Mootha and P. Puigserver (2007). "mTOR controls mitochondrial oxidative function through a YY1-PGC-1alpha transcriptional complex." Nature 450(7170): 736-740.
Cuturic, M., R. K. Abramson, D. Vallini, E. M. Frank and M. Shamsnia (2009). "Sleep patterns in patients with Huntington's disease and their unaffected first-degree relatives: a brief report." Behav Sleep Med 7(4): 245-254.
Dallinger, G., M. Puttaraju, L. G. Mitchell, K. B. Yancey, C. Yee, A. Klausegger, H. Hintner and J. W. Bauer (2003). "Development of spliceosome-mediated RNA trans-splicing (SMaRT) for the correction of inherited skin diseases." Exp Dermatol 12(1): 37-46.
Damiano, M., L. Galvan, N. Deglon and E. Brouillet (2010). "Mitochondria in Huntington's disease." Biochim Biophys Acta 1802(1): 52-61.
Davy, P. and R. Allsopp (2009). "Balancing out the ends during iPSC nuclear reprogramming." Cell Stem Cell 4(2): 95-96.
Delli Carri, A., M. Onorati, V. Castiglioni, A. Faedo, S. Camnasio, M. Toselli, G. Biella and E. Cattaneo (2013). "Human pluripotent stem cell differentiation into authentic striatal projection neurons." Stem Cell Rev 9(4): 461-474.
Demaurex, N., D. Poburko and M. Frieden (2009). "Regulation of plasma membrane calcium fluxes by mitochondria." Biochim Biophys Acta 1787(11): 1383-1394.
Deng, Y. P., R. L. Albin, J. B. Penney, A. B. Young, K. D. Anderson and A. Reiner (2004). "Differential loss of striatal projection systems in Huntington's disease: a quantitative immunohistochemical study." J Chem Neuroanat 27(3): 143-164.
Devine, M. J., M. Ryten, P. Vodicka, A. J. Thomson, T. Burdon, H. Houlden, F. Cavaleri, M. Nagano, N. J. Drummond, J. W. Taanman, A. H. Schapira, K. Gwinn, J. Hardy, P. A. Lewis and T. Kunath (2011). "Parkinson's disease induced pluripotent stem cells with triplication of the alpha-synuclein locus." Nat Commun 2: 440.
Dhuria, S. V., L. R. Hanson and W. H. Frey, 2nd (2010). "Intranasal delivery to the central nervous system: mechanisms and experimental considerations." J Pharm Sci 99(4): 1654-1673.
Dickinson, B. C., V. S. Lin and C. J. Chang (2013). "Preparation and use of MitoPY1 for imaging hydrogen peroxide in mitochondria of live cells." Nat Protoc 8(6): 1249-1259.
DiFiglia, M., E. Sapp, K. O. Chase, S. W. Davies, G. P. Bates, J. P. Vonsattel and N. Aronin (1997). "Aggregation of huntingtin in neuronal intranuclear inclusions and dystrophic neurites in brain." Science 277(5334): 1990-1993.
Djousse, L., B. Knowlton, L. A. Cupples, K. Marder, I. Shoulson and R. H. Myers (2002). "Weight loss in early stage of Huntington's disease." Neurology 59(9): 1325-1330.
Dragatsis, I., D. Goldowitz, N. Del Mar, Y. P. Deng, C. A. Meade, L. Liu, Z. Sun, P. Dietrich, J. Yue and A. Reiner (2009). "CAG repeat lengths > or =335 attenuate the phenotype in the R6/2 Huntington's disease transgenic mouse." Neurobiol Dis 33(3): 315-330.
Drouet, V., V. Perrin, R. Hassig, N. Dufour, G. Auregan, S. Alves, G. Bonvento, E. Brouillet, R. Luthi-Carter, P. Hantraye and N. Deglon (2009). "Sustained effects of nonallele-specific Huntingtin silencing." Ann Neurol 65(3): 276-285.
Drouet, V., M. Ruiz, D. Zala, M. Feyeux, G. Auregan, K. Cambon, L. Troquier, J. Carpentier, S. Aubert, N. Merienne, F. Bourgois-Rocha, R. Hassig, M. Rey, N. Dufour, F. Saudou, A. L. Perrier, P. Hantraye and N. Deglon (2014). "Allele-specific silencing of mutant huntingtin in rodent brain and human stem cells." PLoS One 9(6): e99341.

Duarte, A. I., G. H. Petit, S. Ranganathan, J. Y. Li, C. R. Oliveira, P. Brundin, M. Bjorkqvist and A. C. Rego (2011). "IGF-1 protects against diabetic features in an in vivo model of Huntington's disease." Exp Neurol 231(2): 314-319.
Dunah, A. W., H. Jeong, A. Griffin, Y. M. Kim, D. G. Standaert, S. M. Hersch, M. M. Mouradian, A. B. Young, N. Tanese and D. Krainc (2002). "Sp1 and TAFII130 transcriptional activity disrupted in early Huntington's disease." Science 296(5576): 2238-2243.
Duyao, M., C. Ambrose, R. Myers, A. Novelletto, F. Persichetti, M. Frontali, S. Folstein, C. Ross, M. Franz, M. Abbott and et al. (1993). "Trinucleotide repeat length instability and age of onset in Huntington's disease." Nat Genet 4(4): 387-392.
Dyall, S. D., M. T. Brown and P. J. Johnson (2004). "Ancient invasions: from endosymbionts to organelles." Science 304(5668): 253-257.
Ehrnhoefer, D. E., L. Sutton and M. R. Hayden (2011). "Small changes, big impact: posttranslational modifications and function of huntingtin in Huntington disease." Neuroscientist 17(5): 475-492.
Eigentler, A., S. Boesch, R. Schneider, G. Dechant and R. Nat (2013). "Induced pluripotent stem cells from friedreich ataxia patients fail to upregulate frataxin during in vitro differentiation to peripheral sensory neurons." Stem Cells Dev 22(24): 3271-3282.
Elias, S., M. S. Thion, H. Yu, C. M. Sousa, C. Lasgi, X. Morin and S. Humbert (2014). "Huntingtin regulates mammary stem cell division and differentiation." Stem Cell Reports 2(4): 491-506.
Endesfelder, S., A. Kliche, H. Lochmuller, A. von Moers and A. Speer (2005). "Antisense oligonucleotides and short interfering RNAs silencing the cyclin-dependent kinase inhibitor p21 improve proliferation of Duchenne muscular dystrophy patients' primary skeletal myoblasts." J Mol Med (Berl) 83(1): 64-71.
Engelender, S., A. H. Sharp, V. Colomer, M. K. Tokito, A. Lanahan, P. Worley, E. L. Holzbaur and C. A. Ross (1997). "Huntingtin-associated protein 1 (HAP1) interacts with the p150Glued subunit of dynactin." Hum Mol Genet 6(13): 2205-2212.
Epping, E. A. and J. S. Paulsen (2011). "Depression in the early stages of Huntington disease." Neurodegener Dis Manag 1(5): 407-414.
Evans, M. J. and M. H. Kaufman (1981). "Establishment in culture of pluripotential cells from mouse embryos." Nature 292(5819): 154-156.
Evans, S. J., I. Douglas, M. D. Rawlins, N. S. Wexler, S. J. Tabrizi and L. Smeeth (2013). "Prevalence of adult Huntington's disease in the UK based on diagnoses recorded in general practice records." J Neurol Neurosurg Psychiatry.
Evers, M. M., B. A. Pepers, J. C. van Deutekom, S. A. Mulders, J. T. den Dunnen, A. Aartsma-Rus, G. J. van Ommen and W. M. van Roon-Mom (2011). "Targeting several CAG expansion diseases by a single antisense oligonucleotide." PLoS One 6(9): e24308.
Facucho-Oliveira, J. M., J. Alderson, E. C. Spikings, S. Egginton and J. C. St John (2007). "Mitochondrial DNA replication during differentiation of murine embryonic stem cells." J Cell Sci 120(Pt 22): 4025-4034.
Fan, M. M. and L. A. Raymond (2007). "N-methyl-D-aspartate (NMDA) receptor function and excitotoxicity in Huntington's disease." Prog Neurobiol 81(5-6): 272-293.
Farr, S. A., M. A. Erickson, M. L. Niehoff, W. A. Banks and J. E. Morley (2014). "Central and Peripheral Administration of Antisense Oligonucleotide Targeting Amyloid-beta Protein Precursor Improves Learning and Memory and Reduces Neuroinflammatory Cytokines in Tg2576 (AbetaPPswe) Mice." J Alzheimers Dis 40(4): 1005-1016.

Farr, S. A., J. L. Ripley, R. Sultana, Z. Zhang, M. L. Niehoff, T. L. Platt, M. P. Murphy, J. E. Morley, V. Kumar and D. A. Butterfield (2014). "Antisense oligonucleotide against GSK-3beta in brain of SAMP8 mice improves learning and memory and decreases oxidative stress: Involvement of transcription factor Nrf2 and implications for Alzheimer disease." Free Radic Biol Med 67: 387-395.
Farrer, L. A. (1985). "Diabetes mellitus in Huntington disease." Clin Genet 27(1): 62-67.
Feigin, A., C. Tang, Y. Ma, P. Mattis, D. Zgaljardic, M. Guttman, J. S. Paulsen, V. Dhawan and D. Eidelberg (2007). "Thalamic metabolism and symptom onset in preclinical Huntington's disease." Brain 130(Pt 11): 2858-2867.
Ferlini, A., P. Sabatelli, M. Fabris, E. Bassi, S. Falzarano, G. Vattemi, D. Perrone, F. Gualandi, N. M. Maraldi, L. Merlini, K. Sparnacci, M. Laus, A. Caputo, P. Bonaldo, P. Braghetta and P. Rimessi (2010). "Dystrophin restoration in skeletal, heart and skin arrector pili smooth muscle of mdx mice by ZM2 NP-AON complexes." Gene Ther 17(3): 432-438.
Ferrante, R. J., M. F. Beal, N. W. Kowall, E. P. Richardson, Jr. and J. B. Martin (1987). "Sparing of acetylcholinesterase-containing striatal neurons in Huntington's disease." Brain Res 411(1): 162-166.
Ferrante, R. J., N. W. Kowall, M. F. Beal, J. B. Martin, E. D. Bird and E. P. Richardson, Jr. (1987). "Morphologic and histochemical characteristics of a spared subset of striatal neurons in Huntington's disease." J Neuropathol Exp Neurol 46(1): 12-27.
Ferrante, R. J., N. W. Kowall, M. F. Beal, E. P. Richardson, Jr., E. D. Bird and J. B. Martin (1985). "Selective sparing of a class of striatal neurons in Huntington's disease." Science 230(4725): 561-563.
Ferreira, I. L., T. Cunha-Oliveira, M. V. Nascimento, M. Ribeiro, M. T. Proenca, C. Januario, C. R. Oliveira and A. C. Rego (2011). "Bioenergetic dysfunction in Huntington's disease human cybrids." Exp Neurol 231(1): 127-134.
Ferreira, I. L., M. V. Nascimento, M. Ribeiro, S. Almeida, S. M. Cardoso, M. Grazina, J. Pratas, M. J. Santos, C. Januario, C. R. Oliveira and A. C. Rego (2010). "Mitochondrial-dependent apoptosis in Huntington's disease human cybrids." Exp Neurol 222(2): 243-255.
Ferrick, D. A., A. Neilson and C. Beeson (2008). "Advances in measuring cellular bioenergetics using extracellular flux." Drug Discov Today 13(5-6): 268-274.
Feyeux, M., F. Bourgois-Rocha, A. Redfern, P. Giles, N. Lefort, S. Aubert, C. Bonnefond, A. Bugi, M. Ruiz, N. Deglon, L. Jones, M. Peschanski, N. D. Allen and A. L. Perrier (2012). "Early transcriptional changes linked to naturally occurring Huntington's disease mutations in neural derivatives of human embryonic stem cells." Hum Mol Genet 21(17): 3883-3895.
Fiedorowicz, J. G., J. A. Mills, A. Ruggle, D. Langbehn and J. S. Paulsen (2011). "Suicidal behavior in prodromal Huntington disease." Neurodegener Dis 8(6): 483-490.
Fink, G., I. Schuchardt, J. Colombelli, E. Stelzer and G. Steinberg (2006). "Dynein-mediated pulling forces drive rapid mitotic spindle elongation in Ustilago maydis." EMBO J 25(20): 4897-4908.
Finkbeiner, S. and S. Mitra (2008). "The ubiquitin-proteasome pathway in Huntington's disease." ScientificWorldJournal 8: 421-433.
Fiorini, A., R. Sultana, S. Forster, M. Perluigi, G. Cenini, C. Cini, J. Cai, J. B. Klein, S. A. Farr, M. L. Niehoff, J. E. Morley, V. B. Kumar and D. Allan Butterfield (2013). "Antisense directed against PS-1 gene decreases brain oxidative markers in aged senescence accelerated mice (SAMP8) and reverses learning and memory impairment: a proteomics study." Free Radic Biol Med 65: 1-14.

Fire, A., S. Xu, M. K. Montgomery, S. A. Kostas, S. E. Driver and C. C. Mello (1998). "Potent and specific genetic interference by double-stranded RNA in Caenorhabditis elegans." Nature 391(6669): 806-811.
Folmes, C. D., A. Martinez-Fernandez, E. Perales-Clemente, X. Li, A. McDonald, D. Oglesbee, S. C. Hrstka, C. Perez-Terzic, A. Terzic and T. J. Nelson (2013). "Disease-causing mitochondrial heteroplasmy segregated within induced pluripotent stem cell clones derived from a patient with MELAS." Stem Cells 31(7): 1298-1308.
Folmes, C. D., T. J. Nelson, A. Martinez-Fernandez, D. K. Arrell, J. Z. Lindor, P. P. Dzeja, Y. Ikeda, C. Perez-Terzic and A. Terzic (2011). "Somatic oxidative bioenergetics transitions into pluripotency-dependent glycolysis to facilitate nuclear reprogramming." Cell Metab 14(2): 264-271.
Folstein, S. E., G. A. Chase, W. E. Wahl, A. M. McDonnell and M. F. Folstein (1987). "Huntington disease in Maryland: clinical aspects of racial variation." Am J Hum Genet 41(2): 168-179.
Foroud, T., J. Gray, J. Ivashina and P. M. Conneally (1999). "Differences in duration of Huntington's disease based on age at onset." J Neurol Neurosurg Psychiatry 66(1): 52-56.
Franich, N. R., H. L. Fitzsimons, D. M. Fong, M. Klugmann, M. J. During and D. Young (2008). "AAV vector-mediated RNAi of mutant huntingtin expression is neuroprotective in a novel genetic rat model of Huntington's disease." Mol Ther 16(5): 947-956.
Furtado, S., O. Suchowersky, B. Rewcastle, L. Graham, M. L. Klimek and A. Garber (1996). "Relationship between trinucleotide repeats and neuropathological changes in Huntington's disease." Ann Neurol 39(1): 132-136.
Fusaki, N., H. Ban, A. Nishiyama, K. Saeki and M. Hasegawa (2009). "Efficient induction of transgene-free human pluripotent stem cells using a vector based on Sendai virus, an RNA virus that does not integrate into the host genome." Proc Jpn Acad Ser B Phys Biol Sci 85(8): 348-362.
Fusco, F. R., Q. Chen, W. J. Lamoreaux, G. Figueredo-Cardenas, Y. Jiao, J. A. Coffman, D. J. Surmeier, M. G. Honig, L. R. Carlock and A. Reiner (1999). "Cellular localization of huntingtin in striatal and cortical neurons in rats: lack of correlation with neuronal vulnerability in Huntington's disease." J Neurosci 19(4): 1189-1202.
Gaba, A. M., K. Zhang, K. Marder, C. B. Moskowitz, P. Werner and C. N. Boozer (2005). "Energy balance in early-stage Huntington disease." Am J Clin Nutr 81(6): 1335-1341.
Gabery, S., K. Murphy, K. Schultz, C. T. Loy, E. McCusker, D. Kirik, G. Halliday and A. Petersen (2010). "Changes in key hypothalamic neuropeptide populations in Huntington disease revealed by neuropathological analyses." Acta Neuropathol 120(6): 777-788.
Garneau, J. E., M. E. Dupuis, M. Villion, D. A. Romero, R. Barrangou, P. Boyaval, C. Fremaux, P. Horvath, A. H. Magadan and S. Moineau (2010). "The CRISPR/Cas bacterial immune system cleaves bacteriophage and plasmid DNA." Nature 468(7320): 67-71.
Gatchel, J. R. and H. Y. Zoghbi (2005). "Diseases of unstable repeat expansion: mechanisms and common principles." Nat Rev Genet 6(10): 743-755.
Gauthier, L. R., B. C. Charrin, M. Borrell-Pages, J. P. Dompierre, H. Rangone, F. P. Cordelieres, J. De Mey, M. E. MacDonald, V. Lessmann, S. Humbert and F. Saudou (2004). "Huntingtin controls neurotrophic support and survival of neurons by enhancing BDNF vesicular transport along microtubules." Cell 118(1): 127-138.

Ghule, P. N., R. Medina, C. J. Lengner, M. Mandeville, M. Qiao, Z. Dominski, J. B. Lian, J. L. Stein, A. J. van Wijnen and G. S. Stein (2011). "Reprogramming the pluripotent cell cycle: restoration of an abbreviated G1 phase in human induced pluripotent stem (iPS) cells." J Cell Physiol 226(5): 1149-1156.
Gil, J. M. and A. C. Rego (2008). "Mechanisms of neurodegeneration in Huntington's disease." Eur J Neurosci 27(11): 2803-2820.
Gines, S., I. S. Seong, E. Fossale, E. Ivanova, F. Trettel, J. F. Gusella, V. C. Wheeler, F. Persichetti and M. E. MacDonald (2003). "Specific progressive cAMP reduction implicates energy deficit in presymptomatic Huntington's disease knock-in mice." Hum Mol Genet 12(5): 497-508.
Godin, J. D., K. Colombo, M. Molina-Calavita, G. Keryer, D. Zala, B. C. Charrin, P. Dietrich, M. L. Volvert, F. Guillemot, I. Dragatsis, Y. Bellaiche, F. Saudou, L. Nguyen and S. Humbert (2010). "Huntingtin is required for mitotic spindle orientation and mammalian neurogenesis." Neuron 67(3): 392-406.
Goellner, G. M. and M. Rechsteiner (2003). "Are Huntington's and polyglutamine-based ataxias proteasome storage diseases?" Int J Biochem Cell Biol 35(5): 562-571.
Goldberg, Y. P., B. Kremer, S. E. Andrew, J. Theilmann, R. K. Graham, F. Squitieri, H. Telenius, S. Adam, A. Sajoo, E. Starr and et al. (1993). "Molecular analysis of new mutations for Huntington's disease: intermediate alleles and sex of origin effects." Nat Genet 5(2): 174-179.
Gomes, C. M. and R. Santos (2013). "Neurodegeneration in Friedreich's ataxia: from defective frataxin to oxidative stress." Oxid Med Cell Longev 2013: 487534.
Gonzalez-Alegre, P. (2007). "Therapeutic RNA interference for neurodegenerative diseases: From promise to progress." Pharmacol Ther 114(1): 34-55.
Goodman, A. O., P. R. Murgatroyd, G. Medina-Gomez, N. I. Wood, N. Finer, A. J. Vidal-Puig, A. J. Morton and R. A. Barker (2008). "The metabolic profile of early Huntington's disease--a combined human and transgenic mouse study." Exp Neurol 210(2): 691-698.
Gopalakrishnan, L. and R. C. Scarpulla (1994). "Differential regulation of respiratory chain subunits by a CREB-dependent signal transduction pathway. Role of cyclic AMP in cytochrome c and COXIV gene expression." J Biol Chem 269(1): 105-113.
Graham, R. K., Y. Deng, E. J. Slow, B. Haigh, N. Bissada, G. Lu, J. Pearson, J. Shehadeh, L. Bertram, Z. Murphy, S. C. Warby, C. N. Doty, S. Roy, C. L. Wellington, B. R. Leavitt, L. A. Raymond, D. W. Nicholson and M. R. Hayden (2006). "Cleavage at the caspase-6 site is required for neuronal dysfunction and degeneration due to mutant huntingtin." Cell 125(6): 1179-1191.
Grillo, C. A., G. G. Piroli, R. M. Hendry and L. P. Reagan (2009). "Insulin-stimulated translocation of GLUT4 to the plasma membrane in rat hippocampus is PI3-kinase dependent." Brain Res 1296: 35-45.
Group, H. S. (1996). "Unified Huntington's Disease Rating Scale: reliability and consistency. Huntington Study Group." Mov Disord 11(2): 136-142.
Group, T. H. s. D. C. R. (1993). A novel gene containing a trinucleotide repeat that is expanded and unstable on Huntington's disease chromosomes. The Huntington's Disease Collaborative Research Group. Cell. **72:** 971-983.
Group, T. H. s. D. C. R. (1993). "A novel gene containing a trinucleotide repeat that is expanded and unstable on Huntington's disease chromosomes. The Huntington's Disease Collaborative Research Group." Cell 72(6): 971-983.
Gu, M., M. T. Gash, V. M. Mann, F. Javoy-Agid, J. M. Cooper and A. H. Schapira (1996). "Mitochondrial defect in Huntington's disease caudate nucleus." Ann Neurol 39(3): 385-389.

Guidetti, P., V. Charles, E. Y. Chen, P. H. Reddy, J. H. Kordower, W. O. Whetsell, Jr., R. Schwarcz and D. A. Tagle (2001). "Early degenerative changes in transgenic mice expressing mutant huntingtin involve dendritic abnormalities but no impairment of mitochondrial energy production." Exp Neurol 169(2): 340-350.
Gusella, J. F., N. S. Wexler, P. M. Conneally, S. L. Naylor, M. A. Anderson, R. E. Tanzi, P. C. Watkins, K. Ottina, M. R. Wallace, A. Y. Sakaguchi and et al. (1983). "A polymorphic DNA marker genetically linked to Huntington's disease." Nature 306(5940): 234-238.
Gutekunst, C. A., S. H. Li, H. Yi, J. S. Mulroy, S. Kuemmerle, R. Jones, D. Rye, R. J. Ferrante, S. M. Hersch and X. J. Li (1999). "Nuclear and neuropil aggregates in Huntington's disease: relationship to neuropathology." J Neurosci 19(7): 2522-2534.
Hagopian, K., K. L. Weber, D. T. Hwee, A. L. Van Eenennaam, G. Lopez-Lluch, J. M. Villalba, I. Buron, P. Navas, J. B. German, S. M. Watkins, Y. Chen, A. Wei, R. B. McDonald and J. J. Ramsey (2010). "Complex I-associated hydrogen peroxide production is decreased and electron transport chain enzyme activities are altered in n-3 enriched fat-1 mice." PLoS One 5(9): e12696.
Hanson, L. R. and W. H. Frey, 2nd (2008). "Intranasal delivery bypasses the blood-brain barrier to target therapeutic agents to the central nervous system and treat neurodegenerative disease." BMC Neurosci 9 Suppl 3: S5.
Hansotia, P., R. Wall and J. Berendes (1985). "Sleep disturbances and severity of Huntington's disease." Neurology 35(11): 1672-1674.
Harper, P. S. (1992). "The epidemiology of Huntington's disease." Hum Genet 89(4): 365-376.
Harper, S. Q., P. D. Staber, X. He, S. L. Eliason, I. H. Martins, Q. Mao, L. Yang, R. M. Kotin, H. L. Paulson and B. L. Davidson (2005). "RNA interference improves motor and neuropathological abnormalities in a Huntington's disease mouse model." Proc Natl Acad Sci U S A 102(16): 5820-5825.
Harvey, A., T. Gibson, T. Lonergan and C. Brenner (2011). "Dynamic regulation of mitochondrial function in preimplantation embryos and embryonic stem cells." Mitochondrion 11(5): 829-838.
Hatefi, Y. and D. L. Stiggall (1978). "Preparation and properties of succinate: ubiquinone oxidoreductase (complex II)." Methods Enzymol 53: 21-27.
Heinrichs, R. W. and K. K. Zakzanis (1998). "Neurocognitive deficit in schizophrenia: a quantitative review of the evidence." Neuropsychology 12(3): 426-445.
Heins, N., M. C. Englund, C. Sjoblom, U. Dahl, A. Tonning, C. Bergh, A. Lindahl, C. Hanson and H. Semb (2004). "Derivation, characterization, and differentiation of human embryonic stem cells." Stem Cells 22(3): 367-376.
Henley, S. M., E. J. Wild, N. Z. Hobbs, R. I. Scahill, G. R. Ridgway, D. G. Macmanus, R. A. Barker, N. C. Fox and S. J. Tabrizi (2009). "Relationship between CAG repeat length and brain volume in premanifest and early Huntington's disease." J Neurol 256(2): 203-212.
Hick, A., M. Wattenhofer-Donze, S. Chintawar, P. Tropel, J. P. Simard, N. Vaucamps, D. Gall, L. Lambot, C. Andre, L. Reutenauer, M. Rai, M. Teletin, N. Messaddeq, S. N. Schiffmann, S. Viville, C. E. Pearson, M. Pandolfo and H. Puccio (2013). "Neurons and cardiomyocytes derived from induced pluripotent stem cells as a model for mitochondrial defects in Friedreich's ataxia." Dis Model Mech 6(3): 608-621.
Ho, L. W., R. Brown, M. Maxwell, A. Wyttenbach and D. C. Rubinsztein (2001). "Wild type Huntingtin reduces the cellular toxicity of mutant Huntingtin in mammalian cell models of Huntington's disease." J Med Genet 38(7): 450-452.

Hockemeyer, D., F. Soldner, C. Beard, Q. Gao, M. Mitalipova, R. C. DeKelver, G. E. Katibah, R. Amora, E. A. Boydston, B. Zeitler, X. Meng, J. C. Miller, L. Zhang, E. J. Rebar, P. D. Gregory, F. D. Urnov and R. Jaenisch (2009). "Efficient targeting of expressed and silent genes in human ESCs and iPSCs using zinc-finger nucleases." Nat Biotechnol 27(9): 851-857.
Hockemeyer, D., H. Wang, S. Kiani, C. S. Lai, Q. Gao, J. P. Cassady, G. J. Cost, L. Zhang, Y. Santiago, J. C. Miller, B. Zeitler, J. M. Cherone, X. Meng, S. J. Hinkley, E. J. Rebar, P. D. Gregory, F. D. Urnov and R. Jaenisch (2011). "Genetic engineering of human pluripotent cells using TALE nucleases." Nat Biotechnol 29(8): 731-734.
Hoffner, G. and P. Djian (2005). "Transglutaminase and diseases of the central nervous system." Front Biosci 10: 3078-3092.
Hoffner, G., S. Soues and P. Djian (2007). "Aggregation of expanded huntingtin in the brains of patients with Huntington disease." Prion 1(1): 26-31.
Holmuhamedov, E., A. Jahangir, M. Bienengraeber, L. D. Lewis and A. Terzic (2003). "Deletion of mtDNA disrupts mitochondrial function and structure, but not biogenesis." Mitochondrion 3(1): 13-19.
Horton, T. M., B. H. Graham, M. Corral-Debrinski, J. M. Shoffner, A. E. Kaufman, M. F. Beal and D. C. Wallace (1995). "Marked increase in mitochondrial DNA deletion levels in the cerebral cortex of Huntington's disease patients." Neurology 45(10): 1879-1883.
Horvath, P. and R. Barrangou (2010). "CRISPR/Cas, the immune system of bacteria and archaea." Science 327(5962): 167-170.
Humbert, S., E. A. Bryson, F. P. Cordelieres, N. C. Connors, S. R. Datta, S. Finkbeiner, M. E. Greenberg and F. Saudou (2002). "The IGF-1/Akt pathway is neuroprotective in Huntington's disease and involves Huntingtin phosphorylation by Akt." Dev Cell 2(6): 831-837.
Hunt, M. J. and A. J. Morton (2005). "Atypical diabetes associated with inclusion formation in the R6/2 mouse model of Huntington's disease is not improved by treatment with hypoglycaemic agents." Exp Brain Res 166(2): 220-229.
Imaizumi, Y., Y. Okada, W. Akamatsu, M. Koike, N. Kuzumaki, H. Hayakawa, T. Nihira, T. Kobayashi, M. Ohyama, S. Sato, M. Takanashi, M. Funayama, A. Hirayama, T. Soga, T. Hishiki, M. Suematsu, T. Yagi, D. Ito, A. Kosakai, K. Hayashi, M. Shouji, A. Nakanishi, N. Suzuki, Y. Mizuno, N. Mizushima, M. Amagai, Y. Uchiyama, H. Mochizuki, N. Hattori and H. Okano (2012). "Mitochondrial dysfunction associated with increased oxidative stress and alpha-synuclein accumulation in PARK2 iPSC-derived neurons and postmortem brain tissue." Mol Brain 5: 35.
Ishino, Y., H. Shinagawa, K. Makino, M. Amemura and A. Nakata (1987). "Nucleotide sequence of the iap gene, responsible for alkaline phosphatase isozyme conversion in Escherichia coli, and identification of the gene product." J Bacteriol 169(12): 5429-5433.
Itskovitz-Eldor, J., M. Schuldiner, D. Karsenti, A. Eden, O. Yanuka, M. Amit, H. Soreq and N. Benvenisty (2000). "Differentiation of human embryonic stem cells into embryoid bodies compromising the three embryonic germ layers." Mol Med 6(2): 88-95.
Jackson, S. P. (2002). "Sensing and repairing DNA double-strand breaks." Carcinogenesis 23(5): 687-696.
Jacobsen, J. C., G. C. Gregory, J. M. Woda, M. N. Thompson, K. R. Coser, V. Murthy, I. S. Kohane, J. F. Gusella, I. S. Seong, M. E. MacDonald, T. Shioda and J. M. Lee (2011). "HD CAG-correlated gene expression changes support a simple dominant gain of function." Hum Mol Genet 20(14): 2846-2860.

James, D. E. and R. C. Piper (1994). "Insulin resistance, diabetes, and the insulin-regulated trafficking of GLUT-4." J Cell Biol 126(5): 1123-1126.
Jana, N. R., M. Tanaka, G. Wang and N. Nukina (2000). "Polyglutamine length-dependent interaction of Hsp40 and Hsp70 family chaperones with truncated N-terminal huntingtin: their role in suppression of aggregation and cellular toxicity." Hum Mol Genet 9(13): 2009-2018.
Jenkins, B. G., W. J. Koroshetz, M. F. Beal and B. R. Rosen (1993). "Evidence for impairment of energy metabolism in vivo in Huntington's disease using localized 1H NMR spectroscopy." Neurology 43(12): 2689-2695.
Jiang, H., Y. Ren, E. Y. Yuen, P. Zhong, M. Ghaedi, Z. Hu, G. Azabdaftari, K. Nakaso, Z. Yan and J. Feng (2012). "Parkin controls dopamine utilization in human midbrain dopaminergic neurons derived from induced pluripotent stem cells." Nat Commun 3: 668.
Josefsen, K., M. D. Nielsen, K. H. Jorgensen, T. Bock, A. Norremolle, S. A. Sorensen, B. Naver and L. Hasholt (2008). "Impaired glucose tolerance in the R6/1 transgenic mouse model of Huntington's disease." J Neuroendocrinol 20(2): 165-172.
Juul, A. (2003). "Serum levels of insulin-like growth factor I and its binding proteins in health and disease." Growth Horm IGF Res 13(4): 113-170.
Kahlem, P., H. Green and P. Djian (1998). "Transglutaminase action imitates Huntington's disease: selective polymerization of Huntingtin containing expanded polyglutamine." Mol Cell 1(4): 595-601.
Kang, L., J. Wang, Y. Zhang, Z. Kou and S. Gao (2009). "iPS cells can support full-term development of tetraploid blastocyst-complemented embryos." Cell Stem Cell 5(2): 135-138.
Kannagi, R., N. A. Cochran, F. Ishigami, S. Hakomori, P. W. Andrews, B. B. Knowles and D. Solter (1983). "Stage-specific embryonic antigens (SSEA-3 and -4) are epitopes of a unique globo-series ganglioside isolated from human teratocarcinoma cells." EMBO J 2(12): 2355-2361.
Kardon, J. R. and R. D. Vale (2009). "Regulators of the cytoplasmic dynein motor." Nat Rev Mol Cell Biol 10(12): 854-865.
Karpuj, M. V., H. Garren, H. Slunt, D. L. Price, J. Gusella, M. W. Becher and L. Steinman (1999). "Transglutaminase aggregates huntingtin into nonamyloidogenic polymers, and its enzymatic activity increases in Huntington's disease brain nuclei." Proc Natl Acad Sci U S A 96(13): 7388-7393.
Kelly, R. D., H. Sumer, M. McKenzie, J. Facucho-Oliveira, I. A. Trounce, P. J. Verma and J. C. St John (2013). "The effects of nuclear reprogramming on mitochondrial DNA replication." Stem Cell Rev 9(1): 1-15.
Kermer, P., N. Klocker, M. Labes and M. Bahr (2000). "Insulin-like growth factor-I protects axotomized rat retinal ganglion cells from secondary death via PI3-K-dependent Akt phosphorylation and inhibition of caspase-3 In vivo." J Neurosci 20(2): 2-8.
Keryer, G., J. R. Pineda, G. Liot, J. Kim, P. Dietrich, C. Benstaali, K. Smith, F. P. Cordelieres, N. Spassky, R. J. Ferrante, I. Dragatsis and F. Saudou (2011). "Ciliogenesis is regulated by a huntingtin-HAP1-PCM1 pathway and is altered in Huntington disease." J Clin Invest 121(11): 4372-4382.
Kieburtz, K., M. MacDonald, C. Shih, A. Feigin, K. Steinberg, K. Bordwell, C. Zimmerman, J. Srinidhi, J. Sotack, J. Gusella and et al. (1994). "Trinucleotide repeat length and progression of illness in Huntington's disease." J Med Genet 31(11): 872-874.

Killoran, A., K. M. Biglan, J. Jankovic, S. Eberly, E. Kayson, D. Oakes, A. B. Young and I. Shoulson (2013). "Characterization of the Huntington intermediate CAG repeat expansion phenotype in PHAROS." Neurology 80(22): 2022-2027.
Kim, J., J. P. Moody, C. K. Edgerly, O. L. Bordiuk, K. Cormier, K. Smith, M. F. Beal and R. J. Ferrante (2010). "Mitochondrial loss, dysfunction and altered dynamics in Huntington's disease." Hum Mol Genet 19(20): 3919-3935.
Kim, Y. G., J. Cha and S. Chandrasegaran (1996). "Hybrid restriction enzymes: zinc finger fusions to Fok I cleavage domain." Proc Natl Acad Sci U S A 93(3): 1156-1160.
King, A., M. A. Selak and E. Gottlieb (2006). "Succinate dehydrogenase and fumarate hydratase: linking mitochondrial dysfunction and cancer." Oncogene 25(34): 4675-4682.
Kordasiewicz, H. B., L. M. Stanek, E. V. Wancewicz, C. Mazur, M. M. McAlonis, K. A. Pytel, J. W. Artates, A. Weiss, S. H. Cheng, L. S. Shihabuddin, G. Hung, C. F. Bennett and D. W. Cleveland (2012). "Sustained therapeutic reversal of Huntington's disease by transient repression of huntingtin synthesis." Neuron 74(6): 1031-1044.
Koroshetz, W. J., B. G. Jenkins, B. R. Rosen and M. F. Beal (1997). "Energy metabolism defects in Huntington's disease and effects of coenzyme Q10." Ann Neurol 41(2): 160-165.
Kosodo, Y., K. Roper, W. Haubensak, A. M. Marzesco, D. Corbeil and W. B. Huttner (2004). "Asymmetric distribution of the apical plasma membrane during neurogenic divisions of mammalian neuroepithelial cells." EMBO J 23(11): 2314-2324.
Kotak, S., C. Busso and P. Gonczy (2012). "Cortical dynein is critical for proper spindle positioning in human cells." J Cell Biol 199(1): 97-110.
Kremer, B., P. Goldberg, S. E. Andrew, J. Theilmann, H. Telenius, J. Zeisler, F. Squitieri, B. Lin, A. Bassett, E. Almqvist and et al. (1994). "A worldwide study of the Huntington's disease mutation. The sensitivity and specificity of measuring CAG repeats." N Engl J Med 330(20): 1401-1406.
Kremer, B., S. J. Tallaksen-Greene and R. L. Albin (1993). "AMPA and NMDA binding sites in the hypothalamic lateral tuberal nucleus: implications for Huntington's disease." Neurology 43(8): 1593-1595.
Kremer, H. P., R. A. Roos, G. Dingjan, E. Marani and G. T. Bots (1990). "Atrophy of the hypothalamic lateral tuberal nucleus in Huntington's disease." J Neuropathol Exp Neurol 49(4): 371-382.
Kremer, H. P., R. A. Roos, G. M. Dingjan, G. T. Bots, G. W. Bruyn and M. A. Hofman (1991). "The hypothalamic lateral tuberal nucleus and the characteristics of neuronal loss in Huntington's disease." Neurosci Lett 132(1): 101-104.
Ku, S., E. Soragni, E. Campau, E. A. Thomas, G. Altun, L. C. Laurent, J. F. Loring, M. Napierala and J. M. Gottesfeld (2010). "Friedreich's ataxia induced pluripotent stem cells model intergenerational GAATTC triplet repeat instability." Cell Stem Cell 7(5): 631-637.
Laan, L., N. Pavin, J. Husson, G. Romet-Lemonne, M. van Duijn, M. P. Lopez, R. D. Vale, F. Julicher, S. L. Reck-Peterson and M. Dogterom (2012). "Cortical dynein controls microtubule dynamics to generate pulling forces that position microtubule asters." Cell 148(3): 502-514.
Lalic, N. M., J. Maric, M. Svetel, A. Jotic, E. Stefanova, K. Lalic, N. Dragasevic, T. Milicic, L. Lukic and V. S. Kostic (2008). "Glucose homeostasis in Huntington disease: abnormalities in insulin sensitivity and early-phase insulin secretion." Arch Neurol 65(4): 476-480.

Landles, C. and G. P. Bates (2004). "Huntingtin and the molecular pathogenesis of Huntington's disease. Fourth in molecular medicine review series." EMBO Rep 5(10): 958-963.
Latres, E., A. R. Amini, A. A. Amini, J. Griffiths, F. J. Martin, Y. Wei, H. C. Lin, G. D. Yancopoulos and D. J. Glass (2005). "Insulin-like growth factor-1 (IGF-1) inversely regulates atrophy-induced genes via the phosphatidylinositol 3-kinase/Akt/mammalian target of rapamycin (PI3K/Akt/mTOR) pathway." J Biol Chem 280(4): 2737-2744.
Laviola, L., A. Natalicchio, S. Perrini and F. Giorgino (2008). "Abnormalities of IGF-I signaling in the pathogenesis of diseases of the bone, brain, and fetoplacental unit in humans." Am J Physiol Endocrinol Metab 295(5): E991-999.
Leavitt, B. R., J. A. Guttman, J. G. Hodgson, G. H. Kimel, R. Singaraja, A. W. Vogl and M. R. Hayden (2001). "Wild-type huntingtin reduces the cellular toxicity of mutant huntingtin in vivo." Am J Hum Genet 68(2): 313-324.
Leavitt, B. R. and M. R. Hayden (2006). "Is tetrabenazine safe and effective for suppressing chorea in Huntington's disease?" Nat Clin Pract Neurol 2(10): 536-537.
Lee, Y., C. Ahn, J. Han, H. Choi, J. Kim, J. Yim, J. Lee, P. Provost, O. Radmark, S. Kim and V. N. Kim (2003). "The nuclear RNase III Drosha initiates microRNA processing." Nature 425(6956): 415-419.
Lee, Y., S. El Andaloussi and M. J. Wood (2012). "Exosomes and microvesicles: extracellular vesicles for genetic information transfer and gene therapy." Hum Mol Genet 21(R1): R125-134.
Li, F., Y. Wang, K. I. Zeller, J. J. Potter, D. R. Wonsey, K. A. O'Donnell, J. W. Kim, J. T. Yustein, L. A. Lee and C. V. Dang (2005). "Myc stimulates nuclearly encoded mitochondrial genes and mitochondrial biogenesis." Mol Cell Biol 25(14): 6225-6234.
Li, S. H., A. L. Cheng, H. Zhou, S. Lam, M. Rao, H. Li and X. J. Li (2002). "Interaction of Huntington disease protein with transcriptional activator Sp1." Mol Cell Biol 22(5): 1277-1287.
Li, S. H., C. A. Gutekunst, S. M. Hersch and X. J. Li (1998). "Interaction of huntingtin-associated protein with dynactin P150Glued." J Neurosci 18(4): 1261-1269.
Li, S. H. and X. J. Li (2004). "Huntingtin-protein interactions and the pathogenesis of Huntington's disease." Trends Genet 20(3): 146-154.
Li, W., F. Teng, T. Li and Q. Zhou (2013). "Simultaneous generation and germline transmission of multiple gene mutations in rat using CRISPR-Cas systems." Nat Biotechnol 31(8): 684-686.
Lim, D., L. Fedrizzi, M. Tartari, C. Zuccato, E. Cattaneo, M. Brini and E. Carafoli (2008). "Calcium homeostasis and mitochondrial dysfunction in striatal neurons of Huntington disease." J Biol Chem 283(9): 5780-5789.
Lim, L. P. and C. B. Burge (2001). "A computational analysis of sequence features involved in recognition of short introns." Proc Natl Acad Sci U S A 98(20): 11193-11198.
Lin, S., L. W. Fan, P. G. Rhodes and Z. Cai (2009). "Intranasal administration of IGF-1 attenuates hypoxic-ischemic brain injury in neonatal rats." Exp Neurol 217(2): 361-370.
Liu, J., P. J. Verma, M. V. Evans-Galea, M. B. Delatycki, A. Michalska, J. Leung, D. Crombie, J. P. Sarsero, R. Williamson, M. Dottori and A. Pebay (2011). "Generation of induced pluripotent stem cell lines from Friedreich ataxia patients." Stem Cell Rev 7(3): 703-713.
Liu, Q., D. J. Segal, J. B. Ghiara and C. F. Barbas, 3rd (1997). "Design of polydactyl zinc-finger proteins for unique addressing within complex genomes." Proc Natl Acad Sci U S A 94(11): 5525-5530.

Liu, S., Z. Tian, F. Yin, Q. Zhao and M. Fan (2009). "Generation of dopaminergic neurons from human fetal mesencephalic progenitors after co-culture with striatal-conditioned media and exposure to lowered oxygen." Brain Res Bull 80(1-2): 62-68.
Liu, W., Q. Long, K. Chen, S. Li, G. Xiang, S. Chen, X. Liu, Y. Li, L. Yang, D. Dong, C. Jiang, Z. Feng and D. Qin (2013). "Mitochondrial metabolism transition cooperates with nuclear reprogramming during induced pluripotent stem cell generation." Biochem Biophys Res Commun 431(4): 767-771.
Liu, X., Q. Jiang, S. G. Mansfield, M. Puttaraju, Y. Zhang, W. Zhou, J. A. Cohn, M. A. Garcia-Blanco, L. G. Mitchell and J. F. Engelhardt (2002). "Partial correction of endogenous DeltaF508 CFTR in human cystic fibrosis airway epithelia by spliceosome-mediated RNA trans-splicing." Nat Biotechnol 20(1): 47-52.
Lloyd, R. E., J. H. Lee, R. Alberio, E. J. Bowles, J. Ramalho-Santos, K. H. Campbell and J. C. St John (2006). "Aberrant nucleo-cytoplasmic cross-talk results in donor cell mtDNA persistence in cloned embryos." Genetics 172(4): 2515-2527.
Lombardi, M. S., L. Jaspers, C. Spronkmans, C. Gellera, F. Taroni, E. Di Maria, S. D. Donato and W. F. Kaemmerer (2009). "A majority of Huntington's disease patients may be treatable by individualized allele-specific RNA interference." Exp Neurol 217(2): 312-319.
Lumsden, A. L., T. L. Henshall, S. Dayan, M. T. Lardelli and R. I. Richards (2007). "Huntingtin-deficient zebrafish exhibit defects in iron utilization and development." Hum Mol Genet 16(16): 1905-1920.
Luo, S. and D. C. Rubinsztein (2009). "Huntingtin promotes cell survival by preventing Pak2 cleavage." J Cell Sci 122(Pt 6): 875-885.
Ma, T. C., J. L. Buescher, B. Oatis, J. A. Funk, A. J. Nash, R. L. Carrier and K. R. Hoyt (2007). "Metformin therapy in a transgenic mouse model of Huntington's disease." Neurosci Lett 411(2): 98-103.
Ma, Y. and D. Eidelberg (2007). "Functional imaging of cerebral blood flow and glucose metabolism in Parkinson's disease and Huntington's disease." Mol Imaging Biol 9(4): 223-233.
MacDonald, M. E., S. Gines, J. F. Gusella and V. C. Wheeler (2003). "Huntington's disease." Neuromolecular Med 4(1-2): 7-20.
Mak, S. K., Y. A. Huang, S. Iranmanesh, M. Vangipuram, R. Sundararajan, L. Nguyen, J. W. Langston and B. Schule (2012). "Small molecules greatly improve conversion of human-induced pluripotent stem cells to the neuronal lineage." Stem Cells Int 2012: 140427.
Maksimovic, I. D., M. D. Jovanovic, M. Colic, R. Mihajlovic, D. Micic, V. Selakovic, M. Ninkovic, Z. Malicevic, M. Rusic-Stojiljkovic and A. Jovicic (2001). "Oxidative damage and metabolic dysfunction in experimental Huntington's disease: selective vulnerability of the striatum and hippocampus." Vojnosanit Pregl 58(3): 237-242.
Mali, P., L. Yang, K. M. Esvelt, J. Aach, M. Guell, J. E. DiCarlo, J. E. Norville and G. M. Church (2013). "RNA-guided human genome engineering via Cas9." Science 339(6121): 823-826.
Mandal, S., A. G. Lindgren, A. S. Srivastava, A. T. Clark and U. Banerjee (2011). "Mitochondrial function controls proliferation and early differentiation potential of embryonic stem cells." Stem Cells 29(3): 486-495.
Mangiarini, L., K. Sathasivam, M. Seller, B. Cozens, A. Harper, C. Hetherington, M. Lawton, Y. Trottier, H. Lehrach, S. W. Davies and G. P. Bates (1996). "Exon 1 of the HD gene with an expanded CAG repeat is sufficient to cause a progressive neurological phenotype in transgenic mice." Cell 87(3): 493-506.

Mansfield, S. G., R. H. Clark, M. Puttaraju, J. Kole, J. A. Cohn, L. G. Mitchell and M. A. Garcia-Blanco (2003). "5' exon replacement and repair by spliceosome-mediated RNA trans-splicing." RNA 9(10): 1290-1297.
Mansfield, S. G., J. Kole, M. Puttaraju, C. C. Yang, M. A. Garcia-Blanco, J. A. Cohn and L. G. Mitchell (2000). "Repair of CFTR mRNA by spliceosome-mediated RNA trans-splicing." Gene Ther 7(22): 1885-1895.
Marchetto, M. C., G. W. Yeo, O. Kainohana, M. Marsala, F. H. Gage and A. R. Muotri (2009). "Transcriptional signature and memory retention of human-induced pluripotent stem cells." PLoS One 4(9): e7076.
Margolis, R. L. and C. A. Ross (2003). "Diagnosis of Huntington disease." Clin Chem 49(10): 1726-1732.
Martin, B., W. Chadwick, W. N. Cong, N. Pantaleo, C. M. Daimon, E. J. Golden, K. G. Becker, W. H. Wood, 3rd, O. D. Carlson, J. M. Egan and S. Maudsley (2012). "Euglycemic agent-mediated hypothalamic transcriptomic manipulation in the N171-82Q model of Huntington disease is related to their physiological efficacy." J Biol Chem 287(38): 31766-31782.
Martin, G. R. (1981). "Isolation of a pluripotent cell line from early mouse embryos cultured in medium conditioned by teratocarcinoma stem cells." Proc Natl Acad Sci U S A 78(12): 7634-7638.
Martin, W. R., M. Wieler and C. C. Hanstock (2007). "Is brain lactate increased in Huntington's disease?" J Neurol Sci 263(1-2): 70-74.
Mateizel, I., N. De Temmerman, U. Ullmann, G. Cauffman, K. Sermon, H. Van de Velde, M. De Rycke, E. Degreef, P. Devroey, I. Liebaers and A. Van Steirteghem (2006). "Derivation of human embryonic stem cell lines from embryos obtained after IVF and after PGD for monogenic disorders." Hum Reprod 21(2): 503-511.
Mathieu, J., Z. Zhang, A. Nelson, D. A. Lamba, T. A. Reh, C. Ware and H. Ruohola-Baker (2013). "Hypoxia induces re-entry of committed cells into pluripotency." Stem Cells 31(9): 1737-1748.
Mathieu, J., W. Zhou, Y. Xing, H. Sperber, A. Ferreccio, Z. Agoston, K. T. Kuppusamy, R. T. Moon and H. Ruohola-Baker (2014). "Hypoxia-inducible factors have distinct and stage-specific roles during reprogramming of human cells to pluripotency." Cell Stem Cell 14(5): 592-605.
McKinstry, S. U., Y. B. Karadeniz, A. K. Worthington, V. Y. Hayrapetyan, M. I. Ozlu, K. Serafin-Molina, W. C. Risher, T. Ustunkaya, I. Dragatsis, S. Zeitlin, H. H. Yin and C. Eroglu (2014). "Huntingtin is required for normal excitatory synapse development in cortical and striatal circuits." J Neurosci 34(28): 9455-9472.
Mergenthaler, P., U. Lindauer, G. A. Dienel and A. Meisel (2013). "Sugar for the brain: the role of glucose in physiological and pathological brain function." Trends Neurosci 36(10): 587-597.
Metzler, M., L. Gan, G. Mazarei, R. K. Graham, L. Liu, N. Bissada, G. Lu, B. R. Leavitt and M. R. Hayden (2010). "Phosphorylation of huntingtin at Ser421 in YAC128 neurons is associated with protection of YAC128 neurons from NMDA-mediated excitotoxicity and is modulated by PP1 and PP2A." J Neurosci 30(43): 14318-14329.
Milakovic, T. and G. V. Johnson (2005). "Mitochondrial respiration and ATP production are significantly impaired in striatal cells expressing mutant huntingtin." J Biol Chem 280(35): 30773-30782.
Miller, J. C., S. Tan, G. Qiao, K. A. Barlow, J. Wang, D. F. Xia, X. Meng, D. E. Paschon, E. Leung, S. J. Hinkley, G. P. Dulay, K. L. Hua, I. Ankoudinova, G. J. Cost, F. D. Urnov, H. S. Zhang, M. C. Holmes, L. Zhang, P. D. Gregory and E. J. Rebar (2011).

"A TALE nuclease architecture for efficient genome editing." Nat Biotechnol 29(2): 143-148.
Mills, J. D. and M. Janitz (2012). "Alternative splicing of mRNA in the molecular pathology of neurodegenerative diseases." Neurobiol Aging 33(5): 1012 e1011-1024.
Mitchell, I. G., N. W. Amphlett and R. W. Rees (1994). "Parametric analysis of rank transformed data for statistical assessment of genotoxicity data with examples from cultured mammalian cells." Mutagenesis 9(2): 125-132.
Mitra, S., A. S. Tsvetkov and S. Finkbeiner (2009). "Protein turnover and inclusion body formation." Autophagy 5(7): 1037-1038.
Mochel, F. and R. G. Haller (2011). "Energy deficit in Huntington disease: why it matters." J Clin Invest 121(2): 493-499.
Modregger, J., N. A. DiProspero, V. Charles, D. A. Tagle and M. Plomann (2002). "PACSIN 1 interacts with huntingtin and is absent from synaptic varicosities in presymptomatic Huntington's disease brains." Hum Mol Genet 11(21): 2547-2558.
Molina-Calavita, M., M. Barnat, S. Elias, E. Aparicio, M. Piel and S. Humbert (2014). "Mutant huntingtin affects cortical progenitor cell division and development of the mouse neocortex." J Neurosci 34(30): 10034-10040.
Montoya, A., B. H. Price, M. Menear and M. Lepage (2006). "Brain imaging and cognitive dysfunctions in Huntington's disease." J Psychiatry Neurosci 31(1): 21-29.
Morin, X. and Y. Bellaiche (2011). "Mitotic spindle orientation in asymmetric and symmetric cell divisions during animal development." Dev Cell 21(1): 102-119.
Morrison, P. J. (2010). "Accurate prevalence and uptake of testing for Huntington's disease." Lancet Neurol 9(12): 1147.
Morrison, P. J. (2012). "Prevalence estimates of Huntington disease in Caucasian populations are gross underestimates." Mov Disord 27(13): 1707-1708; author reply 1708-1709.
Morton, A. J., N. I. Wood, M. H. Hastings, C. Hurelbrink, R. A. Barker and E. S. Maywood (2005). "Disintegration of the sleep-wake cycle and circadian timing in Huntington's disease." J Neurosci 25(1): 157-163.
Myers, R. H., M. E. MacDonald, W. J. Koroshetz, M. P. Duyao, C. M. Ambrose, S. A. Taylor, G. Barnes, J. Srinidhi, C. S. Lin, W. L. Whaley and et al. (1993). "De novo expansion of a (CAG)n repeat in sporadic Huntington's disease." Nat Genet 5(2): 168-173.
Myers, R. H., D. S. Sax, W. J. Koroshetz, C. Mastromauro, L. A. Cupples, D. K. Kiely, F. K. Pettengill and E. D. Bird (1991). "Factors associated with slow progression in Huntington's disease." Arch Neurol 48(8): 800-804.
Nance, M. A., V. Mathias-Hagen, G. Breningstall, M. J. Wick and R. C. McGlennen (1999). "Analysis of a very large trinucleotide repeat in a patient with juvenile Huntington's disease." Neurology 52(2): 392-394.
Nance, M. A. and R. H. Myers (2001). "Juvenile onset Huntington's disease--clinical and research perspectives." Ment Retard Dev Disabil Res Rev 7(3): 153-157.
Neganova, I. and M. Lako (2008). "G1 to S phase cell cycle transition in somatic and embryonic stem cells." J Anat 213(1): 30-44.
Nguyen, G. D., S. Gokhan, A. E. Molero and M. F. Mehler (2013). "Selective roles of normal and mutant huntingtin in neural induction and early neurogenesis." PLoS One 8(5): e64368.
Nguyen, H. N., B. Byers, B. Cord, A. Shcheglovitov, J. Byrne, P. Gujar, K. Kee, B. Schule, R. E. Dolmetsch, W. Langston, T. D. Palmer and R. R. Pera (2011). "LRRK2 mutant iPSC-derived DA neurons demonstrate increased susceptibility to oxidative stress." Cell Stem Cell 8(3): 267-280.

Nicoleau, C., C. Varela, C. Bonnefond, Y. Maury, A. Bugi, L. Aubry, P. Viegas, F. Bourgois-Rocha, M. Peschanski and A. L. Perrier (2013). "Embryonic stem cells neural differentiation qualifies the role of Wnt/beta-Catenin signals in human telencephalic specification and regionalization." Stem Cells 31(9): 1763-1774.
Nilsson, P., N. Iwata, S. Muramatsu, L. O. Tjernberg, B. Winblad and T. C. Saido (2010). "Gene therapy in Alzheimer's disease - potential for disease modification." J Cell Mol Med 14(4): 741-757.
Noatynska, A., M. Gotta and P. Meraldi (2012). "Mitotic spindle (DIS)orientation and DISease: cause or consequence?" J Cell Biol 199(7): 1025-1035.
Noctor, S. C., V. Martinez-Cerdeno and A. R. Kriegstein (2008). "Distinct behaviors of neural stem and progenitor cells underlie cortical neurogenesis." J Comp Neurol 508(1): 28-44.
Nopoulos, P. C., E. H. Aylward, C. A. Ross, J. A. Mills, D. R. Langbehn, H. J. Johnson, V. A. Magnotta, R. K. Pierson, L. J. Beglinger, M. A. Nance, R. A. Barker and J. S. Paulsen (2011). "Smaller intracranial volume in prodromal Huntington's disease: evidence for abnormal neurodevelopment." Brain 134(Pt 1): 137-142.
Norremolle, A., E. Budtz-Jorgensen, K. Fenger, J. E. Nielsen, S. A. Sorensen and L. Hasholt (2009). "4p16.3 haplotype modifying age at onset of Huntington disease." Clin Genet 75(3): 244-250.
Norremolle, A., O. Riess, J. T. Epplen, K. Fenger, L. Hasholt and S. A. Sorensen (1993). "Trinucleotide repeat elongation in the Huntingtin gene in Huntington disease patients from 71 Danish families." Hum Mol Genet 2(9): 1475-1476.
Nucifora, F. C., Jr., M. Sasaki, M. F. Peters, H. Huang, J. K. Cooper, M. Yamada, H. Takahashi, S. Tsuji, J. Troncoso, V. L. Dawson, T. M. Dawson and C. A. Ross (2001). "Interference by huntingtin and atrophin-1 with cbp-mediated transcription leading to cellular toxicity." Science 291(5512): 2423-2428.
Okita, K., H. Hong, K. Takahashi and S. Yamanaka (2010). "Generation of mouse-induced pluripotent stem cells with plasmid vectors." Nat Protoc 5(3): 418-428.
Okita, K., T. Ichisaka and S. Yamanaka (2007). "Generation of germline-competent induced pluripotent stem cells." Nature 448(7151): 313-317.
Okita, K., M. Nakagawa, H. Hyenjong, T. Ichisaka and S. Yamanaka (2008). "Generation of mouse induced pluripotent stem cells without viral vectors." Science 322(5903): 949-953.
Olah, J., P. Klivenyi, G. Gardian, L. Vecsei, F. Orosz, G. G. Kovacs, H. V. Westerhoff and J. Ovadi (2008). "Increased glucose metabolism and ATP level in brain tissue of Huntington's disease transgenic mice." FEBS J 275(19): 4740-4755.
Oliveira, J. M., S. Chen, S. Almeida, R. Riley, J. Goncalves, C. R. Oliveira, M. R. Hayden, D. G. Nicholls, L. M. Ellerby and A. C. Rego (2006). "Mitochondrial-dependent Ca2+ handling in Huntington's disease striatal cells: effect of histone deacetylase inhibitors." J Neurosci 26(43): 11174-11186.
Oliveira, J. M., M. B. Jekabsons, S. Chen, A. Lin, A. C. Rego, J. Goncalves, L. M. Ellerby and D. G. Nicholls (2007). "Mitochondrial dysfunction in Huntington's disease: the bioenergetics of isolated and in situ mitochondria from transgenic mice." J Neurochem 101(1): 241-249.
Olsen, P. A., M. Gelazauskaite, M. Randol and S. Krauss (2010). "Analysis of illegitimate genomic integration mediated by zinc-finger nucleases: implications for specificity of targeted gene correction." BMC Mol Biol 11: 35.
Orr, A. L., S. Li, C. E. Wang, H. Li, J. Wang, J. Rong, X. Xu, P. G. Mastroberardino, J. T. Greenamyre and X. J. Li (2008). "N-terminal mutant huntingtin associates with mitochondria and impairs mitochondrial trafficking." J Neurosci 28(11): 2783-2792.

Ostergaard, M. E., A. L. Southwell, H. Kordasiewicz, A. T. Watt, N. H. Skotte, C. N. Doty, K. Vaid, E. B. Villanueva, E. E. Swayze, C. F. Bennett, M. R. Hayden and P. P. Seth (2013). "Rational design of antisense oligonucleotides targeting single nucleotide polymorphisms for potent and allele selective suppression of mutant Huntingtin in the CNS." Nucleic Acids Res 41(21): 9634-9650.
Pan, G. and J. A. Thomson (2007). "Nanog and transcriptional networks in embryonic stem cell pluripotency." Cell Res 17(1): 42-49.
Panopoulos, A. D., O. Yanes, S. Ruiz, Y. S. Kida, D. Diep, R. Tautenhahn, A. Herrerias, E. M. Batchelder, N. Plongthongkum, M. Lutz, W. T. Berggren, K. Zhang, R. M. Evans, G. Siuzdak and J. C. Izpisua Belmonte (2012). "The metabolome of induced pluripotent stem cells reveals metabolic changes occurring in somatic cell reprogramming." Cell Res 22(1): 168-177.
Panov, A. V., L. Andreeva and J. T. Greenamyre (2004). "Quantitative evaluation of the effects of mitochondrial permeability transition pore modifiers on accumulation of calcium phosphate: comparison of rat liver and brain mitochondria." Arch Biochem Biophys 424(1): 44-52.
Pardo, R., E. Colin, E. Regulier, P. Aebischer, N. Deglon, S. Humbert and F. Saudou (2006). "Inhibition of calcineurin by FK506 protects against polyglutamine-huntingtin toxicity through an increase of huntingtin phosphorylation at S421." J Neurosci 26(5): 1635-1645.
Pardo, R., M. Molina-Calavita, G. Poizat, G. Keryer, S. Humbert and F. Saudou (2010). "pARIS-htt: an optimised expression platform to study huntingtin reveals functional domains required for vesicular trafficking." Mol Brain 3: 17.
Park, I. H., N. Arora, H. Huo, N. Maherali, T. Ahfeldt, A. Shimamura, M. W. Lensch, C. Cowan, K. Hochedlinger and G. Q. Daley (2008). "Disease-specific induced pluripotent stem cells." Cell 134(5): 877-886.
Park, S. E., R. Dantzer, K. W. Kelley and R. H. McCusker (2011). "Central administration of insulin-like growth factor-I decreases depressive-like behavior and brain cytokine expression in mice." J Neuroinflammation 8: 12.
Parsons, M. P., R. Kang, C. Buren, A. Dau, A. L. Southwell, C. N. Doty, S. S. Sanders, M. R. Hayden and L. A. Raymond (2014). "Bidirectional control of postsynaptic density-95 (PSD-95) clustering by Huntingtin." J Biol Chem 289(6): 3518-3528.
Patel, S. S., J. Jankovic, A. J. Hood, C. B. Jeter and A. B. Sereno (2012). "Reflexive and volitional saccades: biomarkers of Huntington disease severity and progression." J Neurol Sci 313(1-2): 35-41.
Paulsen Bda, S., R. de Moraes Maciel, A. Galina, M. Souza da Silveira, C. dos Santos Souza, H. Drummond, E. Nascimento Pozzatto, H. Silva, Jr., L. Chicaybam, R. Massuda, P. Setti-Perdigao, M. Bonamino, P. S. Belmonte-de-Abreu, N. G. Castro, H. Brentani and S. K. Rehen (2012). "Altered oxygen metabolism associated to neurogenesis of induced pluripotent stem cells derived from a schizophrenic patient." Cell Transplant 21(7): 1547-1559.
Paulsen, J. S., M. Hayden, J. C. Stout, D. R. Langbehn, E. Aylward, C. A. Ross, M. Guttman, M. Nance, K. Kieburtz, D. Oakes, I. Shoulson, E. Kayson, S. Johnson and E. Penziner (2006). "Preparing for preventive clinical trials: the Predict-HD study." Arch Neurol 63(6): 883-890.
Paulsen, J. S., D. R. Langbehn, J. C. Stout, E. Aylward, C. A. Ross, M. Nance, M. Guttman, S. Johnson, M. MacDonald, L. J. Beglinger, K. Duff, E. Kayson, K. Biglan, I. Shoulson, D. Oakes and M. Hayden (2008). "Detection of Huntington's disease decades before diagnosis: the Predict-HD study." J Neurol Neurosurg Psychiatry 79(8): 874-880.

Paulsen, J. S., H. Zhao, J. C. Stout, R. R. Brinkman, M. Guttman, C. A. Ross, P. Como, C. Manning, M. R. Hayden and I. Shoulson (2001). "Clinical markers of early disease in persons near onset of Huntington's disease." Neurology 57(4): 658-662.
Pellerin, L. and P. J. Magistretti (1994). "Glutamate uptake into astrocytes stimulates aerobic glycolysis: a mechanism coupling neuronal activity to glucose utilization." Proc Natl Acad Sci U S A 91(22): 10625-10629.
Pergolizzi, R. G., A. E. Ropper, R. Dragos, A. C. Reid, K. Nakayama, Y. Tan, J. R. Ehteshami, S. H. Coleman, R. B. Silver, N. R. Hackett, A. Menez and R. G. Crystal (2003). "In vivo trans-splicing of 5' and 3' segments of pre-mRNA directed by corresponding DNA sequences delivered by gene transfer." Mol Ther 8(6): 999-1008.
Perry, S. W., J. P. Norman, J. Barbieri, E. B. Brown and H. A. Gelbard (2011). "Mitochondrial membrane potential probes and the proton gradient: a practical usage guide." Biotechniques 50(2): 98-115.
Persichetti, F., C. M. Ambrose, P. Ge, S. M. McNeil, J. Srinidhi, M. A. Anderson, B. Jenkins, G. T. Barnes, M. P. Duyao, L. Kanaley and et al. (1995). "Normal and expanded Huntington's disease gene alleles produce distinguishable proteins due to translation across the CAG repeat." Mol Med 1(4): 374-383.
Perutz, M. F., T. Johnson, M. Suzuki and J. T. Finch (1994). "Glutamine repeats as polar zippers: their possible role in inherited neurodegenerative diseases." Proc Natl Acad Sci U S A 91(12): 5355-5358.
Petersen, A. and M. Bjorkqvist (2006). "Hypothalamic-endocrine aspects in Huntington's disease." Eur J Neurosci 24(4): 961-967.
Petersen, A., J. Gil, M. L. Maat-Schieman, M. Bjorkqvist, H. Tanila, I. M. Araujo, R. Smith, N. Popovic, N. Wierup, P. Norlen, J. Y. Li, R. A. Roos, F. Sundler, H. Mulder and P. Brundin (2005). "Orexin loss in Huntington's disease." Hum Mol Genet 14(1): 39-47.
Petersson, U., C. J. Ostgren, L. Brudin, K. Brismar and P. M. Nilsson (2009). "Low levels of insulin-like growth-factor-binding protein-1 (IGFBP-1) are prospectively associated with the incidence of type 2 diabetes and impaired glucose tolerance (IGT): the Soderakra Cardiovascular Risk Factor Study." Diabetes Metab 35(3): 198-205.
Peyre, E., F. Jaouen, M. Saadaoui, L. Haren, A. Merdes, P. Durbec and X. Morin (2011). "A lateral belt of cortical LGN and NuMA guides mitotic spindle movements and planar division in neuroepithelial cells." J Cell Biol 193(1): 141-154.
Pfister, E. L., L. Kennington, J. Straubhaar, S. Wagh, W. Liu, M. DiFiglia, B. Landwehrmeyer, J. P. Vonsattel, P. D. Zamore and N. Aronin (2009). "Five siRNAs targeting three SNPs may provide therapy for three-quarters of Huntington's disease patients." Curr Biol 19(9): 774-778.
Pich, S., D. Bach, P. Briones, M. Liesa, M. Camps, X. Testar, M. Palacin and A. Zorzano (2005). "The Charcot-Marie-Tooth type 2A gene product, Mfn2, up-regulates fuel oxidation through expression of OXPHOS system." Hum Mol Genet 14(11): 1405-1415.
Podolsky, S. and N. A. Leopold (1977). "Abnormal glucose tolerance and arginine tolerance tests in Huntington's disease." Gerontology 23(1): 55-63.
Pouladi, M. A., A. J. Morton and M. R. Hayden (2013). "Choosing an animal model for the study of Huntington's disease." Nat Rev Neurosci 14(10): 708-721.
Pouladi, M. A., Y. Xie, N. H. Skotte, D. E. Ehrnhoefer, R. K. Graham, J. E. Kim, N. Bissada, X. W. Yang, P. Paganetti, R. M. Friedlander, B. R. Leavitt and M. R. Hayden (2010). "Full-length huntingtin levels modulate body weight by influencing insulin-like growth factor 1 expression." Hum Mol Genet 19(8): 1528-1538.

Power, C. and J. E. Rasko (2011). "Will cell reprogramming resolve the embryonic stem cell controversy? A narrative review." Ann Intern Med 155(2): 114-121.
Powers, W. J., R. H. Haas, T. Le, T. O. Videen, T. Hershey, L. McGee-Minnich and J. S. Perlmutter (2007). "Normal platelet mitochondrial complex I activity in Huntington's disease." Neurobiol Dis 27(1): 99-101.
Powers, W. J., R. H. Haas, T. Le, T. O. Videen, J. Markham and J. S. Perlmutter (2011). "Platelet mitochondrial complex I and I+III activities do not correlate with cerebral mitochondrial oxidative metabolism." J Cereb Blood Flow Metab 31(1): e1-5.
Pramono, Z. A., K. B. Wee, J. L. Wang, Y. J. Chen, Q. B. Xiong, P. S. Lai and W. C. Yee (2012). "A prospective study in the rational design of efficient antisense oligonucleotides for exon skipping in the DMD gene." Hum Gene Ther 23(7): 781-790.
Pratley, R. E., A. D. Salbe, E. Ravussin and J. N. Caviness (2000). "Higher sedentary energy expenditure in patients with Huntington's disease." Ann Neurol 47(1): 64-70.
Prigione, A. and J. Adjaye (2010). "Modulation of mitochondrial biogenesis and bioenergetic metabolism upon in vitro and in vivo differentiation of human ES and iPS cells." Int J Dev Biol 54(11-12): 1729-1741.
Prigione, A., B. Fauler, R. Lurz, H. Lehrach and J. Adjaye (2010). "The senescence-related mitochondrial/oxidative stress pathway is repressed in human induced pluripotent stem cells." Stem Cells 28(4): 721-733.
Prigione, A., A. M. Hossini, B. Lichtner, A. Serin, B. Fauler, M. Megges, R. Lurz, H. Lehrach, E. Makrantonaki, C. C. Zouboulis and J. Adjaye (2011). "Mitochondrial-associated cell death mechanisms are reset to an embryonic-like state in aged donor-derived iPS cells harboring chromosomal aberrations." PLoS One 6(11): e27352.
Prigione, A., N. Rohwer, S. Hoffmann, B. Mlody, K. Drews, R. Bukowiecki, K. Blumlein, E. E. Wanker, M. Ralser, T. Cramer and J. Adjaye (2014). "HIF1alpha modulates cell fate reprogramming through early glycolytic shift and upregulation of PDK1-3 and PKM2." Stem Cells 32(2): 364-376.
Pruszak, J., K. C. Sonntag, M. H. Aung, R. Sanchez-Pernaute and O. Isacson (2007). "Markers and methods for cell sorting of human embryonic stem cell-derived neural cell populations." Stem Cells 25(9): 2257-2268.
Purdon, S. E., E. Mohr, V. Ilivitsky and B. D. Jones (1994). "Huntington's disease: pathogenesis, diagnosis and treatment." J Psychiatry Neurosci 19(5): 359-367.
Purves, D., G. Augustine, D. Fitzpatric, W. Hall, A. Lamantia, J. McNamara and S. Williams (2004). Neuroscience Chapter 17(3 ed.): Massachusetts U.S.A. .
Purves, D. G. and P. G. Erwin (2004). "Post-traumatic stress and self-disclosure." J Psychol 138(1): 23-33.
Puttaraju, M., S. F. Jamison, S. G. Mansfield, M. A. Garcia-Blanco and L. G. Mitchell (1999). "Spliceosome-mediated RNA trans-splicing as a tool for gene therapy." Nat Biotechnol 17(3): 246-252.
Quarrell, O. W., A. Tyler, M. P. Jones, M. Nordin and P. S. Harper (1988). "Population studies of Huntington's disease in Wales." Clin Genet 33(3): 189-195.
Quintanilla, R. A. and G. V. Johnson (2009). "Role of mitochondrial dysfunction in the pathogenesis of Huntington's disease." Brain Res Bull 80(4-5): 242-247.
Ragan, C. I. (1987). "Structure of NADH-ubiquinone reductase (complex I)." Curr. Top. Bioenerg. 15: 1-36.
Ramaswamy, S., K. M. Shannon and J. H. Kordower (2007). "Huntington's disease: pathological mechanisms and therapeutic strategies." Cell Transplant 16(3): 301-312.
Rand, T. A., S. Petersen, F. Du and X. Wang (2005). "Argonaute2 cleaves the anti-guide strand of siRNA during RISC activation." Cell 123(4): 621-629.

Ratovitski, T., E. Chighladze, N. Arbez, T. Boronina, S. Herbrich, R. N. Cole and C. A. Ross (2012). "Huntingtin protein interactions altered by polyglutamine expansion as determined by quantitative proteomic analysis." Cell Cycle 11(10): 2006-2021.
Razak, S. R., K. Ueno, N. Takayama, N. Nariai, M. Nagasaki, R. Saito, H. Koso, C. Y. Lai, M. Murakami, K. Tsuji, T. Michiue, H. Nakauchi, M. Otsu and S. Watanabe (2013). "Profiling of microRNA in human and mouse ES and iPS cells reveals overlapping but distinct microRNA expression patterns." PLoS One 8(9): e73532.
Razin, S. V., V. V. Borunova, O. G. Maksimenko and O. L. Kantidze (2012). "Cys2His2 zinc finger protein family: classification, functions, and major members." Biochemistry (Mosc) 77(3): 217-226.
Reger, M. A., G. S. Watson, P. S. Green, L. D. Baker, B. Cholerton, M. A. Fishel, S. R. Plymate, M. M. Cherrier, G. D. Schellenberg, W. H. Frey, 2nd and S. Craft (2008). "Intranasal insulin administration dose-dependently modulates verbal memory and plasma amyloid-beta in memory-impaired older adults." J Alzheimers Dis 13(3): 323-331.
Rego, A. C. and L. P. de Almeida (2005). "Molecular targets and therapeutic strategies in Huntington's disease." Curr Drug Targets CNS Neurol Disord 4(4): 361-381.
Rego, A. C., M. S. Santos and C. R. Oliveira (1997). "Adenosine triphosphate degradation products after oxidative stress and metabolic dysfunction in cultured retinal cells." J Neurochem 69(3): 1228-1235.
Rego, A. C., S. Vesce and D. G. Nicholls (2001). "The mechanism of mitochondrial membrane potential retention following release of cytochrome c in apoptotic GT1-7 neural cells." Cell Death Differ 8(10): 995-1003.
Rehman, J., H. J. Zhang, P. T. Toth, Y. Zhang, G. Marsboom, Z. Hong, R. Salgia, A. N. Husain, C. Wietholt and S. L. Archer (2012). "Inhibition of mitochondrial fission prevents cell cycle progression in lung cancer." FASEB J 26(5): 2175-2186.
Reiner, A., R. L. Albin, K. D. Anderson, C. J. D'Amato, J. B. Penney and A. B. Young (1988). "Differential loss of striatal projection neurons in Huntington disease." Proc Natl Acad Sci U S A 85(15): 5733-5737.
Reiner, A., N. Del Mar, Y. P. Deng, C. A. Meade, Z. Sun and D. Goldowitz (2007). "R6/2 neurons with intranuclear inclusions survive for prolonged periods in the brains of chimeric mice." J Comp Neurol 505(6): 603-629.
Reiner, A., E. Shelby, H. Wang, Z. Demarch, Y. Deng, N. H. Guley, V. Hogg, R. Roxburgh, L. J. Tippett, H. J. Waldvogel and R. L. Faull (2013). "Striatal parvalbuminergic neurons are lost in Huntington's disease: implications for dystonia." Mov Disord 28(12): 1691-1699.
Reinhardt, P., B. Schmid, L. F. Burbulla, D. C. Schondorf, L. Wagner, M. Glatza, S. Hoing, G. Hargus, S. A. Heck, A. Dhingra, G. Wu, S. Muller, K. Brockmann, T. Kluba, M. Maisel, R. Kruger, D. Berg, Y. Tsytsyura, C. S. Thiel, O. E. Psathaki, J. Klingauf, T. Kuhlmann, M. Klewin, H. Muller, T. Gasser, H. R. Scholer and J. Sterneckert (2013). "Genetic correction of a LRRK2 mutation in human iPSCs links parkinsonian neurodegeneration to ERK-dependent changes in gene expression." Cell Stem Cell 12(3): 354-367.
Ribeiro, M., T. R. Rosenstock, A. M. Oliveira, C. R. Oliveira and A. C. Rego (2014). "Insulin and IGF-1 improve mitochondrial function in a PI-3K/Akt-dependent manner and reduce mitochondrial generation of reactive oxygen species in Huntington's disease knock-in striatal cells." Free Radic Biol Med 74: 129-144.
Richter, C., J. T. Chang and P. C. Fineran (2012). "Function and regulation of clustered regularly interspaced short palindromic repeats (CRISPR) / CRISPR associated (Cas) systems." Viruses 4(10): 2291-2311.

Richter, H., L. Randau and A. Plagens (2013). "Exploiting CRISPR/Cas: interference mechanisms and applications." Int J Mol Sci 14(7): 14518-14531.
Rigamonti, D., J. H. Bauer, C. De-Fraja, L. Conti, S. Sipione, C. Sciorati, E. Clementi, A. Hackam, M. R. Hayden, Y. Li, J. K. Cooper, C. A. Ross, S. Govoni, C. Vincenz and E. Cattaneo (2000). "Wild-type huntingtin protects from apoptosis upstream of caspase-3." J Neurosci 20(10): 3705-3713.
Rindt, H., P. F. Yen, C. N. Thebeau, T. S. Peterson, G. A. Weisman and C. L. Lorson (2012). "Replacement of huntingtin exon 1 by trans-splicing." Cell Mol Life Sci 69(24): 4191-4204.
Robicsek, O., R. Karry, I. Petit, N. Salman-Kesner, F. J. Muller, E. Klein, D. Aberdam and D. Ben-Shachar (2013). "Abnormal neuronal differentiation and mitochondrial dysfunction in hair follicle-derived induced pluripotent stem cells of schizophrenia patients." Mol Psychiatry 18(10): 1067-1076.
Rockabrand, E., N. Slepko, A. Pantalone, V. N. Nukala, A. Kazantsev, J. L. Marsh, P. G. Sullivan, J. S. Steffan, S. L. Sensi and L. M. Thompson (2007). "The first 17 amino acids of Huntingtin modulate its sub-cellular localization, aggregation and effects on calcium homeostasis." Hum Mol Genet 16(1): 61-77.
Rosen, C. J. and M. Pollak (1999). "Circulating IGF-I: New Perspectives for a New Century." Trends Endocrinol Metab 10(4): 136-141.
Rosenblatt, A., K. Y. Liang, H. Zhou, M. H. Abbott, L. M. Gourley, R. L. Margolis, J. Brandt and C. A. Ross (2006). "The association of CAG repeat length with clinical progression in Huntington disease." Neurology 66(7): 1016-1020.
Rosenfeld, M., H. Brenner-Lavie, S. G. Ari, A. Kavushansky and D. Ben-Shachar (2011). "Perturbation in mitochondrial network dynamics and in complex I dependent cellular respiration in schizophrenia." Biol Psychiatry 69(10): 980-988.
Rosenstock, T. R., C. R. Bertoncini, A. V. Teles, H. Hirata, M. J. Fernandes and S. S. Smaili (2010). "Glutamate-induced alterations in Ca2+ signaling are modulated by mitochondrial Ca2+ handling capacity in brain slices of R6/1 transgenic mice." Eur J Neurosci 32(1): 60-70.
Rubinsztein, D. C., J. Leggo, R. Coles, E. Almqvist, V. Biancalana, J. J. Cassiman, K. Chotai, M. Connarty, D. Crauford, A. Curtis, D. Curtis, M. J. Davidson, A. M. Differ, C. Dode, A. Dodge, M. Frontali, N. G. Ranen, O. C. Stine, M. Sherr, M. H. Abbott, M. L. Franz, C. A. Graham, P. S. Harper, J. C. Hedreen, M. R. Hayden and et al. (1996). "Phenotypic characterization of individuals with 30-40 CAG repeats in the Huntington disease (HD) gene reveals HD cases with 36 repeats and apparently normal elderly individuals with 36-39 repeats." Am J Hum Genet 59(1): 16-22.
Ruocco, H. H., I. Lopes-Cendes, T. L. Laurito, L. M. Li and F. Cendes (2006). "Clinical presentation of juvenile Huntington disease." Arq Neuropsiquiatr 64(1): 5-9.
Rupp, J., M. Dzemidzic, T. Blekher, J. West, S. Hui, J. Wojcieszek, A. J. Saykin, D. A. Kareken and T. Foroud (2012). "Comparison of vertical and horizontal saccade measures and their relation to gray matter changes in premanifest and manifest Huntington disease." J Neurol 259(2): 267-276.
Sadagurski, M., Z. Cheng, A. Rozzo, I. Palazzolo, G. R. Kelley, X. Dong, D. Krainc and M. F. White (2011). "IRS2 increases mitochondrial dysfunction and oxidative stress in a mouse model of Huntington disease." J Clin Invest 121(10): 4070-4081.
Sadri-Vakili, G. and J. H. Cha (2006). "Mechanisms of disease: Histone modifications in Huntington's disease." Nat Clin Pract Neurol 2(6): 330-338.
Saleh, N., S. Moutereau, J. P. Azulay, C. Verny, C. Simonin, C. Tranchant, N. El Hawajri, A. C. Bachoud-Levi and P. Maison (2010). "High insulinlike growth factor I is associated with cognitive decline in Huntington disease." Neurology 75(1): 57-63.

Sanchez-Danes, A., Y. Richaud-Patin, I. Carballo-Carbajal, S. Jimenez-Delgado, C. Caig, S. Mora, C. Di Guglielmo, M. Ezquerra, B. Patel, A. Giralt, J. M. Canals, M. Memo, J. Alberch, J. Lopez-Barneo, M. Vila, A. M. Cuervo, E. Tolosa, A. Consiglio and A. Raya (2012). "Disease-specific phenotypes in dopamine neurons from human iPS-based models of genetic and sporadic Parkinson's disease." EMBO Mol Med 4(5): 380-395.
Sapp, E., C. Schwarz, K. Chase, P. G. Bhide, A. B. Young, J. Penney, J. P. Vonsattel, N. Aronin and M. DiFiglia (1997). "Huntingtin localization in brains of normal and Huntington's disease patients." Ann Neurol 42(4): 604-612.
Sapru, M. K., J. W. Yates, S. Hogan, L. Jiang, J. Halter and M. C. Bohn (2006). "Silencing of human alpha-synuclein in vitro and in rat brain using lentiviral-mediated RNAi." Exp Neurol 198(2): 382-390.
Saretzki, G., T. Walter, S. Atkinson, J. F. Passos, B. Bareth, W. N. Keith, R. Stewart, S. Hoare, M. Stojkovic, L. Armstrong, T. von Zglinicki and M. Lako (2008). "Downregulation of multiple stress defense mechanisms during differentiation of human embryonic stem cells." Stem Cells 26(2): 455-464.
Sawa, A., G. W. Wiegand, J. Cooper, R. L. Margolis, A. H. Sharp, J. F. Lawler, Jr., J. T. Greenamyre, S. H. Snyder and C. A. Ross (1999). "Increased apoptosis of Huntington disease lymphoblasts associated with repeat length-dependent mitochondrial depolarization." Nat Med 5(10): 1194-1198.
Scaduto, R. C., Jr. and L. W. Grotyohann (1999). "Measurement of mitochondrial membrane potential using fluorescent rhodamine derivatives." Biophys J 76(1 Pt 1): 469-477.
Scaggiante, B., B. Dapas, R. Farra, M. Grassi, G. Pozzato, C. Giansante, N. Fiotti and G. Grassi (2011). "Improving siRNA bio-distribution and minimizing side effects." Curr Drug Metab 12(1): 11-23.
Schieke, S. M., M. Ma, L. Cao, J. P. McCoy, Jr., C. Liu, N. F. Hensel, A. J. Barrett, M. Boehm and T. Finkel (2008). "Mitochondrial metabolism modulates differentiation and teratoma formation capacity in mouse embryonic stem cells." J Biol Chem 283(42): 28506-28512.
Schilling, G., M. W. Becher, A. H. Sharp, H. A. Jinnah, K. Duan, J. A. Kotzuk, H. H. Slunt, T. Ratovitski, J. K. Cooper, N. A. Jenkins, N. G. Copeland, D. L. Price, C. A. Ross and D. R. Borchelt (1999). "Intranuclear inclusions and neuritic aggregates in transgenic mice expressing a mutant N-terminal fragment of huntingtin." Hum Mol Genet 8(3): 397-407.
Seibler, P., J. Graziotto, H. Jeong, F. Simunovic, C. Klein and D. Krainc (2011). "Mitochondrial Parkin recruitment is impaired in neurons derived from mutant PINK1 induced pluripotent stem cells." J Neurosci 31(16): 5970-5976.
Seneca, S., D. Fagnart, K. Keymolen, W. Lissens, D. Hasaerts, S. Debulpaep, B. Desprechins, I. Liebaers and L. De Meirleir (2004). "Early onset Huntington disease: a neuronal degeneration syndrome." Eur J Pediatr 163(12): 717-721.
Serviddio, G. and J. Sastre (2010). "Measurement of mitochondrial membrane potential and proton leak." Methods Mol Biol 594: 107-121.
Shen, Q., W. Zhong, Y. N. Jan and S. Temple (2002). "Asymmetric Numb distribution is critical for asymmetric cell division of mouse cerebral cortical stem cells and neuroblasts." Development 129(20): 4843-4853.
Shiraki, N., Y. Shiraki, T. Tsuyama, F. Obata, M. Miura, G. Nagae, H. Aburatani, K. Kume, F. Endo and S. Kume (2014). "Methionine metabolism regulates maintenance and differentiation of human pluripotent stem cells." Cell Metab 19(5): 780-794.

Shirendeb, U., A. P. Reddy, M. Manczak, M. J. Calkins, P. Mao, D. A. Tagle and P. H. Reddy (2011). "Abnormal mitochondrial dynamics, mitochondrial loss and mutant huntingtin oligomers in Huntington's disease: implications for selective neuronal damage." Hum Mol Genet 20(7): 1438-1455.
Shirendeb, U. P., M. J. Calkins, M. Manczak, V. Anekonda, B. Dufour, J. L. McBride, P. Mao and P. H. Reddy (2012). "Mutant huntingtin's interaction with mitochondrial protein Drp1 impairs mitochondrial biogenesis and causes defective axonal transport and synaptic degeneration in Huntington's disease." Hum Mol Genet 21(2): 406-420.
Shyh-Chang, N., J. W. Locasale, C. A. Lyssiotis, Y. Zheng, R. Y. Teo, S. Ratanasirintrawoot, J. Zhang, T. Onder, J. J. Unternaehrer, H. Zhu, J. M. Asara, G. Q. Daley and L. C. Cantley (2013). "Influence of threonine metabolism on S-adenosylmethionine and histone methylation." Science 339(6116): 222-226.
Siller, K. H. and C. Q. Doe (2009). "Spindle orientation during asymmetric cell division." Nat Cell Biol 11(4): 365-374.
Silva, A. C., S. Almeida, M. Laco, A. I. Duarte, J. Domingues, C. R. Oliveira, C. Januario and A. C. Rego (2013). "Mitochondrial respiratory chain complex activity and bioenergetic alterations in human platelets derived from pre-symptomatic and symptomatic Huntington's disease carriers." Mitochondrion 13(6): 801-809.
Singaraja, R. R., S. Hadano, M. Metzler, S. Givan, C. L. Wellington, S. Warby, A. Yanai, C. A. Gutekunst, B. R. Leavitt, H. Yi, K. Fichter, L. Gan, K. McCutcheon, V. Chopra, J. Michel, S. M. Hersch, J. E. Ikeda and M. R. Hayden (2002). "HIP14, a novel ankyrin domain-containing protein, links huntingtin to intracellular trafficking and endocytosis." Hum Mol Genet 11(23): 2815-2828.
Sittler, A., S. Walter, N. Wedemeyer, R. Hasenbank, E. Scherzinger, H. Eickhoff, G. P. Bates, H. Lehrach and E. E. Wanker (1998). "SH3GL3 associates with the Huntingtin exon 1 protein and promotes the formation of polygln-containing protein aggregates." Mol Cell 2(4): 427-436.
Siva, K., G. Covello and M. A. Denti (2014). "Exon-skipping antisense oligonucleotides to correct missplicing in neurogenetic diseases." Nucleic Acid Ther 24(1): 69-86.
Slow, E. J., J. van Raamsdonk, D. Rogers, S. H. Coleman, R. K. Graham, Y. Deng, R. Oh, N. Bissada, S. M. Hossain, Y. Z. Yang, X. J. Li, E. M. Simpson, C. A. Gutekunst, B. R. Leavitt and M. R. Hayden (2003). "Selective striatal neuronal loss in a YAC128 mouse model of Huntington disease." Hum Mol Genet 12(13): 1555-1567.
Smith, R., P. Brundin and J. Y. Li (2005). "Synaptic dysfunction in Huntington's disease: a new perspective." Cell Mol Life Sci 62(17): 1901-1912.
Smith, R. A., T. M. Miller, K. Yamanaka, B. P. Monia, T. P. Condon, G. Hung, C. S. Lobsiger, C. M. Ward, M. McAlonis-Downes, H. Wei, E. V. Wancewicz, C. F. Bennett and D. W. Cleveland (2006). "Antisense oligonucleotide therapy for neurodegenerative disease." J Clin Invest 116(8): 2290-2296.
Snell, R. G., J. C. MacMillan, J. P. Cheadle, I. Fenton, L. P. Lazarou, P. Davies, M. E. MacDonald, J. F. Gusella, P. S. Harper and D. J. Shaw (1993). "Relationship between trinucleotide repeat expansion and phenotypic variation in Huntington's disease." Nat Genet 4(4): 393-397.
Soldner, F., J. Laganiere, A. W. Cheng, D. Hockemeyer, Q. Gao, R. Alagappan, V. Khurana, L. I. Golbe, R. H. Myers, S. Lindquist, L. Zhang, D. Guschin, L. K. Fong, B. J. Vu, X. Meng, F. D. Urnov, E. J. Rebar, P. D. Gregory, H. S. Zhang and R. Jaenisch (2011). "Generation of isogenic pluripotent stem cells differing exclusively at two early onset Parkinson point mutations." Cell 146(2): 318-331.
Sommer, A. G., S. S. Rozelle, S. Sullivan, J. A. Mills, S. M. Park, B. W. Smith, A. M. Iyer, D. L. French, D. N. Kotton, P. Gadue, G. J. Murphy and G. Mostoslavsky (2012).

"Generation of human induced pluripotent stem cells from peripheral blood using the STEMCCA lentiviral vector." J Vis Exp(68).
Sommer, C. A., M. Stadtfeld, G. J. Murphy, K. Hochedlinger, D. N. Kotton and G. Mostoslavsky (2009). "Induced pluripotent stem cell generation using a single lentiviral stem cell cassette." Stem Cells 27(3): 543-549.
Son, M. J., B. R. Jeong, Y. Kwon and Y. S. Cho (2013). "Interference with the mitochondrial bioenergetics fuels reprogramming to pluripotency via facilitation of the glycolytic transition." Int J Biochem Cell Biol 45(11): 2512-2518.
Sorensen, S. A. and K. Fenger (1992). "Causes of death in patients with Huntington's disease and in unaffected first degree relatives." J Med Genet 29(12): 911-914.
Southwell, A. L., N. H. Skotte, C. F. Bennett and M. R. Hayden (2012). "Antisense oligonucleotide therapeutics for inherited neurodegenerative diseases." Trends Mol Med 18(11): 634-643.
Spitkovsky, D., P. Sasse, E. Kolossov, C. Bottinger, B. K. Fleischmann, J. Hescheler and R. J. Wiesner (2004). "Activity of complex III of the mitochondrial electron transport chain is essential for early heart muscle cell differentiation." FASEB J 18(11): 1300-1302.
St John, J. C., A. Amaral, E. Bowles, J. F. Oliveira, R. Lloyd, M. Freitas, H. L. Gray, C. S. Navara, G. Oliveira, G. P. Schatten, E. Spikings and J. Ramalho-Santos (2006). "The analysis of mitochondria and mitochondrial DNA in human embryonic stem cells." Methods Mol Biol 331: 347-374.
St John, J. C., J. Ramalho-Santos, H. L. Gray, P. Petrosko, V. Y. Rawe, C. S. Navara, C. R. Simerly and G. P. Schatten (2005). "The expression of mitochondrial DNA transcription factors during early cardiomyocyte in vitro differentiation from human embryonic stem cells." Cloning Stem Cells 7(3): 141-153.
Starling, A. J., V. M. Andre, C. Cepeda, M. de Lima, S. H. Chandler and M. S. Levine (2005). "Alterations in N-methyl-D-aspartate receptor sensitivity and magnesium blockade occur early in development in the R6/2 mouse model of Huntington's disease." J Neurosci Res 82(3): 377-386.
Steffan, J. S., A. Kazantsev, O. Spasic-Boskovic, M. Greenwald, Y. Z. Zhu, H. Gohler, E. E. Wanker, G. P. Bates, D. E. Housman and L. M. Thompson (2000). "The Huntington's disease protein interacts with p53 and CREB-binding protein and represses transcription." Proc Natl Acad Sci U S A 97(12): 6763-6768.
Stein, C. A., C. Subasinghe, K. Shinozuka and J. S. Cohen (1988). "Physicochemical properties of phosphorothioate oligodeoxynucleotides." Nucleic Acids Res 16(8): 3209-3221.
Stewart, M. H., M. Bosse, K. Chadwick, P. Menendez, S. C. Bendall and M. Bhatia (2006). "Clonal isolation of hESCs reveals heterogeneity within the pluripotent stem cell compartment." Nat Methods 3(10): 807-815.
Stocchi, V., L. Cucchiarini, M. Magnani, L. Chiarantini, P. Palma and G. Crescentini (1985). "Simultaneous extraction and reverse-phase high-performance liquid chromatographic determination of adenine and pyridine nucleotides in human red blood cells." Anal Biochem 146(1): 118-124.
Stojkovic, M., M. Lako, T. Strachan and A. Murdoch (2004). "Derivation, growth and applications of human embryonic stem cells." Reproduction 128(3): 259-267.
Strehlow, A. N., J. Z. Li and R. M. Myers (2007). "Wild-type huntingtin participates in protein trafficking between the Golgi and the extracellular space." Hum Mol Genet 16(4): 391-409.

Suhr, S. T., E. A. Chang, J. Tjong, N. Alcasid, G. A. Perkins, M. D. Goissis, M. H. Ellisman, G. I. Perez and J. B. Cibelli (2010). "Mitochondrial rejuvenation after induced pluripotency." PLoS One 5(11): e14095.
Takahashi, K., K. Tanabe, M. Ohnuki, M. Narita, T. Ichisaka, K. Tomoda and S. Yamanaka (2007). "Induction of pluripotent stem cells from adult human fibroblasts by defined factors." Cell 131(5): 861-872.
Takahashi, K. and S. Yamanaka (2006). "Induction of pluripotent stem cells from mouse embryonic and adult fibroblast cultures by defined factors." Cell 126(4): 663-676.
Takashima, Y., G. Guo, R. Loos, J. Nichols, G. Ficz, F. Krueger, D. Oxley, F. Santos, J. Clarke, W. Mansfield, W. Reik, P. Bertone and A. Smith (2014). "Resetting Transcription Factor Control Circuitry toward Ground-State Pluripotency in Human." Cell 158(6): 1254-1269.
Tang, T. S., E. Slow, V. Lupu, I. G. Stavrovskaya, M. Sugimori, R. Llinas, B. S. Kristal, M. R. Hayden and I. Bezprozvanny (2005). "Disturbed Ca2+ signaling and apoptosis of medium spiny neurons in Huntington's disease." Proc Natl Acad Sci U S A 102(7): 2602-2607.
Thakur, A. K., M. Jayaraman, R. Mishra, M. Thakur, V. M. Chellgren, I. J. Byeon, D. H. Anjum, R. Kodali, T. P. Creamer, J. F. Conway, A. M. Gronenborn and R. Wetzel (2009). "Polyglutamine disruption of the huntingtin exon 1 N terminus triggers a complex aggregation mechanism." Nat Struct Mol Biol 16(4): 380-389.
Thomson, J. A., J. Itskovitz-Eldor, S. S. Shapiro, M. A. Waknitz, J. J. Swiergiel, V. S. Marshall and J. M. Jones (1998). "Embryonic stem cell lines derived from human blastocysts." Science 282(5391): 1145-1147.
Thorne, R. G., G. J. Pronk, V. Padmanabhan and W. H. Frey, 2nd (2004). "Delivery of insulin-like growth factor-I to the rat brain and spinal cord along olfactory and trigeminal pathways following intranasal administration." Neuroscience 127(2): 481-496.
Timmers, H. J., D. F. Swaab, J. A. van de Nes and H. P. Kremer (1996). "Somatostatin 1-12 immunoreactivity is decreased in the hypothalamic lateral tuberal nucleus of Huntington's disease patients." Brain Res 728(2): 141-148.
Todd, L. R., M. N. Damin, R. Gomathinayagam, S. R. Horn, A. R. Means and U. Sankar (2010). "Growth factor erv1-like modulates Drp1 to preserve mitochondrial dynamics and function in mouse embryonic stem cells." Mol Biol Cell 21(7): 1225-1236.
Todd, L. R., R. Gomathinayagam and U. Sankar (2010). "A novel Gfer-Drp1 link in preserving mitochondrial dynamics and function in pluripotent stem cells." Autophagy 6(6): 821-822.
Trottier, Y., D. Devys, G. Imbert, F. Saudou, I. An, Y. Lutz, C. Weber, Y. Agid, E. C. Hirsch and J. L. Mandel (1995). "Cellular localization of the Huntington's disease protein and discrimination of the normal and mutated form." Nat Genet 10(1): 104-110.
Trushina, E., R. D. Singh, R. B. Dyer, S. Cao, V. H. Shah, R. G. Parton, R. E. Pagano and C. T. McMurray (2006). "Mutant huntingtin inhibits clathrin-independent endocytosis and causes accumulation of cholesterol in vitro and in vivo." Hum Mol Genet 15(24): 3578-3591.
Urnov, F. D., J. C. Miller, Y. L. Lee, C. M. Beausejour, J. M. Rock, S. Augustus, A. C. Jamieson, M. H. Porteus, P. D. Gregory and M. C. Holmes (2005). "Highly efficient endogenous human gene correction using designed zinc-finger nucleases." Nature 435(7042): 646-651.

Urnov, F. D., E. J. Rebar, M. C. Holmes, H. S. Zhang and P. D. Gregory (2010). "Genome editing with engineered zinc finger nucleases." Nat Rev Genet 11(9): 636-646.
van Bilsen, P. H., L. Jaspers, M. S. Lombardi, J. C. Odekerken, E. N. Burright and W. F. Kaemmerer (2008). "Identification and allele-specific silencing of the mutant huntingtin allele in Huntington's disease patient-derived fibroblasts." Hum Gene Ther 19(7): 710-719.
van der Burg, J. M., K. Bacos, N. I. Wood, A. Lindqvist, N. Wierup, B. Woodman, J. I. Wamsteeker, R. Smith, T. Deierborg, M. J. Kuhar, G. P. Bates, H. Mulder, C. Erlanson-Albertsson, A. J. Morton, P. Brundin, A. Petersen and M. Bjorkqvist (2008). "Increased metabolism in the R6/2 mouse model of Huntington's disease." Neurobiol Dis 29(1): 41-51.
Van Raamsdonk, J. M., M. Metzler, E. Slow, J. Pearson, C. Schwab, J. Carroll, R. K. Graham, B. R. Leavitt and M. R. Hayden (2007). "Phenotypic abnormalities in the YAC128 mouse model of Huntington disease are penetrant on multiple genetic backgrounds and modulated by strain." Neurobiol Dis 26(1): 189-200.
Varum, S., O. Momcilovic, C. Castro, A. Ben-Yehudah, J. Ramalho-Santos and C. S. Navara (2009). "Enhancement of human embryonic stem cell pluripotency through inhibition of the mitochondrial respiratory chain." Stem Cell Res 3(2-3): 142-156.
Varum, S., A. S. Rodrigues, M. B. Moura, O. Momcilovic, C. A. t. Easley, J. Ramalho-Santos, B. Van Houten and G. Schatten (2011). "Energy metabolism in human pluripotent stem cells and their differentiated counterparts." PLoS One 6(6): e20914.
Vazquez-Martin, A., S. Cufi, B. Corominas-Faja, C. Oliveras-Ferraros, L. Vellon and J. A. Menendez (2012). "Mitochondrial fusion by pharmacological manipulation impedes somatic cell reprogramming to pluripotency: new insight into the role of mitophagy in cell stemness." Aging (Albany NY) 4(6): 393-401.
Verkhratsky, A., J. J. Rodriguez and L. Steardo (2013). "Astrogliopathology: A Central Element of Neuropsychiatric Diseases?" Neuroscientist.
Vig, P. J., S. H. Subramony, D. R. D'Souza, J. Wei and M. E. Lopez (2006). "Intranasal administration of IGF-I improves behavior and Purkinje cell pathology in SCA1 mice." Brain Res Bull 69(5): 573-579.
Vincent, A. M. and E. L. Feldman (2002). "Control of cell survival by IGF signaling pathways." Growth Horm IGF Res 12(4): 193-197.
Vonsattel, J. P. and M. DiFiglia (1998). "Huntington disease." J Neuropathol Exp Neurol 57(5): 369-384.
Vonsattel, J. P., C. Keller and E. P. Cortes Ramirez (2011). "Huntington's disease - neuropathology." Handb Clin Neurol 100: 83-100.
Vonsattel, J. P., C. Keller and M. Del Pilar Amaya (2008). "Neuropathology of Huntington's disease." Handb Clin Neurol 89: 599-618.
Vonsattel, J. P., R. H. Myers, T. J. Stevens, R. J. Ferrante, E. D. Bird and E. P. Richardson, Jr. (1985). "Neuropathological classification of Huntington's disease." J Neuropathol Exp Neurol 44(6): 559-577.
Walker, F. O. (2007). "Huntington's disease." Lancet 369(9557): 218-228.
Wally, V., A. Klausegger, U. Koller, H. Lochmuller, S. Krause, G. Wiche, L. G. Mitchell, H. Hintner and J. W. Bauer (2008). "5' trans-splicing repair of the PLEC1 gene." J Invest Dermatol 128(3): 568-574.
Wang, H., P. J. Lim, M. Karbowski and M. J. Monteiro (2009). "Effects of overexpression of huntingtin proteins on mitochondrial integrity." Hum Mol Genet 18(4): 737-752.

Wang, H., H. Yang, C. S. Shivalila, M. M. Dawlaty, A. W. Cheng, F. Zhang and R. Jaenisch (2013). "One-step generation of mice carrying mutations in multiple genes by CRISPR/Cas-mediated genome engineering." Cell 153(4): 910-918.
Wang, J., P. Alexander, L. Wu, R. Hammer, O. Cleaver and S. L. McKnight (2009). "Dependence of mouse embryonic stem cells on threonine catabolism." Science 325(5939): 435-439.
Wang, J., C. E. Wang, A. Orr, S. Tydlacka, S. H. Li and X. J. Li (2008). "Impaired ubiquitin-proteasome system activity in the synapses of Huntington's disease mice." J Cell Biol 180(6): 1177-1189.
Wang, L., X. Ye, Q. Zhao, Z. Zhou, J. Dan, Y. Zhu, Q. Chen and L. Liu (2014). "Drp1 is dispensable for mitochondria biogenesis in induction to pluripotency but required for differentiation of embryonic stem cells." Stem Cells Dev 23(20): 2422-2434.
Wang, Y. and R. Blelloch (2009). "Cell cycle regulation by MicroRNAs in embryonic stem cells." Cancer Res 69(10): 4093-4096.
Wang, Y. L., W. Liu, E. Wada, M. Murata, K. Wada and I. Kanazawa (2005). "Clinico-pathological rescue of a model mouse of Huntington's disease by siRNA." Neurosci Res 53(3): 241-249.
Warby, S. C., C. N. Doty, R. K. Graham, J. B. Carroll, Y. Z. Yang, R. R. Singaraja, C. M. Overall and M. R. Hayden (2008). "Activated caspase-6 and caspase-6-cleaved fragments of huntingtin specifically colocalize in the nucleus." Hum Mol Genet 17(15): 2390-2404.
Warby, S. C., C. N. Doty, R. K. Graham, J. Shively, R. R. Singaraja and M. R. Hayden (2009). "Phosphorylation of huntingtin reduces the accumulation of its nuclear fragments." Mol Cell Neurosci 40(2): 121-127.
Warby, S. C., A. Montpetit, A. R. Hayden, J. B. Carroll, S. L. Butland, H. Visscher, J. A. Collins, A. Semaka, T. J. Hudson and M. R. Hayden (2009). "CAG expansion in the Huntington disease gene is associated with a specific and targetable predisposing haplogroup." Am J Hum Genet 84(3): 351-366.
Warby, S. C., H. Visscher, J. A. Collins, C. N. Doty, C. Carter, S. L. Butland, A. R. Hayden, I. Kanazawa, C. J. Ross and M. R. Hayden (2011). "HTT haplotypes contribute to differences in Huntington disease prevalence between Europe and East Asia." Eur J Hum Genet 19(5): 561-566.
Waterman-Storer, C. M., S. B. Karki, S. A. Kuznetsov, J. S. Tabb, D. G. Weiss, G. M. Langford and E. L. Holzbaur (1997). "The interaction between cytoplasmic dynein and dynactin is required for fast axonal transport." Proc Natl Acad Sci U S A 94(22): 12180-12185.
Wellington, C. L., L. M. Ellerby, C. A. Gutekunst, D. Rogers, S. Warby, R. K. Graham, O. Loubser, J. van Raamsdonk, R. Singaraja, Y. Z. Yang, J. Gafni, D. Bredesen, S. M. Hersch, B. R. Leavitt, S. Roy, D. W. Nicholson and M. R. Hayden (2002). "Caspase cleavage of mutant huntingtin precedes neurodegeneration in Huntington's disease." J Neurosci 22(18): 7862-7872.
Wellington, C. L., L. M. Ellerby, A. S. Hackam, R. L. Margolis, M. A. Trifiro, R. Singaraja, K. McCutcheon, G. S. Salvesen, S. S. Propp, M. Bromm, K. J. Rowland, T. Zhang, D. Rasper, S. Roy, N. Thornberry, L. Pinsky, A. Kakizuka, C. A. Ross, D. W. Nicholson, D. E. Bredesen and M. R. Hayden (1998). "Caspase cleavage of gene products associated with triplet expansion disorders generates truncated fragments containing the polyglutamine tract." J Biol Chem 273(15): 9158-9167.
Wellington, C. L., R. Singaraja, L. Ellerby, J. Savill, S. Roy, B. Leavitt, E. Cattaneo, A. Hackam, A. Sharp, N. Thornberry, D. W. Nicholson, D. E. Bredesen and M. R. Hayden

(2000). "Inhibiting caspase cleavage of huntingtin reduces toxicity and aggregate formation in neuronal and nonneuronal cells." J Biol Chem 275(26): 19831-19838.
Werther, G. A., A. Hogg, B. J. Oldfield, M. J. McKinley, R. Figdor and F. A. Mendelsohn (1989). "Localization and Characterization of Insulin-Like Growth Factor-I Receptors in Rat Brain and Pituitary Gland Using in vitro Autoradiography and Computerized Densitometry* A Distinct Distribution from Insulin Receptors." J Neuroendocrinol 1(5): 369-377.
Wexler, N. S., J. Lorimer, J. Porter, F. Gomez, C. Moskowitz, E. Shackell, K. Marder, G. Penchaszadeh, S. A. Roberts, J. Gayan, D. Brocklebank, S. S. Cherny, L. R. Cardon, J. Gray, S. R. Dlouhy, S. Wiktorski, M. E. Hodes, P. M. Conneally, J. B. Penney, J. Gusella, J. H. Cha, M. Irizarry, D. Rosas, S. Hersch, Z. Hollingsworth, M. MacDonald, A. B. Young, J. M. Andresen, D. E. Housman, M. M. De Young, E. Bonilla, T. Stillings, A. Negrette, S. R. Snodgrass, M. D. Martinez-Jaurrieta, M. A. Ramos-Arroyo, J. Bickham, J. S. Ramos, F. Marshall, I. Shoulson, G. J. Rey, A. Feigin, N. Arnheim, A. Acevedo-Cruz, L. Acosta, J. Alvir, K. Fischbeck, L. M. Thompson, A. Young, L. Dure, C. J. O'Brien, J. Paulsen, A. Brickman, D. Krch, S. Peery, P. Hogarth, D. S. Higgins, Jr. and B. Landwehrmeyer (2004). "Venezuelan kindreds reveal that genetic and environmental factors modulate Huntington's disease age of onset." Proc Natl Acad Sci U S A 101(10): 3498-3503.
Weydt, P., V. V. Pineda, A. E. Torrence, R. T. Libby, T. F. Satterfield, E. R. Lazarowski, M. L. Gilbert, G. J. Morton, T. K. Bammler, A. D. Strand, L. Cui, R. P. Beyer, C. N. Easley, A. C. Smith, D. Krainc, S. Luquet, I. R. Sweet, M. W. Schwartz and A. R. La Spada (2006). "Thermoregulatory and metabolic defects in Huntington's disease transgenic mice implicate PGC-1alpha in Huntington's disease neurodegeneration." Cell Metab 4(5): 349-362.
Weydt, P., S. M. Soyal, C. Gellera, S. Didonato, C. Weidinger, H. Oberkofler, G. B. Landwehrmeyer and W. Patsch (2009). "The gene coding for PGC-1alpha modifies age at onset in Huntington's Disease." Mol Neurodegener 4: 3.
Wick, A. N., D. R. Drury, H. I. Nakada and J. B. Wolfe (1957). "Localization of the primary metabolic block produced by 2-deoxyglucose." J Biol Chem 224(2): 963-969.
Wiedenheft, B., S. H. Sternberg and J. A. Doudna (2012). "RNA-guided genetic silencing systems in bacteria and archaea." Nature 482(7385): 331-338.
Wiegand, M., A. A. Moller, C. J. Lauer, S. Stolz, W. Schreiber, M. Dose and J. C. Krieg (1991). "Nocturnal sleep in Huntington's disease." J Neurol 238(4): 203-208.
Wild, E. J. and S. J. Tabrizi (2007). "The differential diagnosis of chorea." Pract Neurol 7(6): 360-373.
Willardsen, M. I. and B. A. Link (2011). "Cell biological regulation of division fate in vertebrate neuroepithelial cells." Dev Dyn 240(8): 1865-1879.
Wirtz-Peitz, F., T. Nishimura and J. A. Knoblich (2008). "Linking cell cycle to asymmetric division: Aurora-A phosphorylates the Par complex to regulate Numb localization." Cell 135(1): 161-173.
Woltjen, K., I. P. Michael, P. Mohseni, R. Desai, M. Mileikovsky, R. Hamalainen, R. Cowling, W. Wang, P. Liu, M. Gertsenstein, K. Kaji, H. K. Sung and A. Nagy (2009). "piggyBac transposition reprograms fibroblasts to induced pluripotent stem cells." Nature 458(7239): 766-770.
Wright, H. H., C. N. Still and R. K. Abramson (1981). "Huntington's disease in black kindreds in South Carolina." Arch Neurol 38(7): 412-414.
Wu, J., F. Lin and Z. Qin (2007). "Sequestration of glyceraldehyde-3-phosphate dehydrogenase to aggregates formed by mutant huntingtin." Acta Biochim Biophys Sin (Shanghai) 39(11): 885-890.

Xia, X., H. Zhou, Y. Huang and Z. Xu (2006). "Allele-specific RNAi selectively silences mutant SOD1 and achieves significant therapeutic benefit in vivo." Neurobiol Dis 23(3): 578-586.
Yajima, H., H. Fujisawa, N. I. Nakajima, H. Hirakawa, P. A. Jeggo, R. Okayasu and A. Fujimori (2013). "The complexity of DNA double strand breaks is a critical factor enhancing end-resection." DNA Repair (Amst).
Yamamoto, A., M. L. Cremona and J. E. Rothman (2006). "Autophagy-mediated clearance of huntingtin aggregates triggered by the insulin-signaling pathway." J Cell Biol 172(5): 719-731.
Yamamoto, A., J. J. Lucas and R. Hen (2000). "Reversal of neuropathology and motor dysfunction in a conditional model of Huntington's disease." Cell 101(1): 57-66.
Yamanaka, T., H. Miyazaki, F. Oyama, M. Kurosawa, C. Washizu, H. Doi and N. Nukina (2008). "Mutant Huntingtin reduces HSP70 expression through the sequestration of NF-Y transcription factor." EMBO J 27(6): 827-839.
Yanes, O., J. Clark, D. M. Wong, G. J. Patti, A. Sanchez-Ruiz, H. P. Benton, S. A. Trauger, C. Desponts, S. Ding and G. Siuzdak (2010). "Metabolic oxidation regulates embryonic stem cell differentiation." Nat Chem Biol 6(6): 411-417.
Yao, J. K., S. Leonard and R. D. Reddy (2004). "Increased nitric oxide radicals in postmortem brain from patients with schizophrenia." Schizophr Bull 30(4): 923-934.
Yu, J., K. Hu, K. Smuga-Otto, S. Tian, R. Stewart, Slukvin, II and J. A. Thomson (2009). "Human induced pluripotent stem cells free of vector and transgene sequences." Science 324(5928): 797-801.
Yu, J., M. A. Vodyanik, K. Smuga-Otto, J. Antosiewicz-Bourget, J. L. Frane, S. Tian, J. Nie, G. A. Jonsdottir, V. Ruotti, R. Stewart, Slukvin, II and J. A. Thomson (2007). "Induced pluripotent stem cell lines derived from human somatic cells." Science 318(5858): 1917-1920.
Yu, Z. X., S. H. Li, J. Evans, A. Pillarisetti, H. Li and X. J. Li (2003). "Mutant huntingtin causes context-dependent neurodegeneration in mice with Huntington's disease." J Neurosci 23(6): 2193-2202.
Zala, D., E. Colin, H. Rangone, G. Liot, S. Humbert and F. Saudou (2008). "Phosphorylation of mutant huntingtin at S421 restores anterograde and retrograde transport in neurons." Hum Mol Genet 17(24): 3837-3846.
Zala, D., M. V. Hinckelmann, H. Yu, M. M. Lyra da Cunha, G. Liot, F. P. Cordelieres, S. Marco and F. Saudou (2013). "Vesicular glycolysis provides on-board energy for fast axonal transport." Cell 152(3): 479-491.
Zaugg, K., Y. Yao, P. T. Reilly, K. Kannan, R. Kiarash, J. Mason, P. Huang, S. K. Sawyer, B. Fuerth, B. Faubert, T. Kalliomaki, A. Elia, X. Luo, V. Nadeem, D. Bungard, S. Yalavarthi, J. D. Growney, A. Wakeham, Y. Moolani, J. Silvester, A. Y. Ten, W. Bakker, K. Tsuchihara, S. L. Berger, R. P. Hill, R. G. Jones, M. Tsao, M. O. Robinson, C. B. Thompson, G. Pan and T. W. Mak (2011). "Carnitine palmitoyltransferase 1C promotes cell survival and tumor growth under conditions of metabolic stress." Genes Dev 25(10): 1041-1051.
Zeuschner, D., K. Mildner, H. Zaehres and H. R. Scholer (2010). "Induced pluripotent stem cells at nanoscale." Stem Cells Dev 19(5): 615-620.
Zhang, H., Q. Li, R. K. Graham, E. Slow, M. R. Hayden and I. Bezprozvanny (2008). "Full length mutant huntingtin is required for altered Ca2+ signaling and apoptosis of striatal neurons in the YAC mouse model of Huntington's disease." Neurobiol Dis 31(1): 80-88.
Zhang, J., I. Khvorostov, J. S. Hong, Y. Oktay, L. Vergnes, E. Nuebel, P. N. Wahjudi, K. Setoguchi, G. Wang, A. Do, H. J. Jung, J. M. McCaffery, I. J. Kurland, K. Reue, W.

N. Lee, C. M. Koehler and M. A. Teitell (2011). "UCP2 regulates energy metabolism and differentiation potential of human pluripotent stem cells." EMBO J 30(24): 4860-4873.
Zhang, J., E. Nuebel, D. R. Wisidagama, K. Setoguchi, J. S. Hong, C. M. Van Horn, S. S. Imam, L. Vergnes, C. S. Malone, C. M. Koehler and M. A. Teitell (2012). "Measuring energy metabolism in cultured cells, including human pluripotent stem cells and differentiated cells." Nat Protoc 7(6): 1068-1085.
Zhang, N., M. C. An, D. Montoro and L. M. Ellerby (2010). "Characterization of Human Huntington's Disease Cell Model from Induced Pluripotent Stem Cells." PLoS Curr 2: RRN1193.
Zhang, X., I. Neganova, S. Przyborski, C. Yang, M. Cooke, S. P. Atkinson, G. Anyfantis, S. Fenyk, W. N. Keith, S. F. Hoare, O. Hughes, T. Strachan, M. Stojkovic, P. W. Hinds, L. Armstrong and M. Lako (2009). "A role for NANOG in G1 to S transition in human embryonic stem cells through direct binding of CDK6 and CDC25A." J Cell Biol 184(1): 67-82.
Zhao, W., X. Ji, F. Zhang, L. Li and L. Ma (2012). "Embryonic stem cell markers." Molecules 17(6): 6196-6236.
Zhao, X. Y., W. Li, Z. Lv, L. Liu, M. Tong, T. Hai, J. Hao, C. L. Guo, Q. W. Ma, L. Wang, F. Zeng and Q. Zhou (2009). "iPS cells produce viable mice through tetraploid complementation." Nature 461(7260): 86-90.
Zheng, Z., Q. Wan, J. Liu, H. Zhu, X. Chu and Q. Du (2013). "Evidence for dynein and astral microtubule-mediated cortical release and transport of Galphai/LGN/NuMA complex in mitotic cells." Mol Biol Cell 24(7): 901-913.
Zheng, Z., H. Zhu, Q. Wan, J. Liu, Z. Xiao, D. P. Siderovski and Q. Du (2010). "LGN regulates mitotic spindle orientation during epithelial morphogenesis." J Cell Biol 189(2): 275-288.
Zhou, H., S. Wu, J. Y. Joo, S. Zhu, D. W. Han, T. Lin, S. Trauger, G. Bien, S. Yao, Y. Zhu, G. Siuzdak, H. R. Scholer, L. Duan and S. Ding (2009). "Generation of induced pluripotent stem cells using recombinant proteins." Cell Stem Cell 4(5): 381-384.
Zhou, P., I. L. Derkatch and S. W. Liebman (2001). "The relationship between visible intracellular aggregates that appear after overexpression of Sup35 and the yeast prion-like elements [PSI(+)] and [PIN(+)]." Mol Microbiol 39(1): 37-46.
Zhu, J., W. Wen, Z. Zheng, Y. Shang, Z. Wei, Z. Xiao, Z. Pan, Q. Du, W. Wang and M. Zhang (2011). "LGN/mInsc and LGN/NuMA complex structures suggest distinct functions in asymmetric cell division for the Par3/mInsc/LGN and Galphai/LGN/NuMA pathways." Mol Cell 43(3): 418-431.
Zuccato, C., M. Tartari, A. Crotti, D. Goffredo, M. Valenza, L. Conti, T. Cataudella, B. R. Leavitt, M. R. Hayden, T. Timmusk, D. Rigamonti and E. Cattaneo (2003). "Huntingtin interacts with REST/NRSF to modulate the transcription of NRSE-controlled neuronal genes." Nat Genet 35(1): 76-83.
Zuccato, C., M. Valenza and E. Cattaneo (2010). "Molecular mechanisms and potential therapeutical targets in Huntington's disease." Physiol Rev 90(3): 905-981.